Thesis Submitted for Consideration for the Degree of Doctor of Philosophy

Department of Earth Sciences

University of Oxford

Nickel Stable Isotope Fractionation in Planetary Materials

Naomi Jane Saunders

MEarthSci

Worcester College

Trinity 2018

Supervisors:

Professor Alex N. Halliday and Doctor Jane Barling

Contents

Declaration

I declare that the work presented in this thesis is wholly my own work, except where otherwise stated. The views and interpretations expressed herein are mine, and do not represent those of any other person or group

Naomi J. Saunders

Acknowledgements

This thesis exists thanks to the support and help of many people. Firstly, thanks to my supervisors, Alex and Jane, for their feedback throughout this work but especially in the final weeks. Secondly, Yu-Te Alan Hsieh, manager of the multi-collectors here at Oxford, has been a lifesaver on so many occasions. Alan stayed late with me so often, whenever P4 was behaving badly, and I cannot thank him enough. Thirdly, Phil Holdship, ICPMS manager, for his help using the Quad and Element throughout this work.

The department here at Oxford has been an amazing place to work, and I need to thank all of the friends here who have made my time here both productive and fun. So a big thank you to those, current and past, including Becca, Lauren, Neil, Ally, Ricky, Lawrence, Sietske, Eleanor, and officemates and group mates current and former. Thanks also go to Elizabeth, for letting me 'nest' in her library for the last 3 months. Outside of my academic life, special thanks go to the best of friends: Kiran, Susannah, and Katie. These lovely people have been fantastic throughout my time in Oxford, supplying stress-relief, pizza, cake, fun, and entertainment for years. I also owe thank to the person who is the reason I started AS level Geology in 2008: Jan Fielding, one of my most supportive and inspiring teachers! I should also thank the existence of my favourite 'feel better' things: tea, sherry, and BBC Radio Cumbria!

The greatest thanks go to those responsible for my continued sanity and happiness: my parents, sister Candy, and partner Luke. Thanks go to my parents for their endless long-distance support, especially when I rang in a stress late at night! Candy has supplied escape throughout my time in Oxford (particularly with tea and chat). Luke has made my last two years in Oxford a delight, and has been there for me even through the last and worst parts of PhD life.

Abstract

Nickel is a moderately siderophile and refractory first row transition metal, and a relatively new addition to the field of investigation of mass dependent stable isotope fractionation processes. Nickel is compatible in the magnesium-rich silicate minerals that constitute most upper mantle lithologies. This work provides the first detailed study of Ni stable isotopic compositions for such materials, with a particular focus on ultramafic xenoliths, oceanic basaltic rocks and lunar samples. The methods use ion exchange chromatography and multi-collector ICPMS with double spiking, adapting procedures of Gall et al., 2012. It is found that Ni isotopic compositions are not fractionated by partial melting or fractional crystallisation. There are no significant fractionations between mantle minerals. However, there are variations within the terrestrial mantle and in basalts from the Earth and Moon. On Earth, the deviations toward lighter compositions in enriched mid ocean ridge basalts show a relationship with the presence of enriched trace element chemical compositions. Ocean island basalts also display isotopic heterogeneities. In ultramafic samples it is the more metasomatised and iron-rich lithologies that are isotopically lightest, the most extreme being pyroxenitic material. This provides evidence that recycling of basaltic materials into the mantle leaves a signature of isotopically light Ni. Nickel isotopic compositions can therefore behave as a tracer for the composition of the mantle source region, uncomplicated by melting processes, redox changes, or time since enriched material was added to the mantle source region. On the Moon, variations in Ni isotopic composition have been shown not to relate to cosmogenic effects. The lunar Ni isotopic compositions appear to relate to the abundance of plagioclase and incompatible elements in the sample. Nickel isotopes, therefore, behaved differently in the lunar environment and were fractionated by processes that are insignificant or do not occur on Earth, probably in the lunar magma ocean.

Extended Abstract

Nickel is a first row transition metal, with 5 stable isotopes. It is a moderately siderophile refractory element that is mainly (>90%) concentrated in the core. At the present day Earth's surface, Ni is usually found only in the 2+ oxidation state, making it unlikely that redox plays a role in its distribution or its isotopic fractionation. During mantle melting Ni behaves as a compatible element, largely remaining in olivine. Indeed variations in the concentration of Ni in basalts [Ni] have long been ascribed to fractional crystallisation of olivine. Nickel isotopes have been studied for decades, because excess ^{60}Ni indicates fossil ^{60}Fe (half-life=2.6 Ma (Rugel et al., 2009)), which has been extensively used as a geochronometer of early solar system events and materials. In addition, nucleosynthetic isotopic variations have been found in calcium aluminium refractory inclusions and correlating with effects on ^{96}Zr and formerly live ^{60}Fe (Quitte et al., 2007).

Studies of the level of mass dependent stable isotope fractionation of Ni were first made at high precision using double spiking, by Cameron et al (2009). Much of the early interest focused on low temperature and bio-geochemistry (e.g. Gall et al. 2013). More recently a study investigating Ni isotopic compositions of the terrestrial mantle, minerals, and meteorites was published (Gall et al., 2017). Mass-dependent fractionations in low-temperature (surface) environments are significantly larger than the fractionations predicted for high temperature environments (such as dominate planetary formation and formation of igneous rocks). Smaller fractionations make the resolution of useful variations more difficult. Today, nearly all measurements are made using multiple collector inductively coupled plasma mass spectrometry (MC-ICPMS), which facilitates high degrees of ionization. The techniques for mass bias corrections for mass dependent fractionation studies use Cu-doping or double spiking. In the case of mass independent fractionations, internal normalisation to a fixed isotope ratio is used.

In this work, samples were usually pre-powdered, and this work has shown that no contamination of Ni isotopic composition occurred during the production of archive powdered samples. Samples are weighed with high precision to provide a minimum of 1000 ng of natural Ni (although less was used if sample material was limited). The samples were then dissolved by acid digestion, either on a hotplate or in an oven using high-pressure Parr Bombs. The method used for purification of Ni from geological samples is an adaptation of the ion exchange chromatography method developed by (Gall et al., 2012). Both cation and anion resins are used in three sequential micro-columns of decreasing capacity. Samples are equilibrated with the appropriate amount of double spike prior to loading onto the first column to have a sample/natural Ni to spike Ni ratio of 0.4:1.

The first (and largest) column, uses di-ammonium-hydrogen-citrate (dAHC) and ammonia (NH_3) to cause elements other than Ni, Zn and Cu to wash off the AG50W-X4 cation resin. Nickel, Zn, and Cu are then eluted with 3M hydrochloric acid (HCl) after the ammonia has been removed with a dilute HCl rinse. The second column (using the same resin as the first column) first uses an oxalic acid and HCl mixture as the chelating agent. Elements with valences greater than 2+ are eluted as oxalic complexes. Following this, a HCl and acetone mixture removes divalent elements excluding Ni. Nickel is eluted with the Ni-binding chemical di-methylglyoxime (DMG) in a mixture with acetone and HCl. The third and final column is designed to remove any remaining Fe by causing it to stick to AG1-X8 anion resin in HCl and hydrogen peroxide (H_2O_2) while Ni is eluted.

Analysis is undertaken on a Nu Plasma HR MC-ICPMS, using pseudo high resolution to avoid the influence of polyatomic interferences on mass 58. The array of Faraday collectors is non-standard on the instrument used in this work, the set-up allows monitoring of mass 57 to perform an iron correction, in addition to the Ni masses (58, 60, 61, 62). A microconcentric PFA nebulizer and desolvator (DSN-100) were used to introduce samples to the plasma and all isotopes are simultaneously measured in static collection mode (Gall et al., 2012).

Over one hundred geological samples have been analysed in this work, consisting of 20 mineral separates, 29 mantle xenoliths, 41 mafic samples, and 11 lunar basalts, as well as USGS rock standards. Duplicates were analysed throughout to monitor reproducibility, in addition to the repeated analysis of standards. The 2SD external reproducibility on $\delta^{60/58}Ni_{SRM986}$ during the course of this work/study, assessed on >60 replicate analyses of reference standards, is ±0.06‰ and is comparable to the external reproducibility in earlier work/studies.

Most ultramafic samples have very similar Ni isotopic compositions, but there are notable exceptions. An average of $\delta^{60/58}Ni_{SRM986}$=0.20±0.08‰ (2SD, n=18) representing the bulk silicate Earth, agrees well with the average mantle from the most comprehensive previous study (Gall et al., 2017). Mantle peridotites can undergo metasomatism. Such samples display anomalously light isotopic compositions ($\delta^{60/58}Ni_{SRM986}$=0.02 to 0.13‰). Nickel isotopic compositions in dunites and pyroxenites are also lighter than the average for unmetasomatised peridotites. Two websterites (pyroxenites containing both ortho- and clinopyroxenes) from Cameroon have the lightest Ni isotopic compositions analysed in this thesis by a large margin (-0.26 and -0.38‰). Pyroxenites from Kilbourne Hole have Ni isotopic compositions up to 0.20‰ lighter than the unmetasomatised spinel lherzolites from the same site. This suggests that lighter Ni isotopic compositions are associated with enriched lithologies, and shows that heterogeneity is preserved in Ni isotopes in the terrestrial mantle.

To evaluate whether the light isotopic compositions reflected isotopic disequilibrium between mineral phases, or the modal effects of varying proportions of minerals stemming from differences in mineralogy, the constituent minerals were separated from a number of samples and analysed for their Ni isotopic composition. Eighteen mineral samples from six different host xenoliths plus 2 megacrysts were analysed, consisting of examples of olivine, orthopyroxene, clinopyroxene, spinel, and garnet. Sulfide had too low abundance in the host xenoliths to be separated for analysis. However, from mass balance considerations, both sulfide and garnet are unlikely to contribute significant Ni.

The separated mantle minerals show very limited fractionation in Ni isotopes (<0.12‰). Olivine and orthopyroxene (where both were analysed from a single host) are identical within error, and spinel, where analysed, is the phase with the heaviest Ni isotopic composition. Clinopyroxene is always the phase with the lightest Ni isotopic composition in the peridotites. In the samples with lighter bulk rock Ni isotopic compositions, all the phases have similarly lighter Ni isotopic compositions than normal. Reconstruction of bulk Ni isotopic compositions from constituent mineral compositions, with modal amounts of each mineral, agree within error with the analysed bulk powder. This also suggests that the Ni isotopic composition of the bulk rock is not affected by minor mineral phases, nor interstitial or surficial adherents. Similar to the peridotite xenoliths, the constituent minerals in pyroxenite all show light Ni isotopic compositions, like the bulk rock. However, the clinopyroxene is, if anything, slightly heavier than the orthopyroxene. There is no indication in any of these cases that the Ni isotopic compositions are greatly out of equilibrium on a mineral scale, even when the bulk rock has isotopically light Ni isotopic composition. Therefore, there is no indication that mantle mineralogy influences Ni isotope composition.

A broad negative correlation between $\delta^{60/58}Ni_{SRM986}$ and Fe content suggests that the Ni isotopic composition is related to major element chemistry, and not affected by minor recent interactions. A further positive correlation between $\delta^{60/58}Ni_{SRM986}$ and Nd isotopic composition suggests that the variations observed in ultramafic samples most likely reflect recycling of light Ni into the mantle. The origin of a light component is not obvious at this stage. The nickel isotopic compositions of shales, hydrocarbons, ferromanganese crusts and seawater are isotopically heavy (Gall 2011, Gall et al., 2013, Cameron and Vance, 2014, Porter et al., 2014; Ventura et al 2015, Vance et al., 2016; Ciscero et al., 2018) relative to the BSE. Nickel that is slightly lighter than BSE is produced as a residue to weathering (Gall et al 2012) and in alteration of the oceanic crust (Gall, 2011). However, it is also possible that the Ni isotopes are fractionated during subduction, in a similar way to how it has been suggested Mo isotopes are fractionated in subduction zones (König et al., 2016).

The mafic lavas analysed in this work also display heterogeneity in Ni isotopes, broadly similar in range to that found in the ultramafic rocks with a spread between values that are similar to unmetasomatised peridotite (0.20‰) to significantly lighter (-0.10‰). In order to test whether part of this variability in mafic samples might reflect degree of partial melting a suite of samples from the Cameroon Line were studied. All 15 samples whether hypersthene-normative basalt, alkali basalt, basanite, or nephelinite, yield Ni isotopic compositions that agree within error yielding an average of average $\delta^{60/58}Ni_{SRM986}$=0.08±0.05‰. Geochemical indicators of partial melting and fractional crystallisation also show no relationship with Ni isotopic composition. Therefore, melting processes do not change Ni isotopic compositions and are likely to preserve the Ni isotopic composition of the mantle source.

'Normal' mid ocean ridge basalts (N-MORB) have Ni isotopic compositions that are similar to the BSE (average $\delta^{60/58}Ni_{SRM986}$=0.15±0.11‰, n=4, including 2 samples at 0.19‰). Those with a more enriched component (E-MORB), with elevated La/Sm ratios, are isotopically lighter (average $\delta^{60/58}Ni_{SRM986}$=0.00±0.06‰, n=7). Lighter $\delta^{60/58}Ni_{SRM986}$ in enriched MORB, relative to normal MORB, further supports that enriched lithologies in the mantle preserve light Ni isotopic compositions.

Greater variability in Ni isotopic compositions is found in ocean island basalts (OIBs). Four OIB systems were analysed and differences between the average Ni isotopic compositions of these OIBs, further highlights the mantle heterogeneity in Ni isotopic compositions. The samples from Iceland (average $\delta^{60/58}Ni_{SRM986}$=0.13±0.17‰, n=6) display the greatest range in Ni isotopic compositions from a single locality of 0.01 to 0.23‰. Samples from the Azores (average $\delta^{60/58}Ni_{SRM986}$=-0.10±0.10‰, n=3) and Galápagos (average $\delta^{60/58}Ni_{SRM986}$=-0.01±0.04‰, n=2) are generally lighter, extending down to -0.16‰ (AZP6, Pico, Azores).

Given that partial melting and fractional crystallisation has been shown to have no effect on terrestrial Ni isotopic composition, the most likely explanation for the Ni isotopic variability in MORB and OIB is that enriched components with light Ni isotopic compositions pervade the

upper mantle leading to considerable degrees of heterogeneity. Mass balance calculations suggest that approximately 25% of websterite-like material could reproduce the Ni isotopic compositions of the majority of mafic samples.

The Moon shows no evidence for plate tectonics, and therefore no mechanism to produce recycled components, it might be expected that the Ni isotopic composition of the lunar mantle, hence lunar basalts, would be more uniform than the terrestrial mantle and terrestrial basalts. The nickel isotopic compositions of 11 Apollo basalts define a large range from -0.20 to 0.34‰, exceeding that found in terrestrial basalts. Unspiked aliquots of 5 samples with cosmic ray exposure ages ranging from 95 to 621 Ma were analysed to determine whether there was any indication of cosmogenic modification. All yielded compositions that were identical to terrestrial samples within error. There is also no correlation between the Ni isotopic compositions and cosmic ray exposure age.

Given that the main process apparently affecting the fractionation of Ni isotopes in terrestrial high temperature environments is the presence of recycled enriched material it is surprising that greater variation exists on the Moon. In fact the majority of lunar basalt Ni isotopic compositions are within error of, or even heavier than the average terrestrial unmetasomatised peridotite. One aluminium rich basalt (14053) has an extremely light Ni isotopic composition (-0.20‰). The lunar samples show a negative correlation between Ni isotopic composition and aluminium concentration and plagioclase abundance, in addition to negative correlations with a number of incompatible element concentration. A correlation with S concentration and sulphur isotopic composition, suggests that Ni fractionation in the Moon may relate to experimental results for the partitioning of Ni being affected by oxygen fugacity with high S content. Further work is needed to elucidate whether this is indeed the case.

1. Introduction

1.1. Nickel

Nickel (Ni) is a first row transition metal, with five stable isotopes of wide ranging natural relative abundances 58 (68.077%), 60 (26.22%), 61 (1.114%), 62 (3.635%), and 64 (0.926%) (Gramlich et al., 1989). The name is derived from *kupfernickel,* a Ni ore now called nickeline, and originally believed to have been an ore of copper (Nicholls, 1974).

Nickel preferentially forms strong metallic bonds and, in crystal structures, prefers octahedral coordination, usually as Ni^{2+} (Wedepohl, 1974). Oxidation states of +3 and +4 are also possible, but +2 is the most stable valence state under surface terrestrial redox states (Nicholls, 1974), which causes Ni to be largely insensitive to redox changes. Nickel is abundant in planetary materials as both Fe-Ni metal in elemental form, and as a divalent cationic species, substituting for Fe and Mg in common silicate structures (Elliott and Steele, 2017).

The bulk Earth is estimated to contain 1.82 wt% Ni, of which the majority is in the Fe-Ni core (5.2 wt%) (Henderson and Henderson, 2009) because Ni is moderately siderophile (iron-loving). Nickel is also refractory, as it has a relatively high condensation temperature of 1353°C (Lodders, 2003). Therefore, the Earth is expected to have approximately chondritic proportions of Ni relative to other refractory elements.

Nickel is highly compatible, therefore during partial melting of a mantle source material Ni is enriched in the residual solid phases. Accordingly, 99.97% of Ni in the bulk silicate Earth (BSE) is in the mantle (McDonough and Sun, 1995). Despite this, Ni is still the 15^{th} most abundant element in the Earth's crust at 0.008 wt% (Nicholls, 1974), though it rarely occurs as a native metal.

The advantage of studying Ni in planetary materials is the abundance of Ni in iron and chondrite groups of meteorites. Lithophile elements, in contrast to siderophile Ni, are not present in sufficient quantities in iron meteorites to allow comparison between these groups. As

a first row transition element, Ni behaves similarly to iron, but has the advantage of being unaffected by oxidation state.

As with all the iron-group nuclei, Ni isotopes can be produced from equilibrium processes during silicon burning and production is dependent on temperature, density and neutron enrichment (Morand and Allègre, 1983). In addition, ^{62}Ni and ^{64}Ni are preferentially produced in a neutron rich environment (e- or r- process).

Early work investigating Ni isotopes was focussed on the search in meteorites for radiogenic ^{60}Ni (e.g. Morand et al., 1980), produced by decay of formerly live ^{60}Fe with a half-life 2.6 Ma (Rugel et al., 2009). Investigation of mass independent and stable mass dependent fractionation of Ni has been a relatively new addition to the field.

Further details on the development of the field of stable Ni isotope geochemistry can be found in the review by Elliott and Steele (2017).

1.2. Previous work on Ni isotopes

1.2.1. Background

Until 2006, almost all investigations of Ni isotopic compositions were aimed at providing evidence for the presence and abundance of formerly live ^{60}Fe. Early studies (for example: Birck & Lugmair 1988; A. Shukolyukov & Lugmair 1993; Tachibana & Huss, 2003) found such anomalies and this developed into the ^{60}Fe-^{60}Ni chronometer, used to date very early processes in solar system materials. Study of Ni isotopes began with the investigation of meteorites for radiogenic ^{60}Ni from the decay of the short-lived extinct radioactive isotope ^{60}Fe (Morand et al., 1980).

Analysis of Ni isotopes, unless secondary-ion mass spectrometry (SIMS) is used, requires purification of the sample to limit problems relating to interferences. Different methods of purification have been published, the details of which are presented in Chapter 2. Investigation of isotopic fractionation requires a method of correction for instrumental mass bias inherent to

the mass spectrometer, that does not correct for natural mass dependent fractionation in the sample. For Ni these have included double spike, doping with Cu, and sample-standard bracketing (see Chapter 2). Since 2005, Ni isotopes have been analysed almost exclusively using multiple-collector inductively-coupled-plasma mass spectrometry (MC-ICPMS), because Ni requires high first ionisation potential.

The procedure of purification from Gall and co-workers (2012) is described in detail in Chapter 2, as it formed the basis of this work. This method uses a three micro-column ion exchange procedure, double spike, and MC-ICPMS (Nu plasma HR).

1.2.2. Published studies of Nickel isotopes

Geochronological use of Ni

From 1982 to 1993 a number of research articles reported evidence of formerly live ^{60}Fe in a number of meteorite classes and their components based on excesses in the daughter product ^{60}Ni (Guan et al., 2004; Mostefaoui et al., 2005; Shukolyukov and Lugmair, 1993b, 1993a; Tachibana et al., 2006; Tachibana and Huss, 2003; Chen and co-workers, 2009. Other studies have found deficits in ^{60}Ni, which suggests they formed before decay of fossil ^{60}Fe, potentially relating to segregation of metal phases with live ^{60}Fe (e.g. Cook et al., 2008a).

Nucleosynthetic nickel isotope anomalies

Nucleosynthetic anomalies have also been investigated in solar system materials. The results, normalised to a fixed isotopic ratio, are usually expressed in units of per ten-thousand (ϵ) deviation from terrestrial Ni isotope ratios, as measured with reference to the Ni standard reference material, SRM986 from NIST (Gramlich et al., 1989). The SRM986 has been the reference material for all studies except (Moynier et al., 2007).

Early studies found no evidence of Ni isotopic anomalies in meteorites including examples of chondrites, irons, Allende inclusions and pallasites (Morand et al., 1980; Morand and Allègre, 1983; Shimamura and Lugmair, 1983), due to large errors prior to technological advances in analytical techniques.

Since development of MC-ICPMS, nucleosynthtic anomalies on all Ni isotopes have been found in a number of meteorite classes, and meteoritic components including CAIS, chondrules, and mineral phases (Bizzarro et al., 2006; Chen et al., 2009; Cook et al., 2008b, 2006; Moynier et al., 2005; Quitté et al., 2006; Regelous et al., 2008; Steele et al., 2012, 2011)

Steele and co-workers (2012) also found correlations of Ni isotope anomalies with O, Cr, and Ti isotope ratios and Pb/Yb in the bulk meteorites, suggesting heterogeneous distribution of isotopic anomalies in the early solar system. As on Earth, Ni isotopic anomalies due to early solar system nucleosynthetic heterogeneity are unlikely to be found in the Moon.

Mass dependent nickel isotopic fractionation

Mass dependent stable Ni isotope fractionation is normally expressed as $\delta^{60/58}Ni_{SRM986}$ in units of per mille (‰). Investigation of mass dependent Ni began with Tanimizu and Hirata (2006), and analysis has been done almost exclusively with MC-ICP-MS.

Broadly, low temperature materials have shown large fractionations from as light as -1.5‰ in some microbial cells (Cameron et al., 2009) and ranging up to 2.2‰ in river water (Vance et al., 2016), and 2.5‰ in organic rich sediment (Porter et al., 2014). High temperature materials were expected to show less fractionation, and indeed only sulfide minerals (-1.05‰ (Tanimizu and Hirata, 2006) to 0.76‰ (Gall, 2011)), show large fractionations from SRM986, a range of approximately half that seen in low temperature materials. The published Ni isotope data is summarised in Figure 1 (terrestrial) and Figure 2 (extra-terrestrial).

Natural waters were analysed by Cameron and Vance (2014) and heavy Ni isotopic compositions were found in rivers across the globe, and in ocean water samples. Additional river samples from the sulfidic Black Sea environment were analysed by Vance and co-workers (2016) and found to be generally heavier than those analysed in Cameron and Vance two years earlier. Heavy Ni isotopic compositions are also found in Fe-Mn crusts and nodules (range 0.88 to 2.47‰; Gall et al., 2013; Gueguen et al., 2016) and marine sediments (range 0.03 to 1.15‰; Ciscato et al., 2018), although sulfidic sediments from the Black Sea have a more limited range (0.18 to 0.26‰; (Vance et al., 2016). Organic rich sediments are dominantly heavy in Ni

isotopic composition, ranging from 0.33 to 2.5‰ (Porter et al., 2014). Crude oil itself has a Ni isotopic composition within the range of source rock compositions (0.42 to 0.75‰; Ventura et al., 2015).

Low temperature alteration has been shown to produce lighter Ni isotopic compositions than comparable pristine samples, including serpentinised peridotites (Gall, 2011; Gueguen et al., 2013), and altered basalts (Gall, 2011). Altered dunite has also been shown to be lighter in Ni isotopic composition than unaltered examples (Spivak-Birndorf et al., 2018). Leached olivine, however, showed identical Ni isotopic compositions to pristine samples, suggesting that leaching of Ni from olivine does not drive fractionation or govern the pattern of isotopic compositions in weathering profiles by itself (Spivak-Birndorf et al., 2018) or that the olivine leaching method used was not comparable to the natural weathering processes.

Tropical weathering products are generally variable in Ni isotopic composition. Laterites produced from extreme chemical weathering of ultramafic rocks are mostly heavy relative to SRM986 (Gall, 2011; Spivak-Birndorf et al., 2018). In contrast, Brazilian laterite ores investigated by Ratié and co-workers (2016, 2015) range from -0.12 to 0.90‰. Saprolite, a more highly weathered rock than laterite, has been found to have heavy and light Ni isotopic compositions ranging from -0.61 to 0.30‰ (Gall et al., 2013; Ratié et al., 2015). Other soils are also variable, ranging from -0.30 to 0.72 (Estrade et al., 2015; Ratié et al., 2016, 2015).

Sulfide minerals have been found to be mostly light in Ni isotopic compositions (Gall, 2011; Gueguen et al., 2013; Hofmann et al., 2014), which has been shown to affect bulk host rock composition in komatiites with disseminated sulfide mineralisation (Gall, 2011; Gueguen et al., 2013). There are three heavy exceptions: two samples from Sudbury, which may have a meteoritic component (Gall, 2011; Gall et al., 2017, 2013, 2012), and millerite (Tanimizu and Hirata, 2006), which may indicate the specific sulfide phases can be characterised by very different Ni isotopic compositions (range -1.05 to 0.76‰).

Three $\delta^{60/58}Ni_{SRM986}$ estimates have been published for the bulk silicate Earth (BSE). The first estimate ($\delta^{60/58}Ni_{SRM986}$=0.18±0.04‰) by (Steele et al., 2011), weighted average of analyses of 3

ultramafic standards (PCC1 (Cameron et al., 2009) as well as JP1 and DTS2 from (Steele et al., 2011)). This estimate was followed by Gueguen et al. (2013) with a much lighter estimate of 0.05±0.05‰. The latter estimate used igneous and ultramafic reference materials as well as fresh and altered basalts from Loihi, and clay and basalt samples from IODP core 114. These samples were removed from a new average published by Elliott and Steele (2017) to produce a revised very precise BSE estimate including only samples of mantle and mantle derived melts, of $\delta^{60/58}Ni_{SRM986}$=0.11±0.01‰. The most comprehensive estimate prior to this study, 0.23±0.06‰ (Gall et al., 2017), was based on fertile peridotite xenoliths and Phanerozoic komatiites.

Partial melts of the mantle have very limited published data to date. Komatiites have been found to have variable $\delta^{60/58}Ni_{SRM986}$ apparently depending on the presence of associated sulfide. Archean komatiites with disseminated sulfide mineralisation exhibit a large range in Ni isotopic compositions all significantly lighter than the estimates for BSE (Gall, 2011; Gueguen et al., 2013). Gall and co-workers (Gall et al., 2017) also analysed 5 Phanerozoic komatiites from Gorgona and found them to be in agreement with the BSE estimate in the same work. A picrite sample analysed by Gall (2011) also had a similar composition to the terrestrial mantle. Mid-ocean ridge basalts have generally been lighter than BSE estimates (Cameron et al., 2009; Gall, 2011; Gueguen et al., 2013). Analysis of intrusive igneous rocks has been limited to 5 granite samples, which ranged in Ni isotopic composition from 0.12 to 0.24‰ (Gall, 2011).

The only published study looking directly at the terrestrial mantle was by Gall and co-workers (2017). These authors analysed stable Ni isotopic compositions for 7 ultramafic xenoliths, 6 from Tanzania and 1 from South Africa, 3 ultramafic rock standards, 7 mineral phases from 3 xenoliths, and 2 megacrysts. The xenoliths and komatiites previously mentioned, formed the basis of an estimate of the BSE.

Theoretical and experimental studies of Ni isotopes have been used to investigate particular processes that are difficult to separate from other effects in natural environments, including sorption to ferrihydrite (Wasylenki et al., 2015), and fractionation between sulfide minerals (Liu

et al., 2018); or to investigate a reservoir of Ni that cannot be sampled e.g. Archaean seawater (Wang and Wasylenki, 2017).

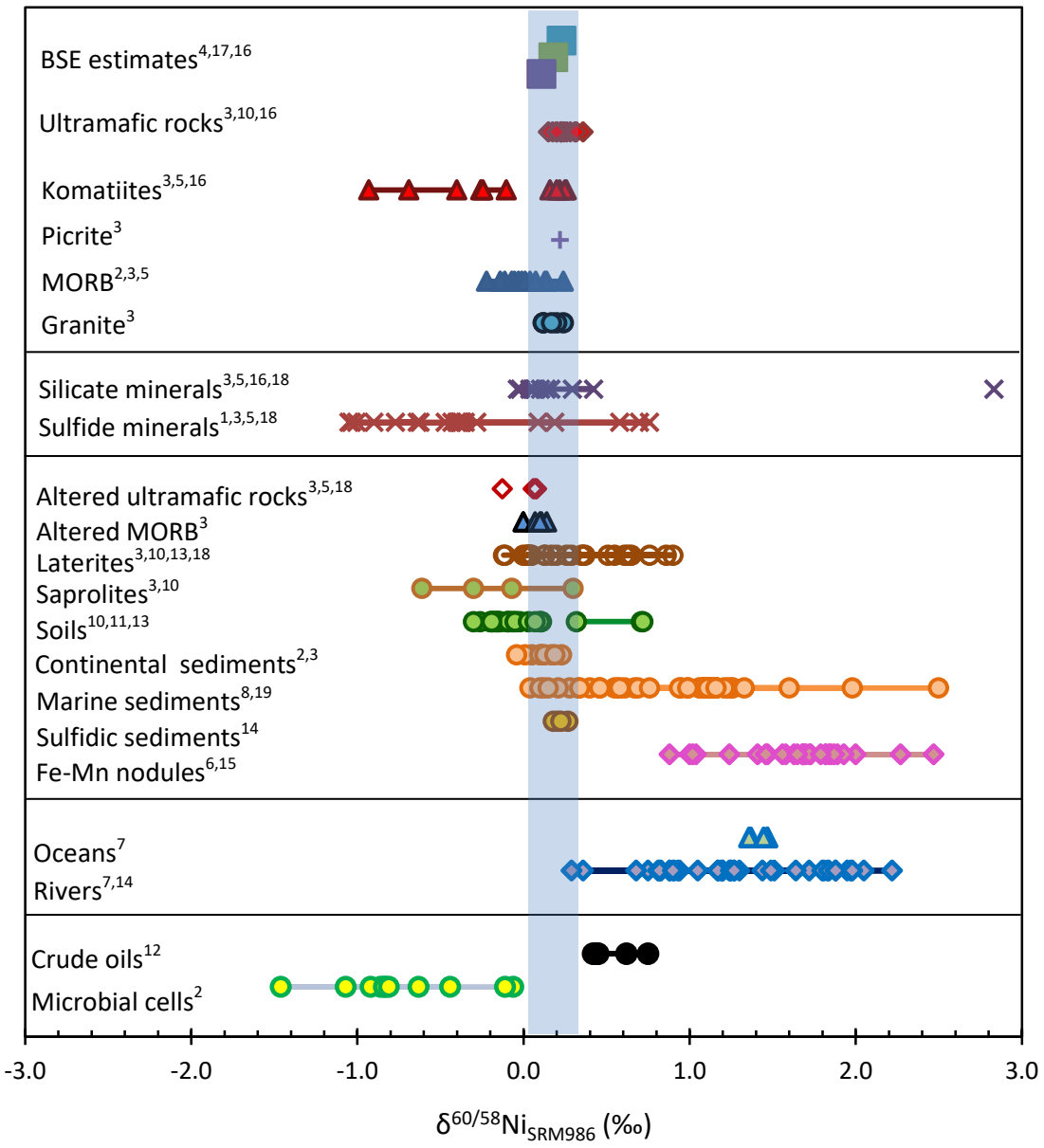

Figure 1

Published $\delta^{60/58}Ni_{SRM986}$ data for terrestrial samples. BSE estimates for comparison, from (Gall et al., 2017; Steele et al., 2011) and with the estimate of Gueguen and co-workers (2013) recalculated by (Elliott and Steele, 2017) to remove sediments.
[1](Tanimizu and Hirata, 2006); [2](Cameron et al., 2009); [3](Gall, 2011); [4](Steele et al., 2011); [5](Gueguen et al., 2013); [6](Gall et al., 2013); [7](Cameron and Vance, 2014); [8](Porter et al., 2014); [9](Hofmann et al., 2014); [10](Ratié et al., 2015); [11](Estrade et al., 2015); [12](Ventura et al., 2015); [13](Ratié et al., 2016); [14](Vance et al., 2016); [15](Gueguen et al., 2016); [16](Gall et al., 2017); [17](Elliott and Steele, 2017); [18](Spivak-Birndorf et al., 2018); [19](Ciscato et al., 2018)

Meteoritic samples have been analysed for stable Ni isotopic composition in several studies. Nickel isotopic compositions of metal from six chondrites analysed by Cook and co-workers

(2007) vary from $\delta^{60/58}Ni_{SRM986}$=0.05 to 0.44‰, recalculated from $\delta^{61/58}Ni$, $\delta^{62/58}Ni$, and $\delta^{64/58}Ni$. Three ordinary chondrites were analysed for Ni isotopic composition by Chernonozhkin and co-workers (2016), and vary from 0.15‰ to 0.24‰. Chernonozhkin and co-workers (2016) also showed that the isotopic composition of fusion crusts of these meteorites was within error of the bulk sample. The metal fraction of mesosiderites was found to be heavier in Ni isotopic composition than the silicate fraction (Chernonozhkin et al., 2016). The reverse was found to be true for pallasite samples, which showed that Ni isotopic compositions of metal were lighter than associated olivine (Chernonozhkin et al., 2016). This result argued against pallasites being formed from the IIIAB iron meteorite parent body, which has heavier Ni stable isotope signatures, as reported by (Chernonozhkin et al., 2016; Cook et al., 2007), and cannot be explained by fractional crystallization of the same body. Chernonozhkin and co-workers (2017) reported in-situ analyses of $\delta^{62/60}Ni_{SRM986}$, and observed that Ni in taenite is isotopically lighter than in kamacite.

Recent papers have extensively studied Ni isotopic compositions of presolar grains (Kodolányi et al., 2018; Trappitsch et al., 2018). Compositions show huge heterogeneity, ranging from $\delta^{60/58}Ni_{SRM986}$=-111±90‰ to 1613±6814‰, with some errors over an order of magnitude larger than the fractionation measured (e.g. $\delta^{60/58}Ni_{SRM986}$=1±54‰).

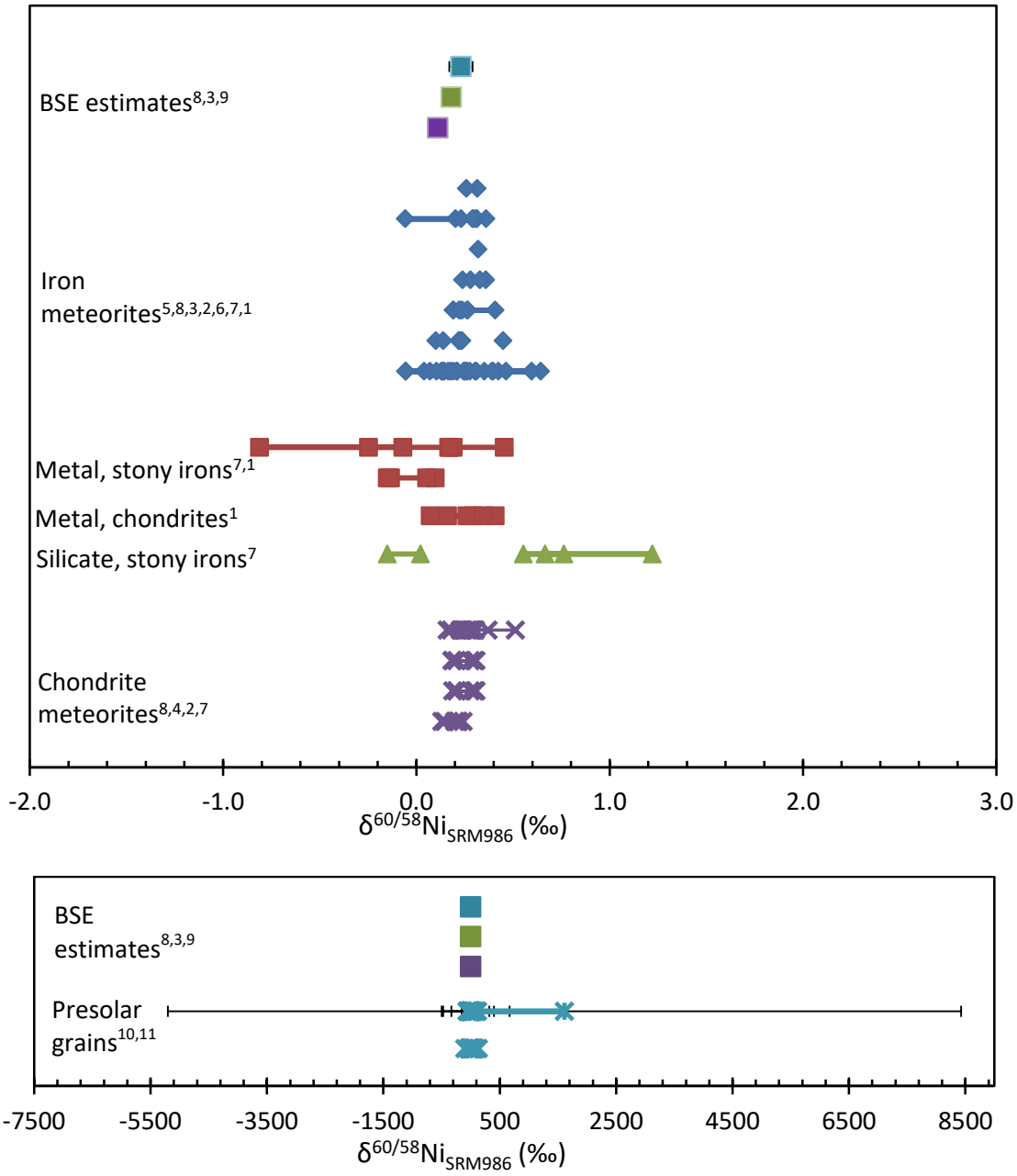

Figure 2

Published $\delta^{60/58}Ni_{SRM986}$ data for extra-terrestrial samples. Top (meteoritic material) and bottom (presolar grains); NB presented with different x-axis scales. BSE estimates for comparison, from (Gall et al., 2017; Steele et al., 2011) and with the estimate of Gueguen and co-workers (2013) recalculated by (Elliott and Steele, 2017) to remove sediments.

[1](Cook et al., 2007); [2](Cameron et al., 2009); [3](Steele et al., 2011); [4](Steele et al., 2012), [5](Gueguen et al., 2013); [6](Chernonozhkin et al., 2015); [7](Chernonozhkin et al., 2016); [8](Gall et al., 2017); [9](Elliott and Steele, 2017); [10](Kodolányi et al., 2018); [11](Trappitsch et al., 2018)

1.3. Motivation for this study

1.3.1. Terrestrial

As highlighted above, limited data have been published for Ni stable isotopes in ultramafic samples excluding industrially processed reference materials. Initial work by Gall (2011) showed some heterogeneity in MORB, which suggested heterogeneity in the mantle in Ni isotopes, or a fractionation process occurring during partial melting of the mantle. A mineralogical control on Ni isotope heterogeneity in the mantle was postulated (Gall et al., 2017). Gall (2011) considered it unlikely, given the dominance of mantle Ni over that in the crust, that any signature of recycling of crustal material into the mantle at subduction zones would be resolvable, but this has not yet been investigated.

This study establishes a more representative dataset for the mantle. Samples were targeted from a range of high temperature environments including more samples of fertile peridotites, depleted dunites and enriched pyroxenites. This study also investigated metasomatised mantle samples. This study also includes an in depth study of mafic samples produced from normal partial melting regimes, such as those that produce alkali basalts and tholeiites, as well as small degree partial melts, such as nephelinites, that have not been investigated beyond a few analyses of MORB (Cameron et al., 2009; Gall, 2011; Gueguen et al., 2013). No OIB samples have been analysed prior to this work outside of reference materials.

1.3.2. Lunar

Isotopically the Moon has been shown to be extremely similar to the Earth, however no Ni isotopic compositions have been so far published. The vast majority of elements that have so far been measured show no resolvable difference between the Moon and Earth (examples: O (Wiechert et al., 2001), Si (Armytage et al., 2012), Sr (Moynier et al., 2010), Ca (Simon and DePaolo, 2010), Cu (Moynier et al., 2006), Fe (Wang et al., 2015), Mg (Sedaghatpour et al., 2013) etc.). Some evidence for differences between the isotopic composition of the Earth and Moon has been found in Zn (e.g Paniello et al., 2012)

Nickel, as a non-volatile element, is expected to show a lunar isotopic composition identical to the silicate Earth. Nickel concentrations are depleted in the lunar mantle relative to CI chondrites (Rai and Westrenen, 2014), and the Moon has much lower basalt [Ni] compared with terrestrial basalts. Volcanic glass from the Moon has a higher Ni concentration than the mare basalts, which has been suggested to imply low-pressure fractionation of trace elements during emplacement of the mare basalts (Delano, 1985). Without ultramafic lunar xenoliths, the Moon's mantle geochemistry is estimated from the trace element data of lunar basalt samples that are likely to be partial melts of the lunar mantle (Rai and Westrenen, 2014). Nickel isotopic compositions may be able to provide information on the mantle source regions of the basalts sampled.

The formation of the small lunar core may have fractionated Ni isotopes, although there is no evidence for this having occurred during the formation of the terrestrial core (Gall et al., 2017; Steele et al., 2011).

Analysis of Ni isotopic compositions of lunar samples could provide further evidence for the formation mechanism for the Moon and the development of the layered solid body we have today. Nickel concentration has shown initial difference between lunar Ni and terrestrial, which investigation of isotopes may further elucidate.

1.4. References

Aigner-Torres, M., Blundy, J., Ulmer, P., Pettke, T., 2007. Laser Ablation ICPMS study of trace element partitioning between plagioclase and basaltic melts: an experimental approach. Contrib Miner. Pet. 153, 647–667. https://doi.org/10.1007/s00410-006-0168-2

Arai, T., Maruyama, S., 2017. Formation of anorthosite on the Moon through magma ocean fractional crystallization. Geosci. Front. 8, 299–308. https://doi.org/10.1016/j.gsf.2016.11.007

Armytage, R.M.G., Georg, R.B., Williams, H.M., Halliday, A.N., 2012. Silicon isotopes in lunar rocks : Implications for the Moon's formation and the early history of the Earth. Geochim. Cosmochim. Acta 77, 504–514. https://doi.org/10.1016/j.gca.2011.10.032

Aulbach, S., Rudnick, R.L., McDonough, W.F., 2008. Li-Sr-Nd isotope signatures of the plume and cratonic lithospheric mantle beneath the margin of the rifted Tanzanian craton (Labait). Contrib. to Mineral. Petrol. 155, 79–92. https://doi.org/10.1007/s00410-007-0226-4

Becker, J.S., 2007. Inorganic mass spectrometry : principles and applications. John Wiley & Sons.

Bédard, J.H., 2005. Trace element partitioning in plagioclase feldspar. Geochim. Cosmochim. Acta 70, 3717–3742. https://doi.org/10.1016/j.gca.2006.05.003

Bindeman, I.N., Davis, A.M., 2000. Trace element partitioning between plagioclase and melt: Investigation of dopant influence on partition behavior.

Birck, J.L., Lugmair, G.W., 1988. Nickel and chromium isotopes in Allende inclusions. Earth Planet. Sci. Lett. 90, 131–143. https://doi.org/10.1016/0012-821X(88)90096-9

Bizzarro, M., Ulfbeck, D., Thrane, K., 2006. Nickel isotopes in meteorites: evidence for live 60Fe and distinct 62Ni isotope reservoirs in the early solar system. Lunar Planet. Sci. XXXVII 37.

Bizzarro, M., Ulfbeck, D., Trinquier, A., Thrane, K., Connelly, J.N., Meyer, B.S., 2007. Evidence for a late supernova injection of 60Fe into the protoplanetary disk. Science 316, 1178–81. https://doi.org/10.1126/science.1141040

Bourdon, B., Langmuir, C.H., Zindler, A., 1996. Ridge-hotspot interaction along the Mid-Atlantic Ridge between 37'30' and 40'30'N: the U-Th disequilibrium evidence, Earth and Planetary Science Letters.

Bouvier, A., Vervoort, J.D., Patchett, P.J., 2008. The Lu-Hf and Sm-Nd isotopic composition of CHUR: Constraints from unequilibrated chondrites and implications for the bulk composition of terrestrial planets. Earth Planet. Sci. Lett. 273, 48–57. https://doi.org/10.1016/j.epsl.2008.06.010

Burton, K.W., Schiano, P., Birck, J.-L., Allègre, C.J., Rehkämper, M., Halliday, A.N., Dawson, J.B., 2000. The distribution and behaviour of rhenium and osmium amongst mantle minerals and the age of the lithospheric mantle beneath Tanzania. Earth Planet. Sci. Lett. 183, 93–106. https://doi.org/10.1016/S0012-821X(00)00259-4

Bussod, G.Y.A., Williams, D.R., 1991. Thermal and kinematic model of the southern Rio Grande rift: inferences from crustal and mantle xenoliths from Kilboume Hole, New Mexico. Tectonophysics 197, 373–389.

Cameron, V., Vance, D., 2014. Heavy nickel isotope compositions in rivers and the oceans. Geochim. Cosmochim. Acta 128, 195–211. https://doi.org/10.1016/j.gca.2013.12.007

Cameron, V., Vance, D., Archer, C., House, C.H., 2009. A biomarker based on the stable isotopes of nickel. Proc. Natl. Acad. Sci. U. S. A. 106, 10944–10948.

https://doi.org/10.1073/pnas.0900726106

Canil, D., Pearson RL Rudnick, N.D., McDonough Carswell, W. DA, 1994. Ferric iron in peridotites and mantle oxidation states. Earth Planet. Sci. Lett. 123, 205–220.

Canup, R.M., 2012. Forming a Moon with an Earth-like Composition via a Giant Impact. Science 338, 1052–1055. https://doi.org/10.1126/science.1106818

Canup, R.M., Asphaug, E., 2001. Origin of the Moon in a giant impact near the end of the Earth's formation. Nature 412, 708–712. https://doi.org/10.1038/35089010

Canup, R.M., Barr, A.C., Crawford, D.A., 2013. Lunar-forming impacts: High-resolution SPH and AMR-CTH simulations. Icarus 222, 200–219. https://doi.org/10.1016/J.ICARUS.2012.10.011

Capobianco, C.J., Amelin, A.A., 1994. Metal-silicate partitioning of nickel and cobalt: The influence of temperature and oxygen fugacity. Geochim. Cosmochim. Acta 58, 125–140.

Chako Tchamabé, B., Youmen, D., Owona, S., Ohba, T., Németh, K., Nsangou Ngapna, M., E Asaah, A.N., Aka, F.T., Tanyileke, G., Hell, J. V, 2013. Eruptive history of the Barombi Mbo Maar, Cameroon Volcanic Line, Central Africa: Constraints from volcanic facies analysis. Cent. Eur. J. Geosci 5, 480–496. https://doi.org/10.2478/s13533-012-0147-2

Chen, J.H., Papanastassiou, D.A., 2006. NICKEL ISOTOPE INVESTIGATION BY MC-ICP-MS AND PTIMS, in: Lunar and Planetary Science XXXVII. pp. 61–62.

Chen, J.H., Papanastassiou, D.A., Wasserburg, G.J., 2009. A search for nickel isotopic anomalies in iron meteorites and chondrites. Geochim. Cosmochim. Acta 73, 1461–1471. https://doi.org/10.1016/j.gca.2008.11.040

Chernonozhkin, S.M., Goderis, S., Costas-Rodríguez, M., Claeys, P., Vanhaecke, F., 2016. Effect of parent body evolution on equilibrium and kinetic isotope fractionation: a combined Ni and Fe isotope study of iron and stony-iron meteorites. Geochim. Cosmochim. Acta 186, 168–188. https://doi.org/10.1016/j.gca.2016.04.050

Chernonozhkin, S.M., Goderis, S., Lobo, L., Claeys, P., Vanhaecke, F., 2015. Development of an isolation procedure and MC-ICP-MS measurement protocol for the study of stable isotope ratio variations of nickel. J. Anal. At. Spectrom. 30, 1518–1530. https://doi.org/10.1039/C5JA00080G

Chernonozhkin, S.M., Weyrauch, M., Goderis, S., Oeser, M., McKibbin, S.J., Horn, I., Hecht, L., Weyer, S., Claeys, P., Vanhaecke, F., 2017. Thermal equilibration of iron meteorite and pallasite parent bodies recorded at the mineral scale by Fe and Ni isotope systematics. Geochim. Cosmochim. Acta 217, 95–111. https://doi.org/10.1016/J.GCA.2017.08.022

Ciscato, E.R., Bontognali, T.R.R., Vance, D., 2018. Nickel and its isotopes in organic-rich sediments: implications for oceanic budgets and a potential record of ancient seawater. Earth Planet. Sci. Lett. 494, 239–250. https://doi.org/10.1016/j.epsl.2018.04.061

Cisowski, S.M., Collinson, D.W., Runcorn, S.K., Stephenson, A., Fuller, M., 1983. A REVIEW OF LUNAR PALEOINTENSITY DATA AND IMPLICATIONS FOR THE ORIGIN OF LUNAR MAGNETISM. J. Geophys. Res. 88, A691–A704.

Cook, D.L., Clayton, R.N., Wadhwa, M., Janney, P.E., Davis, A.M., 2008a. Nickel isotopic anomalies in troilite from iron meteorites. Geophys. Res. Lett. 35, 1–5. https://doi.org/10.1029/2007GL032431

Cook, D.L., Clayton, R.N., Wadhwa, M., Janney, P.E., Davis, A.M., 2008b. Nickel isotopic anomalies in troilite from iron meteorites. Geophys. Res. Lett. 35, L01203. https://doi.org/10.1029/2007GL032431

Cook, D.L., Wadhwa, M., Clayton, R.N., Dauphas, N., Janney, P.E., Davis, A.M., 2007. Mass-dependent fractionation of nickel isotopes in meteoritic metal. Meteorit. Planet. Sci. 42,

2067–2077. https://doi.org/10.1111/j.1945-5100.2007.tb01008.x

Cook, D.L., Wadhwa, M., Janney, P.E., Dauphas, N., Clayton, R.N., Davis, A.M., 2006. High precision measurements of non-mass-dependent effects in nickel isotopes in meteoritic metal via multicollector ICPMS. Anal. Chem. 78, 8477–84. https://doi.org/10.1021/ac061285m

Cornen, G., Bandet, Y., Giresse, P., Maley, J., 1992. The nature and chronostratigraphy of Quaternary pyroclastic accumulations from Lake Barombi Mbo (West-Cameroon). J. Volcanol. Geotherm. Res. 51, 357–374.

Dauphas, N., Teng, F.-Z., Arndt, N.T., 2010. Magnesium and iron isotopes in 2.7 Ga Alexo komatiites: Mantle signatures, no evidence for Soret diffusion, and identification of diffusive transport in zoned olivine. Geochim. Cosmochim. Acta 74, 3274–3291. https://doi.org/10.1016/J.GCA.2010.02.031

Dauritria, J.M., Girod, M., 1987. Cenozoaic Volcanism associated with Swells and Rifts, in: Nixon, P.. (Ed.), Mantle Xenoliths. pp. 195–215.

Dawson, J.B., 2012. Nephelinite-melilitite-carbonatite relationships: Evidence from Pleistocene-recent volcanism in northern Tanzania. Lithos 152, 3–10. https://doi.org/10.1016/j.lithos.2012.01.008

Dawson, J.B., 2002. Metasomatism and Partial Melting in Upper-Mantle Peridotite Xenoliths from the Lashaine Volcano, Northern Tanzania. J. Petrol. 43, 1749–1777. https://doi.org/10.1093/petrology/43.9.1749

Dawson, J.B., 1992. Neogene tectonics and volcanicity in the North Tanzania sector of the Gregory Rift Valley: contrasts with the Kenya sector. Tectonophysics 204, 81–92. https://doi.org/10.1016/0040-1951(92)90271-7

Dawson, J.B., 1964a. Carbonate Tuff Cones in Northern Tanganyika. Geol. Mag. 101, 129. https://doi.org/10.1017/S0016756800048561

Dawson, J.B., 1964b. Carbonatitic volcanic ashes in Northern Tanganyika. Bull. Volcanol. 27, 81–91. https://doi.org/10.1007/BF02597513

Dawson, J.B., Powell, D.G., Reid, A.M., 1970. Ultrabasic Xenoliths and Lava from the Lashaine Volcano, Northern Tanzania. J. Petrol. 11, 519–548. https://doi.org/10.1093/petrology/11.3.519

Day, J.M.D., Pearson, D.G., Macpherson, C.G., Lowry, D., Carracedo, J.-C., 2009. Pyroxenite-rich mantle formed by recycled oceanic lithosphere: Oxygen-osmium isotope evidence from Canary Island lavas. Geology 37, 555–558. https://doi.org/10.1130/G25613A.1

Delano, J.W., 1985. Mare Volcanic Glasses, II: Abundances of Trace Ni and the Composition of the Moon.

Dingwell, D.B., O'Neill, H.S.C., Ertel, W., Spettel, B., 1994. The solubility and oxidation state of nickel in silicate melt at low oxygen fugacities: Results using a mechanically assisted equilibration technique. Geochim. Cosmochim. Acta 58, 1967–1974. https://doi.org/10.1016/0016-7037(94)90428-6

Dosso, L., Bougault, H., Langmuir, C., Bollinger, C., Bonnier, O., Etoubleau, J., 1999. The age and distribution of mantle heterogeneity along the Mid-Atlantic ridge (31-41°N). Earth Planet. Sci. Lett. 170, 269–286. https://doi.org/10.1016/S0012-821X(99)00109-0

Dziewonski, A.M., Anderson, D.L., 1981. Preliminary reference Earth model. Phys. Earth Planet. Inter. 25, 297–356. https://doi.org/10.1016/0031-9201(81)90046-7

Eberhardt, P., Geiss, J., Graf, H., Grögler, N., Krähenbühl, U., Schwaller, H., Schwarzmüller, J., Stettler, A., 1970. Correlation between rock type and irradiation history of Apollo 11 igneous rocks. Earth Planet. Sci. Lett. 10, 67–72. https://doi.org/10.1016/0012-

821X(70)90065-8

Ehlers, K., Grove, T.L., Sisson, T.W., Recca, S.I., Zervas, D.A., 1992. The effect of oxygen fugacity on the partitioning of nickel and cobalt between olivine, silicate melt, and metal. Geochim. Cosmochim. Acta 56, 3733–3743. https://doi.org/10.1016/0016-7037(92)90166-G

El Goresy, A., Ramdohr, P., Taylor, L.A., 1971. The opaque minerals in the lunar rocks from Oceanus Procellarum, in: 2ns Lunar Science Conference. The M.I.T. Press, pp. 219–235.

Elliott, T., Steele, R.C.J., 2017. The Isotope Geochemistry of Ni, in: Reviews in Mineralogy and Geochemistry.

Estrade, N., Cloquet, C., Echevarria, G., Sterckeman, T., Deng, T., Tang, Y., Morel, J.-L., 2015. Weathering and vegetation controls on nickel isotope fractionation in surface ultramafic environments (Albania). Earth Planet. Sci. Lett. 423, 24–35. https://doi.org/10.1016/j.epsl.2015.04.018

Faure, G., Mensing, T.M., Faure, G., 2005. Isotopes : principles and applications. Wiley.

Feigenson, M.D., 1986. Continental alkali basalts as mixtures of kimberlite and depleted mantle: Evidence from Kilbourne Hole Maar, New Mexico. Geophys. Res. Lett. 13, 965–968. https://doi.org/10.1029/GL013i009p00965

Finnerty, A.A., Boyd, F.R., 1987. Thermobarometry for Garnet Peridotites, in: Nixon, P.H. (Ed.), Mantle Xenoltihs. Wiley, pp. 381–402.

Fischer, R.A., Nakajima, Y., Campbell, A.J., Frost, D.J., Harries, D., Langenhorst, F., Miyajima, N., Pollok, K., Rubie, D.C., 2015. High pressure metal-silicate partitioning of Ni, Co, V, Cr, Si, and O. Geochim. Cosmochim. Acta 167, 177–194. https://doi.org/10.1016/j.gca.2015.06.026

Fitton, J.G., 2007. The OIB Paradox, in: Foulger, G.R., Jurdy, D.M. (Eds.), Plates, Plumes, and Planetary Processes. The Geological Society of America, pp. 387–409.

Fitton, J.G., 1987. The Cameroon line, West Africa: a comparison between oceanic and continental alkaline volcanism. Geol. Soc. London, Spec. Publ. 30, 273–291. https://doi.org/10.1144/GSL.SP.1987.030.01.13

Fitton, J.G., Dunlop, H.M., 1985. The Cameroon line, West Africa, and its bearing on the origin of oceanic and continental alkali basalt. Earth Planet. Sci. Lett. 72, 23–38. https://doi.org/10.1016/0012-821X(85)90114-1

Fitton, J.G., Saunders, A.D., Kempton, P.D., Hardarson, B.S., 2003. Does depleted mantle form an intrinsic part of the Iceland plume? Geochemistry, Geophys. Geosystems 4. https://doi.org/10.1029/2002GC000424

Freeth, S.J., 1979. Deformation of the African plate as a consequence of membrane stress domains generated by post-Jurassic drift. Earth Planet. Sci. Lett. 45, 93–104. https://doi.org/10.1016/0012-821X(79)90111-0

Frost, D.J., Liebske, C., Langenhorst, F., McCammon, C.A., Trønnes, R.G., Rubie, D.C., 2004. Experimental evidence for the existence of iron-rich metal in the Earth's lower mantle. Nature 428, 409–412. https://doi.org/10.1038/nature02413

Gale, A., Dalton, C.A., Langmuir, C.H., Su, Y., Schilling, J.-G., 2013. The mean composition of ocean ridge basalts. Geochemistry, Geophys. Geosystems 14, 489–518. https://doi.org/10.1029/2012GC004334

Gall, L., 2011. Development and Application of Nickel Stable Isotopes as a New Geochemical Tracer. University Of Oxford.

Gall, L., Williams, H., Siebert, C., Halliday, A.N., 2012. Determination of mass-dependent variations in nickel isotope compositions using double spiking and MC-ICPMS. J. Anal.

At. Spectrom. 27, 137. https://doi.org/10.1039/c1ja10209e

Gall, L., Williams, H.M., Halliday, A.N., Kerr, A.C., 2017. Nickel isotopic composition of the mantle. Geochim. Cosmochim. Acta 199, 196–209. https://doi.org/10.1016/j.gca.2016.11.016

Gall, L., Williams, H.M., Siebert, C., Halliday, A.N., Herrington, R.J., Hein, J.R., 2013. Nickel isotopic compositions of ferromanganese crusts and the constancy of deep ocean inputs and continental weathering effects over the Cenozoic. Earth Planet. Sci. Lett. 375, 148–155. https://doi.org/10.1016/j.epsl.2013.05.019

Garcia, R.F., Gagnepain-Beyneix, J., Chevrot, S., Lognonné, P., 2011. Very preliminary reference Moon model. Phys. Earth Planet. Inter. 188, 96–113. https://doi.org/10.1016/J.PEPI.2011.06.015

Gessmann, C.K., Rubie, D.C., 2000. The origin of the depletions of V, Cr and Mn in the mantles of the Earth and Moon. Earth Planet. Sci. Lett. 184, 95–107. https://doi.org/10.1016/S0012-821X(00)00323-X

Gibson, S.A., McMahon, S.C., Day, J.A., Dawson, J.B., 2013. Highly Refractory Lithospheric Mantle beneath the Tanzanian Craton: Evidence from Lashaine Pre-metasomatic Garnet-bearing Peridotites. J. Petrol. 54, 1503–1546. https://doi.org/10.1093/petrology/egt020

Gramlich, J.W., Machlan, L.A., Barnes, I.L., Paulsen, P.J., 1989. Absolute isotopic abundance ratios and atomic weight of a reference sample of nickel. J. Res. Natl. Inst. Stand. Technol. 94, 347. https://doi.org/10.6028/jres.094.034

Guan, Y., Huss, G.R., Leshin, L.A., 2004. SIMS analyses of Mg, Cr, and Ni isotopes in primitive meteorites and short-lived radionuclides in the early solar system. Appl. Surf. Sci. 231–232, 899–902. https://doi.org/10.1016/j.apsusc.2004.03.163

Gueguen, B., Rouxel, O., Ponzevera, E., Bekker, A., Fouquet, Y., 2013. Nickel Isotope Variations in Terrestrial Silicate Rocks and Geological Reference Materials Measured by MC-ICP-MS. Geostand. Geoanalytical Res. 37, 297–317. https://doi.org/10.1111/j.1751-908X.2013.00209.x

Gueguen, B., Rouxel, O., Rouget, M.-L., Bollinger, C., Ponzevera, E., Germain, Y., Fouquet, Y., 2016. Comparative geochemistry of four ferromanganese crusts from the Pacific Ocean and significance for the use of Ni isotopes as paleoceanographic tracers. Geochim. Cosmochim. Acta 189, 214–235. https://doi.org/10.1016/J.GCA.2016.06.005

Gueguen, B., Sorensen, J. V., Lalonde, S. V., Peña, J., Toner, B.M., Rouxel, O., 2018. Variable Ni isotope fractionation between Fe-oxyhydroxides and implications for the use of Ni isotopes as geochemical tracers. Chem. Geol. 481, 38–52. https://doi.org/10.1016/J.CHEMGEO.2018.01.023

Haase, K.M., Regelous, M., Duncan, R.A., Brandl, P.A., Stroncik, N., Grevemeyer, I., 2011. Insights into mantle composition and mantle melting beneath mid-ocean ridges from postspreading volcanism on the fossil Galapagos Rise Theme: Geochemical Heterogeneities in Oceanic Island Basalt and Mid-ocean Ridge Basalt Sources: Implications for Melting. Geochem. Geophys. Geosyst 12. https://doi.org/10.1029/2010GC003482

Haase, K.M., Regelous, M., Duncan, R.A., Brandl, P.A., Stroncik, N., Grevemeyer, I., 2011. Insights into mantle composition and mantle melting beneath mid-ocean ridges from postspreading volcanism on the fossil Galapagos Rise. Geochemistry, Geophys. Geosystems 12, 1–21. https://doi.org/10.1029/2010GC003482

Halliday, A.N., 2000. Terrestrial accretion rates and the origin of the Moon. Earth Planet. Sci. Lett. 176, 17–30. https://doi.org/10.1016/S0012-821X(99)00317-9

Halliday, A.N., Davidson, J.P., Holden, P., DeWolf, C., Lee, D.-C., Fitton, J.G., 1990. Trace-

element fractionation in plumes and the origin of HIMU mantle beneather the Cameroon line. Nature 346, 523–528. https://doi.org/10.1038/346183a0

Halliday, A.N., Davies, G.R., Lee, D.-C., Tommasini, S., Paslick, C.R., Fitton, J.G., James, D.E., 1992a. Lead isotope evidence for young trace element enrichment in the oceanic upper mantle. Nature 359, 623–627. https://doi.org/10.1038/359623a0

Halliday, A.N., Davies, G.R., Lee, D.-C., Tommasini, S., Paslick, C.R., Fitton, J.G., James, D.E., 1992b. Lead isotope evidence for young trace element enrichment in the oceanic upper mantle. Nature 359, 623–627. https://doi.org/10.1038/359623a0

Halliday, A.N., Davies, G.R., Lee, D.C., 1992. Lead isotope evidence for young trace-element enrichment in the oceanic upper mantle. Nature 359, 623–627.

Halliday, A.N., Dickin, A.P., Fallick, A.E., Fitton, J.G., 1988. Mantle dynamics: A Nd, Sr, Pb and O isotopic study of the Cameroon line volcanic chain. J. Petrol. 29, 181–211. https://doi.org/10.1093/petrology/29.1.181

Halliday, A.N., Lee, D.-C., Christensen, J.N., Rehkämper, M., Yi, W., Luo, X., Hall, C.M., Ballentine, C.J., Pettke, T., Stirling, C., 1998. Applications of Multiple Collector-ICPMS to Cosmochemistry, Geochemistry, and Paleoceanography. Geochim. Cosmochim. Acta 62, 919–940. https://doi.org/10.1016/S0016-7037(98)00057-X

Halliday, A.N., Lee, D.-C., Tommasini, S., Davies, G.R., Paslick, C.R., Godfrey Fitton, J., James, D.E., 1995. Incompatible trace elements in OIB and MORB and source enrichment in the sub-oceanic mantle. Earth Planet. Sci. Lett. 133, 379–395. https://doi.org/10.1016/0012-821X(95)00097-V

Hardarson, B.S., Fitton, J.G., 1997. Mechanisms of crustal accretion in Iceland. Geology 25, 1043–1046.

Harpp, K.S., White, W.M., 2001a. Tracing a mantle plume: Isotopic and trace element variations of Galápagos seamounts. Geochemistry, Geophys. Geosystems 2, n/a-n/a. https://doi.org/10.1029/2000GC000137

Harpp, K.S., White, W.M., 2001b. Tracing a mantle plume: Isotopic and trace element variations of Galápagos seamounts. Geochemistry, Geophys. Geosystems 2, n/a-n/a. https://doi.org/10.1029/2000GC000137

Hart, S.R., 1988. Heterogeneous mantle domains: signatures, genesis and mixing chronologies. Earth Planet. Sci. Lett. 90, 273–296. https://doi.org/10.1016/0012-821X(88)90131-8

Hart, S.R., Davis, K.E., 1978. Nickel partitioning between olivine and silicate melt. Earth Planet. Sci. Lett. 40, 203–219.

Hartmann, W.K., Davis, D.R., 1975. Satellite-Sized Planetesimals and Lunar Origin, ICARUS.

Harvey, J., Dale, C.W., Gannoun, A., Burton, K.W., 2011. Osmium mass balance in peridotite and the effects of mantle-derived sulfides on basalt petrogenesis. Geochim. Cosmochim. Acta 75, 5574–5596. https://doi.org/10.1016/j.gca.2011.07.001

Harvey, J., Konig, S., Luguet, A., 2015. The effects of melt depletion and metasomatism on highly siderophile and strongly chalcophile elements: S-Se-Te-Re-PGE systematics of peridotite xenoliths from Kilbourne Hole, New Mexico. Geochim. Cosmochim. Acta 166, 210–233. https://doi.org/10.1016/j.gca.2015.06.028

Harvey, J., Yoshikawa, M., Hammond, S.J., Burton, K.W., 2012. Deciphering the trace element characteristics in kilbourne hole peridotite xenoliths: Melt-rock interaction and metasomatism beneath the Rio Grande Rift, SW USA. J. Petrol. 53, 1709–1742. https://doi.org/10.1093/petrology/egs030

Hauri, E.H., 1996. Major-element variability in the Hawaiian mantle plume. Nature 382, 415–419. https://doi.org/10.1038/382415a0

Henderson, P., Henderson, G., 2009. The Cambridge Handbook of Earth Science Data. Cambridge University Press.

Herzberg, C., Vidito, C., Starkey, N.A., 2016. Nickel–cobalt contents of olivine record origins of mantle peridotite and related rocks. Am. Mineral. 101, 1952–1966. https://doi.org/10.2138/am-2016-5538

Hiesinger, H., Head III, J.W., 2006. New Views of Lunar Geoscience: An Introduction and Overview, in: Reviews in Mineralogy & Geochemistry Volume 60: New Views of the Moon. pp. 1–67.

Hofmann, A., Bekker, A., Dirks, P., Gueguen, B., Rumble, D., Rouxel, O.J., 2014. Comparing orthomagmatic and hydrothermal mineralization models for komatiite-hosted nickel deposits in Zimbabwe using multiple-sulfur, iron, and nickel isotope data. Miner. Depos. 49, 75–100. https://doi.org/10.1007/s00126-013-0476-1

Holzheid, A., Palme, H., Chakraborty, S., 1997. The activities of NiO, CoO and FeO in silicate melts. Chem. Geol. 139, 21–38.

Irving, A.J., 1980. Petrology and geochemistry of composite ultramafic xenoliths in alkalic basalts and implications for magmatic processes within the mantle. Am. J. Sci. 280–A, 389–426.

James, D.E., Padovani, E.R., Hart, S.R., 1980. Preliminary results on the oxygen isotopic composition of the lower crust, Kilbourne Hole Maar, New Mexico. Geophys. Res. Lett. 7, 321–324. https://doi.org/10.1029/GL007i005p00321

Jana, D., Walker, D., 1997. The influence of silicate melt composition on distribution of siderophile elements among metal and silicate liquids. Earth Planet. Sci. Lett. 150, 463–472. https://doi.org/10.1016/S0012-821X(97)00079-4

Kegler, P., Holzheid, A., Frost, D.J., Rubie, D.C., Dohmen, R., Palme, H., 2008. New Ni and Co metal-silicate partitioning data and their relevance for an early terrestrial magma ocean. Earth Planet. Sci. Lett. 268. https://doi.org/10.1016/j.epsl.2007.12.020

Keller, G.R., Morgan, P., Seager, W.R., 1990. Crustal structure, gravity anomalies and heat flow in the southern Rio Grande rift and their relationship to extensional tectonics. Tectonophysics 174, 21–37.

Kempton, P.D., Fitton, J.G., Saunders, A.D., Nowell, G.M., Taylor, R.N., Hardarson, B.S., Pearson, G., 2000. The Iceland plume in space and time: a Sr–Nd–Pb–Hf study of the North Atlantic rifted margin, Earth and Planetary Science Letters. Elsevier. https://doi.org/10.1016/S0012-821X(00)00047-9

Kirsten, T., Deubner, J., Horn, P., Kaneoka, I., Kiko, J., Schaeffer, O.A., Thio, S.K., 1972. The rare gas record of Apollo 14 and 15 samples. Proc. Third Lunar Sci. Conf. vol. 3, p. 1865 - 1889 3, 1865–1889.

Kodolányi, J., Stephan, T., Trappitsch, R., Pignatari, M., Davis, A.M., Pellin, M.J., 2018. Iron and nickel isotope compositions of presolar silicon carbide grains from supernovae. Geochim. Cosmochim. Acta 221, 127–144. https://doi.org/10.1016/J.GCA.2017.05.029

König, S., Wille, M., Voegelin, A., Schoenberg, R., 2016. Molybdenum isotope systematics in subduction zones. Earth Planet. Sci. Lett. 447, 95–102. https://doi.org/10.1016/j.epsl.2016.04.033

Koornneef, J.M., Davies, G.R., Döpp, S.P., Vukmanovic, Z., Nikogosian, I.K., Mason, P.R.D., 2009. Nature and timing of multiple metasomatic events in the sub-cratonic lithosphere beneath Labait, Tanzania. Lithos 112, 896–912. https://doi.org/10.1016/J.LITHOS.2009.04.039

Korotev, R.L., 2018. List of Lunar Meteorites [WWW Document]. http://meteorites.wustl.edu/lunar/moon_meteorites_list_alpha.htm.

Krawczynski, M.J., Grove, T.L., 2012. Experimental investigation of the influence of oxygen fugacity on the source depths for high titanium lunar ultramafic magmas. Geochim. Cosmochim. Acta 79, 1–19. https://doi.org/10.1016/j.gca.2011.10.043

Langmuir, C.H., Klein, E.M., Plank, T., 1992. Petrological Systematics of Mid-Ocean Ridge Basalts: Constraints on Melt Generation Beneath Ocean Ridges, in: Phipps Morgan, J., Blackman, D.K., Sinton, J.M. (Eds.), Mantle Flow and Melt Generation at Mantle Ridges. American Geophysical Union (AGU), pp. 183–280. https://doi.org/10.1029/GM071p0183

Lazar, C., Young, E.D., Manning, C.E., 2012. Experimental determination of equilibrium nickel isotope fractionation between metal and silicate from 500 °C to 950 °C. Geochim. Cosmochim. Acta 86, 276–295. https://doi.org/10.1016/J.GCA.2012.02.024

Lee, D.-C., 1994. A Chemical, Isotopic, and Geochronological Study of the Cameroon Line, West Africa. University of Michigan.

Lee, D.-C., Halliday, A.N., Davies, G.R., Essene, E.J., Fitton, J.G., Temdjim, R., 1996. Melt Enrichment of Shallow Depleted Mantle: a Detailed Petrological, Trace Element and Isotopic Study of Mantle- Derived Xenoliths and Megacrysts from the Cameroon Line. J. Petrol. 37, 15–441.

Lee, D., Halliday, A.N., Davies, G.R., Essene, E.J., Fitton, J.G., Temdjim, R., 1996. Melt Enrichment of Shallow Depleted Mantle: a Detailed Petrological, Trace Element and Isotopic Study of Mantle- Derived Xenoliths and Megacrysts from the Cameroon Line. J. Petrol. 37, 415–441.

Liang, Y.-H., Halliday, A.N., Siebert, C., Fitton, J.G., Burton, K.W., Wang, K.-L., Harvey, J., 2017. Molybdenum isotope fractionation in the mantle. Geochim. Cosmochim. Acta 199, 91–111. https://doi.org/10.1016/J.GCA.2016.11.023

Liu, L., Spasojević, S., Gurnis, M., 2008. Reconstructing Farallon Plate Subduction Beneath North America Back to the Late Cretaceous. Science (80-.). 322. https://doi.org/10.1126/science.1164170

Liu, S., Li, Y., Ju, Y., Liu, J., Liu, J., Shi, Y., 2018. Equilibrium nickel isotope fractionation in nickel sulfide minerals. Geochim. Cosmochim. Acta 222, 1–16. https://doi.org/10.1016/J.GCA.2017.10.018

Lodders, K., 2003. Solar System Abundances and Condensation Temperatures of the Elements. Astrophys. Journal, 591, 1220–1247.

Ma, Z., Thompson, R.N., Lykke, K.R., Pellin, M.J., Davis, A.M., 1995. Time-of-Flight Mass Spectrometer with Improved Resolution Review of. Cit. Rev. Sci. Instruments 66, 1150. https://doi.org/10.1063/1.1145546

Maley, J., Livingstone, D.A., Giresse, P., Thouveny, N., Brenac, P., Kelts, K., Kling, G., Stager, C., Haag, M., Fournier, M., Bandet, Y., Williamson, D., Zogning, A., 1990. Lithostratigraphy, volcanism, paleomagnetism and palynology of Quaternary lacustrine deposits from Barombi Mbo (West Cameroon): preliminary results. J. Volcanol. Geotherm. Res. 42, 319–335.

McCammon, C., 2005. The Paradox of Mantle Redox. Science (80-.). 308. https://doi.org/10.1126/science.1108162

McDonough, W.F., Sun, S. s., 1995. The composition of the Earth. Chem. Geol. 120, 223–253. https://doi.org/10.1016/0009-2541(94)00140-4

Menzies, M.A., Arculus, R.J., G, B.M., Bergman, S.C., Ehrenberg, S.N., Irving, A.J., Roden, M.F., Schulze, D.J., 1987. A record of subduction processes and within-plate volcanism in lithospheric xenoliths of southwestern USA, in: Nixon, P.. (Ed.), Mantle Xenoliths. pp. 59–74.

Meyer, C., 2011. Lunar Sample Compendium.

Meyer, C., 2003. Lunar Regolith - NASA Lunar Petrographic Educational Thin Section Set.

Moorbath, S., Sigurdsson, H., Goodwin, R., 1968. K-Ar ages of the oldest exposed rocks in Iceland. Earth Planet. Sci. Lett. 4, 197–205. https://doi.org/10.1016/0012-821X(68)90035-6

Morand, P., Allègre, C.J., 1983. Nickel isotopic studies in meteorites. Earth Planet. Sci. Lett. 63, 167–176. https://doi.org/10.1016/0012-821X(83)90034-1

Morand, P., Audouze, J., Allègre, C.J., 1980. Search for nickel isotopic anomaly of meteorites, in: 43rd Annual Meeting of the Meteoritical Society.

Moreau, C., Regnoult, J.-M., Déruelle, B., Robineau, B., 1987. A new tectonic model for the Cameroon Line, Central Africa. Tectonophysics 141, 317–334. https://doi.org/10.1016/0040-1951(87)90206-X

Morgan, W.J., 1983. Hotspot tracks and the early rifting of the Atlantic. Tectonophysics 94, 123–139. https://doi.org/10.1016/0040-1951(83)90013-6

Mostefaoui, S., Lugmair, G.W., Hoppe, P., 2005. 60 Fe: A Heat Source for Planetary Differentiation from a Nearby Supernova Explosion. Astrophys. J. 625, 271–277. https://doi.org/10.1086/429555

Moynier, F., Agranier, A., Hezel, D.C., Bouvier, A., 2010. Sr stable isotope composition of Earth, the Moon, Mars, Vesta and meteorites, Earth and Planetary Science Letters. https://doi.org/10.1016/j.epsl.2010.10.017

Moynier, F., Albarède, F., Herzog, G.F., 2006. Isotopic composition of zinc, copper, and iron in lunar samples. Geochim. Cosmochim. Acta 70, 6103–6117. https://doi.org/10.1016/j.gca.2006.02.030

Moynier, F., Blichert-Toft, J., Telouk, P., Luck, J.-M., Albarède, F., 2007. Comparative stable isotope geochemistry of Ni, Cu, Zn, and Fe in chondrites and iron meteorites. Geochim. Cosmochim. Acta 71, 4365–4379. https://doi.org/10.1016/j.gca.2007.06.049

Moynier, F., Blichert-Toft, J.F., Telouk, P., Albarede, F., 2005. Excesses of 60Ni in chondrites and iron meteorites, in: Lunar and Planetary Science XXXVI.

Neal, C.R., 2001. The Interior of the Moon: The presence of garnet in the primitive deep lunar mantle. J. Geophys. Res. 106, 27865–27885.

Neal, C.R., Taylor, L.A., 1992. Petrogenesis of mare basalts: A record of lunar volcanism*. Geochim. Cosmochim. Acta 56, 2177–2211.

Neal, C.R., Taylor, L.A., 1991. Evidence for metasomatism of the lunar highlands and the origin of whitlockite. Geochim. Cosmochim. Acta 55, 2965–2980.

Newsom, H.E., 1986. Constraints on the Origin of the Moon from the Abundance of Molybdenum and Other Siderophile Elements.

Nicholls, D., 1974. Complexes and First Row Transition Elements. Macmillan, London.

Nier, A.O., 1940. A Mass Spectrometer for Routine Isotope Abundance Measurements. Rev. Sci. Instrum. 11. https://doi.org/10.1063/1.1751688

Niu, Y., Batiza, R., 1997. Trace element evidence from seamounts for recycled oceanic crust in the Eastern Pacific mantle. Earth Planet. Sci. Lett. 148, 471–483. https://doi.org/10.1016/S0012-821X(97)00048-4

Nixon, P.., 1987. Introduction, in: Mantle Xenoliths. pp. 1–3.

Norton, I.O., 2007. Speculations on Cretaceous tectonic history of the northwest Pacific and a tectonic origin for the Hawaii hotspot, in: Plates, Plumes, and Planetary Processes. pp. 451–470.

O'Neill, H.S.C., 1981. The transition between spinel lherzolite and garnet lherzolite, and its use as a Geobarometer. Contrib. to Mineral. Petrol. 77, 185–194. https://doi.org/10.1007/BF00636522

Palme, H., Spettel, B., Bischoff, A., St6ffler, D., 1984. Early Differentiation of the Moon' Evidence from Trace Elements in Plagioclase, in: PROCEEDINGS OF THE FIFTEENTH LUNAR AND PLANETARY SCIENCE CONFERENCE, PART 1 JOURNAL OF GEOPHYSICAL RESEARCH. https://doi.org/10.1029/JB089iS01p000C3

Paniello, R.C., Day, J.M.D., Moynier, F., 2012. Zinc isotopic evidence for the origin of the Moon. Nature 490, 376–379. https://doi.org/10.1038/nature11507

Papanastassiou, D.A., Wasserburg, G.J., 1971. Rb-Sr AGES OF IGNEOUS ROCKS FROM THE APOLLO 14 MISSION AND THE AGE OF THE FRA MAURO FORMATION. Earth Planet. Sci. Lett. 12, 36–48.

Papike, J.J., Fowler, G.W., Adcock, C.T., Shearer, C.K., 1999. Systematics of Ni and Co in olivine from planetary melt systems: Lunar mare basalts. Am. Mineral. 84, 392–399. https://doi.org/10.2138/am-1999-0324

Paslick, C., Halliday, A.N., James, D., Dawson, J.B., 1995. Enrichment of the continental lithosphere by OIB melts: Isotopic evidence from the volcanic province of northern Tanzania. Earth Planet. Sci. Lett. 130, 109–126.

Paslick, C.R., 1995. A Geochemical Study of Volcanism associated with the early stages of Continental Rifting in Northern Tanzanian. University of Michigan.

Paslick, C.R., Halliday, A.N., Lange, R.A., James, D., Dawson, J.B., 1996. Indirect crustal contamination: evidence from isotopic and chemical disequilibria in minerals from alkali basalts and nephelinites from northern Tanzania. Contrib. to Mineral. Petrol. 125, 277–292. https://doi.org/10.1007/s004100050222

Peale, S.J., Cassen, P., 1978. Contribution of tidal dissipation to lunar thermal history. Icarus 36, 245–269. https://doi.org/10.1016/0019-1035(78)90109-4

Perkins, D., Anthony, E.Y., 2011. The evolution of spinel lherzolite xenoliths and the nature of the mantle at Kilbourne Hole, New Mexico. Contrib. to Mineral. Petrol. 162, 1139–1157. https://doi.org/10.1007/s00410-011-0644-1

Pike, J.E.N., Meyer, C.E., Wilshire, H.G., 1980. Petrography and Chemical Composition of a Suite of Ultramafic Xenoliths from Lashaine, Tanzania. J. Geol. 88, 343–352. https://doi.org/10.1086/628512

Pinter, Z., Patko, L., Djoukam, F.T.J., Kovacs, I., Tchouankoue, J.P., Falus, G., Konc, Z., Tommasi, A., Barou, F., Mihaly, J., Nemeth, C., Jeffries, T., 2015. Characterization of the sub-continental lithospheric mantle beneath the Cameroon volcanic line inferred from alkaline basalt hosted peridotite xenoliths from Barombi Mbo and Nyos Lakes. J. African Earth Sci. 111, 170–193. https://doi.org/10.1016/j.jafrearsci.2015.07.006

Porter, S.J., Selby, D., Cameron, V., 2014. Characterising the nickel isotopic composition of organic-rich marine sediments. Chem. Geol. 387, 12–21. https://doi.org/10.1016/j.chemgeo.2014.07.017

Quitte, G., Halliday, A.N., Meyer, B.S., Markowski, A., Latkoczy, C., Gunther, D., 2007. Correlated Iron 60, Nickel 62, and Zirconium 96 in Refractory Inclusions and the Origin of the Solar System. Astrophys. J. 655, 678–684. https://doi.org/10.1086/509771

Quitté, G., Meier, M., Latkoczy, C., Halliday, A.N., Günther, D., Gunther, D., Günther, D., Gunther, D., Günther, D., 2006. Nickel isotopes in iron meteorites–nucleosynthetic anomalies in sulfides with no effects in metals and no trace of 60Fe. Earth Planet. Sci. Lett. 242, 16–25. https://doi.org/10.1016/j.epsl.2005.11.053

Quitté, G., Oberli, F., 2006. Quantitative extraction and high precision isotope measurements of

nickel by MC-ICPMS. J. Anal. At. Spectrom. 21, 1249. https://doi.org/10.1039/b607569j

Rai, N., Westrenen, W. Van, 2014. Lunar core formation : New constraints from metal – silicate partitioning of siderophile elements. Earth Planet. Sci. Lett. 388, 343–352. https://doi.org/10.1016/j.epsl.2013.12.001

Ratié, G., Jouvin, D., Garnier, J., Rouxel, O., Miska, S., Guimaraes, E., Cruz Vieira, L., Sivry, Y., Zelano, I., Montarges-Pelletier, E., Thil, F., Quantin, C., 2015. Nickel isotope fractionation during tropical weathering of ultramafic rocks. Chem. Geol. 402, 68–76. https://doi.org/10.1016/j.chemgeo.2015.02.039

Ratié, G., Quantin, C., Jouvin, D., Calmels, D., Ettler, V., Sivry, Y., Vieira, L.C., Ponzevera, E., Garnier, J., Cruz Vieira, L., Ponzevera, E., Garnier, J., 2016. Nickel isotope fractionation during laterite Ni ore smelting and refining : Implications for tracing the sources of Ni in smelter-affected soils. Appl. Geochemistry 64, 136–145. https://doi.org/10.1016/j.apgeochem.2015.09.005

Reedy, R.C., Englert, P., 1986. Workshop on COSMOGENIC NUCLIDES.

Regelous, M., Elliott, T., Coath, C.D., 2008. Nickel isotope heterogeneity in the early Solar System. Earth Planet. Sci. Lett. 272, 330–338. https://doi.org/10.1016/j.epsl.2008.05.001

Reid, A.M., Donaldson, C.H., Brown, R.W., Ridley, W.I., Dawson, J.B., 1975. Mineral chemistry of peridotite xenoliths from the Lashaine volcano, Tanzania. Phys. Chem. Earth 9, 525–543. https://doi.org/10.1016/0079-1946(75)90037-3

Rhodes, J.M., Dawson, J.B., 1975. Major and trace element chemistry of peridotite inclusions from the Lashaine volcano, Tanzania. Phys. Chem. Earth 9, 545–557. https://doi.org/10.1016/0079-1946(75)90038-5

Righter, K., 2002. Does the Moon Have a Metallic Core? Constraints from Giant Impact Modeling and Siderophile Elements. Icarus 158, 1–13. https://doi.org/10.1006/icar.2002.6859

Righter, K., Drake, M.J., Yaxley, G., 1997. Prediction of siderophile element metal-silicate partition coefficients to 20 GPa and 2800°C: the effects of pressure, temperature, oxygen fugacity, and silicate and metallic melt compositions. Phys. Earth Planet. Inter. 100, 115–134. https://doi.org/10.1016/S0031-9201(96)03235-9

Righter, K., Pando, K.M., Danielson, L., Lee, C.-T., 2010. Partitioning of Mo, P and other siderophile elements (Cu, Ga, Sn, Ni, Co, Cr, Mn, V, and W) between metal and silicate melt as a function of temperature and silicate melt composition. Earth Planet. Sci. Lett. 291, 1–9. https://doi.org/10.1016/J.EPSL.2009.12.018

Roden, M.F., Irving, A.J., Murthy, V.R., 1988. Isotopic and trace element composition of the upper mantle beneath a young continental rift: Results from Kilbourne Hole, New Mexico. Geochim. Cosmochim. Acta 52, 461–473. https://doi.org/10.1016/0016-7037(88)90101-9

Rugel, G., Faestermann, T., Knie, K., Korschinek, G., Poutivtsev, M., Schumann, D., Kivel, N., Günther-Leopold, I., Weinreich, R., Wohlmuther, M., 2009. New Measurement of the ^{60}Fe Half-Life. Phys. Rev. Lett. 103, 072502. https://doi.org/10.1103/PhysRevLett.103.072502

Sato, M., Hickling, N.L., McLane, J.E., 1973. Oxygen fugacity values of Apollo 12, 14, and 15 lunar samples and reduced state of lunar magmas, in: Proceedings of the Fourth Lunar Science Conference. pp. 1061–1079.

Satsukawa, T., Michibayashi, K., Anthony, E.Y., Stern, R.J., Gao, S.S., Liu, K.H., 2011. Seismic anisotropy of the uppermost mantle beneath the Rio Grande rift: Evidence from Kilbourne Hole peridotite xenoliths, New Mexico. Earth Planet. Sci. Lett. 311, 172–181. https://doi.org/10.1016/J.EPSL.2011.09.013

Sedaghatpour, F., Teng, F.Z., Liu, Y., Sears, D.W.G., Taylor, L.A., 2013. Magnesium isotopic

composition of the Moon. Geochim. Cosmochim. Acta 120, 1–16. https://doi.org/10.1016/j.gca.2013.06.026

Sharp, Z.D., Shearer, C.K., McKeegan, K.D., Barnes, J.D., Wang, Y.Q., 2010. The Chlorine Isotope Composition of the Moon and Implications for an Anhydrous Mantle. Science (80-.). 329. https://doi.org/10.1126/science.1191349

Shearer, C.K., Hess, P.C., Wieczorek, M.A., Pritchard, M.E., Parmentier, E.M., Borg, L.E., Longhi, J., Elkins-Tanton, L.T., Neal, C.R., Antonenko, I., Canup, R.M., Halliday, A.N., Grove, T.L., Hager, B.H., Lee, D.C., Wiechert, U., 2006. Thermal and Magmatic Evolution of the Moon, in: Reviews in Mineralogy & Geochemistry Volume 60: New Views of the Moon. pp. 365–502.

Shimamura, T., Lugmair, G.W., 1983. Ni isotopic compositions in Allende and other meteorites. Earth Planet. Sci. Lett. 63, 177–188. https://doi.org/10.1016/0012-821X(83)90035-3

Shukolyukov, A., Lugmair, G.W., 1993a. 60Fe in eucrites. Earth Planet. Sci. Lett. 119, 159–166. https://doi.org/10.1016/0012-821X(93)90013-Y

Shukolyukov, A., Lugmair, G.W., 1993b. Live Iron-60 in the Early Solar System. Science (80-.). 259, 1138–1142.

Siebert, C., Nägler, T.F., Kramers, J.D., 2001. Determination of molybdenum isotope fractionation by double-spike multicollector inductively coupled plasma mass spectrometry. Geochemistry, Geophys. Geosystems 2, n/a-n/a. https://doi.org/10.1029/2000GC000124

Silveira, G., Stutzmann, E., Davaille, A., Montagner, J.-P., Mendes-Victor, L., Sebai, A., 2006. Azores hotspot signature in the upper mantle. J. Volcanol. Geotherm. Res. 156, 23–34. https://doi.org/10.1016/J.JVOLGEORES.2006.03.022

Simon, J.I., DePaolo, D.J., 2010. Stable calcium isotopic composition of meteorites and rocky planets, Earth and Planetary Science Letters. https://doi.org/10.1016/j.epsl.2009.11.035

Sobolev, A. V, Hofmann, A.W., Kuzmin, D. V, Yaxley, G.M., Arndt, N.T., Chung, S.-L., Danyushevsky, L. V, Elliott, T., Frey, F.A., Garcia, M.O., Gurenko, A.A., Kamenetsky, V.S., Kerr, A.C., Krivolutskaya, N.A., Matvienkov, V. V, Nikogosian, I.K., Rocholl, A., Sigurdsson, I.A., Sushchevskaya, N.M., Teklay, M., 2007. The Amount of Recycled Crust in Sources of Mantle-Derived Melts. Science (80-.). 316.

Sobolev, A. V, Hofmann, A.W., Sobolev, S. V, Nikogosian, I.K., 2005. An olivine-free mantle source of Hawaiian shield basalts. Nature 434.

Spivak-Birndorf, L.J., Wang, S.-J., Bish, D.L., Wasylenki, L.E., 2018. Nickel isotope fractionation during continental weathering. Chem. Geol. 476, 316–326. https://doi.org/10.1016/J.CHEMGEO.2017.11.028

Steele, A.M., Colson, R.O., Haskin, L.A., 1991. Co and Ni as Incompatible elements in the Lunar Mantle: Implications for fO2 and the Petrogenesis of Apollo 15 Green Glass, in: LPSC XXII.

Steele, R.C.J., Coath, C.D., Regelous, M., Russell, S., Elliott, T., 2012. Neutron-poor nickel isotope anomalies in meteorites. Astrophys. J. 758, 59. https://doi.org/10.1088/0004-637X/758/1/59

Steele, R.C.J., Elliott, T., Coath, C.D., Regelous, M., 2011. Confirmation of mass-independent Ni isotopic variability in iron meteorites. Geochim. Cosmochim. Acta 75, 7906–7925. https://doi.org/10.1016/J.GCA.2011.08.030

Steenstra, E.S., Rai, N., Knibbe, J.S., Lin, Y.H., Van Westrenen, W., 2016. New geochemical models of core formation in the Moon from metal-silicate partitioning of 15 siderophile elements. Earth Planet. Sci. Lett. 441, 1–9. https://doi.org/10.1016/j.epsl.2016.02.028

Strelow, F.W.E., 1990. Distribution coefficients and cation-exchange behaviour of some ammines and aquo complexes of metallic elements in ammonium nitrate solution. Anal. Chim. Acta 233, 129–134. https://doi.org/10.1016/S0003-2670(00)83468-6

Strelow, F.W.E., Weinert, C.H.S.W., Eloff, C., 1972. Distribution coefficients and anion exchange behavior of elements in oxalic acid-hydrochloric acid mixtures. Anal. Chem. 44, 2352–2356. https://doi.org/10.1021/ac60322a001

Sun, C., Graff, M., Liang, Y., 2017. Trace element partitioning between plagioclase and silicate melt: The importance of temperature and plagioclase composition, with implications for terrestrial and lunar magmatism. Geochim. Cosmochim. Acta 206, 273–295. https://doi.org/10.1016/j.gca.2017.03.003

Tachibana, S., Huss, G.R., 2003. The Initial Abundance of 60 Fe in the Solar System. Astrophys. J. 588, L41–L44. https://doi.org/10.1086/375362

Tachibana, S., Huss, G.R., Kita, N.T., Shimoda, G., Morishita, Y., 2006. 60 Fe in Chondrites: Debris from a Nearby Supernova in the Early Solar System? Astrophys. J. 639, L87–L90. https://doi.org/10.1086/503201

Tanimizu, M., Hirata, T., 2006. Determination of natural isotopic variation in nickel using inductively coupled plasma mass spectrometry. J. Anal. At. Spectrom. 21, 1423. https://doi.org/10.1039/b609543g

Taylor, S.R., 1982. A Lunar Perspective. Lunar and Planetary Institute.

Taylor, S.R., 1975. Lunar Science: A Post-Apollo View.

Teng, F.-Z., Dauphas, N., Huang, S., Marty, B., 2013. Iron isotopic systematics of oceanic basalts. Geochim. Cosmochim. Acta 107, 12–26. https://doi.org/10.1016/J.GCA.2012.12.027

Thompson, G., Bryan, W.B., Humphris, S.E., 1989. Axial volcanism on the East Pacific Rise, in: Magmatism in the Ocean Basins. pp. 181–200.

Trappitsch, R., Stephan, T., Savina, M.R., Davis, A.M., Pellin, M.J., Rost, D., Gyngard, F., Gallino, R., Bisterzo, S., Cristallo, S., Dauphas, N., 2018. Simultaneous iron and nickel isotopic analyses of presolar silicon carbide grains. Geochim. Cosmochim. Acta 221, 87–108. https://doi.org/10.1016/J.GCA.2017.05.031

van Kan Parker, M., Sanloup, C., Sator, N., Guillot, B., Tronche, E.J., Perrillat, J.-P., Mezouar, M., Rai, N., van Westrenen, W., 2012. Neutral buoyancy of titanium-rich melts in the deep lunar interior. Nat. Geosci. 5, 186–189. https://doi.org/10.1038/ngeo1402

Vance, D., Little, S.H., Archer, C., Cameron, V., Andersen, M.B., Rijkenberg, M.J.A., Lyons, T.W., 2016. The oceanic budgets of nickel and zinc isotopes: the importance of sulfidic environments as illustrated by the Black Sea. Philos. Trans. A. Math. Phys. Eng. Sci. 374, 20150294. https://doi.org/10.1098/rsta.2015.0294

Vauchez, A., Dineur, F., Rudnick, R., 2005. Microstructure, texture and seismic anisotropy of the lithospheric mantle above a mantle plume: Insights from the Labait volcano xenoliths (Tanzania). Earth Planet. Sci. Lett. 232, 295–314. https://doi.org/10.1016/J.EPSL.2005.01.024

Ventura, G.T., Gall, L., Siebert, C., Prytulak, J., Szatmari, P., Hürlimann, M., Halliday, A.N., 2015. The stable isotope composition of vanadium, nickel, and molybdenum in crude oils. Appl. Geochemistry 59, 104–117. https://doi.org/10.1016/j.apgeochem.2015.04.009

Victor, A.H., 1986. Selective separation of Nickel from other elements by cation-exchange chromatography in dimethylglyoxime/hydrochloric acid/acetone media. Anal. Chim. Acta 183, 155–161.

Wadhwa, M., 2008. Redox Conditions on Small Bodies, the Moon and Mars, in: Reviews in

Mineralogy and Geochemistry. GeoScienceWorld, pp. 493–510. https://doi.org/10.2138/rmg.2008.68.17

Walter, L.S., French, B.M., Heinrich, K.F.J., Lowman, P.D., Doan, A.S., Adler, I., 1971. Mineralogical studies of Apollo 12 samples, in: 2nd Lunar Science Conference. M.I.T. Press, pp. 343–358.

Wang, K., Jacobsen, S.B., Sedaghatpour, F., Chen, H., Korotev, R.L., 2015. The earliest Lunar Magma Ocean differentiation recorded in Fe isotopes. Earth Planet. Sci. Lett. 430, 202–208. https://doi.org/10.1016/j.epsl.2015.08.019

Wang, S.-J., Wasylenki, L.E., 2017. Experimental constraints on reconstruction of Archean seawater Ni isotopic composition from banded iron formations. Geochim. Cosmochim. Acta 206, 137–150. https://doi.org/10.1016/J.GCA.2017.02.023

Warren, P.H., 1985. THE MAGMA OCEAN CONCEPT AND LUNAR EVOLUTION. Ann. Rev. Earth planet. Sci 13, 201–241.

Warren, P.H., Wasson, J.T., 1979. The Origin of KREEP. Rev. Geophys. Sp. Phys. 17.

Wasylenki, L.E., Howe, H.D., Spivak-Birndorf, L.J., Bish, D.L., 2015. Ni isotope fractionation during sorption to ferrihydrite: Implications for Ni in banded iron formations. Chem. Geol. 400, 56–64. https://doi.org/10.1016/j.chemgeo.2015.02.007

Weber, R.C., Lin, P., Garnero, E.J., Williams, Q., Lognonné, P., 2011. Seismic Detection of the Lunar Core 331, 309–312.

Wedepohl, K.H., 1974. Nickel, in: Wedepohl, K.H. (Ed.), Handbook of Geochemistry. Springer.

Weis, D., Kieffer, B., Maerschalk, C., Barling, J., de Jong, J., Williams, G.A., Hanano, D., Pretorius, W., Mattielli, N., Scoates, J.S., Goolaerts, A., Friedman, R.M., Mahoney, J.B., 2006. High-precision isotopic characterization of USGS reference materials by TIMS and MC-ICP-MS. Geochemistry, Geophys. Geosystems 7, n/a-n/a. https://doi.org/10.1029/2006GC001283

Weyer, S., Anbar, A.D., Brey, G.P., Münker, C., Mezger, K., Woodland, A.B., 2007. Fe-isotope fractionation during partial melting on Earth and the current view on the Fe-isotope budgets of the planets (reply to the comment of F. Poitrasson and to the comment of B.L. Beard and C.M. Johnson on “Iron isotope fractionation during planetary differentiation” by S. Weyer, A.D. Anbar, G.P. Brey, C. Münker, K. Mezger and A.B. Woodland). Earth Planet. Sci. Lett. 256, 638–646. https://doi.org/10.1016/J.EPSL.2007.01.038

White, W.M., 1985. Sources of oceanic basalts: Radiogenic isotopic evidence. Geology 13, 115. https://doi.org/10.1130/0091-7613(1985)13<115:SOOBRI>2.0.CO;2

White, W.M., McBirney, A.R., Duncan, R.A., 1993. Petrology and geochemistry of the Galápagos Islands: Portrait of a pathological mantle plume. J. Geophys. Res. Solid Earth 98, 19533–19563. https://doi.org/10.1029/93JB02018

White, W.M., Tapia, M.D.M., Schilling, J.-G., 1979. The petrology and geochemistry of the Azores Islands. Contrib. to Mineral. Petrol. 69, 201–213. https://doi.org/10.1007/BF00372322

Wiechert, U., Halliday, A.N., Lee, D.-C., Snyder, G.A., Taylor, L.A., Rumble, D., 2001. Oxygen Isotopes and the Moon-Forming Giant Impact. Science (80-.). 294, 345–348.

Wieczorek, M.A., Jolliff, B.L., Khan, A., Pritchard, M.E., Weiss, B.P., Williams, J.G., Hood, L.L., Righter, K., Neal, C.R., Shearer, C.K., McCallum, I.S., Tompkins, S., Hawke, B.R., Peterson, C., Gillis, J.J., Bussey, B., 2006. The Constitution and Structure of the Lunar Interior, in: Reviews in Mineralogy & Geochemistry Volume 60: New Views of the Moon. pp. 221–343.

Willbold, M., Stracke, A., 2006. Trace element composition of mantle end-members: Implications for recycling of oceanic and upper and lower continental crust. Geochemistry, Geophys. Geosystems 7, 1–30. https://doi.org/10.1029/2005GC001005

Williams, H.M., Bizimis, M., 2014. Iron isotope tracing of mantle heterogeneity within the source regions of oceanic basalts. Earth Planet. Sci. Lett. 404, 396–407. https://doi.org/10.1016/J.EPSL.2014.07.033

Williams, H.M., Mccammon, C.A., Peslier, A.H., Halliday, A.N., Teutsch, N., Levasseur, S., Burg, J.-P., 2004. Iron Isotope Fractionation and the Oxygen Fugacity of the Mantle. Source Sci. New Ser. 304, 1656–1659.

Williams, H.M., Nielsen, S.G., Renac, C., Griffin, W.L., O'Reilly, S.Y., Mccammon, C.A., Pearson, N., Viljoen, F., Alt, J.C., Halliday, A.N., 2009. Fractionation of oxygen and iron isotopes by partial melting processes: Implications for the interpretation of stable isotope signatures in mafic rocks. Earth Planet. Sci. Lett. 283, 156–166. https://doi.org/10.1016/j.epsl.2009.04.011

Williams, H.M., Peslier, A.H., Mccammon, C., Halliday, A.N., 2005. Systematic iron isotope variations in mantle rocks and minerals : The effects of partial melting and oxygen fugacity. Earth Planet. Sci. Lett. 235, 435–452. https://doi.org/10.1016/j.epsl.2005.04.020

Williams, H.M., Prytulak, J., Woodhead, J.D., Kelley, K.A., Brounce, M., Plank, T., 2018. Interplay of crystal fractionation, sulfide saturation and oxygen fugacity on the iron isotope composition of arc lavas: An example from the Marianas. Geochim. Cosmochim. Acta 226, 224–243. https://doi.org/10.1016/J.GCA.2018.02.008

Wing, B.A., Farquhar, J., 2015. Sulfur isotope homogeneity of lunar mare basalts. https://doi.org/10.1016/j.gca.2015.09.003

Wood, B.J., Bryndzia, L.T., Johnson, K., 1990. Mantle Oxidation State and Its Relationship to Tectonic Environment and Fluid Speciation. Science (80-.). 248.

Wood, B.J., Kiseeva, E.S., Mirolo, F.J., 2014. Accretion and core formation: The effects of sulfur on metal-silicate partition coefficients. Geochim. Cosmochim. Acta 145, 248–267. https://doi.org/10.1016/j.gca.2014.09.002

Yi, W., Halliday, A.N., Alt, J.C., Lee, D.-C., Rehkämper, M., Garcia, M.O. 0, Langmuir, C.H., Su, Y., Rehkämper, M., Garcia, M.O. 0, Langmuir, C.H., Su, Y., 2000. Cadmium, indium, tin, tellurium, and sulfur in oceanic basalts: Implications for chalcophile element fractionation in the Earth. J. Geophys. Res. 105, 18,927-18,948. https://doi.org/10.1029/2000JB900152

Yi, W., Halliday, A.N., Lee, D.-C., Christensen, J.N., 1995a. Indium and tin in basalts, sulfides, and the mantle. Geochim. Cosmochim. Acta 59, 5081–5090.

Yi, W., Halliday, A.N., Lee, D.-C., Christensen, J.N., 1995b. Indium and tin in basalts, sulfides, and the mantle. Geochim. Cosmochim. Acta 59, 5081–5090. https://doi.org/10.1016/0016-7037(95)00342-8

Zhao, Y., Xue, C., Liu, S.-A., Symons, D.T.A., Zhao, X., Yang, Y., Ke, J., 2017. Copper isotope fractionation during sulfide-magma differentiation in the Tulaergen magmatic Ni–Cu deposit, NW China. Lithos 286–287, 206–215. https://doi.org/10.1016/J.LITHOS.2017.06.007

Zindler, A., Hart, S., 1986. CHEMICAL GEODYNAMICS, Ann. Rev. Earth Planet. Sci.

2. Sample Preparation and Analysis

2.1 Introduction

To determine accurate Ni isotopic compositions in natural samples it is necessary to remove other elements prior to analysis, unless deploying *in situ* techniques like secondary ion mass spectrometry (SIMS). Insufficiently purified samples can introduce matrix effects, such as mass bias, suppression of ionization and spectral interferences, which may be difficult to resolve from the peaks corresponding to the isotopes of Ni. Some polyatomic interferences require the use of high mass resolution mass spectrometry.

Several methods for the purification of Ni isotopes exist in the literature (Morand and Allègre 1983; Shimamura and Lugmair, 1983; Birck & Lugmair 1988; Shukolyukov & Lugmair 1993b; Shukolyukov & Lugmair 1993a; Quitté & Oberli 2006; Cameron et al. 2009; Gall et al. 2012; Gueguen et al. 2013; Chernonozhkin et al. 2015; Spivak-Birndorf et al. 2018). Purification methods can vary depending on sample type and method of analysis. Meteoritic metal with its high Ni content and limited matrix elements requires a procedure particularly targeting iron removal (Quitté and Oberli, 2006).

Morand and Allègre (1983), used both ion exchange and liquid-liquid extraction then analysis on TIMS. The method of purification in Shimamura and Lugmair (1983) also used both ion exchange and liquid-liquid extraction, and was the basis for future purification including (Birck and Lugmair, 1988; Shukolyukov and Lugmair, 1993b, 1993a). Quitté and Oberli (2006) investigated an existing liquid-liquid extraction method and found it to have a yield of 70%, leading to development of a method using both ion-exchange and liquid-liquid extraction that used the complexation of Ni with dimethylglyoxime, with improved recovery, and analysis on a double focussing MC-ICPMS. Quitté and co-workers (2006) proved that dissolution protocol does not affect results if the sample is in chloride form before chemistry. Cameron and co-workers (2009) developed a technique to purify Ni samples and analyse Ni isotopic

compositions using Ni resin. Variations on ion-exchange purification procedures have been extensively used (Bizzarro et al., 2006; Chen et al., 2009; Cook et al., 2006; Moynier et al., 2005; Quitté et al., 2006; Steele et al., 2011). Moynier and co-workers (2005) also used sulfide precipitation using gaseous H_2S.

Other studies that deviated from variations on the usual ion-exchange and analysis include Tanimizu and Hirata (2006), who used a solvent extraction chemistry to purify Ni due to concerns about the potential for mass dependent fractionation during ion exchange column. Chen and co-workers (2009) analysed samples without Fe correction. Cook and co-workers (2007) did not report $\delta^{60/58}Ni_{SRM986}$ because of concerns of the possibility of radiogenic isotope effects on ^{60}Ni. Spivak-Birndorf and co-workers (2018) developed a new DMG-free ion exchange method. Kodolányi and co-workers (2018) analysed the Ni isotopic composition of presolar grains using the new Chicago Instrument for Laser Ionization (CHILI) and Trappitsch and co-workers (2018) using CHILI and CHARISMA (a refectron time-of-flight mass spectrometer for surface analysis that incorporates a Schwarzschild all-reflecting microscope (Ma et al., 1995)).

The method used for this study, described below, is a development of the method of Gall (2011; 2012). All the work was conducted in the Earth Sciences Department, University of Oxford. The purification of the samples was preceded by the addition of double spike for instrumental mass bias correction (see 49). This procedure was originally developed to miniaturise the chemistry and reduce the amount of di-methylglyoxime - an organic compound that strongly binds Ni but can compromise analysis of Ni isotopic compositions. Analysis used multi-collector ICPMS, with instrumental mass bias corrected by use of double-spike, with data reduction following the procedures of Siebert et al. (2001).

.

2.2 Sample preparation

The samples were chosen in order to investigate Ni isotope fractionation in high temperature environments on Earth and the Moon, covering a range of geographical localities and melting regimes.

Most samples investigated in this study were powdered archive materials. A test of the reliability of using such materials was carried out on low Ni samples with equivalent splits prepared by hand from rock specimens. Similarly, hand preparation was used for preparing material for mineral picking. All samples were weighed accurately into cleaned PFA Teflon vials and all double spike was accurately weighed into the sample as early in the process as practical for that sample. Sample dissolution was kept broadly similar but with differing volumes of acid depending on sample type. Most samples used hotplate dissolution methods; others required a high-pressure Parr bomb to dissolve refractory phases. All reagents were analytical grade or better, with acids distilled in-house by sub-boiling, and dilutions made by volume with ultrapure distilled water (MQ, 18.2 MΩ/cm).

2.2.1 Preparation of rock samples from hand specimens

The samples that were prepared from hand specimen were done for investigation of preparation techniques and for preparation of mineral separates. The nephelinite samples from Etinde volcano in Cameroon, provided by Prof J G Fitton, University of Edinburgh, had extremely low Ni concentrations, which were the most likely to render any perturbation in Ni isotopic composition by the processing method significant and easily detectable. Therefore, part of the Cameroon Line project was looking to test for any difference in the Ni isotopic composition, or Ni concentration, between the original rock powders prepared by Prof G. Fitton in the 1970s and 1980s, and duplicates prepared from original hand specimens to current geochemistry standards. Samples were stored in MQ washed glass bottles until ready for weighing and dissolution. The samples for preparation of mineral separates were ultramafic xenoliths from

Kilbourne Hole, from Dr J Harvey, University of Leeds. All preparation from hand specimens was completed in-house, after initial mineral picking training at the University of Leeds.

The hand specimens had saw marks, obvious weathering, or country rock rind removed by sanding with silicon carbide (SiC) sandpaper, and were then sealed in plastic in order to isolate the rock samples from all steel throughout the process. The wrapped sample was then broken with a mallet and steel plate. A piece was selected that included proportionate phenocryst / crystal distribution sufficient to be considered representative of the bulk rock. This piece was then visually inspected for weathering that might alter the chemistry of the rock. The wet-dry Si-C sandpaper was submerged in MQ to remove risk of air-borne dust cross contamination, and was used to remove all weathered and sawn edges to the samples. Samples were further broken. At this point techniques diverged for production of either bulk powder, or mineral separates.

Samples that required powder for bulk rock analysis were, if coarse grained or porphyritic, powdered to rock flour texture, in a new blank-tested agate pestle and mortar. The use of transparent film to cover the mortar prevented loss of material and minimised contamination. Two batches of high purity quartz sand were ground between samples to ensure no cross contamination, and wiped with MQ and ethanol between grindings. Samples were tipped from the pestle and mortar onto clean paper, with a fresh wooden spatula for each sample. Each sample was transferred to a MQ-washed glass vial to await digestion.

Samples that were to be prepared for mineral separation were carefully hand crushed until individual grains were separated. This crushate was separated from the bulk stock and sieved into a fine and a coarse fraction. A single clean fine plastic sieve of ~0.5 mm aperture was used to separate a fine fraction for potential future separation of sulfides by magnet, and the coarser fraction used for mineral picking.

The coarser fraction was washed in MQ until all dust was removed and then dried in an oven at ~40-70°C. Using clean glass petri dishes, a clean fine fibre brush, and a binocular microscope (Wild M8 stereo-zoom) with light source, minerals phases were separated in small batches

('first pick'). During the second or 'clean pick', every mineral grain was examined under 50× magnification at all angles until it was identified as completely clean of grain boundaries, inclusions, surficial adhesions, weathering/alteration, abraded edges, that might compromise the purity of the final sample. Discarded grains were kept for possible re-crushing and re-picking later. The 'clean pick' continued until sufficient mass was separated for analysis.

The clean mineral separates were given a final wash in MQ before weighing and dissolution. Spinel, as a refractory phase, was sometimes crushed to powder after the MQ wash prior to weighing, in order to increase surface area for acid attack.

2.1.1 Weighing and dissolution of silicate rock powders

Samples were weighed into PFA vials using a Sartorius® 5 figure electronic analytical balance (Model ME 2355). To reduce the weighing error, sample aliquots were usually >10 mg. The exact amount of rock sample to be weighed was based on the natural Ni concentration and the >1000 ng of natural Ni needed per analysis. Above 10 mg, the amount weighed was correlated inversely with the Ni concentration to achieve 1000 ng of natural Ni. Mineral separates were exceptions, because of the effort required to produce and dissolve extra material over that specifically needed for analysis.

Double spike analysis is a method for correcting for instrumental mass bias used in the majority of studies of Ni isotopic compositions. Double spike analysis is explained in further detail in section 2.3.3, including its reason for use. The appropriate spike volume was calculated from the optimum sample:spike Ni ratio = 0.4:1 (Gall, 2011; Gall et al., 2012), and Ni concentration of sample and double spike solution. If the sample:spike ratio is considerably different to the optimum, the deconvolution of the double spike data cannot produce reliable data (see figure 3, Gall et al. 2012).

It was necessary to weigh both the sample amount and the spike volume as accurately as possible in order to extract an accurate concentration of natural Ni in the sample using the

isotope ratios resulting from analysis (by isotope dilution). Seven measurements within 0.05 mg of each other, without directional drift throughout, were deemed sufficient for the purposes of this study, with the resulting average taken as an accurate weight.

The double spike can be weighed into the powder before dissolution, or weighed into an aliquot of dissolved sample. The former technique is considered ideal, as the double spike can account for any fractionation of Ni during the dissolution process. The latter technique was used for samples with high Ni concentration, in order to reduce wastage of the double spike, and for samples first needing ICPMS analysis for determination of accurate Ni concentration. Where double spike was added after dissolution, samples needed to reflux at 85-90°C in dilute nitric acid for at least 15 hours before loading onto the column, in order for full equilibration between double spike and sample. No difference between these approaches was found when tested with a USGS duplicate that compared spike added at either stage (see 2.3.7).

All reagents were reagent grade or better with HCl, HNO_3, HF, and oxalic acid further purified in house, all but the latter by sub-boiling distillation. Oxalic acid was purified by dissolving in MQ water and re-precipitating. Acid dilutions were made by volume with ultrapure water (18.2 MΩ/cm hereafter MQ water). Concentrated HNO_3 and concentrated HF acids in a 3:1 mixing ratio to a total volume of 2 ml was usually sufficient to dissolve the silicates in the rock samples. Avoiding larger volumes of HF reduced the probability of formation of insoluble fluorides. The samples had a minimum of 48 hours on a hotplate at 85°C. This relatively low temperature was used to prevent the formation of insoluble fluorides during the dissolution. If the presence of fluorides was observed the sample was dried and re-dissolved in concentrated HNO_3, before the sample was dissolved in 6M HCl, and refluxed at 120°C until the solution was completely clear. If no fluorides were observed the samples were evaporated gently and then refluxed in 2-3 ml 6M HCl at 120°C for 48 hours. If the sample was not clear in this volume, more acid was added until the sample was entirely in solution. For voluminous sample sizes, which required greater volumes of acid to dissolve completely, and correspondingly

greater load volumes for the first column, it was necessary to use more than one column per sample.

In cases where there were refractory phases, e.g. spinel, it was necessary to use a high-pressure Parr bomb to dissolve the sample fully. The samples were dried and 6M HCl was added. The sample was sealed in the PTFE Teflon liner and then the Parr Bomb steel jacket and then placed in an oven at ~180°C until the solution was clear. This process usually took 4 days for silicate samples with minor insoluble phases, but up to 3 weeks longer was required for spinel mineral separates.

Given the scarcity of material it was decided to explore using the lunar samples in two forms. Firstly, homogenous powders were weighed and dissolved as described above. Second, matrix eluents were utilised following ion exchange for the purification of Zn (Sean Hopkins, University of Oxford). The eluents were dried and then had Ni double spike weighed into them. Five duplicate samples were analysed from both approaches to test that no fractionation of Ni took place on the Zn column prior to the Ni double spike being added (see Chapter 5). The procedure was the same for the evaluation of potential cosmogenic isotope effects on the Moon, but excluding the addition of double spike (see 2.2.3, and Chapter 5).

2.2 Purification of nickel in geological samples

The early purification methods for Ni for isotopic analysis used both ion-exchange and liquid-liquid extraction in combination, followed by analysis on TIMS (Birck and Lugmair, 1988; Morand and Allègre, 1983; Shimamura and Lugmair, 1983; Shukolyukov and Lugmair, 1993b, 1993a). These studies were followed by a series of published studies using SIMS including ion microprobes where purification of Ni prior to analysis was not possible (Guan et al., 2004; Mostefaoui et al., 2005; Tachibana et al., 2006; Tachibana and Huss, 2003). Ion exchange and sulfide precipitation was used with the first work analysed on MC-ICPMS (Moynier et al.,

2005). The liquid-liquid extraction was found to have recovery of only 70% (Quitté and Oberli, 2006), and several purification methods were developed to improved yield once MC-ICPMS was developed. These methods largely focussed on ion-exchange chromatography (Bizzarro et al., 2006; Cook et al., 2006; Quitté et al., 2006). The first purification for of Ni for investigation of stable mass dependent Ni isotopes in geological materials was by Tanimizu and Hirata (Tanimizu and Hirata, 2006) using a procedure involving solvent extraction, chosen because of the suspicion of mass dependent fractionation during ion exchange chromatography. This is less of a concern when using double spiking

The importance of the purification method is paramount for analysis by MC-ICPMS because of the propensity of the plasma to form polyatomic and isobaric interferences, and the difficulty with matrix effects from impure sample introduction. Quitté and Oberli (2006) identified the main problem isobaric interferences as ^{58}Fe, and ^{64}Zn. Doubly charged ions can also interfere on Ni masses including ^{116}Cd, $^{116, 120, 122, 124}$Sn, $^{120, 122, 124}$Te, and ^{124}Xe. Although the method uses an online correction for any residual iron (see section 2.3.4), these other interferences make the purity of the separated Ni critical to the acquisition of high quality data.

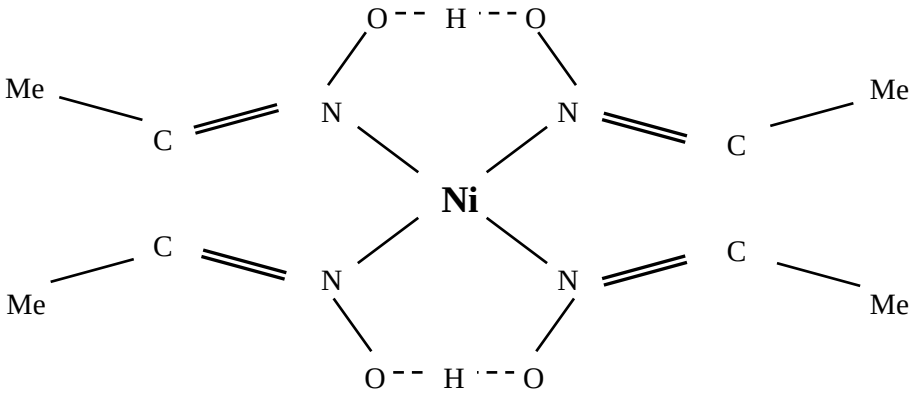

Figure 3

Nickel bound with DMG into bis(dimethylglyoximato)nickel(II), adapted from (Nicholls, 1974)

Since 2006, most Ni purification methods have relied on di-methylglyoxime (DMG). The DMG acts as a chelating agent in neutral or ammoniacal solutions of Ni^{2+} so that Ni is bound into the structure at the centre of a square plane of nitrogen atoms (Nicholls, 1974) (Figure 3). Methods for purification of Ni by ion exchange before Gall (2011; 2012), and especially those using commercial Nickel Resin (Eichrom Technologies®) (Cameron et al., 2009; Quitté and Oberli, 2006), resulted in large quantities of DMG and related organic compounds in the purified Ni cut, which were difficult to break down. These compounds need to be eliminated before analysis because otherwise Ni may remain bound to the DMG and be lost during analysis (Gall et al., 2012). Therefore, Gall (2011; 2012) developed a method that greatly reduced the amount of DMG used in the purification protocol. This method was used, with recalibration and minor development, for this study.

2.2.1 Differences to published method

There are a number of changes between the method used here and the method of Gall (2011; 2012) including the normal required recalibration, to adapt to a new batch of resin and other reagents.

Gall (pers comm, 2015) advised certain changes to the published method developed since publication in 2012. These changes included the half hour reaction time for the di-ammonium-hydrogen-citrate (dAHC) and sample before adding the ammonia before the first column, and an extra dry down and addition of concentrated HNO_3 after the second column.

To test the efficiency of the published purification method without modification, a set of final Ni cuts of samples were analysed for their elemental content in addition to Ni. This test, analysed on a Thermo-Finnigan™ Element 2, would indicate if the new batch of AG50W-X4 resin (200-400 mesh, Bio-Rad®) was working as expected.

The results of this test indicated that calcium was a major problem because it was much higher in the Ni cuts than in the blank, indicating this was sample Ca not being removed by the

chemistry. Calcium can be a major interference on Ni masses in the MC-ICPMS through oxide formation (CaO^+). Other elements that were potentially sufficiently abundant to cause problems were Mg, Cr, and Zn.

These results meant that a change in protocol was necessary. As the first column should remove the matrix elements found to be present in the final Ni cut, and this column has the new batch of resin, efforts were focussed on recalibrating this column. The first column was designed to remove Ca, other alkaline earth elements, and d block transition elements (Gall et al., 2012). These elements should all form citrate complexes in the load and first rinse solution (a mixture of di-Ammonium-hydrogen-citrate and ammonia), which do not stick to the resin, and are therefore eluted to waste. Nickel, Zn, and Cu, bond with free ammonia and stick to the resin until eluted (Gall et al., 2012). The chemistry was altered to increase the volume of dAHC and ammonia in the load solution by a factor of two, to provide more citrate to bind matrix elements. This should improve the potential for all the relevant ions to be bound to the citrate and removed from the purified solution.

A set of 5 samples which had been put through both chemistry methods was analysed on the Thermo-Finnigan™ Element 2, for matrix elements and Ni to compare the cleanliness of each method. The samples from the initial method showed levels of Fe in most Ni cuts that were below a detection limit of 6.6 ng, making the [Fe]/[Ni] ratio <0.007. Calcium is the other matrix element of concern in the analysis of Ni. Gall (2012) suggests that an absolute maximum value of [Ca]/[Ni] =0.3, and ideally [Ca]/[Ni]<0.1 should be sought, as unlike Fe there is no correction that can be made during analysis. However, the level of Ca in the Ni cut from the method before recalibration was below this limit, suggesting another problem, or a larger sensitivity to Ca in new conditions of analysis. The method after recalibration lowered the ratio of the matrix elements to Ni in most samples and did not add to the blank. Therefore, the extended load method was used thereon. The extended load also enabled continuity between procedures for samples of differing sample volumes (which were not always in solution in the half-sized load), except the very lowest Ni concentration rocks (nephelinites).

Table 2-1

Concentrations for each measured matrix element relative to the measured Ni content in the sample. N = normal load solution as described by (Gall et al., 2012), el = extended load solution as used since April 2016. V, Co, Cu, Ga also analysed but below detection in all samples. DL = detection limit calculated by the dtandard deviation on repeated blank analysis multiplied by 3.

	^{24}Mg/ ^{60}Ni (wt)		^{27}Al/ ^{60}Ni (wt)		^{42}Ca/ ^{60}Ni (wt)		^{52}Cr/ ^{60}Ni (wt)		^{55}Mn/ ^{60}Ni (wt)		^{56}Fe/ ^{60}Ni (wt)		^{66}Zn/ ^{60}Ni (wt)	
	n	**el**	**n**	**el**	**n**	**el**	**n**	**el**	**n**	**el**	**n**	**el**	**n**	**el**
BHV02	0.013	0.017	0.004	0.048	0.176	0.071	0.002	0.004	0.002	0.004	< DL	< DL	< DL	< DL
DTS2	0.015	0.015	0.002	0.004	0.039	0.073	0.025	0.003	0.001	0.002	< DL	< DL	0.002	< DL
BIR1a	0.007	0.007	0.003	0.002	0.091	0.035	0.001	0.002	0.001	0.002	< DL	< DL	< DL	< DL
BD825	0.005	0.014	0.002	0.006	0.077	0.038	0.003	0.004	0.001	0.003	< DL	0.050	0.002	< DL
C235D	0.004	0.025	0.064	0.006	0.024	0.196	0.002	0.003	0.002	0.004	0.020	< DL	0.007	< DL

Resin-related organics in the sample after column purification adversely affected the performance of the mass spectrometer, and this necessitated the development of a method for destroying these organic compounds after the final column. Dissolution in concentrated HNO_3 and subsequent dry down was used, and repeated as necessary. Any resin observable in the sample required centrifuging to allow a resin-free sample solution to be removed.

2.2.2 Method of Purification of nickel used in this study

The ion exchange method used for this study is summarised in Table 2-3, Table 2-4, Table 2-5.

Ultrapure MQ water (18.2 MΩ/cm) was produced by Millipore Elix® water purification system and an in lab Millipore MilliQ® Advantage A10 QPod. Acids were purified by in house sub-boiling distillation (in quartz for HCl and HNO_3, in PTFE Teflon for HF), and were periodically blank tested. Both HCl and HNO_3 concentrated stocks were titrated (for values see Appendix 7.2) upon receipt and dilutions were made by volume using MQ water.

The chemistry also used ammonia (NH_3, concentrated (25%)), acetone ($(CH_3)_2CO$, analytical grade or higher), and hydrogen peroxide (H_2O_2, (ultrapure <10ppt levels of trace elements), 30% solution). Dry reagents included oxalic acid (dry commercial grade, purified in house by

dissolving in MQ water and re-precipitating, made up to 0.5M), di-ammonium-hydrogen-citrate (dAHC, dry commercial grade and made up to 1M in MQ), and di-methylglyoxime (DMG, dry commercial grade, made up to 0.105M in acetone, discarded once discoloured). The DMG should be collected as a separate waste product to other reagents in this chemistry. The dry DMG powder was weighed and diluted with acetone into a stock solution of 0.105M, and discarded after 2 weeks or when discoloured from clear. Stock solutions of dAHC and oxalic acid were inherited from previous work. Reagents H_2O_2, and NH_3, as well as stocks of ICPMS element standards and the double spike, were stored in refrigerated conditions.

All mixtures of these reagents were made by volume, into clean FEP Teflon bottles. For the first column, a mixture of 0.1M dAHC and 3M NH_3 is needed with MQ dilution. The second column required mixtures to be made of 0.1M HCl and 0.05M oxalic acid, 0.05M HCl and 95% acetone, and 0.5M HCl, 95% acetone and 0.1M DMG. The final column required a mixture of 6M HCl and 0.05% H_2O_2. Mixtures involving H_2O_2, and those including both HCl and acetone were made immediately before use and then discarded, because the mixtures degraded.

Pre-cleaned PFA Teflon vials (Savillex™) were used to hold samples, at all times when not on the column. All columns were made in house, with shrink-wrap Teflon and moulds (for dimensions see Table 2-2) made specifically for the Ni chemistry specifications, pre-cleaned prior to use. The first two columns used a chloride form cation resin (Bio-Rad®, AG50W-X4, 200-400 mesh), and the final column used a chloride form anion resin (Bio-Rad®, AG1-X8, 200-400 mesh). All resins were pre-cleaned in bulk, pre-cleaned once in the column, and finally conditioned with the same solvent as the sample was to be loaded in.

Table 2-2

Dimensions for column moulds used in the Ni purfication.
NB the 1st column uses a laregr size of shrink Teflon than the two smaller sizes.

	Volume of column (exc. frit)	Column diameter (mould)	Column length (mould)
	µl	mm	mm
Column 1	615	Tapered 4.4-3.5	50
Column 2	250	3.5	25
Column 3	120	3.5	12.5

Before each column, it was necessary to convert the sample to chloride form by sequential dissolution in and evaporation of, 6M HCl, before the load solution was made up (Gall et al., 2012). In load solutions involving dilute HCl, it was necessary to re-dissolve the sample in a small volume of more concentrated HCl, and add MQ to dilute to the correct concentration and volume. If the sample was not in solution in the correct volume of dilute HCl an increase in the volume of load solution was required. After each column, the sample was refluxed at 150°C in concentrated HNO_3. The resin was discarded after each use, due to breakdown of the resin structure by the reagents (Gall, pers comm, 2015). The mixtures used in Columns 2 and 3 had to be made immediately before use; and not stored (Gall, pers comm, 2015).

In column 1 (see Table 2-3), the load solution was dilute HCl, di-ammonium-hydrogen-citrate (dAHC), and ammonia. On this column, Ni, Zn, and Cu (the more electronegative divalent cations) bound with ammonia and stuck to the resin, other elements (such as Mg and other alkaline earths, Fe and most other d block elements, and Al) formed non-sticking citrates (Gall et al., 2012; Strelow, 1990). If dAHC were not added before ammonia, Mg and Ca would precipitate as hydroxides. To allow the dAHC time to react fully with the sample 30 minutes was allowed between adding it and the ammonia. Once the load solution had gone through the column, a short rinse of the dAHC and ammonia mixture ensured all matrix material had interacted with the resin, and the citrate complexes had eluted. A rinse of 0.4M HCl ensured all excess ammonia was removed from the resin to waste. The Ni, Cu, and Zn, were eluted in a 3M

HCl solution into a Teflon vial, and dried at 125°C. Concentrated HNO_3 was then added to the sample to break down the Ni-ammonium complex (Gall et al., 2012).

In column 2 (see Table 2-4), the load solution was dilute HCl and oxalic acid. On this column, elements in any valence state greater than 2+ (residual ammonium salts, and remaining Mg, Ca, Na, Al, Ti, and Cr) formed non-sticking oxalic complexes (Gall et al., 2012; Strelow et al., 1972). Once the load solution had gone through the column, short rinses of the HCl and oxalic mixture ensured that all matrix material had interacted with the resin, and >2+ elements had eluted. Remaining divalent elements were eluted to waste as chloro-complexes with a second set of short rinses of HCl and acetone (Gall et al., 2012; Victor, 1986). This also conditioned the resin for the final elution of Ni. The Ni was then selectively eluted in a solution of dilute HCl and DMG in acetone into a Teflon beaker that contained 0.15 ml MQ, and dried at 85°C. The MQ and low drying temperature prevented volatilisation of Ni in acetone, and splattering of the sample during drying. Concentrated HNO_3 was added to the sample to break down the Ni-DMG complex (Gall et al., 2012), which required 30 minutes until the reaction was completed. The sample was then dried, and refluxed in concentrated nitric acid overnight.

In column 3 (see Table 2-5), the only anion resin column, the load solution was 6M HCl and dilute H_2O_2. Nickel was eluted immediately, whereas Fe formed a sticking complex in 6M HCl (Gall et al., 2012). Once the load solution had gone through the column, a short rinse of the HCl and H_2O_2 mixture ensured that all Ni had eluted into a Teflon beaker, and dried at 120°C. Concentrated HNO_3 was added to the sample to convert the Ni to nitrate form (Gall et al., 2012), and dried and re-dissolved in concentrated HNO_3 until no organics remained in the sample. A visual check for any grains of resin in the sample was made, and if present, was removed prior to analysis.

Table 2-3

Summary of process of purification of Ni in column 1

Column 1	Column Volume 610µl	Resin	Bio-Rad® AG50W-X4 200-400 mesh	Notes
	Reagents		Volume (ml)	
Equilibration	0.1M NH_4-citrate + 3M NH_4		4	
Load	0.5M HCl + 0.1M NH_4-citrate[§] + 3M NH_3		6	
Cleaning Step 1	0.1M NH_4-citrate + 3M NH_4		1	Citrate complexes eluting
Cleaning Step 2	0.4M HCl*		1	Citrate complexes eluting, and excess ammonia
Elution into clean PFA vials	3M HCl		2	Ni, Zn, Cu eluting
	Temperature			
Dry to small drop	125°C			
Reflux in conc nitric Min 14 hours	150°C		0.3	

Table 2-4

Summary of process of purification of Ni in column 2

Column 2	Column Volume 250µl	Resin	Bio-Rad® AG50W-X4 200-400 mesh	Notes
	Reagents		Volume (ml)	
Equilibration	0.1M HCl + 0.05M oxalic acid		1	
Load	0.1M HCl + 0.05M oxalic acid		1	
Cleaning Step 1	0.1M HCl + 0.05M oxalic acid		3 in 1ml rinses	Elutes elements in >2+ valence state
Cleaning Step 2	0.5M HCl + 95% acetone		3 in 1ml rinses	Elutes elements in 2+ valence state (except Ni)
Elution into clean PFA vials 0.15 ml MQ in vial	0.5MHCl + 95% acetone + 0.1 M DMG		1	Elute Ni
	Temperature			
Dry	< 85°C			
React with conc nitric acid for 30 mins	-		0.1	
Dry	125°C			
Reflux in conc nitric Min 14 hours	150°C		0.1	

Table 2-5

Summary of process of purification of Ni in column 3

Column 3	Column Volume 120µl	Resin	Bio-Rad® AG1-X8 200-400 mesh	Notes
	Reagents		Volume (ml)	
Equilibration	6M HCl + 0.05% H_2O_2		0.5	
Load into clean PFA vial	6M HCl + 0.05% H_2O_2		0.2	Ni elutes immediately
Elution	6M HCl + 0.05% H_2O_2		0.2	
Add then dry @125°C	Conc nitric acid		0.1	
Add then dry @125°C	Conc nitric acid		0.1	

2.2.3 Adaptation of procedure for investigation of cosmogenic effects

Investigation of cosmogenic effects requires a completely separate processing environment from mass dependent work. If any double spike, with its artificially altered isotopic composition, is incorporated into a sample, it will lead to unreliable results.

Samples for investigation of potential cosmogenic effects were, therefore, processed entirely separately to mass dependent samples. The purification of these samples took place in a laminar flow hood that had been in contact with Ni double spike, which was cleaned before use, along with cleaned column racks and new waste beakers. The Teflon used for the chemistry, including the Teflon micro-columns, had never been in contact with Ni double spike, and all other Teflon were thoroughly cleaned and used minimally. Dispensing containers for common reagents were replaced with those that had never seen double spike, and clean new column racks were also used, as well as new waste beakers.

Samples for this investigation were either lunar samples prepared from homogenised powder or lunar samples prepared from matrix column cuts of a Zn purification column (performed by

Sean Hopkins), plus two terrestrial standards. The matrix cuts were stored in centrifuge tubes for some time before the Ni chemistry, and dried in PFA Teflon. Powdered samples were weighed and dissolved as described previously.

The purification procedure was exactly as for investigation of mass dependent effects, but more natural Ni was needed to compensate for the lack of additional Ni from double spike. More Ni was able to be used for the samples from Zn matrix column cuts because the solutions were otherwise going to waste, whereas the powders were pristine and more valuable. The amount of Ni needed was calculated so that the smallest analysed isotope (mass 61) exceeded 200mV during analysis to minimise the error on the peak.

2.3 Mass spectrometry

2.3.1 Introduction

Mass spectrometry

The mass spectrometer separates ions and charged molecules by their mass/charge ratio (m/z) based on their behaviour upon being accelerated through electric and magnetic fields. The mass spectrometer has a method of sample introduction, a source of ions, a method of ion separation, and a collector that measures the ions in a specific m/z.

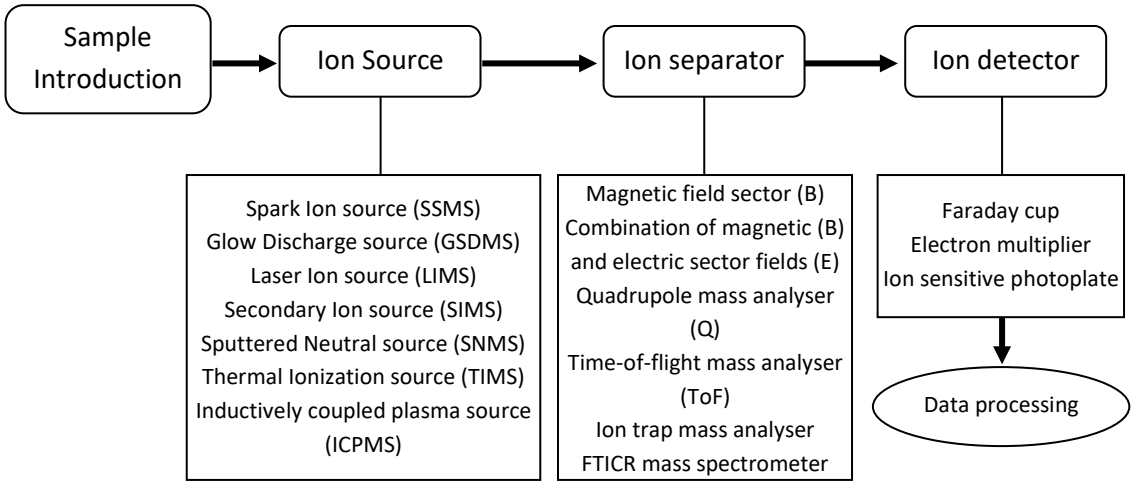

Figure 4

Adapted from Fig 1.1 (Becker, 2007), diagram of basic mass spectrometer structure with some variations available for each part

Mass spectrometers were invented over 100 years ago and most modern designs of mass spectrometer are still based on those of Nier (1940). Originally, mass spectrometry was only aimed at analysing isotopic abundances, however techniques and instrumentation developed to allow investigation of isotopic ratios as well. There are now many types of mass spectrometer including secondary ion MS, thermal ionization MS, accelerator MS, and inductively coupled plasma MS. In SIMS the sample is ionized by an incident primary ion beam releasing secondary sample ions that are then analysed, whereas in TIMS the sample is ionized by heating of an metal ribbon by a high current. Accelerator MS uses acceleration to high velocities to separate rare ions from ions of similar mass. ICPMS was developed in 1980, and is now one of the most versatile mass spectrometry techniques (Becker, 2007). One advantage of ICPMS is the ability to have varied sample introduction methods, for example, ICPMS can be coupled to a laser ablation system.

The ICPMS mass spectrometer utilises a quartz torch to support the plasma, which is surrounded by a copper load coil at one end. An RF generator supplies a high frequency current through the coil at high power, producing an electromagnetic field. A high-voltage spark ignites the plasma, stripping electrons from the Ar, which are then accelerated within the RF field. The collisions caused by this start a chain reaction of released electrons, which then collide and in doing so heat the gas to 5000-8000K, producing the plasma. This high temperature can ionize most elements, if the plasma is sustainable by constant gas and energy supply.

Solution samples are introduced to the ICPMS in one of two main ways. The first is by direct aspiration of the sample solution by a self-aspirating PFA Teflon nebuliser, which sprays a fine aerosol into an externally cooled spray chamber, which then transfers the sample to the plasma. This method is very reliable, and yields a stable ion beam, however it has a very low transfer efficiency (Gall, 2011). The second method of sample introduction uses a desolvation system. This system uses a PFA Teflon nebuliser as well; however, the desolvation system uses a heated spray chamber, and the aerosol partly evaporates, producing smaller droplets. These droplets are then transported through a heated Teflon membrane that separates the analyte from the solvent.

This method reduces the solvent amount entering the plasma, thereby increasing the sensitivity of the mass spectrometer, and reduces isobaric interferences from solvent molecules (Gall, 2011).

Once the sample is inside the torch, the plasma ionizes the constituent atoms, which is then extracted through the two cones (sampler and skimmer) of the interface (also known as double cone extraction), by the pressure difference between the plasma at atmospheric pressure and the mass spectrometer at high vacuum. The sample ions are then accelerated as an ion beam by potential differences and focussed by optical lenses into the mass analyser. The extraction of ions through the interface produces significant instrumental mass fractionation (Gall, 2011), resulting in the mass bias that needs correcting for with methods described in section 2.3.3.

Development of Multi Collector ICPMS (MC-ICPMS) allowed the simultaneous analysis of multiple isotopes by having numerous collectors receiving different m/z ratio ions at once. Use of multiple collectors allowed beam fluctuations (e.g. due to plasma flicker) to be cancelled out, producing a more exact ratio measurement, and therefore higher precision. The MC-ICPMS can analyse a broader range of measurable elements; including those with high ionization potential, which are difficult to analyse by TIMS (Halliday et al., 1998). An MC-ICPMS can be fitted with either laser ablation or solution aspirators (such as in this work), which allows flexibility in sample introduction. The MC-ICPMS also has superior ionisation efficiency and achieves better peak shapes than preceding mass spectrometers (Halliday et al., 1998), and quickly became the method of choice for analysing geochemical samples in most isotope systems.

The MC-ICPMS used in this work uses a double focussing magnetic sector for ion separation (Gall, 2011). The technique uses magnetic sector separation of mass/charge. The plasma source produces ions with a significant energy spread that the peak shape will be degraded without energy focusing using an electrostatic analyser (ESA) (Halliday et al., 1998).

Every mass spectrometer has a different capability for mass resolution, usually expressed as $m/\Delta m$, which shows how small a mass unit is separable for analysis. The MC-ICPMS used here allows for three different modes of resolution to be used: low, medium and high. In low

resolution mode the m/Δm equals ~400, with the source and alpha slits fully open. Reducing the width of these slits allows for higher resolution (medium resolution m/Δm equals ~ 4000, and in high resolution m/Δm equals ~8000) by cutting off the sides of the ion beams. However, if low resolution allows 100% transmission of the beam, then at high resolution only 5% of the beam is left (Gall, 2011). Therefore, a balance between resolution and transmission is needed to make the most of any given sample. A compromise between increasing resolution without reducing transmission can be made with 'pseudo-high resolution', whereby an interference that is not sufficiently resolved from the peak of interest can have its effects removed by analysing on an interference-free shoulder. This technique is further described in section 2.3.5.

Analysis of nickel

The investigation of radiogenic and nucleosynthetic effects in nickel isotopes in planetary materials has used various types of mass spectrometers, including thermal ionization mass spectrometry (TIMS) (Morand & Allègre 1983; Shimamura & Lugmair 1983; Birck & Lugmair 1988; Shukolyukov & Lugmair 1993), and secondary ion mass spectrometry (SIMS) (Tachibana & Huss 2003; Guan et al. 2004; Mostefaoui et al. 2005; Tachibana et al. 2006), and multi-collector inductively-coupled-plasma mass spectrometry or MC-ICPMS (e.g. Bizzarro et al. 2007; Regelous et al. 2008; Steele et al. 2012). With the development of MC-ICPMS came investigation of mass dependent fractionation, as MC-ICPMS provides the ability to control mass bias and correct for isobaric interferences, to achieve significantly better precision on Ni isotope ratios. Therefore, since 2005, Ni isotopes have been measured almost entirely by MC-ICPMS (Moynier et al. 2005; Quitté et al. 2006; Cook et al. 2006; etc).

Analysis by SIMS can provide high spatial resolution but suffers from relatively poor precision (Cook et al., 2006). Direct analysis of solid samples by SIMS is also vulnerable to isobaric interferences on ^{58}Ni by ^{58}Fe and on ^{64}Ni by ^{64}Zn making it difficult to measure these Ni isotopes. Resolution on SIMS is only sufficient to identify ^{60}Ni anomalies in samples with high Fe/Ni ratios, such as troilite (Quitté and Oberli, 2006).

Analysis by TIMS allows for the measurement of all Ni isotopes and for the correction of ^{58}Fe and ^{64}Zn interferences, with typically better precision than SIMS, but only on the ^{60}Ni/^{58}Ni ratio (Cook et al., 2006) for samples with low Fe/Ni ratio. Other Ni isotope ratios on TIMS have errors of several epsilon units (Birck and Lugmair, 1988; Morand and Allègre, 1983; Shimamura and Lugmair, 1983). Double focussing and MC TIMS instruments were used to some success to identify ^{60}Ni excesses in some planetary materials, but these were hard to resolve.

A comparison between MC-ICPMS and TIMS was undertaken by Chen and Papanastassiou (2006) who came to the conclusion that MC-ICPMS introduced more interferences despite the benefit of better ionisation capabilities. However, high resolution MC-ICPMS provides the ability to measure all Ni isotopes and correct for the isobaric interferences, with significantly better precision on all Ni isotope ratios.

Tanimizu and Hirata (2006) analysed samples using Cu-doping for correction of instrumental mass bias, as did Moynier and co-workers (2007). Instrumental mass bias correction by double spike analysis has been used extensively of Ni including (Cameron et al., 2009; Gall et al., 2012; Gueguen et al., 2013; Spivak-Birndorf et al., 2018). All studies that have used the double spike analysis technique for correction of instrumental mass bias have used isotopes 61 and 62. All studies except Moynier (Moynier et al., 2007), have normalised to SRM986, however, due to work published on the fractionation induced in production of pure Ni metals and reagents (Tanimizu and Hirata, 2006), the composition of SRM986 is not representative of terrestrial reservoirs (Elliott and Steele, 2017).

The MC-ICPMS used to analyse Ni in this work is a Nu Plasma High Resolution in the Department of Earth Sciences, University of Oxford. It is used currently to measure Ni, V, Li, and Sr. The set up includes a microcentric PFA nebuliser and a DSN-100 from Nu instruments, with a set of Ni type B cones (further details in section 2.3.5). It has 12 Faraday cups arranged in a fixed array custom designed for measuring low-medium mass isotopes (see 2.3.5). This particular arrangement allowed simultaneous analyses of six isotopes with ion beams in every

third collector, including monitoring of ^{57}Fe in addition to the four Ni isotopes of interest (58, 60, 61, 62). From monitoring ^{57}Fe a correction can be made for any ^{58}Fe acting on the Ni peak as these peaks are not resolvable. Testing of this correction has shown this to be robust and necessary (Gall et al. 2012).

2.3.2 Delta notation

The delta (δ) notation is a way to express the stable isotopic ratios variations. The delta is reported in per mill (‰) relative to a standard (Equation 1). The standard used for nickel is Standard Reference Material (SRM) 986 from the National Institute of Standards and Technologies (NIST).

Equation 1

$$\delta^{\frac{60}{58}}Ni = \left[\frac{\left(\left(\frac{^{60}Ni}{^{58}Ni}\right)_{sample} - \left(\frac{^{60}Ni}{^{58}Ni}\right)_{SRM986}\right)}{\left(\frac{^{60}Ni}{^{58}Ni}\right)_{SRM986}}\right] \times 10^3$$

2.3.3 Instrumental mass fractionation correction

Double Spike Analysis Theory

A spike in isotope geochemistry is a solution, which contains a known concentration of a particular element, and is enriched in one of its isotopes, to change the isotopic composition. Therefore, the term ‘double spike’ refers to a mixture of two such spikes so that the resulting solution has a known concentration of the element and a known ratio of two enriched isotopes.

By adding a known quantity of double spike to the sample before processing, the fractionation induced by the instrument and/or chemistry can be corrected for during deconvolution of the data. Once equilibrated the added Ni behaves in exactly the same way as the natural Ni. The double spike analysis technique can also allow accurate determination of the natural concentration of the element of interest in the sample with sufficiently accurate weighing

information on the sample and spike amounts, through isotope dilution (as described in Faure et al. 2005).

Gall (pers comm, 2016) calibrated the spike solution used throughout this work in 2013. The spike solutions were obtained from the Oak Ridge National Laboratory, and issued with assays of purity. The double spike used enriched ^{61}Ni and ^{62}Ni with a ratio ^{61}Ni/^{62}Ni of 0.4386 (Gall, pers comm, 2016). The Ni concentration in the mixed spike was 101 ppm (Gall, pers comm, 2016). The ratio of sample Ni (natural) to spike Ni was 0.4:1, and outside of the acceptable range reliable data could not be produced (Gall et al., 2012).

2.3.4 Interferences

One of the main problems with analysing any isotopic ratio is spectral interferences, as discussed previously. Interferences can be other isotopes of other elements with the same mass, doubly charged ions, or molecules that have approximately the same charge/mass ratio as the isotopes of interest. Molecular interferences can come from combinations of Ar, H, O, N etc. from the Ar support gas and air entrainment through the cones. Polyatomic interferences from uptake of impure sample solutions, and matrix effects are dealt with previously. It is necessary regardless to minimise the production of interferences in the plasma through tuning and proper calibration of the purification chemistry, as discussed previously, to limit the presence of available ions to form interferences.

One of the major interferences on the Ni masses of interest comes from the isobaric interference of ^{58}Fe with ^{58}Ni. For this reason Gall (2012) developed an online iron correction using the voltage of 57 to correct for the amount of the 58 voltage caused by Fe. Iron might come from the desolvator, internal parts of the mass spectrometer, or in the analysis solution (Gall et al., 2012), although the chemistry is maximised specifically to reduce this. Testing of this correction has shown this to be robust and necessary (Gall et al. 2012) up to Fe/Ni = 2.

The other major interferences on Ni are the presence of $^{40}Ar^{18}O$ and/or $^{40}Ar^{17}OH$ on mass 58 and similarly $^{40}Ar^{17}O$ and/or $^{40}Ar^{16}OH$ on mass 57. The former can be seen on the peak scan in Figure 6. These polyatomic interferences on the masses 58 and 57 therefore made the centre peak offset monitoring (as described in section 2.3.5) necessary to maintain alignment of the interference free shoulders for the duration of an analysis run, and allow the Fe correction to work as intended.

2.3.5 Analytical set up

The Nu Plasma HR MC-ICPMS has a specially adapted array of collectors designed for measuring low-medium mass isotopes. This arrangement (see Figure 5) allows simultaneous analyses of six isotopes with ion beams in every third collector, allowing the monitoring of ^{57}Fe, for the previously mentioned Fe correction, as well as the four Ni isotopes of interest.

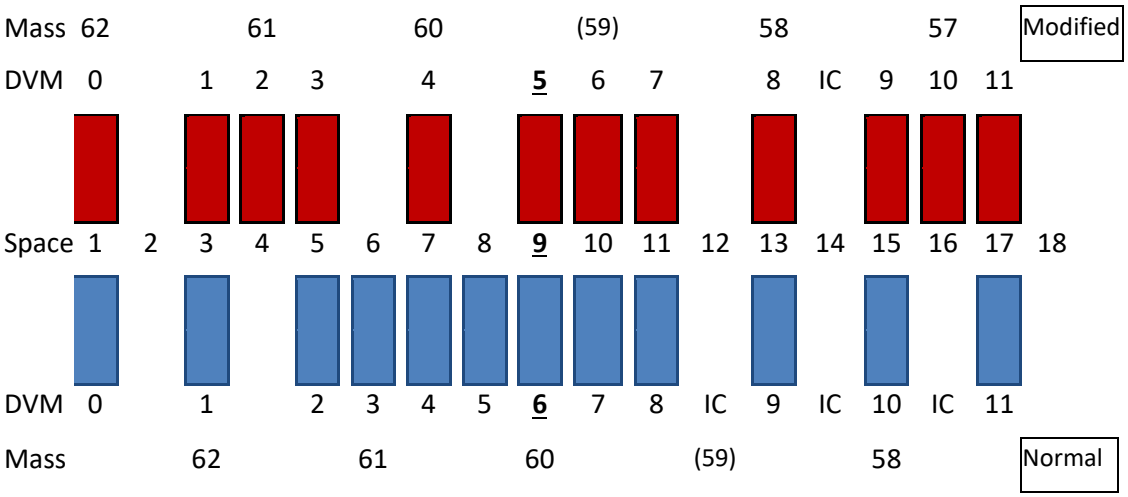

Figure 5

Collector array configuration on the mass spectrometer used in this work (top) compared to normal array (bottom) which could measure Ni only without ^{57}Fe.
IC = Ion counter. Bold and underlined = axial collector. Numbers 57 – 62 indicate the placement of the ion beams of these mass units. Numbers 1-11 = the DVM numbers i.e. in the mass spectrometer used in this work arrangement mass beam 58 is measured in DVM 8.

The normal amount of natural Ni used for analysis in medium resolution is ~1 µg, with 2.5 µg of added spike (ratio 0.4:1). The faraday cup resistors are 10^{11} Ω and can measure currents up to 10^{10} A, equivalent to an ion beam of 10V. The total Ni received as volts in the detectors was usually ~14V. Lower natural Ni has been successfully analysed where sample material is extremely limited, or fewer replicates have been used to maximise the available signal in volts.

Sample solution is introduced to the plasma using a desolvator (DSN-100 from Nu instruments), which is cleaned regularly. The microcentric PFA Teflon nebuliser used is reserved for only measuring Ni with double spike analysis. Nebuliser 75-1141 (actual flow rate 90-100 µl/min), which had previously been used for Mo analyses, has been used exclusively for Ni isotope measurements, since February 2016.

The set of cones used (Ni, Type B) are reserved for only measuring Ni. These are cleaned as necessary, especially if instability or problematic results are an issue. Nickel background from the cones and internal steel parts was investigated by Gall (2012) and found to be constant, and no bias has been detected between analyses using on-peak-zero background measurement in the blank acid and those done using background measurement by ESA deflection (Gall et al., 2012). In this study, the background acid has a total Ni volts of <1mV relative to ~14V total in analyses (sample and spike). The concentration of all samples was adjusted to within ~10% (or better) of the bracketing SRM and each other.

Medium resolution and pseudo-high-resolution (centre peak offset monitoring)

It is necessary to measure Ni in medium resolution mode because there are numerous interferences that must be resolved. Medium resolution reduces the sensitivity of the instrument, increasing the amount of Ni needed to measure a sample's isotopic Ni composition successfully. Nickel is susceptible to perturbations in delta value with interferences, especially CaO^+ and ArO^+; and problems are also known be caused by TiO^+, $MgAr^+$, and $ArOH^+$ (Gall et al., 2012). Testing has suggested that the greatest interference and effect on delta is due to interferences on

the masses of 58 and 57, as previously mentioned. This necessitates measuring on the shoulder of the peak in a narrow area of interference free Ni mass.

There is a risk when measuring on a narrow interference free shoulder that even a small amount of drift in the magnet can affect the mass where the measurement is being undertaken, by causing the analytical mass to drift off the peak entirely or into the part of the peak that also has the interference. In this work, programming was developed and used to centre the 58 peak with each measurement and move a set offset from there to measure on a part of the peak seen to be interference free. This value of the offset was not constant and was determined before beginning measurements in any session. This was done by scanning a solution with a low concentration of Ni (for 58) and Fe (for 57), and identifying the field number of the interference free shoulder compared to the field number of the peak centre. The difference between these was the offset to

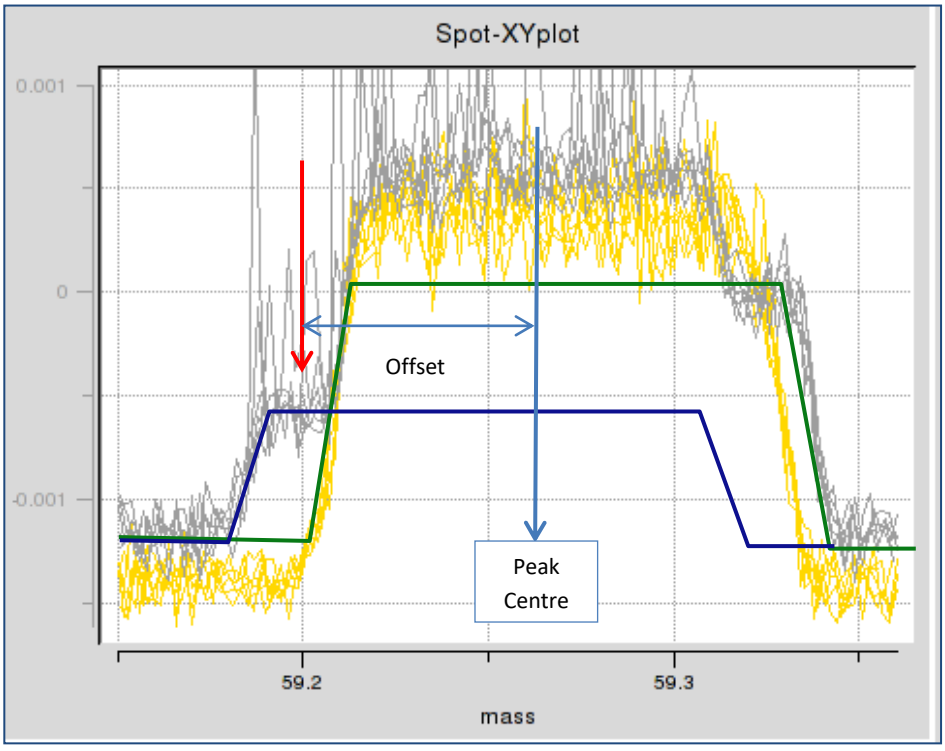

Figure 6

Screenshot of effect of interference on an extremely low concentration Ni solution highlighting the narrow interference free shoulder (red arrow). The grey line indicates the readout of the peak scanning over the mass range of interest of the 58 mass. True Ni is highlighted by the blue peak, and the green indicates the interference's peak. Only when sitting on the interference free shoulder can we get accurate and reproducible results, however at normal Ni concentrations of solutions being measured the interference is optically swamped and cannot be seen, but it still affects the delta measurements adversely.

be input into the programme to measure Ni without interference related perturbations.

The centre peak monitoring could only check the 58 peak. Therefore the other peaks were not perfectly aligned with the 58 during tuning in order that there was sufficient drift room on the other masses. However, the 57 peak was aligned with the 58 peak that allowed the interference on 57 to be removed from influencing the Fe correction made using the voltage from mass 57.

Typical analytical protocol

Between analyses, the system is washed with clean dilute HNO_3 from three separate wash stations for a total of 5 minutes. Analysis of total Ni in these wash stations are measured prior to and after each run of samples. These blanks have never shown any appreciable contamination of Ni into the wash stations during a run. After the dilute HNO_3 wash, ESA deflection, for 20 seconds prior to measurement, was used to measure electronic background noise. All isotopes were measured simultaneously in static collection mode. Each measurement consisted of 40 cycles of 10s integrations of the ion beam intensity.

Initial tuning used an unspiked 20 ppb Ni tuning solution, to find optimum torch and gas flow, and to transition to medium resolution. A solution of leftover spiked SRM is used to tune peak shape and check all other settings are optimum. A very dilute solution of Ni and Fe is used to find the optimum peak offset for the pseudo-high resolution. Several analyses of leftover solutions of SRM and secondary standards are used to check the tuning, and that the method is producing the correct results before a run begins.

In order to account for the differing conditions in the plasma between and within runs, each sample was bracketed between analyses of the SRM986, at the same concentration as the samples. Analyses of several in house secondary standards and USGS rock samples were interspersed within each run of samples. The Fe correction was tested by analysis of both secondary standards (Fe-Ni Sulfides) that had not been purified through chemistry. There was

no difference between the resulting delta of these solutions and the solutions that had been purified, confirming the Fe correction worked correctly.

2.3.6 The nickel blank

One column per chemistry session contained a full procedural blank. The Ni in this column was the sum of the Ni contamination in all of the reagents used in the chemistry from dissolution to dilution for analysis. These blanks were analysed periodically on the Thermo-Finnigan™ Element 2, or the PerkinElmer™ NexION Quad 350D and have generally shown an insignificant Ni blank of <3.6 ng, which compared with an average natural Ni load 1000 ng plus. Blanks for samples that used a large load solution (~10 times normal) to the 1st column to keep the samples with large amounts of matrix elements due to low Ni concentration showed higher blanks by a factor of ~2.

Table 2-6

Mass of Ni analysed in total procedural blanks from the chemistries analysed during the first 18 months of this work

Date of chemistry	Instrument	Volume of 1st column load	Ni (ng)
17-Apr-16	Element	6	3.586
04-Apr-16	Element	6	2.231
13-Mar-16	Element	6	2.631
10-Aug-16	Element	6	3.038
18-Oct-16	Element	6	2.753
05-Nov-16	NA	6	NA
30-Nov-16	Element	6	2.966
24-Jan-17	Quad	6	2.492
31-Jan-17	Quad	6	2.774
15-Mar-17	Quad	60	8.188
12-May-17	Quad	6	2.390
17-May-17	Quad	45	8.587
15-Jun-17	Quad	6	3.557
20-Jun-17	Quad	6	1.943
23-Jun-17	Quad	40	7.915
09-Oct-17	Quad	6	2.135
13-Oct-17	Quad	6	2.588
Further procedural blanks not analysed			

There is a higher contribution to the blank in a sample dissolved using the Parr Bomb technique than those dissolved using a hotplate only digestion. a digestion using a Parr bomb.

Table 2-7 shows a direct comparison between two different bomb digestions (using different vessels) and a standard hotplate digestion. The standard blank for a hotplate digestion is up to two orders of magnitude less than a digestion using a Parr bomb.

Table 2-7

Comparison of Ni blank between hotplate dissolution and dissolution in high pressure Parr Bomb

Digestion Method	Instrument	Ni (ng) after digestion only
Hotplate	Element	0.080
Bomb (3)	Element	2.190
Bomb (1)	Quad	0.775

2.3.7 Reproducibility

In the literature published values of well known, easily acquired rock standards, such as USGS reference materials (see Table 2-8), show limited variation since the first paper on Ni isotopes to analyse an international rock standard (Cameron et al., 2009). This indicates that despite the many different methods currently in use for extracting and analysing stable Ni, reproducible data can be produced.

In this study, USGS reference materials have been analysed in each analytical session, with at least one sample per chemistry being a USGS reference material. Averages are displayed below, with comparable published data (Table 2-8). The results for the analyses from this study are all within error of the published values (excluding (Cameron et al., 2009), for which the deltas are outside the range of all subsequent studies. The 2SE of this study, which takes into account the greater n than in published studies prior, is comparable to earlier work. Cameron (2009) did not present the number of analyses in their average, and the 2SE could not be calculated.

Table 2-8

Table of published values for $\delta^{60/58}$Ni in ‰ normalised to NIST SRM 986.
2se is uncertainty as 2 times the standard deviation of the measurements divided by the square root of the number of analyses. 'n' is the number of separate analyses of the sample. In most cases this is separate digestions and chemistries also, for some data this is not clear. For my work 'n' represents the total number of analyses from multiple runs of each dissolution. PCC1 and DTS2b is the same dissolution with separate chemistry, BHVO2 and BIR1a are from numerous dissolutions.

	BIR1a			BHVO2			PCC1			DTS2b		
	δ^{60}Ni	**2se**	**n**	**δ^{60}Ni**	**2se**	**n**	**δ^{60}Ni**	**2se**	**n**	**δ^{60}Ni**	**2se**	**n**
Average all published	**0.14**			**0.05**			**0.18**					
Average excluding (Cameron et al, 2009)	**0.14**			**0.039**			**0.128**					
Cameron et al, 2009				**0.13**			**0.34**					
Gall et al, 2012	**0.13**	0.01	68	**0.05**	0.01	90	**0.12**	0.012	34			
Gueguen et al, 2013	**0.12**	0.02	3	**0.01**	0.01	11	**0.12**	0.022	5			
Ratie et al, 2015				**0.01**	0.01	4						
Chernonozhkin et al, 2015	**0.19**	0.01	2	**0.08**	0.01	5						
Steele et al, 2012										0.128	0.040	4
L. Gall Pers Comm, 2015	**0.120**	0.011	40	**0.045**	0.008	35	**0.145**	0.012	15			
This study	**0.147**	0.013	22	**0.028**	0.010	39	**0.145**	0.014	19	**0.157**	0.016	16

The effects of fractionation by the column purification itself were tested by comparing SRM986, Kambalda, and Sudbury, which had all been through chemistry, with the bracketing standard of SRM986 that had not been through chemistry. This is shown in Table 2-9. The results show no difference within error between the samples that have passed through ion exchange and those that have not, therefore, no mass dependent fractionation occurs during ion-exchange purification. The error on the secondary samples that have not been through chemistry is greater, because the high Fe content in these samples increases the error on the reproducibility.

The error presented throughout this work of ±0.06‰ is 2SD on total number of analyses of rock standards (processed through the same column procedure), and therefore is most appropriate. The full number of analyses for the calculation of this is presented in Appendix 7.4, where each number (n) is the product of 30 replicates. Where data tables present a 2sd and n this is the

replicates of the samples where 2sd is on the sample means of the number of replicates, where each replicate is 30 ratios.

Table 2-9

Table comparing the Ni isotopic compositions of secondary standards used in this study (through chemistry) and in previous work in this department by L. Gall (pers. comm).
The SRM (column) is a test of SRM through the whole chemistry with the samples bracketed to the SRM without chemistry used to bracket all samples in this study. The isotopic composition is within error of zero (the defined value of SRM986) showing no fractionation of Ni occurs during processing in the Ni purification columns.

	SRM			Kambalda			Sudbury		
	$\delta^{60/58}$Ni	2SD	n	**$\delta^{60/58}$Ni**	2SD	n	**$\delta^{60/58}$Ni**	2SD	n
L. Gall Average				**-1.03**	0.083	25	**0.75**	0.082	45
This study average with chemistry	**0.018**	**0.058**	**29**	**-0.891**	**0.064**	**66**	**0.771**	**0.049**	**60**
This study average without chemistry	**0.000**	by definition		**-0.888**	**0.088**	**52**	**0.761**	**0.074**	**53**

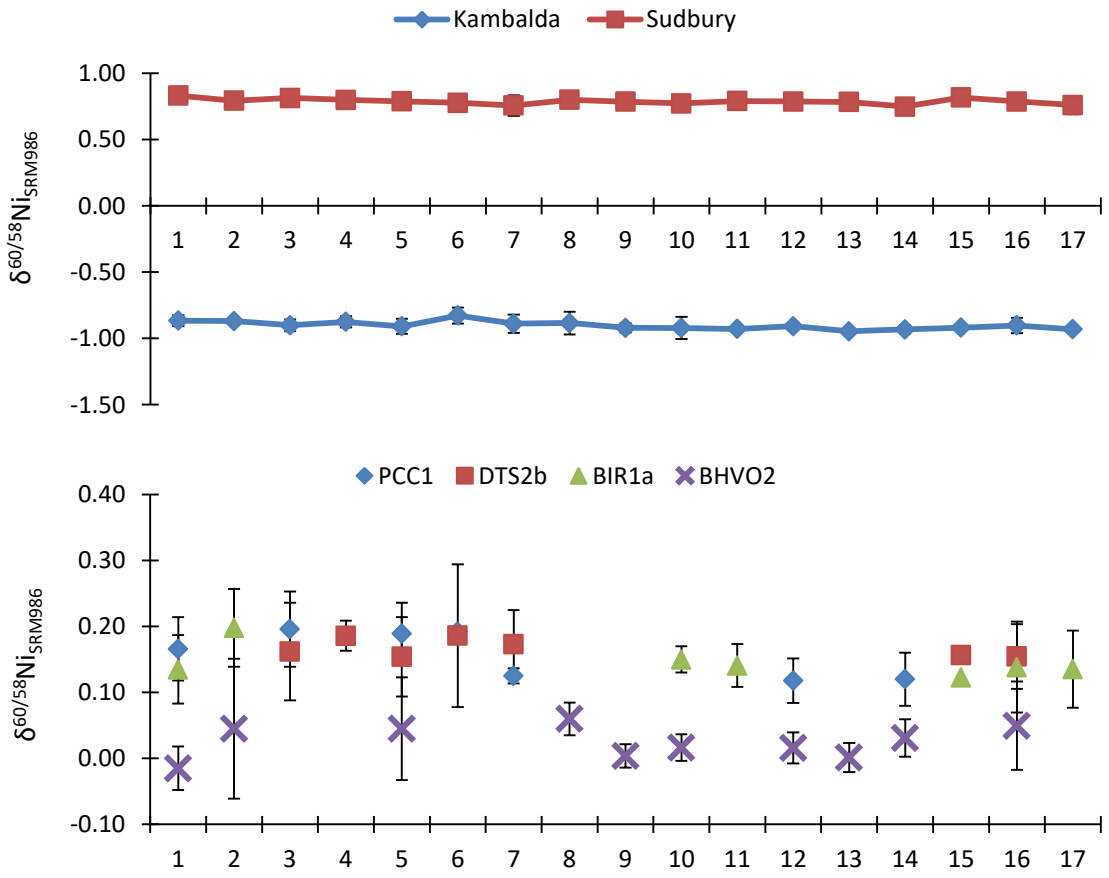

Figure 7

Nickel isotopic composition for secondary standards (top) and USGS reference materials (bottom) through time. Each data point is the result of numerous analysis within a single run.

As referred to in section 2.1.1, if the Ni concentration in the weighed sample was high enough that double spike would be wasted if all the weighed sample was spiked, or if a Ni concentration needed to be determined, the double spike could be added to an aliquot after dissolution. To test whether there is a difference in those samples spiked at dissolution, and those spiked onto an aliquot, a sample of USGS standard BIR was spiked prior to dissolution and compared to the analyses done on spiked aliquots. The resulting $^{60/58}$Ni is identical within error (see Table 2-10) for both samples, suggesting there is no difference between both methods of spiking in the course of this work.

Table 2-10

Comparison of Ni isotopic composition between BHVO2 spiked onto powder, and spiked after dissolution
External reproducibility 0.06‰, n equals number of analyses.

Sample BIR1a	$\delta^{60/58}$Ni	2sd	n
Spike added to powder	**0.135**	0.044	4
Spike added to aliquot	**0.150**	0.064	18

2.3.8 Adaptation of procedure for analysis of cosmogenic effects

The MC-ICPMS used in the investigation of lunar cosmogenic effects is the same as used throughout this project, although it, and the lab, was cleaned and had many consumables replaced. This included a new torch, new cones, and new nebuliser, and a replacement DSN that had never seen double spike. The bracketing standard of unspiked SRM986 did not go through chemistry, but an in-house standard (Sudbury NiS) and a USGS sample (BHVO2) were purified with the samples. For the measurements of standard materials and samples all dilution preparation was done in the DS-free laminar flow hood in the MFL, including using fresh diluting acid and freshly cleaned vials.

The programming was suitably altered to report the ratios needed, and the maths updated to remove double spike deconvolution and replace with exponential power law mass fractionation correction, relative to fixed natural isotopic ratios, and with iron correction based on the voltage received for mass 57. The maths was set up to report ratios relative to different pairs as the fixed

natural ratio based on the values of Gramlich (1989). In this work we investigated normalisation ratios 61/58 (Quitté and Oberli, 2006) and 62/58 (Chen et al., 2009; Cook et al., 2006; Quitté et al., 2006; Quitté and Oberli, 2006), and 58/61 (Regelous et al., 2008; Steele et al., 2012, 2011) and 62/61 (Steele et al., 2012). In general, normalisations involving ^{61}Ni isotope have greater errors due to the lower voltage on this smallest beam. Normalisations involving 58 are vulnerable to any error in the Fe correction propagating into the isotopic ratio, particularly if 58 is the denominator, causing errors to propagate into all isotopic ratios.

Analysis of cosmogenic Ni effects comes with many potential problems including that nucleosynthetic anomalies have been identified on isotope ^{62}Ni, as it is overproduced in type Ia supernovae (Steele et al., 2011), and isotope ^{60}Ni has a contribution from decay of short lived radioactive isotope ^{60}Fe. However, these should not be relevant to lunar samples. Other potential problems include the low magnitude of isotope ^{61}Ni without the addition of double spike, and that isotope ^{58}Ni also has the Fe correction, which if imperfect and then used in the normalisation process can propagate any error in the correction into all the isotope ratios reported.

Once the instrument was set up, analysis of DS-free SRM986 were analysed repeatedly, to test whether we could reproduce the natural terrestrial isotopic Ni ratio (Gramlich et al., 1989) long term.

The samples had limited Ni available and the decision was made to analyse increased ratios but with extra ESA deflections, rather than full duplicates. All samples were analysed for >55 ratios in total, but with ESA deflection baseline recalculated after each 20 ratios. Only the standard materials could be analysed more than once, because of the limited lunar material. Results are shown in Chapter 5.

2.4 References

Aigner-Torres, M., Blundy, J., Ulmer, P., Pettke, T., 2007. Laser Ablation ICPMS study of trace element partitioning between plagioclase and basaltic melts: an experimental approach. Contrib Miner. Pet. 153, 647–667. https://doi.org/10.1007/s00410-006-0168-2

Arai, T., Maruyama, S., 2017. Formation of anorthosite on the Moon through magma ocean fractional crystallization. Geosci. Front. 8, 299–308. https://doi.org/10.1016/j.gsf.2016.11.007

Armytage, R.M.G., Georg, R.B., Williams, H.M., Halliday, A.N., 2012. Silicon isotopes in lunar rocks : Implications for the Moon's formation and the early history of the Earth. Geochim. Cosmochim. Acta 77, 504–514. https://doi.org/10.1016/j.gca.2011.10.032

Aulbach, S., Rudnick, R.L., McDonough, W.F., 2008. Li-Sr-Nd isotope signatures of the plume and cratonic lithospheric mantle beneath the margin of the rifted Tanzanian craton (Labait). Contrib. to Mineral. Petrol. 155, 79–92. https://doi.org/10.1007/s00410-007-0226-4

Becker, J.S., 2007. Inorganic mass spectrometry : principles and applications. John Wiley & Sons.

Bédard, J.H., 2005. Trace element partitioning in plagioclase feldspar. Geochim. Cosmochim. Acta 70, 3717–3742. https://doi.org/10.1016/j.gca.2006.05.003

Bindeman, I.N., Davis, A.M., 2000. Trace element partitioning between plagioclase and melt: Investigation of dopant influence on partition behavior.

Birck, J.L., Lugmair, G.W., 1988. Nickel and chromium isotopes in Allende inclusions. Earth Planet. Sci. Lett. 90, 131–143. https://doi.org/10.1016/0012-821X(88)90096-9

Bizzarro, M., Ulfbeck, D., Thrane, K., 2006. Nickel isotopes in meteorites: evidence for live 60Fe and distinct 62Ni isotope reservoirs in the early solar system. Lunar Planet. Sci. XXXVII 37.

Bizzarro, M., Ulfbeck, D., Trinquier, A., Thrane, K., Connelly, J.N., Meyer, B.S., 2007. Evidence for a late supernova injection of 60Fe into the protoplanetary disk. Science 316, 1178–81. https://doi.org/10.1126/science.1141040

Bourdon, B., Langmuir, C.H., Zindler, A., 1996. Ridge-hotspot interaction along the Mid-Atlantic Ridge between 37'30' and 40'30'N: the U-Th disequilibrium evidence, Earth and Planetary Science Letters.

Bouvier, A., Vervoort, J.D., Patchett, P.J., 2008. The Lu-Hf and Sm-Nd isotopic composition of CHUR: Constraints from unequilibrated chondrites and implications for the bulk composition of terrestrial planets. Earth Planet. Sci. Lett. 273, 48–57. https://doi.org/10.1016/j.epsl.2008.06.010

Burton, K.W., Schiano, P., Birck, J.-L., Allègre, C.J., Rehkämper, M., Halliday, A.N., Dawson, J.B., 2000. The distribution and behaviour of rhenium and osmium amongst mantle minerals and the age of the lithospheric mantle beneath Tanzania. Earth Planet. Sci. Lett. 183, 93–106. https://doi.org/10.1016/S0012-821X(00)00259-4

Bussod, G.Y.A., Williams, D.R., 1991. Thermal and kinematic model of the southern Rio Grande rift: inferences from crustal and mantle xenoliths from Kilboume Hole, New Mexico. Tectonophysics 197, 373–389.

Cameron, V., Vance, D., 2014. Heavy nickel isotope compositions in rivers and the oceans. Geochim. Cosmochim. Acta 128, 195–211. https://doi.org/10.1016/j.gca.2013.12.007

Cameron, V., Vance, D., Archer, C., House, C.H., 2009. A biomarker based on the stable isotopes of nickel. Proc. Natl. Acad. Sci. U. S. A. 106, 10944–10948.

https://doi.org/10.1073/pnas.0900726106

Canil, D., Pearson RL Rudnick, N.D., McDonough Carswell, W. DA, 1994. Ferric iron in peridotites and mantle oxidation states. Earth Planet. Sci. Lett. 123, 205–220.

Canup, R.M., 2012. Forming a Moon with an Earth-like Composition via a Giant Impact. Science 338, 1052–1055. https://doi.org/10.1126/science.1106818

Canup, R.M., Asphaug, E., 2001. Origin of the Moon in a giant impact near the end of the Earth's formation. Nature 412, 708–712. https://doi.org/10.1038/35089010

Canup, R.M., Barr, A.C., Crawford, D.A., 2013. Lunar-forming impacts: High-resolution SPH and AMR-CTH simulations. Icarus 222, 200–219. https://doi.org/10.1016/J.ICARUS.2012.10.011

Capobianco, C.J., Amelin, A.A., 1994. Metal-silicate partitioning of nickel and cobalt: The influence of temperature and oxygen fugacity. Geochim. Cosmochim. Acta 58, 125–140.

Chako Tchamabé, B., Youmen, D., Owona, S., Ohba, T., Németh, K., Nsangou Ngapna, M., E Asaah, A.N., Aka, F.T., Tanyileke, G., Hell, J. V, 2013. Eruptive history of the Barombi Mbo Maar, Cameroon Volcanic Line, Central Africa: Constraints from volcanic facies analysis. Cent. Eur. J. Geosci 5, 480–496. https://doi.org/10.2478/s13533-012-0147-2

Chen, J.H., Papanastassiou, D.A., 2006. NICKEL ISOTOPE INVESTIGATION BY MC-ICP-MS AND PTIMS, in: Lunar and Planetary Science XXXVII. pp. 61–62.

Chen, J.H., Papanastassiou, D.A., Wasserburg, G.J., 2009. A search for nickel isotopic anomalies in iron meteorites and chondrites. Geochim. Cosmochim. Acta 73, 1461–1471. https://doi.org/10.1016/j.gca.2008.11.040

Chernonozhkin, S.M., Goderis, S., Costas-Rodríguez, M., Claeys, P., Vanhaecke, F., 2016. Effect of parent body evolution on equilibrium and kinetic isotope fractionation: a combined Ni and Fe isotope study of iron and stony-iron meteorites. Geochim. Cosmochim. Acta 186, 168–188. https://doi.org/10.1016/j.gca.2016.04.050

Chernonozhkin, S.M., Goderis, S., Lobo, L., Claeys, P., Vanhaecke, F., 2015. Development of an isolation procedure and MC-ICP-MS measurement protocol for the study of stable isotope ratio variations of nickel. J. Anal. At. Spectrom. 30, 1518–1530. https://doi.org/10.1039/C5JA00080G

Chernonozhkin, S.M., Weyrauch, M., Goderis, S., Oeser, M., McKibbin, S.J., Horn, I., Hecht, L., Weyer, S., Claeys, P., Vanhaecke, F., 2017. Thermal equilibration of iron meteorite and pallasite parent bodies recorded at the mineral scale by Fe and Ni isotope systematics. Geochim. Cosmochim. Acta 217, 95–111. https://doi.org/10.1016/J.GCA.2017.08.022

Ciscato, E.R., Bontognali, T.R.R., Vance, D., 2018. Nickel and its isotopes in organic-rich sediments: implications for oceanic budgets and a potential record of ancient seawater. Earth Planet. Sci. Lett. 494, 239–250. https://doi.org/10.1016/j.epsl.2018.04.061

Cisowski, S.M., Collinson, D.W., Runcorn, S.K., Stephenson, A., Fuller, M., 1983. A REVIEW OF LUNAR PALEOINTENSITY DATA AND IMPLICATIONS FOR THE ORIGIN OF LUNAR MAGNETISM. J. Geophys. Res. 88, A691–A704.

Cook, D.L., Clayton, R.N., Wadhwa, M., Janney, P.E., Davis, A.M., 2008a. Nickel isotopic anomalies in troilite from iron meteorites. Geophys. Res. Lett. 35, 1–5. https://doi.org/10.1029/2007GL032431

Cook, D.L., Clayton, R.N., Wadhwa, M., Janney, P.E., Davis, A.M., 2008b. Nickel isotopic anomalies in troilite from iron meteorites. Geophys. Res. Lett. 35, L01203. https://doi.org/10.1029/2007GL032431

Cook, D.L., Wadhwa, M., Clayton, R.N., Dauphas, N., Janney, P.E., Davis, A.M., 2007. Mass-dependent fractionation of nickel isotopes in meteoritic metal. Meteorit. Planet. Sci. 42,

2067–2077. https://doi.org/10.1111/j.1945-5100.2007.tb01008.x

Cook, D.L., Wadhwa, M., Janney, P.E., Dauphas, N., Clayton, R.N., Davis, A.M., 2006. High precision measurements of non-mass-dependent effects in nickel isotopes in meteoritic metal via multicollector ICPMS. Anal. Chem. 78, 8477–84. https://doi.org/10.1021/ac061285m

Cornen, G., Bandet, Y., Giresse, P., Maley, J., 1992. The nature and chronostratigraphy of Quaternary pyroclastic accumulations from Lake Barombi Mbo (West-Cameroon). J. Volcanol. Geotherm. Res. 51, 357–374.

Dauphas, N., Teng, F.-Z., Arndt, N.T., 2010. Magnesium and iron isotopes in 2.7 Ga Alexo komatiites: Mantle signatures, no evidence for Soret diffusion, and identification of diffusive transport in zoned olivine. Geochim. Cosmochim. Acta 74, 3274–3291. https://doi.org/10.1016/J.GCA.2010.02.031

Dauritria, J.M., Girod, M., 1987. Cenozoaic Volcanism associated with Swells and Rifts, in: Nixon, P.. (Ed.), Mantle Xenoliths. pp. 195–215.

Dawson, J.B., 2012. Nephelinite-melilitite-carbonatite relationships: Evidence from Pleistocene-recent volcanism in northern Tanzania. Lithos 152, 3–10. https://doi.org/10.1016/j.lithos.2012.01.008

Dawson, J.B., 2002. Metasomatism and Partial Melting in Upper-Mantle Peridotite Xenoliths from the Lashaine Volcano, Northern Tanzania. J. Petrol. 43, 1749–1777. https://doi.org/10.1093/petrology/43.9.1749

Dawson, J.B., 1992. Neogene tectonics and volcanicity in the North Tanzania sector of the Gregory Rift Valley: contrasts with the Kenya sector. Tectonophysics 204, 81–92. https://doi.org/10.1016/0040-1951(92)90271-7

Dawson, J.B., 1964a. Carbonate Tuff Cones in Northern Tanganyika. Geol. Mag. 101, 129. https://doi.org/10.1017/S0016756800048561

Dawson, J.B., 1964b. Carbonatitic volcanic ashes in Northern Tanganyika. Bull. Volcanol. 27, 81–91. https://doi.org/10.1007/BF02597513

Dawson, J.B., Powell, D.G., Reid, A.M., 1970. Ultrabasic Xenoliths and Lava from the Lashaine Volcano, Northern Tanzania. J. Petrol. 11, 519–548. https://doi.org/10.1093/petrology/11.3.519

Day, J.M.D., Pearson, D.G., Macpherson, C.G., Lowry, D., Carracedo, J.-C., 2009. Pyroxenite-rich mantle formed by recycled oceanic lithosphere: Oxygen-osmium isotope evidence from Canary Island lavas. Geology 37, 555–558. https://doi.org/10.1130/G25613A.1

Delano, J.W., 1985. Mare Volcanic Glasses, II: Abundances of Trace Ni and the Composition of the Moon.

Dingwell, D.B., O'Neill, H.S.C., Ertel, W., Spettel, B., 1994. The solubility and oxidation state of nickel in silicate melt at low oxygen fugacities: Results using a mechanically assisted equilibration technique. Geochim. Cosmochim. Acta 58, 1967–1974. https://doi.org/10.1016/0016-7037(94)90428-6

Dosso, L., Bougault, H., Langmuir, C., Bollinger, C., Bonnier, O., Etoubleau, J., 1999. The age and distribution of mantle heterogeneity along the Mid-Atlantic ridge (31-41°N). Earth Planet. Sci. Lett. 170, 269–286. https://doi.org/10.1016/S0012-821X(99)00109-0

Dziewonski, A.M., Anderson, D.L., 1981. Preliminary reference Earth model. Phys. Earth Planet. Inter. 25, 297–356. https://doi.org/10.1016/0031-9201(81)90046-7

Eberhardt, P., Geiss, J., Graf, H., Grögler, N., Krähenbühl, U., Schwaller, H., Schwarzmüller, J., Stettler, A., 1970. Correlation between rock type and irradiation history of Apollo 11 igneous rocks. Earth Planet. Sci. Lett. 10, 67–72. https://doi.org/10.1016/0012-

821X(70)90065-8

Ehlers, K., Grove, T.L., Sisson, T.W., Recca, S.I., Zervas, D.A., 1992. The effect of oxygen fugacity on the partitioning of nickel and cobalt between olivine, silicate melt, and metal. Geochim. Cosmochim. Acta 56, 3733–3743. https://doi.org/10.1016/0016-7037(92)90166-G

El Goresy, A., Ramdohr, P., Taylor, L.A., 1971. The opaque minerals in the lunar rocks from Oceanus Procellarum, in: 2ns Lunar Science Conference. The M.I.T. Press, pp. 219–235.

Elliott, T., Steele, R.C.J., 2017. The Isotope Geochemistry of Ni, in: Reviews in Mineralogy and Geochemistry.

Estrade, N., Cloquet, C., Echevarria, G., Sterckeman, T., Deng, T., Tang, Y., Morel, J.-L., 2015. Weathering and vegetation controls on nickel isotope fractionation in surface ultramafic environments (Albania). Earth Planet. Sci. Lett. 423, 24–35. https://doi.org/10.1016/j.epsl.2015.04.018

Faure, G., Mensing, T.M., Faure, G., 2005. Isotopes : principles and applications. Wiley.

Feigenson, M.D., 1986. Continental alkali basalts as mixtures of kimberlite and depleted mantle: Evidence from Kilbourne Hole Maar, New Mexico. Geophys. Res. Lett. 13, 965–968. https://doi.org/10.1029/GL013i009p00965

Finnerty, A.A., Boyd, F.R., 1987. Thermobarometry for Garnet Peridotites, in: Nixon, P.H. (Ed.), Mantle Xenoltihs. Wiley, pp. 381–402.

Fischer, R.A., Nakajima, Y., Campbell, A.J., Frost, D.J., Harries, D., Langenhorst, F., Miyajima, N., Pollok, K., Rubie, D.C., 2015. High pressure metal-silicate partitioning of Ni, Co, V, Cr, Si, and O. Geochim. Cosmochim. Acta 167, 177–194. https://doi.org/10.1016/j.gca.2015.06.026

Fitton, J.G., 2007. The OIB Paradox, in: Foulger, G.R., Jurdy, D.M. (Eds.), Plates, Plumes, and Planetary Processes. The Geological Society of America, pp. 387–409.

Fitton, J.G., 1987. The Cameroon line, West Africa: a comparison between oceanic and continental alkaline volcanism. Geol. Soc. London, Spec. Publ. 30, 273–291. https://doi.org/10.1144/GSL.SP.1987.030.01.13

Fitton, J.G., Dunlop, H.M., 1985. The Cameroon line, West Africa, and its bearing on the origin of oceanic and continental alkali basalt. Earth Planet. Sci. Lett. 72, 23–38. https://doi.org/10.1016/0012-821X(85)90114-1

Fitton, J.G., Saunders, A.D., Kempton, P.D., Hardarson, B.S., 2003. Does depleted mantle form an intrinsic part of the Iceland plume? Geochemistry, Geophys. Geosystems 4. https://doi.org/10.1029/2002GC000424

Freeth, S.J., 1979. Deformation of the African plate as a consequence of membrane stress domains generated by post-Jurassic drift. Earth Planet. Sci. Lett. 45, 93–104. https://doi.org/10.1016/0012-821X(79)90111-0

Frost, D.J., Liebske, C., Langenhorst, F., McCammon, C.A., Trønnes, R.G., Rubie, D.C., 2004. Experimental evidence for the existence of iron-rich metal in the Earth's lower mantle. Nature 428, 409–412. https://doi.org/10.1038/nature02413

Gale, A., Dalton, C.A., Langmuir, C.H., Su, Y., Schilling, J.-G., 2013. The mean composition of ocean ridge basalts. Geochemistry, Geophys. Geosystems 14, 489–518. https://doi.org/10.1029/2012GC004334

Gall, L., 2011. Development and Application of Nickel Stable Isotopes as a New Geochemical Tracer. University Of Oxford.

Gall, L., Williams, H., Siebert, C., Halliday, A.N., 2012. Determination of mass-dependent variations in nickel isotope compositions using double spiking and MC-ICPMS. J. Anal.

At. Spectrom. 27, 137. https://doi.org/10.1039/c1ja10209e

Gall, L., Williams, H.M., Halliday, A.N., Kerr, A.C., 2017. Nickel isotopic composition of the mantle. Geochim. Cosmochim. Acta 199, 196–209. https://doi.org/10.1016/j.gca.2016.11.016

Gall, L., Williams, H.M., Siebert, C., Halliday, A.N., Herrington, R.J., Hein, J.R., 2013. Nickel isotopic compositions of ferromanganese crusts and the constancy of deep ocean inputs and continental weathering effects over the Cenozoic. Earth Planet. Sci. Lett. 375, 148–155. https://doi.org/10.1016/j.epsl.2013.05.019

Garcia, R.F., Gagnepain-Beyneix, J., Chevrot, S., Lognonné, P., 2011. Very preliminary reference Moon model. Phys. Earth Planet. Inter. 188, 96–113. https://doi.org/10.1016/J.PEPI.2011.06.015

Gessmann, C.K., Rubie, D.C., 2000. The origin of the depletions of V, Cr and Mn in the mantles of the Earth and Moon. Earth Planet. Sci. Lett. 184, 95–107. https://doi.org/10.1016/S0012-821X(00)00323-X

Gibson, S.A., McMahon, S.C., Day, J.A., Dawson, J.B., 2013. Highly Refractory Lithospheric Mantle beneath the Tanzanian Craton: Evidence from Lashaine Pre-metasomatic Garnet-bearing Peridotites. J. Petrol. 54, 1503–1546. https://doi.org/10.1093/petrology/egt020

Gramlich, J.W., Machlan, L.A., Barnes, I.L., Paulsen, P.J., 1989. Absolute isotopic abundance ratios and atomic weight of a reference sample of nickel. J. Res. Natl. Inst. Stand. Technol. 94, 347. https://doi.org/10.6028/jres.094.034

Guan, Y., Huss, G.R., Leshin, L.A., 2004. SIMS analyses of Mg, Cr, and Ni isotopes in primitive meteorites and short-lived radionuclides in the early solar system. Appl. Surf. Sci. 231–232, 899–902. https://doi.org/10.1016/j.apsusc.2004.03.163

Gueguen, B., Rouxel, O., Ponzevera, E., Bekker, A., Fouquet, Y., 2013. Nickel Isotope Variations in Terrestrial Silicate Rocks and Geological Reference Materials Measured by MC-ICP-MS. Geostand. Geoanalytical Res. 37, 297–317. https://doi.org/10.1111/j.1751-908X.2013.00209.x

Gueguen, B., Rouxel, O., Rouget, M.-L., Bollinger, C., Ponzevera, E., Germain, Y., Fouquet, Y., 2016. Comparative geochemistry of four ferromanganese crusts from the Pacific Ocean and significance for the use of Ni isotopes as paleoceanographic tracers. Geochim. Cosmochim. Acta 189, 214–235. https://doi.org/10.1016/J.GCA.2016.06.005

Gueguen, B., Sorensen, J. V., Lalonde, S. V., Peña, J., Toner, B.M., Rouxel, O., 2018. Variable Ni isotope fractionation between Fe-oxyhydroxides and implications for the use of Ni isotopes as geochemical tracers. Chem. Geol. 481, 38–52. https://doi.org/10.1016/J.CHEMGEO.2018.01.023

Haase, K.M., Regelous, M., Duncan, R.A., Brandl, P.A., Stroncik, N., Grevemeyer, I., 2011. Insights into mantle composition and mantle melting beneath mid-ocean ridges from postspreading volcanism on the fossil Galapagos Rise Theme: Geochemical Heterogeneities in Oceanic Island Basalt and Mid-ocean Ridge Basalt Sources: Implications for Melting. Geochem. Geophys. Geosyst 12. https://doi.org/10.1029/2010GC003482

Haase, K.M., Regelous, M., Duncan, R.A., Brandl, P.A., Stroncik, N., Grevemeyer, I., 2011. Insights into mantle composition and mantle melting beneath mid-ocean ridges from postspreading volcanism on the fossil Galapagos Rise. Geochemistry, Geophys. Geosystems 12, 1–21. https://doi.org/10.1029/2010GC003482

Halliday, A.N., 2000. Terrestrial accretion rates and the origin of the Moon. Earth Planet. Sci. Lett. 176, 17–30. https://doi.org/10.1016/S0012-821X(99)00317-9

Halliday, A.N., Davidson, J.P., Holden, P., DeWolf, C., Lee, D.-C., Fitton, J.G., 1990. Trace-

element fractionation in plumes and the origin of HIMU mantle beneather the Cameroon line. Nature 346, 523–528. https://doi.org/10.1038/346183a0

Halliday, A.N., Davies, G.R., Lee, D.-C., Tommasini, S., Paslick, C.R., Fitton, J.G., James, D.E., 1992a. Lead isotope evidence for young trace element enrichment in the oceanic upper mantle. Nature 359, 623–627. https://doi.org/10.1038/359623a0

Halliday, A.N., Davies, G.R., Lee, D.-C., Tommasini, S., Paslick, C.R., Fitton, J.G., James, D.E., 1992b. Lead isotope evidence for young trace element enrichment in the oceanic upper mantle. Nature 359, 623–627. https://doi.org/10.1038/359623a0

Halliday, A.N., Davies, G.R., Lee, D.C., 1992. Lead isotope evidence for young trace-element enrichment in the oceanic upper mantle. Nature 359, 623–627.

Halliday, A.N., Dickin, A.P., Fallick, A.E., Fitton, J.G., 1988. Mantle dynamics: A Nd, Sr, Pb and O isotopic study of the Cameroon line volcanic chain. J. Petrol. 29, 181–211. https://doi.org/10.1093/petrology/29.1.181

Halliday, A.N., Lee, D.-C., Christensen, J.N., Rehkämper, M., Yi, W., Luo, X., Hall, C.M., Ballentine, C.J., Pettke, T., Stirling, C., 1998. Applications of Multiple Collector-ICPMS to Cosmochemistry, Geochemistry, and Paleoceanography. Geochim. Cosmochim. Acta 62, 919–940. https://doi.org/10.1016/S0016-7037(98)00057-X

Halliday, A.N., Lee, D.-C., Tommasini, S., Davies, G.R., Paslick, C.R., Godfrey Fitton, J., James, D.E., 1995. Incompatible trace elements in OIB and MORB and source enrichment in the sub-oceanic mantle. Earth Planet. Sci. Lett. 133, 379–395. https://doi.org/10.1016/0012-821X(95)00097-V

Hardarson, B.S., Fitton, J.G., 1997. Mechanisms of crustal accretion in Iceland. Geology 25, 1043–1046.

Harpp, K.S., White, W.M., 2001a. Tracing a mantle plume: Isotopic and trace element variations of Galápagos seamounts. Geochemistry, Geophys. Geosystems 2, n/a-n/a. https://doi.org/10.1029/2000GC000137

Harpp, K.S., White, W.M., 2001b. Tracing a mantle plume: Isotopic and trace element variations of Galápagos seamounts. Geochemistry, Geophys. Geosystems 2, n/a-n/a. https://doi.org/10.1029/2000GC000137

Hart, S.R., 1988. Heterogeneous mantle domains: signatures, genesis and mixing chronologies. Earth Planet. Sci. Lett. 90, 273–296. https://doi.org/10.1016/0012-821X(88)90131-8

Hart, S.R., Davis, K.E., 1978. Nickel partitioning between olivine and silicate melt. Earth Planet. Sci. Lett. 40, 203–219.

Hartmann, W.K., Davis, D.R., 1975. Satellite-Sized Planetesimals and Lunar Origin, ICARUS.

Harvey, J., Dale, C.W., Gannoun, A., Burton, K.W., 2011. Osmium mass balance in peridotite and the effects of mantle-derived sulfides on basalt petrogenesis. Geochim. Cosmochim. Acta 75, 5574–5596. https://doi.org/10.1016/j.gca.2011.07.001

Harvey, J., Konig, S., Luguet, A., 2015. The effects of melt depletion and metasomatism on highly siderophile and strongly chalcophile elements: S-Se-Te-Re-PGE systematics of peridotite xenoliths from Kilbourne Hole, New Mexico. Geochim. Cosmochim. Acta 166, 210–233. https://doi.org/10.1016/j.gca.2015.06.028

Harvey, J., Yoshikawa, M., Hammond, S.J., Burton, K.W., 2012. Deciphering the trace element characteristics in kilbourne hole peridotite xenoliths: Melt-rock interaction and metasomatism beneath the Rio Grande Rift, SW USA. J. Petrol. 53, 1709–1742. https://doi.org/10.1093/petrology/egs030

Hauri, E.H., 1996. Major-element variability in the Hawaiian mantle plume. Nature 382, 415–419. https://doi.org/10.1038/382415a0

Henderson, P., Henderson, G., 2009. The Cambridge Handbook of Earth Science Data. Cambridge University Press.

Herzberg, C., Vidito, C., Starkey, N.A., 2016. Nickel–cobalt contents of olivine record origins of mantle peridotite and related rocks. Am. Mineral. 101, 1952–1966. https://doi.org/10.2138/am-2016-5538

Hiesinger, H., Head III, J.W., 2006. New Views of Lunar Geoscience: An Introduction and Overview, in: Reviews in Mineralogy & Geochemistry Volume 60: New Views of the Moon. pp. 1–67.

Hofmann, A., Bekker, A., Dirks, P., Gueguen, B., Rumble, D., Rouxel, O.J., 2014. Comparing orthomagmatic and hydrothermal mineralization models for komatiite-hosted nickel deposits in Zimbabwe using multiple-sulfur, iron, and nickel isotope data. Miner. Depos. 49, 75–100. https://doi.org/10.1007/s00126-013-0476-1

Holzheid, A., Palme, H., Chakraborty, S., 1997. The activities of NiO, CoO and FeO in silicate melts. Chem. Geol. 139, 21–38.

Irving, A.J., 1980. Petrology and geochemistry of composite ultramafic xenoliths in alkalic basalts and implications for magmatic processes within the mantle. Am. J. Sci. 280–A, 389–426.

James, D.E., Padovani, E.R., Hart, S.R., 1980. Preliminary results on the oxygen isotopic composition of the lower crust, Kilbourne Hole Maar, New Mexico. Geophys. Res. Lett. 7, 321–324. https://doi.org/10.1029/GL007i005p00321

Jana, D., Walker, D., 1997. The influence of silicate melt composition on distribution of siderophile elements among metal and silicate liquids. Earth Planet. Sci. Lett. 150, 463–472. https://doi.org/10.1016/S0012-821X(97)00079-4

Kegler, P., Holzheid, A., Frost, D.J., Rubie, D.C., Dohmen, R., Palme, H., 2008. New Ni and Co metal-silicate partitioning data and their relevance for an early terrestrial magma ocean. Earth Planet. Sci. Lett. 268. https://doi.org/10.1016/j.epsl.2007.12.020

Keller, G.R., Morgan, P., Seager, W.R., 1990. Crustal structure, gravity anomalies and heat flow in the southern Rio Grande rift and their relationship to extensional tectonics. Tectonophysics 174, 21–37.

Kempton, P.D., Fitton, J.G., Saunders, A.D., Nowell, G.M., Taylor, R.N., Hardarson, B.S., Pearson, G., 2000. The Iceland plume in space and time: a Sr–Nd–Pb–Hf study of the North Atlantic rifted margin, Earth and Planetary Science Letters. Elsevier. https://doi.org/10.1016/S0012-821X(00)00047-9

Kirsten, T., Deubner, J., Horn, P., Kaneoka, I., Kiko, J., Schaeffer, O.A., Thio, S.K., 1972. The rare gas record of Apollo 14 and 15 samples. Proc. Third Lunar Sci. Conf. vol. 3, p. 1865 - 1889 3, 1865–1889.

Kodolányi, J., Stephan, T., Trappitsch, R., Pignatari, M., Davis, A.M., Pellin, M.J., 2018. Iron and nickel isotope compositions of presolar silicon carbide grains from supernovae. Geochim. Cosmochim. Acta 221, 127–144. https://doi.org/10.1016/J.GCA.2017.05.029

König, S., Wille, M., Voegelin, A., Schoenberg, R., 2016. Molybdenum isotope systematics in subduction zones. Earth Planet. Sci. Lett. 447, 95–102. https://doi.org/10.1016/j.epsl.2016.04.033

Koornneef, J.M., Davies, G.R., Döpp, S.P., Vukmanovic, Z., Nikogosian, I.K., Mason, P.R.D., 2009. Nature and timing of multiple metasomatic events in the sub-cratonic lithosphere beneath Labait, Tanzania. Lithos 112, 896–912. https://doi.org/10.1016/J.LITHOS.2009.04.039

Korotev, R.L., 2018. List of Lunar Meteorites [WWW Document]. http://meteorites.wustl.edu/lunar/moon_meteorites_list_alpha.htm.

Krawczynski, M.J., Grove, T.L., 2012. Experimental investigation of the influence of oxygen fugacity on the source depths for high titanium lunar ultramafic magmas. Geochim. Cosmochim. Acta 79, 1–19. https://doi.org/10.1016/j.gca.2011.10.043

Langmuir, C.H., Klein, E.M., Plank, T., 1992. Petrological Systematics of Mid-Ocean Ridge Basalts: Constraints on Melt Generation Beneath Ocean Ridges, in: Phipps Morgan, J., Blackman, D.K., Sinton, J.M. (Eds.), Mantle Flow and Melt Generation at Mantle Ridges. American Geophysical Union (AGU), pp. 183–280. https://doi.org/10.1029/GM071p0183

Lazar, C., Young, E.D., Manning, C.E., 2012. Experimental determination of equilibrium nickel isotope fractionation between metal and silicate from 500 °C to 950 °C. Geochim. Cosmochim. Acta 86, 276–295. https://doi.org/10.1016/J.GCA.2012.02.024

Lee, D.-C., 1994. A Chemical, Isotopic, and Geochronological Study of the Cameroon Line, West Africa. University of Michigan.

Lee, D.-C., Halliday, A.N., Davies, G.R., Essene, E.J., Fitton, J.G., Temdjim, R., 1996. Melt Enrichment of Shallow Depleted Mantle: a Detailed Petrological, Trace Element and Isotopic Study of Mantle- Derived Xenoliths and Megacrysts from the Cameroon Line. J. Petrol. 37, 15–441.

Lee, D., Halliday, A.N., Davies, G.R., Essene, E.J., Fitton, J.G., Temdjim, R., 1996. Melt Enrichment of Shallow Depleted Mantle: a Detailed Petrological, Trace Element and Isotopic Study of Mantle- Derived Xenoliths and Megacrysts from the Cameroon Line. J. Petrol. 37, 415–441.

Liang, Y.-H., Halliday, A.N., Siebert, C., Fitton, J.G., Burton, K.W., Wang, K.-L., Harvey, J., 2017. Molybdenum isotope fractionation in the mantle. Geochim. Cosmochim. Acta 199, 91–111. https://doi.org/10.1016/J.GCA.2016.11.023

Liu, L., Spasojević, S., Gurnis, M., 2008. Reconstructing Farallon Plate Subduction Beneath North America Back to the Late Cretaceous. Science (80-.). 322. https://doi.org/10.1126/science.1164170

Liu, S., Li, Y., Ju, Y., Liu, J., Liu, J., Shi, Y., 2018. Equilibrium nickel isotope fractionation in nickel sulfide minerals. Geochim. Cosmochim. Acta 222, 1–16. https://doi.org/10.1016/J.GCA.2017.10.018

Lodders, K., 2003. Solar System Abundances and Condensation Temperatures of the Elements. Astrophys. Journal, 591, 1220–1247.

Ma, Z., Thompson, R.N., Lykke, K.R., Pellin, M.J., Davis, A.M., 1995. Time-of-Flight Mass Spectrometer with Improved Resolution Review of. Cit. Rev. Sci. Instruments 66, 1150. https://doi.org/10.1063/1.1145546

Maley, J., Livingstone, D.A., Giresse, P., Thouveny, N., Brenac, P., Kelts, K., Kling, G., Stager, C., Haag, M., Fournier, M., Bandet, Y., Williamson, D., Zogning, A., 1990. Lithostratigraphy, volcanism, paleomagnetism and palynology of Quaternary lacustrine deposits from Barombi Mbo (West Cameroon): preliminary results. J. Volcanol. Geotherm. Res. 42, 319–335.

McCammon, C., 2005. The Paradox of Mantle Redox. Science (80-.). 308. https://doi.org/10.1126/science.1108162

McDonough, W.F., Sun, S. s., 1995. The composition of the Earth. Chem. Geol. 120, 223–253. https://doi.org/10.1016/0009-2541(94)00140-4

Menzies, M.A., Arculus, R.J., G, B.M., Bergman, S.C., Ehrenberg, S.N., Irving, A.J., Roden, M.F., Schulze, D.J., 1987. A record of subduction processes and within-plate volcanism in lithospheric xenoliths of southwestern USA, in: Nixon, P.. (Ed.), Mantle Xenoliths. pp. 59–74.

Meyer, C., 2011. Lunar Sample Compendium.

Meyer, C., 2003. Lunar Regolith - NASA Lunar Petrographic Educational Thin Section Set.

Moorbath, S., Sigurdsson, H., Goodwin, R., 1968. K-Ar ages of the oldest exposed rocks in Iceland. Earth Planet. Sci. Lett. 4, 197–205. https://doi.org/10.1016/0012-821X(68)90035-6

Morand, P., Allègre, C.J., 1983. Nickel isotopic studies in meteorites. Earth Planet. Sci. Lett. 63, 167–176. https://doi.org/10.1016/0012-821X(83)90034-1

Morand, P., Audouze, J., Allègre, C.J., 1980. Search for nickel isotopic anomaly of meteorites, in: 43rd Annual Meeting of the Meteoritical Society.

Moreau, C., Regnoult, J.-M., Déruelle, B., Robineau, B., 1987. A new tectonic model for the Cameroon Line, Central Africa. Tectonophysics 141, 317–334. https://doi.org/10.1016/0040-1951(87)90206-X

Morgan, W.J., 1983. Hotspot tracks and the early rifting of the Atlantic. Tectonophysics 94, 123–139. https://doi.org/10.1016/0040-1951(83)90013-6

Mostefaoui, S., Lugmair, G.W., Hoppe, P., 2005. 60 Fe: A Heat Source for Planetary Differentiation from a Nearby Supernova Explosion. Astrophys. J. 625, 271–277. https://doi.org/10.1086/429555

Moynier, F., Agranier, A., Hezel, D.C., Bouvier, A., 2010. Sr stable isotope composition of Earth, the Moon, Mars, Vesta and meteorites, Earth and Planetary Science Letters. https://doi.org/10.1016/j.epsl.2010.10.017

Moynier, F., Albarède, F., Herzog, G.F., 2006. Isotopic composition of zinc, copper, and iron in lunar samples. Geochim. Cosmochim. Acta 70, 6103–6117. https://doi.org/10.1016/j.gca.2006.02.030

Moynier, F., Blichert-Toft, J., Telouk, P., Luck, J.-M., Albarède, F., 2007. Comparative stable isotope geochemistry of Ni, Cu, Zn, and Fe in chondrites and iron meteorites. Geochim. Cosmochim. Acta 71, 4365–4379. https://doi.org/10.1016/j.gca.2007.06.049

Moynier, F., Blichert-Toft, J.F., Telouk, P., Albarede, F., 2005. Excesses of 60Ni in chondrites and iron meteorites, in: Lunar and Planetary Science XXXVI.

Neal, C.R., 2001. The Interior of the Moon: The presence of garnet in the primitive deep lunar mantle. J. Geophys. Res. 106, 27865–27885.

Neal, C.R., Taylor, L.A., 1992. Petrogenesis of mare basalts: A record of lunar volcanism*. Geochim. Cosmochim. Acta 56, 2177–2211.

Neal, C.R., Taylor, L.A., 1991. Evidence for metasomatism of the lunar highlands and the origin of whitlockite. Geochim. Cosmochim. Acta 55, 2965–2980.

Newsom, H.E., 1986. Constraints on the Origin of the Moon from the Abundance of Molybdenum and Other Siderophile Elements.

Nicholls, D., 1974. Complexes and First Row Transition Elements. Macmillan, London.

Nier, A.O., 1940. A Mass Spectrometer for Routine Isotope Abundance Measurements. Rev. Sci. Instrum. 11. https://doi.org/10.1063/1.1751688

Niu, Y., Batiza, R., 1997. Trace element evidence from seamounts for recycled oceanic crust in the Eastern Pacific mantle. Earth Planet. Sci. Lett. 148, 471–483. https://doi.org/10.1016/S0012-821X(97)00048-4

Nixon, P.., 1987. Introduction, in: Mantle Xenoliths. pp. 1–3.

Norton, I.O., 2007. Speculations on Cretaceous tectonic history of the northwest Pacific and a tectonic origin for the Hawaii hotspot, in: Plates, Plumes, and Planetary Processes. pp. 451–470.

O'Neill, H.S.C., 1981. The transition between spinel lherzolite and garnet lherzolite, and its use as a Geobarometer. Contrib. to Mineral. Petrol. 77, 185–194. https://doi.org/10.1007/BF00636522

Palme, H., Spettel, B., Bischoff, A., St6ffler, D., 1984. Early Differentiation of the Moon' Evidence from Trace Elements in Plagioclase, in: PROCEEDINGS OF THE FIFTEENTH LUNAR AND PLANETARY SCIENCE CONFERENCE, PART 1 JOURNAL OF GEOPHYSICAL RESEARCH. https://doi.org/10.1029/JB089iS01p000C3

Paniello, R.C., Day, J.M.D., Moynier, F., 2012. Zinc isotopic evidence for the origin of the Moon. Nature 490, 376–379. https://doi.org/10.1038/nature11507

Papanastassiou, D.A., Wasserburg, G.J., 1971. Rb-Sr AGES OF IGNEOUS ROCKS FROM THE APOLLO 14 MISSION AND THE AGE OF THE FRA MAURO FORMATION. Earth Planet. Sci. Lett. 12, 36–48.

Papike, J.J., Fowler, G.W., Adcock, C.T., Shearer, C.K., 1999. Systematics of Ni and Co in olivine from planetary melt systems: Lunar mare basalts. Am. Mineral. 84, 392–399. https://doi.org/10.2138/am-1999-0324

Paslick, C., Halliday, A.N., James, D., Dawson, J.B., 1995. Enrichment of the continental lithosphere by OIB melts: Isotopic evidence from the volcanic province of northern Tanzania. Earth Planet. Sci. Lett. 130, 109–126.

Paslick, C.R., 1995. A Geochemical Study of Volcanism associated with the early stages of Continental Rifting in Northern Tanzanian. University of Michigan.

Paslick, C.R., Halliday, A.N., Lange, R.A., James, D., Dawson, J.B., 1996. Indirect crustal contamination: evidence from isotopic and chemical disequilibria in minerals from alkali basalts and nephelinites from northern Tanzania. Contrib. to Mineral. Petrol. 125, 277–292. https://doi.org/10.1007/s004100050222

Peale, S.J., Cassen, P., 1978. Contribution of tidal dissipation to lunar thermal history. Icarus 36, 245–269. https://doi.org/10.1016/0019-1035(78)90109-4

Perkins, D., Anthony, E.Y., 2011. The evolution of spinel lherzolite xenoliths and the nature of the mantle at Kilbourne Hole, New Mexico. Contrib. to Mineral. Petrol. 162, 1139–1157. https://doi.org/10.1007/s00410-011-0644-1

Pike, J.E.N., Meyer, C.E., Wilshire, H.G., 1980. Petrography and Chemical Composition of a Suite of Ultramafic Xenoliths from Lashaine, Tanzania. J. Geol. 88, 343–352. https://doi.org/10.1086/628512

Pinter, Z., Patko, L., Djoukam, F.T.J., Kovacs, I., Tchouankoue, J.P., Falus, G., Konc, Z., Tommasi, A., Barou, F., Mihaly, J., Nemeth, C., Jeffries, T., 2015. Characterization of the sub-continental lithospheric mantle beneath the Cameroon volcanic line inferred from alkaline basalt hosted peridotite xenoliths from Barombi Mbo and Nyos Lakes. J. African Earth Sci. 111, 170–193. https://doi.org/10.1016/j.jafrearsci.2015.07.006

Porter, S.J., Selby, D., Cameron, V., 2014. Characterising the nickel isotopic composition of organic-rich marine sediments. Chem. Geol. 387, 12–21. https://doi.org/10.1016/j.chemgeo.2014.07.017

Quitte, G., Halliday, A.N., Meyer, B.S., Markowski, A., Latkoczy, C., Gunther, D., 2007. Correlated Iron 60, Nickel 62, and Zirconium 96 in Refractory Inclusions and the Origin of the Solar System. Astrophys. J. 655, 678–684. https://doi.org/10.1086/509771

Quitté, G., Meier, M., Latkoczy, C., Halliday, A.N., Günther, D., Gunther, D., Günther, D., Gunther, D., Günther, D., 2006. Nickel isotopes in iron meteorites–nucleosynthetic anomalies in sulfides with no effects in metals and no trace of 60Fe. Earth Planet. Sci. Lett. 242, 16–25. https://doi.org/10.1016/j.epsl.2005.11.053

Quitté, G., Oberli, F., 2006. Quantitative extraction and high precision isotope measurements of

nickel by MC-ICPMS. J. Anal. At. Spectrom. 21, 1249. https://doi.org/10.1039/b607569j

Rai, N., Westrenen, W. Van, 2014. Lunar core formation : New constraints from metal – silicate partitioning of siderophile elements. Earth Planet. Sci. Lett. 388, 343–352. https://doi.org/10.1016/j.epsl.2013.12.001

Ratié, G., Jouvin, D., Garnier, J., Rouxel, O., Miska, S., Guimaraes, E., Cruz Vieira, L., Sivry, Y., Zelano, I., Montarges-Pelletier, E., Thil, F., Quantin, C., 2015. Nickel isotope fractionation during tropical weathering of ultramafic rocks. Chem. Geol. 402, 68–76. https://doi.org/10.1016/j.chemgeo.2015.02.039

Ratié, G., Quantin, C., Jouvin, D., Calmels, D., Ettler, V., Sivry, Y., Vieira, L.C., Ponzevera, E., Garnier, J., Cruz Vieira, L., Ponzevera, E., Garnier, J., 2016. Nickel isotope fractionation during laterite Ni ore smelting and refining : Implications for tracing the sources of Ni in smelter-affected soils. Appl. Geochemistry 64, 136–145. https://doi.org/10.1016/j.apgeochem.2015.09.005

Reedy, R.C., Englert, P., 1986. Workshop on COSMOGENIC NUCLIDES.

Regelous, M., Elliott, T., Coath, C.D., 2008. Nickel isotope heterogeneity in the early Solar System. Earth Planet. Sci. Lett. 272, 330–338. https://doi.org/10.1016/j.epsl.2008.05.001

Reid, A.M., Donaldson, C.H., Brown, R.W., Ridley, W.I., Dawson, J.B., 1975. Mineral chemistry of peridotite xenoliths from the Lashaine volcano, Tanzania. Phys. Chem. Earth 9, 525–543. https://doi.org/10.1016/0079-1946(75)90037-3

Rhodes, J.M., Dawson, J.B., 1975. Major and trace element chemistry of peridotite inclusions from the Lashaine volcano, Tanzania. Phys. Chem. Earth 9, 545–557. https://doi.org/10.1016/0079-1946(75)90038-5

Righter, K., 2002. Does the Moon Have a Metallic Core? Constraints from Giant Impact Modeling and Siderophile Elements. Icarus 158, 1–13. https://doi.org/10.1006/icar.2002.6859

Righter, K., Drake, M.J., Yaxley, G., 1997. Prediction of siderophile element metal-silicate partition coefficients to 20 GPa and 2800°C: the effects of pressure, temperature, oxygen fugacity, and silicate and metallic melt compositions. Phys. Earth Planet. Inter. 100, 115–134. https://doi.org/10.1016/S0031-9201(96)03235-9

Righter, K., Pando, K.M., Danielson, L., Lee, C.-T., 2010. Partitioning of Mo, P and other siderophile elements (Cu, Ga, Sn, Ni, Co, Cr, Mn, V, and W) between metal and silicate melt as a function of temperature and silicate melt composition. Earth Planet. Sci. Lett. 291, 1–9. https://doi.org/10.1016/J.EPSL.2009.12.018

Roden, M.F., Irving, A.J., Murthy, V.R., 1988. Isotopic and trace element composition of the upper mantle beneath a young continental rift: Results from Kilbourne Hole, New Mexico. Geochim. Cosmochim. Acta 52, 461–473. https://doi.org/10.1016/0016-7037(88)90101-9

Rugel, G., Faestermann, T., Knie, K., Korschinek, G., Poutivtsev, M., Schumann, D., Kivel, N., Günther-Leopold, I., Weinreich, R., Wohlmuther, M., 2009. New Measurement of the ^{60}Fe Half-Life. Phys. Rev. Lett. 103, 072502. https://doi.org/10.1103/PhysRevLett.103.072502

Sato, M., Hickling, N.L., McLane, J.E., 1973. Oxygen fugacity values of Apollo 12, 14, and 15 lunar samples and reduced state of lunar magmas, in: Proceedings of the Fourth Lunar Science Conference. pp. 1061–1079.

Satsukawa, T., Michibayashi, K., Anthony, E.Y., Stern, R.J., Gao, S.S., Liu, K.H., 2011. Seismic anisotropy of the uppermost mantle beneath the Rio Grande rift: Evidence from Kilbourne Hole peridotite xenoliths, New Mexico. Earth Planet. Sci. Lett. 311, 172–181. https://doi.org/10.1016/J.EPSL.2011.09.013

Sedaghatpour, F., Teng, F.Z., Liu, Y., Sears, D.W.G., Taylor, L.A., 2013. Magnesium isotopic

composition of the Moon. Geochim. Cosmochim. Acta 120, 1–16. https://doi.org/10.1016/j.gca.2013.06.026

Sharp, Z.D., Shearer, C.K., McKeegan, K.D., Barnes, J.D., Wang, Y.Q., 2010. The Chlorine Isotope Composition of the Moon and Implications for an Anhydrous Mantle. Science (80-.). 329. https://doi.org/10.1126/science.1191349

Shearer, C.K., Hess, P.C., Wieczorek, M.A., Pritchard, M.E., Parmentier, E.M., Borg, L.E., Longhi, J., Elkins-Tanton, L.T., Neal, C.R., Antonenko, I., Canup, R.M., Halliday, A.N., Grove, T.L., Hager, B.H., Lee, D.C., Wiechert, U., 2006. Thermal and Magmatic Evolution of the Moon, in: Reviews in Mineralogy & Geochemistry Volume 60: New Views of the Moon. pp. 365–502.

Shimamura, T., Lugmair, G.W., 1983. Ni isotopic compositions in Allende and other meteorites. Earth Planet. Sci. Lett. 63, 177–188. https://doi.org/10.1016/0012-821X(83)90035-3

Shukolyukov, A., Lugmair, G.W., 1993a. 60Fe in eucrites. Earth Planet. Sci. Lett. 119, 159–166. https://doi.org/10.1016/0012-821X(93)90013-Y

Shukolyukov, A., Lugmair, G.W., 1993b. Live Iron-60 in the Early Solar System. Science (80-.). 259, 1138–1142.

Siebert, C., Nägler, T.F., Kramers, J.D., 2001. Determination of molybdenum isotope fractionation by double-spike multicollector inductively coupled plasma mass spectrometry. Geochemistry, Geophys. Geosystems 2, n/a-n/a. https://doi.org/10.1029/2000GC000124

Silveira, G., Stutzmann, E., Davaille, A., Montagner, J.-P., Mendes-Victor, L., Sebai, A., 2006. Azores hotspot signature in the upper mantle. J. Volcanol. Geotherm. Res. 156, 23–34. https://doi.org/10.1016/J.JVOLGEORES.2006.03.022

Simon, J.I., DePaolo, D.J., 2010. Stable calcium isotopic composition of meteorites and rocky planets, Earth and Planetary Science Letters. https://doi.org/10.1016/j.epsl.2009.11.035

Sobolev, A. V, Hofmann, A.W., Kuzmin, D. V, Yaxley, G.M., Arndt, N.T., Chung, S.-L., Danyushevsky, L. V, Elliott, T., Frey, F.A., Garcia, M.O., Gurenko, A.A., Kamenetsky, V.S., Kerr, A.C., Krivolutskaya, N.A., Matvienkov, V. V, Nikogosian, I.K., Rocholl, A., Sigurdsson, I.A., Sushchevskaya, N.M., Teklay, M., 2007. The Amount of Recycled Crust in Sources of Mantle-Derived Melts. Science (80-.). 316.

Sobolev, A. V, Hofmann, A.W., Sobolev, S. V, Nikogosian, I.K., 2005. An olivine-free mantle source of Hawaiian shield basalts. Nature 434.

Spivak-Birndorf, L.J., Wang, S.-J., Bish, D.L., Wasylenki, L.E., 2018. Nickel isotope fractionation during continental weathering. Chem. Geol. 476, 316–326. https://doi.org/10.1016/J.CHEMGEO.2017.11.028

Steele, A.M., Colson, R.O., Haskin, L.A., 1991. Co and Ni as Incompatible elements in the Lunar Mantle: Implications for fO2 and the Petrogenesis of Apollo 15 Green Glass, in: LPSC XXII.

Steele, R.C.J., Coath, C.D., Regelous, M., Russell, S., Elliott, T., 2012. Neutron-poor nickel isotope anomalies in meteorites. Astrophys. J. 758, 59. https://doi.org/10.1088/0004-637X/758/1/59

Steele, R.C.J., Elliott, T., Coath, C.D., Regelous, M., 2011. Confirmation of mass-independent Ni isotopic variability in iron meteorites. Geochim. Cosmochim. Acta 75, 7906–7925. https://doi.org/10.1016/J.GCA.2011.08.030

Steenstra, E.S., Rai, N., Knibbe, J.S., Lin, Y.H., Van Westrenen, W., 2016. New geochemical models of core formation in the Moon from metal-silicate partitioning of 15 siderophile elements. Earth Planet. Sci. Lett. 441, 1–9. https://doi.org/10.1016/j.epsl.2016.02.028

Strelow, F.W.E., 1990. Distribution coefficients and cation-exchange behaviour of some ammines and aquo complexes of metallic elements in ammonium nitrate solution. Anal. Chim. Acta 233, 129–134. https://doi.org/10.1016/S0003-2670(00)83468-6

Strelow, F.W.E., Weinert, C.H.S.W., Eloff, C., 1972. Distribution coefficients and anion exchange behavior of elements in oxalic acid-hydrochloric acid mixtures. Anal. Chem. 44, 2352–2356. https://doi.org/10.1021/ac60322a001

Sun, C., Graff, M., Liang, Y., 2017. Trace element partitioning between plagioclase and silicate melt: The importance of temperature and plagioclase composition, with implications for terrestrial and lunar magmatism. Geochim. Cosmochim. Acta 206, 273–295. https://doi.org/10.1016/j.gca.2017.03.003

Tachibana, S., Huss, G.R., 2003. The Initial Abundance of 60 Fe in the Solar System. Astrophys. J. 588, L41–L44. https://doi.org/10.1086/375362

Tachibana, S., Huss, G.R., Kita, N.T., Shimoda, G., Morishita, Y., 2006. 60 Fe in Chondrites: Debris from a Nearby Supernova in the Early Solar System? Astrophys. J. 639, L87–L90. https://doi.org/10.1086/503201

Tanimizu, M., Hirata, T., 2006. Determination of natural isotopic variation in nickel using inductively coupled plasma mass spectrometry. J. Anal. At. Spectrom. 21, 1423. https://doi.org/10.1039/b609543g

Taylor, S.R., 1982. A Lunar Perspective. Lunar and Planetary Institute.

Taylor, S.R., 1975. Lunar Science: A Post-Apollo View.

Teng, F.-Z., Dauphas, N., Huang, S., Marty, B., 2013. Iron isotopic systematics of oceanic basalts. Geochim. Cosmochim. Acta 107, 12–26. https://doi.org/10.1016/J.GCA.2012.12.027

Thompson, G., Bryan, W.B., Humphris, S.E., 1989. Axial volcanism on the East Pacific Rise, in: Magmatism in the Ocean Basins. pp. 181–200.

Trappitsch, R., Stephan, T., Savina, M.R., Davis, A.M., Pellin, M.J., Rost, D., Gyngard, F., Gallino, R., Bisterzo, S., Cristallo, S., Dauphas, N., 2018. Simultaneous iron and nickel isotopic analyses of presolar silicon carbide grains. Geochim. Cosmochim. Acta 221, 87–108. https://doi.org/10.1016/J.GCA.2017.05.031

van Kan Parker, M., Sanloup, C., Sator, N., Guillot, B., Tronche, E.J., Perrillat, J.-P., Mezouar, M., Rai, N., van Westrenen, W., 2012. Neutral buoyancy of titanium-rich melts in the deep lunar interior. Nat. Geosci. 5, 186–189. https://doi.org/10.1038/ngeo1402

Vance, D., Little, S.H., Archer, C., Cameron, V., Andersen, M.B., Rijkenberg, M.J.A., Lyons, T.W., 2016. The oceanic budgets of nickel and zinc isotopes: the importance of sulfidic environments as illustrated by the Black Sea. Philos. Trans. A. Math. Phys. Eng. Sci. 374, 20150294. https://doi.org/10.1098/rsta.2015.0294

Vauchez, A., Dineur, F., Rudnick, R., 2005. Microstructure, texture and seismic anisotropy of the lithospheric mantle above a mantle plume: Insights from the Labait volcano xenoliths (Tanzania). Earth Planet. Sci. Lett. 232, 295–314. https://doi.org/10.1016/J.EPSL.2005.01.024

Ventura, G.T., Gall, L., Siebert, C., Prytulak, J., Szatmari, P., Hürlimann, M., Halliday, A.N., 2015. The stable isotope composition of vanadium, nickel, and molybdenum in crude oils. Appl. Geochemistry 59, 104–117. https://doi.org/10.1016/j.apgeochem.2015.04.009

Victor, A.H., 1986. Selective separation of Nickel from other elements by cation-exchange chromatography in dimethylglyoxime/hydrochloric acid/acetone media. Anal. Chim. Acta 183, 155–161.

Wadhwa, M., 2008. Redox Conditions on Small Bodies, the Moon and Mars, in: Reviews in

Mineralogy and Geochemistry. GeoScienceWorld, pp. 493–510. https://doi.org/10.2138/rmg.2008.68.17

Walter, L.S., French, B.M., Heinrich, K.F.J., Lowman, P.D., Doan, A.S., Adler, I., 1971. Mineralogical studies of Apollo 12 samples, in: 2nd Lunar Science Conference. M.I.T. Press, pp. 343–358.

Wang, K., Jacobsen, S.B., Sedaghatpour, F., Chen, H., Korotev, R.L., 2015. The earliest Lunar Magma Ocean differentiation recorded in Fe isotopes. Earth Planet. Sci. Lett. 430, 202–208. https://doi.org/10.1016/j.epsl.2015.08.019

Wang, S.-J., Wasylenki, L.E., 2017. Experimental constraints on reconstruction of Archean seawater Ni isotopic composition from banded iron formations. Geochim. Cosmochim. Acta 206, 137–150. https://doi.org/10.1016/J.GCA.2017.02.023

Warren, P.H., 1985. THE MAGMA OCEAN CONCEPT AND LUNAR EVOLUTION. Ann. Rev. Earth planet. Sci 13, 201–241.

Warren, P.H., Wasson, J.T., 1979. The Origin of KREEP. Rev. Geophys. Sp. Phys. 17.

Wasylenki, L.E., Howe, H.D., Spivak-Birndorf, L.J., Bish, D.L., 2015. Ni isotope fractionation during sorption to ferrihydrite: Implications for Ni in banded iron formations. Chem. Geol. 400, 56–64. https://doi.org/10.1016/j.chemgeo.2015.02.007

Weber, R.C., Lin, P., Garnero, E.J., Williams, Q., Lognonné, P., 2011. Seismic Detection of the Lunar Core 331, 309–312.

Wedepohl, K.H., 1974. Nickel, in: Wedepohl, K.H. (Ed.), Handbook of Geochemistry. Springer.

Weis, D., Kieffer, B., Maerschalk, C., Barling, J., de Jong, J., Williams, G.A., Hanano, D., Pretorius, W., Mattielli, N., Scoates, J.S., Goolaerts, A., Friedman, R.M., Mahoney, J.B., 2006. High-precision isotopic characterization of USGS reference materials by TIMS and MC-ICP-MS. Geochemistry, Geophys. Geosystems 7, n/a-n/a. https://doi.org/10.1029/2006GC001283

Weyer, S., Anbar, A.D., Brey, G.P., Münker, C., Mezger, K., Woodland, A.B., 2007. Fe-isotope fractionation during partial melting on Earth and the current view on the Fe-isotope budgets of the planets (reply to the comment of F. Poitrasson and to the comment of B.L. Beard and C.M. Johnson on “Iron isotope fractionation during planetary differentiation” by S. Weyer, A.D. Anbar, G.P. Brey, C. Münker, K. Mezger and A.B. Woodland). Earth Planet. Sci. Lett. 256, 638–646. https://doi.org/10.1016/J.EPSL.2007.01.038

White, W.M., 1985. Sources of oceanic basalts: Radiogenic isotopic evidence. Geology 13, 115. https://doi.org/10.1130/0091-7613(1985)13<115:SOOBRI>2.0.CO;2

White, W.M., McBirney, A.R., Duncan, R.A., 1993. Petrology and geochemistry of the Galápagos Islands: Portrait of a pathological mantle plume. J. Geophys. Res. Solid Earth 98, 19533–19563. https://doi.org/10.1029/93JB02018

White, W.M., Tapia, M.D.M., Schilling, J.-G., 1979. The petrology and geochemistry of the Azores Islands. Contrib. to Mineral. Petrol. 69, 201–213. https://doi.org/10.1007/BF00372322

Wiechert, U., Halliday, A.N., Lee, D.-C., Snyder, G.A., Taylor, L.A., Rumble, D., 2001. Oxygen Isotopes and the Moon-Forming Giant Impact. Science (80-.). 294, 345–348.

Wieczorek, M.A., Jolliff, B.L., Khan, A., Pritchard, M.E., Weiss, B.P., Williams, J.G., Hood, L.L., Righter, K., Neal, C.R., Shearer, C.K., McCallum, I.S., Tompkins, S., Hawke, B.R., Peterson, C., Gillis, J.J., Bussey, B., 2006. The Constitution and Structure of the Lunar Interior, in: Reviews in Mineralogy & Geochemistry Volume 60: New Views of the Moon. pp. 221–343.

Willbold, M., Stracke, A., 2006. Trace element composition of mantle end-members: Implications for recycling of oceanic and upper and lower continental crust. Geochemistry, Geophys. Geosystems 7, 1–30. https://doi.org/10.1029/2005GC001005

Williams, H.M., Bizimis, M., 2014. Iron isotope tracing of mantle heterogeneity within the source regions of oceanic basalts. Earth Planet. Sci. Lett. 404, 396–407. https://doi.org/10.1016/J.EPSL.2014.07.033

Williams, H.M., Mccammon, C.A., Peslier, A.H., Halliday, A.N., Teutsch, N., Levasseur, S., Burg, J.-P., 2004. Iron Isotope Fractionation and the Oxygen Fugacity of the Mantle. Source Sci. New Ser. 304, 1656–1659.

Williams, H.M., Nielsen, S.G., Renac, C., Griffin, W.L., O'Reilly, S.Y., Mccammon, C.A., Pearson, N., Viljoen, F., Alt, J.C., Halliday, A.N., 2009. Fractionation of oxygen and iron isotopes by partial melting processes: Implications for the interpretation of stable isotope signatures in mafic rocks. Earth Planet. Sci. Lett. 283, 156–166. https://doi.org/10.1016/j.epsl.2009.04.011

Williams, H.M., Peslier, A.H., Mccammon, C., Halliday, A.N., 2005. Systematic iron isotope variations in mantle rocks and minerals : The effects of partial melting and oxygen fugacity. Earth Planet. Sci. Lett. 235, 435–452. https://doi.org/10.1016/j.epsl.2005.04.020

Williams, H.M., Prytulak, J., Woodhead, J.D., Kelley, K.A., Brounce, M., Plank, T., 2018. Interplay of crystal fractionation, sulfide saturation and oxygen fugacity on the iron isotope composition of arc lavas: An example from the Marianas. Geochim. Cosmochim. Acta 226, 224–243. https://doi.org/10.1016/J.GCA.2018.02.008

Wing, B.A., Farquhar, J., 2015. Sulfur isotope homogeneity of lunar mare basalts. https://doi.org/10.1016/j.gca.2015.09.003

Wood, B.J., Bryndzia, L.T., Johnson, K., 1990. Mantle Oxidation State and Its Relationship to Tectonic Environment and Fluid Speciation. Science (80-.). 248.

Wood, B.J., Kiseeva, E.S., Mirolo, F.J., 2014. Accretion and core formation: The effects of sulfur on metal-silicate partition coefficients. Geochim. Cosmochim. Acta 145, 248–267. https://doi.org/10.1016/j.gca.2014.09.002

Yi, W., Halliday, A.N., Alt, J.C., Lee, D.-C., Rehkämper, M., Garcia, M.O. 0, Langmuir, C.H., Su, Y., Rehkämper, M., Garcia, M.O. 0, Langmuir, C.H., Su, Y., 2000. Cadmium, indium, tin, tellurium, and sulfur in oceanic basalts: Implications for chalcophile element fractionation in the Earth. J. Geophys. Res. 105, 18,927-18,948. https://doi.org/10.1029/2000JB900152

Yi, W., Halliday, A.N., Lee, D.-C., Christensen, J.N., 1995a. Indium and tin in basalts, sulfides, and the mantle. Geochim. Cosmochim. Acta 59, 5081–5090.

Yi, W., Halliday, A.N., Lee, D.-C., Christensen, J.N., 1995b. Indium and tin in basalts, sulfides, and the mantle. Geochim. Cosmochim. Acta 59, 5081–5090. https://doi.org/10.1016/0016-7037(95)00342-8

Zhao, Y., Xue, C., Liu, S.-A., Symons, D.T.A., Zhao, X., Yang, Y., Ke, J., 2017. Copper isotope fractionation during sulfide-magma differentiation in the Tulaergen magmatic Ni–Cu deposit, NW China. Lithos 286–287, 206–215. https://doi.org/10.1016/J.LITHOS.2017.06.007

Zindler, A., Hart, S., 1986. CHEMICAL GEODYNAMICS, Ann. Rev. Earth Planet. Sci.

3. Nickel isotopic fractionation in the terrestrial mantle

3.1. Introduction

The bulk Earth is estimated to contain 1.8 wt% Ni, of which the majority is in the core (estimated at 5.2 wt%) (Henderson and Henderson, 2009). An estimated 99.97% of the Ni budget of the bulk silicate Earth (BSE, the combined mantle and crust) resides in the mantle (McDonough and Sun, 1995). Terrestrial Ni is abundant in both Fe-Ni metal in elemental form, and substituting for Fe and Mg in common silicate structures as a divalent cationic species. In terrestrial natural environments the 2+ valence state dominates almost exclusively, as the most stable oxidation state (Nicholls, 1974).

The partitioning of Ni does not depend on the Ni concentration in the system, although melt composition does play a strong role (Hart and Davis, 1978). Nickel has a similar ionic radius and charge to magnesium; the radii of Mg^{2+} and Ni^{2+} are 0.072 nm, and 0.069 nm respectively (Henderson and Henderson, 2009). Therefore, the Ni^{2+} ion partitions readily into the octahedral metal sites in olivine, usually in place of Mg^{2+}. For this reason, Ni is highly concentrated in olivine, and to a lesser degree in other ferromagnesian silicates, and is highly compatible during basalt melting. The strongly compatible behaviour means that Ni concentrations are highly variable in particular because of olivine fractionation. Nickel concentrations in basaltic magmas and their partially melted mantle residues, depend on the partitioning between liquid and residual solid or cumulate phases, T-P conditions of fractional crystallization and partial melting, the Ni contents of the sources, and melt-rock reaction (Herzberg et al., 2016).

Unlike iron (Fe), which also is in solid solution with Mg in mantle silicates, Ni is not redox sensitive. Iron can be in the +2 or +3 form depending on the degree of oxidation. Stable Fe isotopes are fractionated during partial melting (e.g. Williams et al. 2004; 2005). Investigation of Ni provides the opportunity to investigate such processes without the complication of effects associated with changes in oxidation state.

Analysis of stable Ni isotope composition of mantle samples, excluding reference materials analysed for inter-laboratory comparison, has so far been limited (Figure 8). Three estimates have been published for the bulk silicate Earth (BSE). The first estimate ($\delta^{60/58}Ni_{SRM986}$=0.18±0.04‰, (Steele et al., 2011)) was taken from 3 rock standards from Cameron (2009) and Steele (2011). This was followed by Gueguen and co-workers (2013) much lighter estimate of $\delta^{60/58}Ni_{SRM986}$=0.05±0.05‰, using igneous and ultramafic reference materials as well as fresh and altered basalts from Loihi, and clay and basalt samples from IODP core 1149. The Gueguen estimate was later revised by Elliott and Steele (2017) to produce a very precise BSE estimate including only samples of mantle and mantle derived melts, of $\delta^{60/58}Ni_{SRM986}$=0.11±0.01‰. The most comprehensive estimate, $\delta^{60/58}Ni_{SRM986}$=0.23±0.06‰, consisted only of fertile peridotite xenoliths and Phanerozoic komatiites (Gall et al., 2017).

Four peridotite samples were sampled by Ratié and co-workers (2015) as the parent rock for their study on tropical weathering of ultramafic bedrock, and yielded $\delta^{60/58}Ni_{SRM986}$ of 0.23 to 0.32‰. Seven ultramafic xenoliths were analysed by Gall and co-workers (2017) including a single pyroxenite with a relatively heavy Ni isotopic composition. This large study by Gall and co-workers (2017), provided preliminary evidence that Ni isotopic variation in the mantle might be controlled by mineralogical variations. The authors found a strong positive correlation between bulk rock $\delta^{60/58}Ni_{SRM986}$ and modal clinopyroxene abundance (between 1% and 3.5%). Such a control would be surprising given that Ni substitutes into the same Mg site in the lattice structure of all analysed minerals. The implication would be that Ni isotope compositions of mantle partial melts derived from depleted (olivine-dominated) versus enriched (pyroxene-dominated) lithologies may be distinguishable with Ni isotopes (Gall et al., 2017). Therefore, the stable nickel isotope compositions of primitive melts may be a potential tracer of mantle source lithology (Gall et al., 2017).

In addition to the published xenolith data, ultramafic rock standards have been analysed for inter-laboratory comparison. These consist of fertile peridotites PCC1 (Cameron et al., 2009; Chernonozhkin et al., 2015; Gall et al., 2017, 2012; Gueguen et al., 2013), and JP1

(Chernonozhkin et al., 2015; Steele et al., 2012, 2011), and dunites DTS1 (Chernonozhkin et al., 2015; Gall, 2011; Gall et al., 2017; Gueguen et al., 2013), DTS2 (Steele et al., 2012, 2011) and NHM1 (Gall et al., 2017). These samples are not shown on Figure 8.

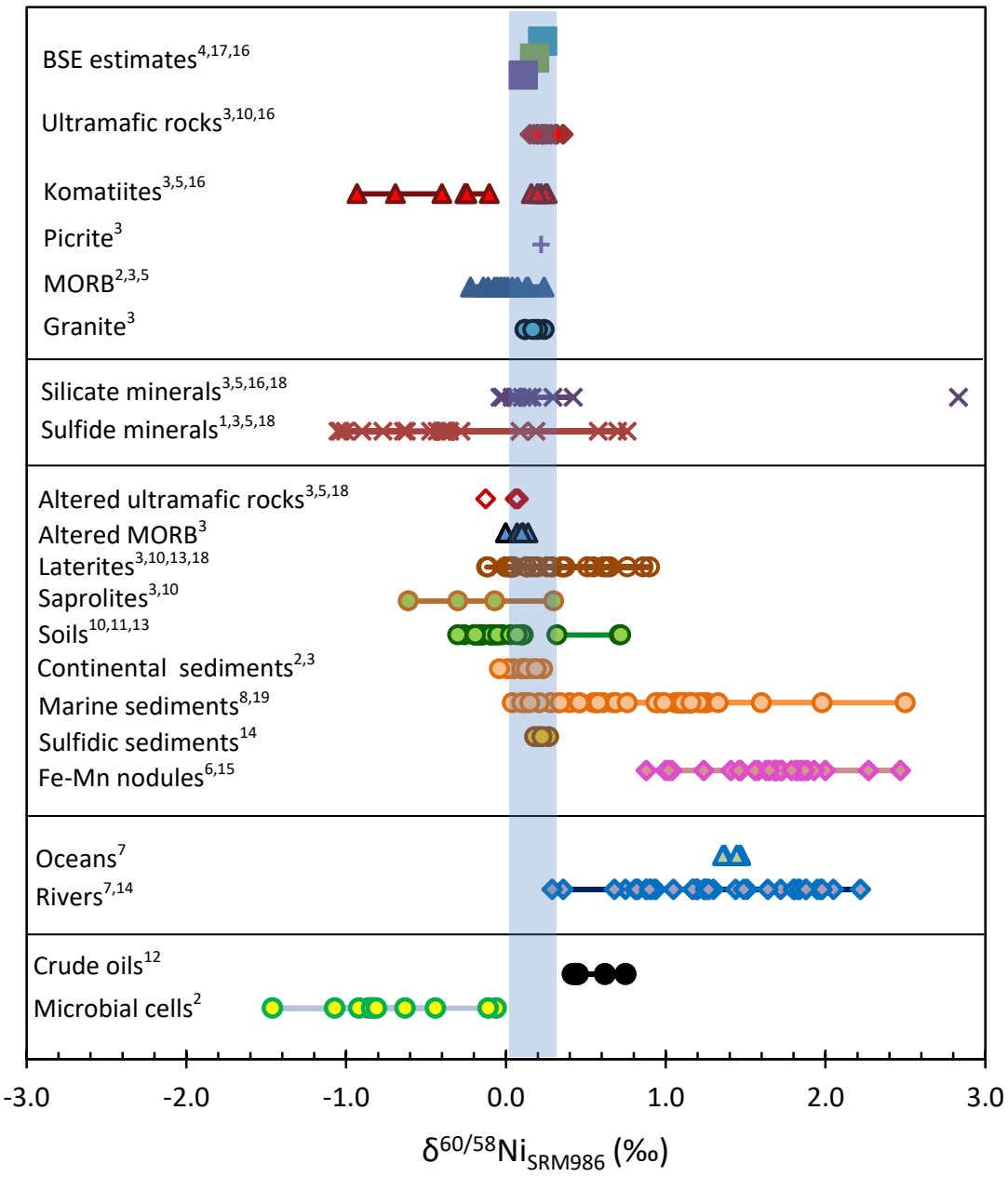

Figure 8

Published $\delta^{60/58}Ni_{SRM986}$ data for terrestrial samples. BSE estimates for comparison, from (Gall et al., 2017; Steele et al., 2011) and with the estimate of Gueguen and co-workers (2013) recalculated by (Elliott and Steele, 2017) to remove sediments.

[1](Tanimizu and Hirata, 2006); [2](Cameron et al., 2009); [3](Gall, 2011); [4](Steele et al., 2011); [5](Gueguen et al., 2013); [6](Gall et al., 2013); [7](Cameron and Vance, 2014); [8](Porter et al., 2014); [9](Hofmann et al., 2014); [10](Ratié et al., 2015); [11](Estrade et al., 2015); [12](Ventura et al., 2015); [13](Ratié et al., 2016); [14](Vance et al., 2016); [15](Gueguen et al., 2016); [16](Gall et al., 2017); [17](Elliott and Steele, 2017); [18](Spivak-Birndorf et al., 2018); [19](Ciscato et al., 2018)

Komatiites are igneous rocks formed from such high degrees of partial melting of the mantle that they are often assumed to represent the composition of the mantle at the time and place of formation (e.g. Dauphas and co-workers (2010)). Gall and co-workers (2017) analysed 5 Phanerozoic komatiites and found them to be within the range of mantle xenoliths analysed in this study (average $\delta^{60/58}Ni_{SRM986}$=0.21±0.08‰, ranging from 0.15 to 0.26‰). Archean komatiite samples have been found to be more variable in Ni isotopic composition. Three samples with disseminated sulfide mineralisation from Australia were analysed at 0.93 to -0.40‰ (n=3) and found to also have light Ni isotopic compositions (Gall 2011). Gueguen and co-workers (2013) also analysed Archean komatiite samples with sulfide mineralisation and found a large range in Ni isotopic compositions from =-0.10 to -1.04‰.

Serpentinised peridotites gave lighter values of $\delta^{60/58}Ni_{SRM986}$=0.07 and 0.08‰ (Gall 2011), which compares with a serpentinite analysed by Gueguen and co-workers (2013) at $\delta^{60/58}Ni_{SRM986}$=-0.13‰. Dunite samples are limited to Spivak-Birndorf and co-workers (2018) single examples of altered ($\delta^{60/58}Ni_{SRM986}$=0.06‰) and unaltered dunite ($\delta^{60/58}Ni_{SRM986}$=0.20‰). Seawater, rivers, ferromanganese crusts and sediments are heavy in Ni isotopic composition (Figure 8). Laterites produced from extreme chemical weathering of ultramafic rocks are mostly relatively heavy (Gall, 2011; Ratié et al., 2015). Other soils are more variable.

In early work by Gall (2011), MORB samples were shown to be significantly lighter than the estimate for bulk mantle, and hence it was suggested that Ni isotopes fractionate with partial melting, with lighter isotopes preferentially enriched in the melt phase during melting. In Gall (2011), a relationship was also found between ridge spreading rate and Ni isotopic composition of the pillow basalt, with slow ridges having heavier compositions than fast-spreading ones.

In this work, a variety of bulk ultramafic xenoliths were analysed from Kilbourne Hole (New Mexico, USA), Lashaine and Labait Hill (Tanzania), and the Cameroon Line (Cameroon) in order to investigate potential heterogeneity in Ni isotopic composition in the mantle. The samples include fertile peridotites, as representative of the majority of the upper mantle, and also several samples of dunite and pyroxenite.

Previously published mantle mineral Ni isotopic composition data is limited to a single basalt-hosted olivine from (Gueguen et al., 2013), a leaching experiment on olivine (Spivak-Birndorf et al., 2018), and 7 minerals from 3 xenoliths (including olivine, orthopyroxene, clinopyroxene) and 2 megacrysts (clinopyroxene, garnet) from (Gall et al., 2017).

In this study, we analysed a variety of separated mineral phases from ultramafic xenoliths from Kilbourne Hole (New Mexico, USA), Lashaine (Tanzania), and the Cameroon Line (Cameroon), in order to investigate Ni isotope fractionation in the mantle. The major phases in ultramafic rocks: olivine, orthopyroxene, clinopyroxene, and spinel were analysed from several xenoliths. Where all major phases were analysed and modal mineralogy was available, reconstructed bulk Ni isotopic compositions were calculated and compared to the analysed bulk values. Additionally, 2 megacrysts from the Cameroon Line were analysed. The formation of megacrysts and their relationship to host rocks are not well understood; they are not always in equilibrium with their host magmas (Menzies et al., 1987). Megacryst data may not be representative of mantle minerals. Megacrysts from Cameroon Line display comparable Nd and Sr isotopic as the lavas (Lee, 1994), suggesting a co-genetic origin. The N12 megacryst samples (clinopyroxene, garnet, and feldspar – latter not analysed here) are from the same lava flow, but the REE evidence suggests all 3 megacrysts cannot be all cogenetic (Lee, 1994).

In summary, this study aims to address the causes of previously reported Ni isotope variations in the mantle, by greatly expanding the dataset of bulk rock mantle samples and further exploring the Ni isotopic fractionation between mineral phases in the mantle and the reported relationship between Ni isotopic compositions and mineral abundance. Of these, the Kilbourne Hole suite is thoroughly documented and, relatively simple offering investigation of relatively pristine samples across a range of mantle lithologies and constituent minerals, from a single locality.

3.2 Sample strategy

The samples in this work were chosen to investigate all major mantle lithologies, sourced from two cratons and various geographical localities. The samples were collected from Tanzania, Cameroon, and New Mexico (USA) and of these, preference was given to samples with published geochemical and petrological data.

Kilbourne Hole allows for investigation of fresh and unaltered samples of the full range of fertile mantle lithologies and constituent minerals, from a single xenolith locality. In contrast, Tanzanian xenoliths exhibit a range of alteration and metasomatism. Analysis of Cameroon Line xenoliths can be contrasted directly with the in depth study of partial melting (see Chapter 4). Comparison between analyses from different geographical localities can also allow assessment of large-scale mantle heterogeneity.

Xenoliths of ultramafic material are frequently brought to the surface during the eruption of intraplate magmas. Entrainment of mantle samples is relatively random aiding in investigating average mantle composition and basalt source regions over a range of depths (Harvey et al., 2011). A single sampling locality may include xenoliths entrained from depths a hundred of kilometres apart vertically (Nixon, 1987). The rapidity of the exhumation limits the effects of serpentinization and tectonism (Harvey et al., 2012).

In general, the mineralogy, and therefore lithology, of xenoliths depends on bulk composition and pressure with certain minerals diagnostic of different pressure ranges (plagioclase=low, spinel=moderate, and garnet=high) (Perkins and Anthony, 2011). Peridotite is defined as an ultramafic coarse-grained rock containing >40% olivine, which includes lherzolites, harzburgite and dunites.

Lherzolite is defined as having between 40% and 90% olivine, and >5% of both orthopyroxene and clinopyroxene. Samples analysed in this study include garnet and spinel bearing lherzolites from localities from two continents (Africa, USA). Lherzolites can host spinel or garnet depending on an exchange reaction that is depth dependent and sensitive to the Cr^{3+} and Fe^{3+}

content of the rock. This equilibrium exchange reaction has been used as a successful geobarometer (O'Neill, 1981). However, garnet lherzolites also include two suites, a low temperature suite <1100°C, and a high temperature one of deeper origin (Finnerty and Boyd, 1987).

Although the majority of mantle samples are lherzolites, other lithologies are important to consider. Harzburgite is defined as having between 40% and 90% olivine, and less than 5% clinopyroxene. Dunite is defined as being >90% olivine, with either pyroxenes or accessory minerals. Pyroxenite is defined as having >60% pyroxene, with websterites specifically having >90% pyroxene and both pyroxenes in abundance >5%. Both harzburgites and dunites are thought to be residues of up to 40% adiabatic decompression melting of fertile peridotites such as garnet and spinel lherzolites. Dunites can also be formed from accumulation of olivine in crustal magma chambers (Dawson et al., 1970).

Potentially significant mantle minerals that were not analysed in this study include sulfides and mantle garnet. Sulfides occur in very small amounts and garnets have low Ni concentrations (basaltic garnet 4-16 ppm, ultramafic garnet 40-300 ppm (Wedepohl, 1974)). Neither contributes significantly to the Ni budget. Arguments for this are presented in section 3.5.2.

3.2.1 African xenoliths

Tanzania

The two Tanzanian localities (Lashaine and Labait Hill) bracket the Eastern branch of the East African Rift, the main active continental rift on Earth. Tanzanian magmatic activity relating to the EAR began with voluminous basaltic to trachytic magmatism around 5 Ma and was followed eventually small-volume explosive, highly alkaline nephelinitic to carbonatitic volcanism (Dawson, 1992) until ending about 1 Ma (Aulbach et al., 2008). Interstitial clinopyroxene, melt veins, melt pockets, and rims of phlogopite have been inferred to relate to rift-related metasomatism beneath Tanzania (Koornneef et al., 2009). These features are all in chemical disequilibrium with the original xenolith mineralogy (Koornneef et al., 2009). Dawson (2012) suggested that both Lashaine and Labait sampled un-metasomatised mantle as well as

metasomatised mantle. Xenoliths from both localities have similar ranges in Sr, Nd, and Pb isotopic compositions (Paslick, 1995).

Lashaine

Lashaine, Tanzania (3°22'S, 36°26'E) is an ankaramitic and carbonatitic tuff cone ~90 km SE of Oldoinyo Loolmurwak, on the Monduli plains (Dawson, 1964a). Seismic data indicates a low velocity zone beneath Lashaine (Gibson et al., 2013). The 700 ft cone consists of glassy scoria and numerous ultramafic xenoliths (Dawson et al., 1970). The first discovery of ultramafic xenoliths at this site was by J. B. Dawson in 1961 (Dawson, 1964b), described as "blocks of garnetiferous peridotite, harzburgite and dunite … highly reminiscent of the cognate xenoliths found in kimberlite pipes". A different collection of xenoliths were described in (Pike et al., 1980) as only up to 18% garnetiferous peridotite. Lashaine is also known as one of the first locations where hydrous minerals of demonstrably mantle origin were found (Dauritria and Girod, 1987). The earliest eruptions were of ankaramitic scoria, with the majority of the xenoliths found in the later the carbonatitic tuff (Dawson et al., 1970; Rhodes and Dawson, 1975).

Xenoliths found in the Lashaine Tuff are generally smaller than 15 cm in any dimension (maximum 25 cm) (Dawson, 2002), and Gibson and co-workers (2013) found no evidence of significant hydrothermal alteration. The xenoliths are described as fresh, and having minimal interaction with the host rock (Rhodes and Dawson, 1975). The temperature and pressure of the last equilibration of the garnetiferous xenoliths was estimated at 960 to 1085°C and 3.2 to 5.0 GPa (Gibson et al., 2013).

Reid and co-workers (1975) found the xenolith assemblages had been altered locally by three different secondary processes. These are proposed based on evidence of a reaction between of garnet and adjacent olivine (producing reaction rims of aluminous orthopyroxene, aluminous clinopyroxene and spinel); marginal or total alteration of some chrome-diopside (thought to be secondary melting); and evidence of extremely localised partial melting at some grain

boundaries (producing quenched interstitial melt in various combinations of olivine, clinopyroxene, orthopyroxene, spinel, phlogopite, and glass (Reid et al., 1975).

Evidence for 2 episodes of metasomatism, preceded by a major element depletion was presented in Dawson (2002). These are identified at >3.4 Ga (major element depletion, producing high-olivine restite protolith, dated by Os isotopes (Burton et al., 2000)), >2.0 Ga (K, Fe, Ca, Ti, and Rb metasomatism, which produced Cr-diopside and phlogopite, dated using Nd and Pb isotopic model ages (Burton et al., 2000)), and one later but undated (influx of K, Fe, Ca, Ti, Nb, and Ti, producing non-equilibrated Ti phlogopite, Ti-Cr diopside, enstatite-bronzite, ilmenite and rutile) (Dawson, 2002). The recognition of two episodes of metasomatism explained previously identified major differences in the isotopic chemistry of diopsides in the Lashaine peridotite xenoliths (Dawson, 2002).

Labait Hill

Labait Hill (4°35′S, 35°26′E) is a small, recently discovered Quaternary cone, 150 km SW of Lashaine, between the Mozambique belt and Tanzanian Craton (Dawson, 2002; Gibson et al., 2013). The xenoliths were extruded recently therefore sampling the present day Tanzanian mantle (Vauchez et al., 2005). The mantle beneath the Tanzanian craton is perturbed by a mantle plume and by the eastern branch of the East African Rift (seismic evidence) (Vauchez et al., 2005). Labait is described in Paslick (1995) as a small cratered cone, on the suture zone between Archean craton (Tanzanian Craton) and Proterozoic mobile belt (Mozambique belt).

Lavas erupted by the Labait volcano sample the mantle from >140 km (lithosphere-asthenosphere boundary) to <70 km (the spinel-peridotite domain) (Vauchez et al., 2005). Underneath Labait, the mantle lithosphere is highly refractory to ~140 km, and then increases in fertility until 150 km (Aulbach et al., 2008). Labait is described as being formed of melilite-dominated flows (Dawson, 2012), but there are limited publications on the host material in this xenolith location.

The xenoliths are dominantly lherzolites at this location with only ~10% being harzburgitic (Gibson et al., 2013). However, Koornneef and co-workers (2009) sampled a different set of

xenoliths (500 samples) and found ~70 % were dunites, with lherzolites and harzburgites being ~10% each.

Paslick (1995) prepared the samples used here but did not obtain chemical compositions for bulk rocks because of "various degrees of alteration of the xenoliths". Both spinel lherzolites and garnet lherzolites are found at this locality. Equilibration temperatures for these xenoliths range from 920°C to 1300°C, with estimated depths of equilibration for the garnetiferous samples of 110-140 km (Paslick, 1995). The mineral chemistry of Labait xenoliths is distinct from that of the Lashaine xenoliths (Gibson et al., 2013).

In garnetiferous xenoliths the garnet has reacted to form spinel-orthopyroxene-diopside intergrowths, with a temperature of 1270-1350°C (Paslick, 1995). The olivine is not zoned, and is chemically similar to other Tanzanian localities (Paslick, 1995). Labait samples have very enriched μ values (μ = $^{238}U/^{204}Pb$, more enriched at Labait than other localities across the world) indicating a recent metasomatic event (Paslick, 1995). Dawson (2012) presents evidence for a series of metasomatic events at Labait, similar to those proposed for Lashaine, dated at 2.8 Ga and 2.4 Ga as well as "pervasive Fe enrichment".

Cameroon Line

The Cameroon Line is a roughly linear volcanic system with volcanoes in Nigeria, Cameroon, Equatorial Guinea (through the island Bioko), and São Tomé and Príncipe. There are 17 plutonic complexes (all on the continental sector and emplaced between ~65-30 Ma) and 12 major volcanic centres (active from ~42 Ma, but Mount Cameroon is the only one currently active) (e.g. (D.-C. Lee et al., 1996)). The Cameroon Line is a unique geological situation, as it is the only known intra-plate alkaline volcanic province to transect the oceanic to continental boundary (Fitton, 1987).

The Cameroon Line has a disputed origins including a mega-shear zone, a continental rift, a series of horsts and grabens (Moreau et al., 1987), membrane tectonics (Freeth, 1979), and rifting associated with a hotspot (Morgan, 1983). A hotspot source was considered unlikely by Fitton and Dunlop (1985) due to the lack of migration of volcanism with time, with their

explanation involving a laterally displaced (by movement of the African plate) region of volcanism previously related to upwelling under the Benue Trough. A fracture zone model is also excluded as an origin because it cannot explain the partial melting of the mantle (Lee, 1994). Halliday and co-workers (1990), identified high $^{206}Pb/^{204}Pb$ ratios in lavas from the continent-ocean-boundary of the Cameroon Line characteristic of the HIMU mantle endmember, suggesting a fossil mantle plume with diminishing lateral effects.

Ultramafic xenoliths examined in this study were erupted in various host lavas from Cameroon, specifically from Ngaoundéré and a site near Lake Barombi Mbo (~54 km NE of Mount Cameroon). Ngaoundéré is the Eastern extremity of the Cameroon Line and one of only two volcanic plateaux in the system (the other being Biu plateau, Nigeria, the most Northern extremity) e.g. (D.-C. Lee et al., 1996). The plateau is built up from alkali basalt flows, with a central volcano that produced basanite with minor trachyte and phonolite (Lee, 1994). The central volcano, Nganha, dates to 10-7 Ma (K-Ar, (Lee, 1994)). Lake Barombi Mbo is a Quaternary maar (crater formed from phreatomagmatic explosions) approximately half way between Manengouba and Mount Cameroon (4°39'45"N and 9°24'15"E), near the town of Kumba (Maley et al., 1990). Ages of one basaltic lava flow range from 4.7 to 1.1 Ma (Maley et al., 1990), with the younger endmember related to alteration. Fragments of peridotite xenoliths are described in Cornen and co-workers (1992) as widespread, in a sequence of 3 main deposits (old basaltic lavas, cindercones and phreatomagmatic units, and a vesicular basaltic lava flow) totalling 126 m thickness (Chako Tchamabé et al., 2013). The xenoliths at Lake Barombi Mbo are of similar lithologies to elsewhere in the Cameroon Line, with samples showing some chemical heterogeneity (Pinter et al., 2015). Barombi Mbo xenoliths record a small degree of partial melting (Pinter et al., 2015).

3.2.2 Kilbourne Hole, New Mexico, USA

Kilbourne Hole (31°59’N, 106°57’W) is part of the Late Pleistocene Potrillo Volcanic Field (PVF) on the axis of the Rio Grande Rift (Harvey et al., 2012). The Rio Grande Rift is an asymmetric graben system, stretching through Colorado, New Mexico, and Texas for >1000 km

(Harvey et al., 2011). The area is characterised by high heat flow (James et al., 1980), and is thought to sample depleted mantle with some "enriching events" (Feigenson, 1986). The crust at this locality has been estimated at <28 km, from gravity and teleseismic studies (Keller et al., 1990), which is therefore the upper limit of the depth for the origin of the xenoliths.

The PVF is one of the largest silica-undersaturated volcanic fields in the Rio Grande Rift (Satsukawa et al., 2011) and hosts abundant mantle and crustal xenoliths, especially around Kilbourne Hole, which dominantly have protogranular textures (Harvey et al., 2012). Due to the relatively young age of the extrusion (with published age estimates from 141 to 10 Ka (Satsukawa et al., 2011)), the xenoliths can be assumed directly representative of the modern day mantle underneath Kilbourne Hole.

The ultramafic samples from Kilbourne Hole include a range of spinel lherzolite, harzburgite and pyroxenite xenoliths from the Kilbourne Hole volcanic maar. Pyroxenite xenoliths from Kilbourne Hole have been successfully modelled as crystal segregates from an alkali magma (Irving, 1980; Roden et al., 1988). The peridotite xenoliths are described in Harvey and co-workers (2012) as relatively simple petrologically but affected by a number of processes potentially including melt depletion, melt-rock reaction, refertilization, and metasomatic events.

The xenoliths were all originally >1 kg, to limit potential effects from infiltration of the host basanite, and ensure sufficient interior to homogenise the bulk sample, with the range chosen to include a variety of amounts clinopyroxene (Harvey et al., 2012). Geothermometry calculations by Harvey and co-workers (2012) reveal equilibrium temperatures between 939 and 1180°C.

The xenoliths from Kilbourne Hole are remarkably fresh and no serpentinization or discernable alteration of the silicates or spinel was observed (Harvey et al., 2015). Previous studies of this locality have unanimously found no discrete metasomatic phases. Some evidence is seen in KH03-10 and KH03-27 for interaction with (or infiltration of) host basanite (Harvey et al., 2015), but generally sampling from the centre of large xenoliths is thought to have limited this. Harvey and co-workers (2012) suggested that clinopyroxene and host basanite dominate the range of bulk rock Sr-Nd isotope ratios in the bulk xenoliths. Evidence for melt depletion is also

provided by the strong correlation (r^2 = 0·93) between some moderately incompatible elements within the xenolith suite (Harvey et al., 2012).

The host rock for the Kilbourne Hole xenoliths is a basanite (Harvey et al., 2011; Roden et al., 1988), with high Al_2O_3 and CaO, but low MgO. The host basanite chemically resembles the high-field-strength-elements (HFSE) depleted interstitial glass of the xenoliths (Harvey et al., 2012), suggesting that this glass was derived during a similar process of low degree aesthenospheric melting as formed the lavas of the PVF.

3.3 Sample preparation

The samples used in this study were either given for investigation by the late Prof Barry Dawson (samples from Tanzania), by Dr Jason Harvey from his collection (New Mexico, USA), or collected during various fieldwork expeditions by teams including Prof Alex Halliday, Prof Godfrey Fitton, Dr Cassi Paslick, and Dr Der-Chuen Lee. Prof Sally Gibson, University of Cambridge, supplied further information, thin sections, and samples left in her care by Prof Barry Dawson.

The bulk ultramafic samples were mostly archive powders, with the exception of H93-X series, which were fine crushates. The mineral separates were hand-picked under 50x magnification and no alteration products, inclusions, composite grains, surficial adherents, or weathered edges were permitted to affect any picked grain (see Chapter 2).

Details of purification and analysis are fully described in described in Chapter 2, therefore, only a short summary is provided here. All acids used were distilled in house by sub-boiling and diluted by volume with ultrapure 18MΩ MQ water. Samples were accurately weighed into PFA Teflon vials and dissolved using 1 part HF and 3 parts HNO3 (2 ml total) followed by dissolution in 6M HCl (up to 5 ml), and the latter usually used a high-pressure Parr Bomb. The double spike was applied after dissolution to a ratio of 2.5 part double spike Ni to 1 part sample Ni. Ultramafic samples were dissolved without adding double spike, because of the high Ni

concentrations, in order not to waste the spike. The mineral separates were dissolved without adding double spike, in order to allow for determination of Ni concentrations by ICP-MS, and therefore allow accurate spiking. Purification of Ni is completed by three ion exchange Teflon microcloumns of diminishing size, using cation and anion resins in sequence with a method adapted from (Gall et al., 2012). Analysis was performed in pseudo-high resolution on a Nu Instruments Nu Plasma HR MC-ICPMS.

3.4 Results of bulk ultramafic samples and minerals

The Ni isotopic compositions of twenty-nine ultramafic bulk samples consisting of lherzolites, harzburgites, dunites and pyroxenites are presented in Table 3-1 and Figure 9. Additionally, 18 minerals from six rocks have been analysed in this work, including samples of olivine (4), orthopyroxene (6), clinopyroxene (6), and spinel (2). In addition to the minerals from ultramafic xenoliths, two megacrysts (garnet and clinopyroxene) were analysed. These data are presented in Table 3-2 and Figure 10.

Table 3-1

Table of Ni isotopic compositions from ultramafic samples

Nickel concentrations from isotope dilution, and n is the number of separate analyses of the sample (>3 means was run more than once from separate chemistries). External reproducibility of Ni isotopic compositions=0.06‰.

Sample Code	Lithology	Ni (ppm)	$\delta^{60/58}$Ni	2sd	n
Lashaine, Tanzania					
BD806	Fe rich mica dunite	1394	0.127	0.058	3
BD825	Spinel dunite	1552	0.098	0.053	3
BD822	Spinel harzburgite	2359	0.148	0.044	5
BD774	Lherzolite	2244	0.260	0.012	3
Labait, Tanzania					
H93-X1	Garnet lherzolite	2597	0.243	0.031	4
H93-X9	Garnet lherzolite	2575	0.173	0.073	3
H93-X8	Spinel lherzolite	2303	0.236	0.036	4
Ngaoundéré, Cameroon					
P6	Spinel-garnet-pargasite websterite	462.7	-0.256	0.007	2

P12	Spinel-garnet websterite	442.7	-0.375	0.028	6
P13	Spinel lherzolite	1978	0.147	0.047	6
Lake Barombi Mbo (Nr Mt Cameroon)					
C235D	Spinel lherzolite	1645	0.241	0.042	5
Kilbourne Hole, New Mexico					
J06	Pyroxenite with diopside, enstatite, spinel	632.6	0.156	0.022	3
J10	Pyroxenite with diopside, enstatite, olivine	232.9	0.002	0.036	3
J22	Pyroxenite with enstatite, diopside, olivine	1756.7	-0.003	0.046	2
KH03-03	Group 2 Spinel lherzolite (clinopyroxene high)	1628	0.235	0.038	3
KH03-02	Group 1 Spinel lherzolite	2070	0.131	0.069	5
KH03-06	Group 1 Spinel lherzolite	1769	0.209	0.030	3
KH03-07	Group 1 Spinel lherzolite	1829	0.212	0.047	3
KH03-10	Group 1 Spinel lherzolite with recent melt rock interaction	2003	0.111	0.064	5
KH03-11	Group 1 Spinel lherzolite	1984	0.161	0.052	3
KH03-21	Group 2 Spinel lherzolite with recent melt rock interaction	1612	0.025	0.034	5
KH03-24	Group 2 Spinel lherzolite with recent melt rock interaction	1680	0.018	0.034	4
KH03-25	Group 1 Spinel lherzolite	2195	0.205	0.039	5
KH96-2	Group 1 Spinel lherzolite	2497	0.158	0.078	3
KH96-8	Group 2 Spinel lherzolite	1862	0.199	0.033	3
KH96-18	Group 1 Spinel lherzolite	1578	0.235	0.029	4
KH03-15	Group 2 Harzburgite with recent melt rock interaction	1923	0.178	0.064	4
KH03-16	Group 2 Harzburgite (clinopyroxene low)	2203	0.234	0.050	3
KH03-27	Group 1 Harzburgite with recent melt rock interaction	2198	0.094	0.047	5

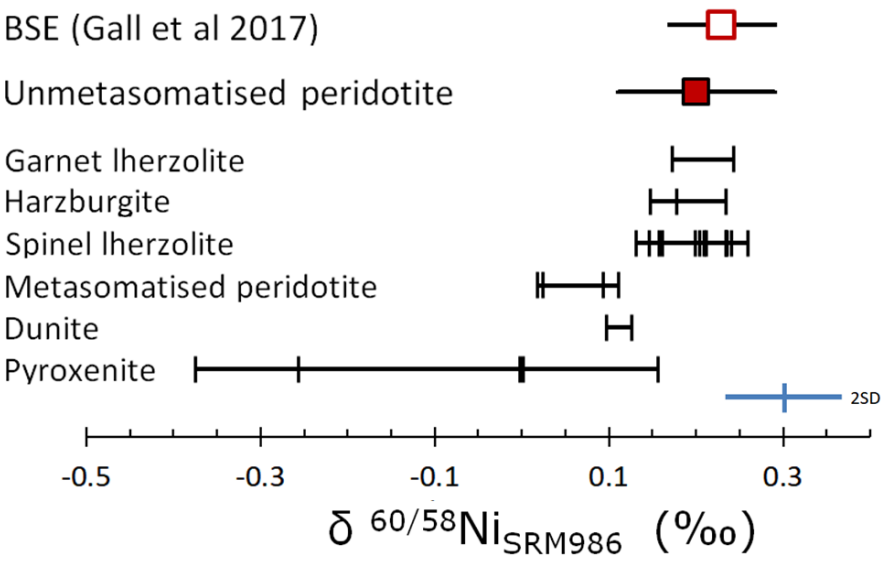

Figure 9

Nickel isotopic compositions analysed in this study for ultramafic bulk rocks samples. Samples from Cameroon, Tanzania, and Kilbourne Hole, USA. Square symbols represent the average value for (open) BSE from Gall et al 2017, and (filled) normal mantle as represented by unmetasomatised peridotites

from this work. External reproducibility on Ni isotopic composition (0.06‰) represented with the error bar presented.

Table 3-2

Table of Ni isotopic compositions from mineral separates

Nickel concentrations from isotope dilution, and n is the number of separate analyses of the sample (>3 means was run more than once from separate chemistries). External on Ni isotopic composition =0.06‰.

Mineral	Ni (ppm)	$\delta^{60/58}$Ni	2sd	n
Kilbourne Hole, New Mexico				
KH03-27, metasomatised harzburgite				
Olivine	2714	0.094	0.046	3
Orthopyroxene	1590	0.083	0.012	3
Clinopyroxene	243.4	0.036	0.012	3
Spinel	2133	0.128	0.079	6
KH03-25, spinel lherzolite				
Olivine	2745	0.172	0.045	5
Orthopyroxene	731.1	0.152	0.025	5
Clinopyroxene	327.8	0.048	0.007	2
KH03-24, metasomatised harzburgite				
Olivine	2384	-0.021	0.018	3
Orthopyroxene	661.3	-0.041		1
Clinopyroxene	323.5	-0.082	0.020	3
Spinel	2057	0.032	0.022	4
KH03-06, spinel lherzolite				
Olivine	2597	0.161		1
Orthopyroxene	711.9	0.183		1
Clinopyroxene	336.7	0.076	0.024	2
Cameroon Line				
C235D, spinel lherzolite, Lake Barombi Mbo				
Orthopyroxene	631.9	0.173	0.010	2
Clinopyroxene	262.4	0.070	0.021	2
P6, websterite, Ngaoundéré				
Orthopyroxene	625.1	-0.311	0.037	4
Clinopyroxene	270.1	-0.235	0.006	4
N12, harzburgite, Biu Plateau				
Clinopyroxene megacryst	348.8	-0.026	0.055	4
Garnet megacryst	71.78	0.069	0.026	4

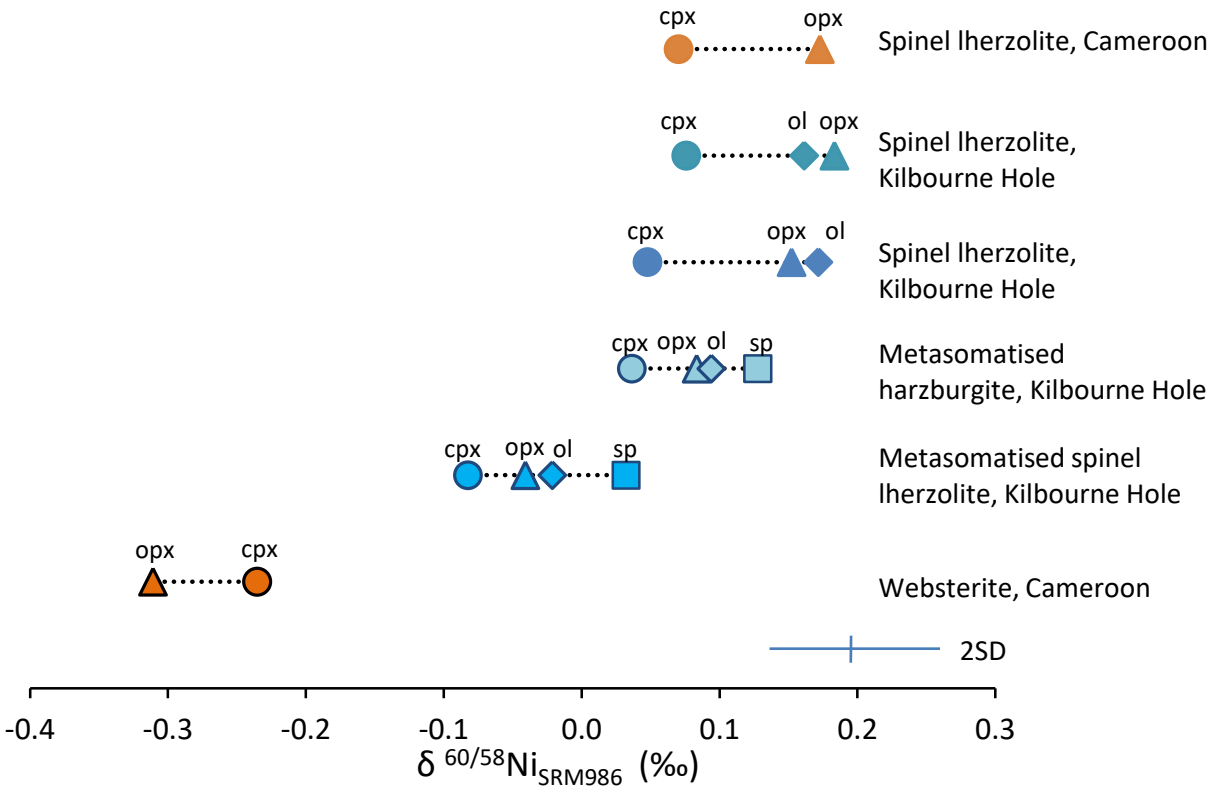

Figure 10

Nickel isotopic compositions for mineral separates from ultramafic xenoliths analysed in this work. External reproducibility on Ni isotopic composition (0.06‰) represented with the error bar presented.

3.4.1 Lherzolites and harzburgites

Most of the samples studied are spinel lherzolites (n=16) and have variable Ni isotopic compositions averaging 0.17±0.14‰. The Tanzanian samples are from Labait Hill (H93-X8 0.24‰) and Lashaine (BD774 0.26‰). The Cameroon samples are from Lake Barombi Mbo (C235D 0.24‰), and from Ngaoundéré (P13 0.15‰). The 12 USA samples are all from Kilbourne Hole (average =0.16±0.14‰). The Kilbourne Hole samples are the most variable but also the most sampled locality. However, the range in Kilbourne Hole far exceeds that seen in any other locality with $\delta^{60/58}Ni_{SRM986}$ ranging from 0.02 to 0.24‰.

The two garnet lherzolite samples (H93-X1 0.24‰, H93-X9 0.17 ‰) are both from Labait Hill (Tanzania). These Ni isotopic compositions are consistent with those of the spinel lherzolites.

The harzburgite samples (1 from Tanzania and 3 from Kilbourne Hole) average $\delta^{60/58}Ni_{SRM986}$=0.16±0.10‰ (n=4), with one sample (KH03-27) showing a significantly lighter composition of 0.09‰.

The reason for such wide variation in Kilbourne Hole is that several of the samples have anomalously light Ni isotopic compositions. The samples with these lighter Ni isotopic compositions all show petrographic features related to recent melt rock interaction including reaction rims observable in thin section around clinopyroxene grains (Harvey et al., 2012). These samples are harzburgite KH03-27 (0.09‰) and spinel lherzolites KH03-10 (0.11‰), KH03-21 (0.03‰), and KH03-24 (0.02‰). KH03-15 and KH03-16 are said to have some evidence of recent melt interaction according to Harvey (2012) but do not show light Ni isotopic compositions (0.18 and 0.23‰ respectively).

If these light samples are excluded on the basis that there has been some metasomatism the average Ni isotopic composition for lherzolites and harzburgites is 0.20±0.09‰ (n=18). This can be considered the average for unmetasomatised fertile peridotite, assumed equivalent to the BSE or 'normal mantle'.

3.4.2 Dunites and pyroxenites

The dunite samples (both Tanzanian) from this work average 0.11±0.03‰ (n=2). This average is between published analyses from Spivak-Birndorf and co-workers (2018) of altered (0.06‰) and unaltered dunite (0.20‰). The dunite average of this work is lighter than the unmetasomatised fertile peridotite average but has a low number of samples and both are from a locality thought to have metasomatism (Gibson et al., 2013).

Five pyroxenite samples were analysed in this study, including three from Kilbourne Hole (Harvey, pers. comm) and two from Ngaoundéré, Cameroon (D.-C. Lee et al., 1996).

Two of the Kilbourne Hole samples show Ni isotopic compositions of 0.00‰, much lighter than the average lherzolite samples from this locality. The third sample is the only one with spinel present and has a heavier Ni isotopic composition of 0.16‰, which is within error of the

lherzolitic average but still fractionally light. The average $\delta^{60/58}Ni_{SRM986}$ of all the Kilbourne Hole pyroxenites is 0.05±0.15‰ (n=3).

The pyroxenites from Ngaoundéré are both spinel-garnet websterites with/without pargasite (P6/P12). These samples have extremely light Ni isotopic compositions (P6 -0.26‰; P12 -0.38‰). These samples are described in (D.-C. Lee et al., 1996) as "having variable degrees of alteration", and because of this no bulk analysis was done in that paper. Both P6 and P12 have REE depletions, to a lesser extent in P6. However, bulk Ni isotope compositions are corroborated by those of pure hand-picked unaltered mineral data, suggesting surficial alterations are not causing an observable effect in Ni isotopes.

3.4.3 Mineral separates

The variation in bulk rock isotopic composition discussed above raises the question of whether Ni fractionates during melting and crystallisation. Therefore, an investigation of mantle mineral phases was undertaken. Nickel is hosted in the octahedral site of garnet, clinopyroxene, orthopyroxene, olivine, and spinel, often substituting for Mg^{2+} (Gall et al., 2017). Olivine (generally >50% of upper mantle lithologies) and spinel (<5%) host the majority of mantle Ni, with concentrations of up to 3000 ppm. Three samples with 'normal' bulk Ni isotopic compositions were analysed for multiple major mineral phases, and compared with three samples with 'light' bulk Ni isotopic compositions. For both selections, 2 from Kilbourne Hole and 1 from Cameroon were investigated.

Sample KH03-06, spinel lherzolite (Kilbourne Hole), has a bulk rock Ni isotopic composition of 0.21‰. Three mineral phases were analysed: olivine (0.16‰), orthopyroxene (0.18‰), and clinopyroxene (0.08‰). Olivine and orthopyroxene are identical within error and within error of the bulk composition as well. The other major phase, spinel, was not analysed.

Sample KH03-25, also spinel lherzolite (Kilbourne Hole), has a bulk rock Ni isotopic composition of 0.21‰. Three mineral phases were analysed: olivine (0.18‰), orthopyroxene

(0.15‰), and clinopyroxene (0.05‰). Olivine and orthopyroxene in this sample are also identical within error and but lighter than the bulk composition.

Sample C235D, spinel lherzolite (Lake Barombi Mbo, Cameroon), has a bulk rock Ni isotopic composition of 0.24‰. Two mineral phases were analysed: orthopyroxene (0.17‰), and clinopyroxene (0.07‰). These two mineral phases are significantly lighter than the bulk Ni isotopic composition, and hence one or more major phase or phases is missing from the data set and must be heavier than those so far measured.

These minerals from the unmetasomatised samples with 'normal' bulk Ni isotopic compositions, show individual mineral phases from different xenoliths with analysed Ni isotopic compositions that agree within error, despite the different host xenoliths (Figure 10). Clinopyroxene samples average $\delta^{60/58}Ni_{SRM986}$=0.06±0.03‰, and are consistently the lightest phase in Ni isotopic composition. Olivine and orthopyroxene samples are identical within error with $\delta^{60/58}Ni_{SRM986}$=0.17±0.02‰.

Sample KH03-24, spinel lherzolite (Kilbourne Hole) with evidence of recent melt-rock interaction, has a light bulk rock Ni isotopic composition of 0.02‰. Four phases were analysed: olivine (-0.02‰), orthopyroxene (-0.04‰), clinopyroxene (-0.08‰), and spinel (0.03‰). Olivine, orthopyroxene, and spinel are identical within error and within error of the bulk composition.

Sample KH03-27, harzburgite (Kilbourne Hole), shows similar evidence for recent melt-rock interaction, and has a bulk rock Ni isotopic composition of 0.09‰. Four phases were analysed: olivine (0.09‰), orthopyroxene (0.08‰), clinopyroxene (0.04‰), and spinel (0.13‰) were picked and analysed. Olivine and orthopyroxene are identical within error and within error of the bulk composition.

Sample P6, spinel-garnet-pargasite websterite (Ngaoundéré, Cameroon), has an extremely light bulk rock Ni isotopic composition of -0.26‰. Two major phases were analysed: orthopyroxene (-0.31‰) and clinopyroxene (-0.27‰). This is the only sample for which clinopyroxene is not

the phase with the lightest Ni isotopic composition. Clinopyroxene is the major phase in this rock (D.-C. Lee et al., 1996), and clinopyroxene is identical within error to the bulk Ni isotopic composition.

Of the minerals from samples with light bulk Ni isotopic compositions, no samples of the same phase from different rock samples agree within error. All the phases from the rocks showing light bulk Ni isotopic compositions are lighter than the same phases in 'normal' xenoliths, showing the process that fractionates the Ni towards lighter isotopes is affecting all the major mineral phases in the rock, though apparently to varying degrees.

As in the unmetasomatised samples, clinopyroxene is generally the lightest phase, with olivine and orthopyroxene agreeing with each other within error within that sample. Spinel is the heaviest phase where measured. The difference between the heaviest and lightest mineral Ni isotopic composition for all xenoliths analysed is consistently and never greater than 0.12‰. There is no evidence in these data that mineralogy and mineral isotopic fractionation is causing the heterogeneity in bulk rock Ni isotopic composition. In fact, the data indicate that mineralogy is unlikely to play any significant role in Ni isotopic variations in the mantle or in mantle melting.

Megacrysts

Megacrysts were also analysed to afford a comparison with the data of Gall et al (Gall et al., 2017) and with the other mantle phases analysed. Sample N12 clinopyroxene, a megacryst from Biu Plateau (Cameroon), hosted in a harzburgite, has a previously published Ni isotopic composition of 0.42‰ (Gall et al., 2017). This study re-analysed the sample with a fresh dissolution for which we obtained the result -0.03‰, which is considerably lighter, and in agreement with other clinopyroxene analyses. Sample N12 garnet, also a megacryst from Biu Plateau (Cameroon), has a previously published Ni isotopic composition of 0.30‰ (Gall et al., 2017). This study re-analysed the sample with a fresh dissolution and gave $\delta^{60/58}Ni_{SRM986}$=0.07‰, which is also considerably lighter than the previously published value.

The cause for the discrepancy between the analyses here and those of previous studies (Gall et al., 2017) is unclear. Both sets of analyses were completed on the same powder. Lighter Ni isotopic compositions for clinopyroxene is however consistent with the other analyses in this work.

3.5 Discussion

3.5.1 The bulk silicate Earth

The bulk silicate earth (BSE) describes the composition of the Earth without the Fe-Ni metal core, representative of the "primitive mantle" after accretion and core segregation, but prior to further compositional processing. In practice, the BSE represents the average composition of the mantle and crust combined, and therefore the BSE composition is volumetrically dominated by the terrestrial mantle. Any estimate of the composition of the BSE for compatible elements such as Ni requires analysis of primarily mantle samples, sufficient to be representative of the bulk mantle. The mantle is generally agreed to be heterogeneous, and its composition can be altered by physical processes (e.g. mixing, slab fall-off) as well as igneous and metamorphic processes.

The previous published estimates of Ni isotopic composition of the BSE include 0.23±0.06‰ (n=6) of Gall and co-workers (2017), and an estimate by Steele and co-workers (2011) taken from a weighted average of 3 rock standards (Cameron et al., 2009; Steele et al., 2011), of 0.18±0.04‰. Gueguen and co-workers (2013) presented a much lighter value of 0.05±0.05‰, using igneous and ultramafic reference materials as well as fresh and altered basalts from Loihi, and clay and basalt samples from IODP core 1149. Given the trivial contribution to BSE nickel of sediments, and the potential for isotopic fractionation induced by pelagic biology, Elliott and Steele (2017) removed these samples to produce a revised BSE estimate including only samples of mantle and mantle derived melts, resulting in $\delta^{60/58}Ni_{SRM986}$=0.11±0.01‰, which is still lighter than other published estimates, although less extreme.

Excluding the average of Gueguen (2013), the published averages bracket the average for unmetasomatised fertile peridotite from this work of $\delta^{60/58}Ni_{SRM986}$=0.20±0.08‰ (n=18). This average was calculated with several exclusions from the dataset. First, this work does not include rock standards in any consideration of averages because of the published problems with the preparation of some rock standards being contaminated by during production (Weis et al., 2006). Second, dunites and pyroxenites were excluded based on not being representative of bulk mantle, e.g. dunites being leftovers from adiabatic decompression melting (Gibson et al., 2013) or cumulates of olivine (Dawson et al., 1970). Third, four samples with anomalously light Ni isotopic compositions were excluded, due to the apparent association with metasomatic effects. Including USGS peridotite PCC1, however, does not alter the average composition. This suggests that the BSE Ni isotopic composition can now be considered well defined. The exception to the agreement in the estimates of Ni isotopic composition of the BSE is the composition of Gueguen and co-workers (2013), which even when recalculated by Elliott and Steele (2017) is ~0.10‰ lighter than other estimates (Gall et al., 2017; Steele et al., 2011).

Analyses of the Ni isotopic compositions of iron and chondritic meteorites has been used to estimate the Ni isotopic composition of a planetary reference value of $\delta^{60/58}Ni_{SRM986}$=0.25±0.02‰ (Elliott and Steele, 2017). This is within error of, although 0.05‰ heavier than, estimates for the BSE. This implies that the fractionation between Ni^{2+} in silicate materials and Ni^{0} in Fe-Ni metal is small and consistent with the partitioning experiments of Lazar and co-workers (2012), who predicted only 0.02‰ fractionation between bulk metal and silicate at 2500K for a single core-mantle equilibrium. Larger fractionations were predicted for a Rayleigh process with well-mixed mantle magma ocean (Elliott and Steele, 2017; Lazar et al., 2012). The conclusion that there was no fractionation between chondrites and the BSE was also reached by Gall and co-workers (2017) whose own chondrite average Ni isotope composition of 0.26±0.12‰ (n=71), was entirely consistent with previous estimates and with their own BSE estimate (0.23±0.06‰).

3.5.2 The role of minerals

Published Ni isotopic compositions for mantle minerals are limited to 5 phases from 3 lherzolite xenoliths and 2 megacrysts from the Cameroon Line from Gall and co-workers (2017); an olivine separate from a basalt host by Gueguen and co-workers (2013), and some leaching experiments of olivine by Spivak-Birndorf and co-workers (2018). Two olivine samples were analysed in Gall and co-workers (Gall et al., 2017) at 0.14±0.04‰, and 0.17±0.05‰, which agree well with the samples from un-metasomatised hosts analysed in this study. The basalt hosted olivines analysed in Gueguen and co-workers (2013) (0.10±0.03‰) and Spivak-Birndorf and co-workers (2018) (0.06±0.05‰, n=14, variously leached) may not be representative of Ni isotopic compositions of minerals in equilibrium with the mantle reservoir of Ni, but agree with the olivine analysed in this study from hosts with lighter Ni isotopic compositions. Two orthopyroxene samples were analysed in Gall and co-workers (2017) at -0.04±0.03‰, and -0.02±0.06‰, which are within error of the orthopyroxene from metasomatised hosts from this work.

The single clinopyroxene sample from a xenolith from Gall and co-workers (Gall et al., 2017) yielded an extreme heavy Ni isotopic composition of 2.83±0.11‰. Analysis of other minerals and bulk xenoliths in this study have been unable to find similarly heavy compositions in the mantle. Gall and co-workers (2017) suggest a potential reason for the extremely heavy Ni isotopic composition in this clinopyroxene sample to be undiscovered mineral inclusions in the sample. Gall and co-workers (2017) highlight that this phase could not be base metal without skewing Ni concentration data for the sample, and the Fe isotopic composition (Williams et al., 2005) done on the same separate, and found to be completely within the normal range of the samples in that work.

The positive correlation between bulk rock $\delta^{60/58}Ni_{SRM986}$ and clinopyroxene abundance observed in Gall and co-workers (2017), is not substantiated with the additional samples in this study. There are, in fact, no correlations with any mineralogical indicators with the addition of the further samples in this work (see Figure 11). The conclusion of Gall and co-workers (2017) that

mineralogy of the sample strongly controls the bulk Ni isotopic composition is not supported by this work.

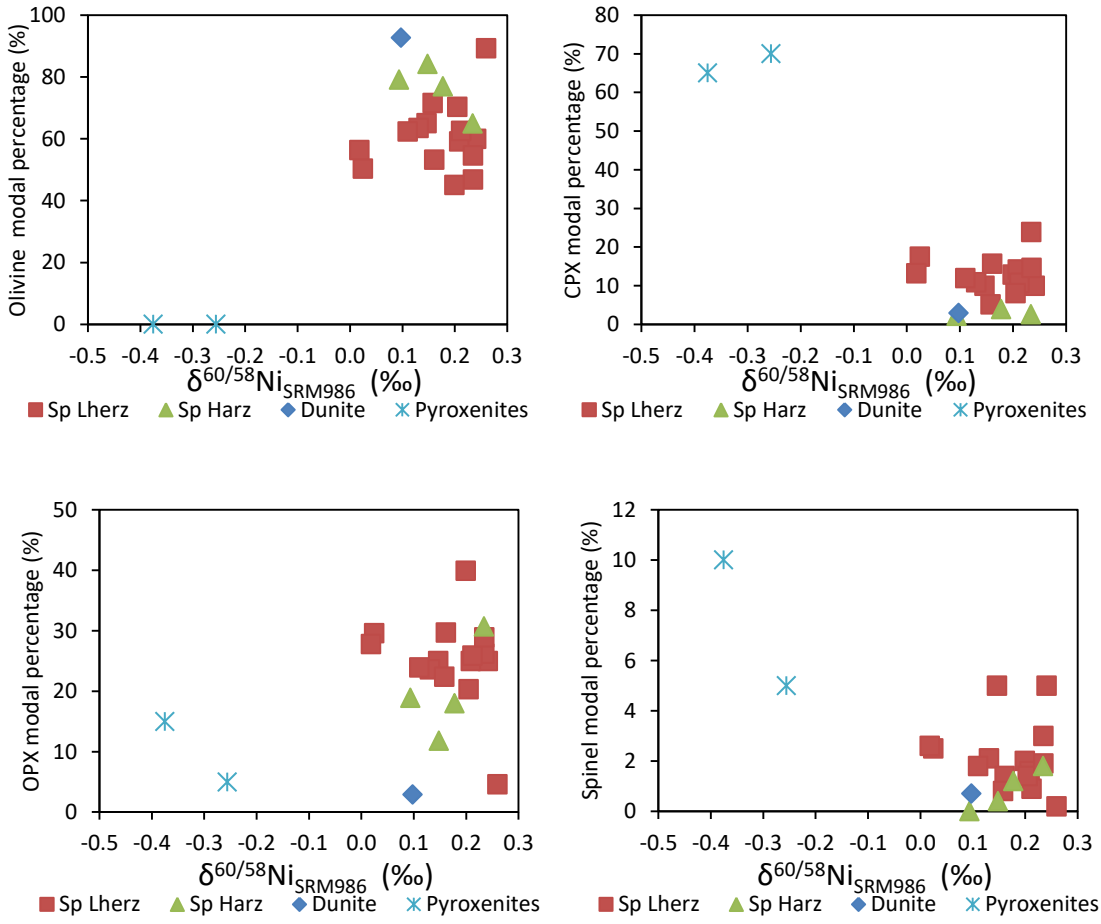

Figure 11

Modal percentage of major mineral phases with Ni isotopic composition of bulk xenoliths analysed in this study. Modal mineralogy from (Harvey et al., 2012; Lee, 1994; Reid et al., 1975). No mineralogical data exists for 1 dunite, 1 spinel lherzolite, and 2 garnet lherzolite and samples from Tanzania and also 3 pyroxenites from Kilbourne Hole. Abbreviations: Sp Lerhz = Spinel lherzolite; Sp Harz = spinel harzburgite. External reproducibility of the Ni isotopic compositions is 0.06‰.

This study has shown limited fractionation between mineral phases, with no rock so far investigated having a Ni isotopic fractionation between its heaviest and lightest mineral of greater than 0.12‰. In general, clinopyroxene is the lightest phase and spinel the heaviest, with olivine and orthopyroxene within error of each other. There is no indication that presence of specific minerals can impart a particular Ni isotopic signature to its host rock. On crystallisation in the mantle, these minerals inherit a largely unfractionated Ni isotopic composition dominated by that of the region of formation.

Mantle minerals from peridotites with bulk compositions within error of the average unmetasomatised fertile peridotite have isotopic compositions that are comparable between samples. All major mineral phases from the xenoliths with lighter bulk Ni isotopic compositions have lighter Ni isotopic compositions than their corresponding phases from the other samples, and do not have consistent compositions. The variation between the Ni isotopic signatures of minerals from these hosts is greater than comparable unmetasomatised minerals, however, the fractionation between phases in the same host remains limited, and the minerals are evidently in equilibrium (see Figure 12 showing systematic variation in Ni isotopic composition with FeO content within phases from a single xenolith).

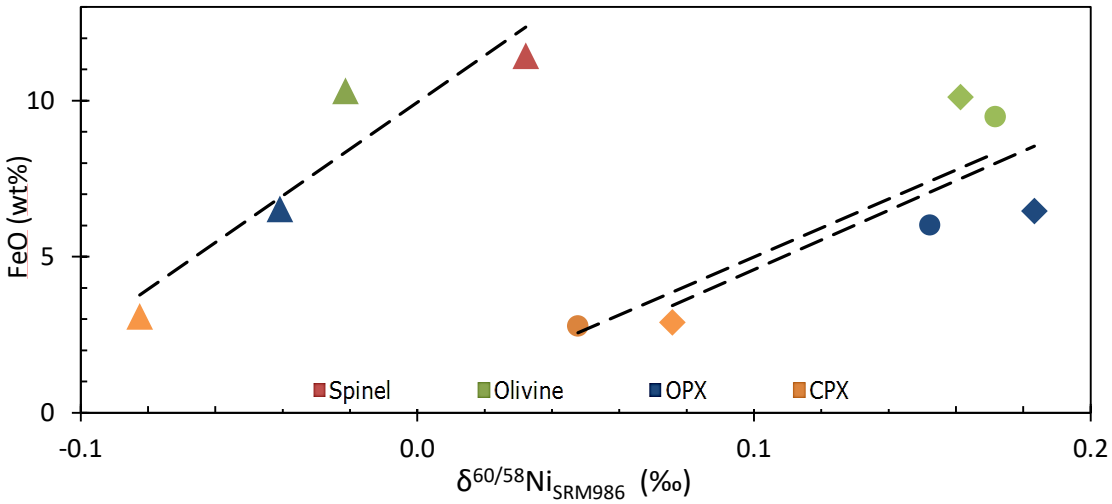

Figure 12

Systematic variation in mineral FeO (wt%) with Ni isotopic composition of the mineral phases (orange=clinopyroxene, blue=orthopyroxene, green=olivine, red=spinel) within three separate Kilbourne Hole xenoliths (triangles=KH03-24, circles=KH03-25, diamonds=KH03-06). External reproducibility of the Ni isotopic compositions is 0.06‰.

Gall et al (2017) suggested that spinel could not have a large influence on mantle Ni isotopic composition, because despite the high Ni concentration, the concentration of spinels in the mantle is insufficiently high. The reconstructions of bulk Ni isotopic compositions from the analysed spinels in this study have shown this is correct, as removing the influence of spinel from the reconstruction has limited to no effect on the resulting bulk composition.

Garnet is assumed to have no influence on the bulk mantle because it has both a low abundance and low Ni concentration. This is supported by the near zero Ni isotopic composition of a garnet megacryst analysed during this work, and the indistinguishable Ni isotopic compositions of spinel and garnet lherzolites from Tanzania. These facts suggest garnet does not have a sufficiently extreme Ni isotopic composition to perturb the mantle reservoir when the Ni concentration is nearly 30 times less than the bulk mantle.

Similarly, the influence of sulfides on the Ni isotopic composition of bulk xenoliths is considered negligible, despite the high Ni concentration. Concentration of sulfides in Kilbourne Hole xenoliths are estimated at 0.03 wt% (Harvey et al., 2011), suggesting that mantle sulfides cannot be a large Ni reservoir in the mantle. A simple mass-balance model was used to investigate this, using Ni and S concentration data for sulfides and bulk peridotite xenoliths. Sulfide grains from Kilbourne Hole average 21 wt% Ni, and 36 wt% S (range 1 to 36 wt% Ni, and 32 to 38 wt% S) (Harvey et al., 2011). The Ni concentration of the peridotite xenoliths, by isotope dilution, averages 1935 ppm (range 1580-2500 ppm), with a lower concentration in pyroxenites of 875 ppm (but with a much greater range than seen in the more numerous peridotite samples of 233 to 1760 ppm). The sulphur concentration in the bulk xenoliths averages 70 ppm, with a range of <3 ppm to 130 ppm (Harvey et al., 2015), providing a limit for sulfide.

The modelling of the potential influence of sulfides on bulk mantle Ni isotopic compositions has shown that the necessary amounts or isotopic composition of the sulfide must be well outside of plausible estimates. There is also the problem of lower Ni concentration in those samples with lighter Ni isotopic signatures than in the normal mantle, which requires loss of Ni-rich sulfide rather than addition. Presence of sulfides dominating the Ni isotopic composition of the mantle would cause the bulk xenolith compositions to plot along a mixing line between the pristine mantle and the composition of pure sulfides, highlighted, in both Ni isotopic composition, [S], and [S]/[Ni]. This assumes identical Ni isotopic compositions of all the

sulfides in this area of the mantle.

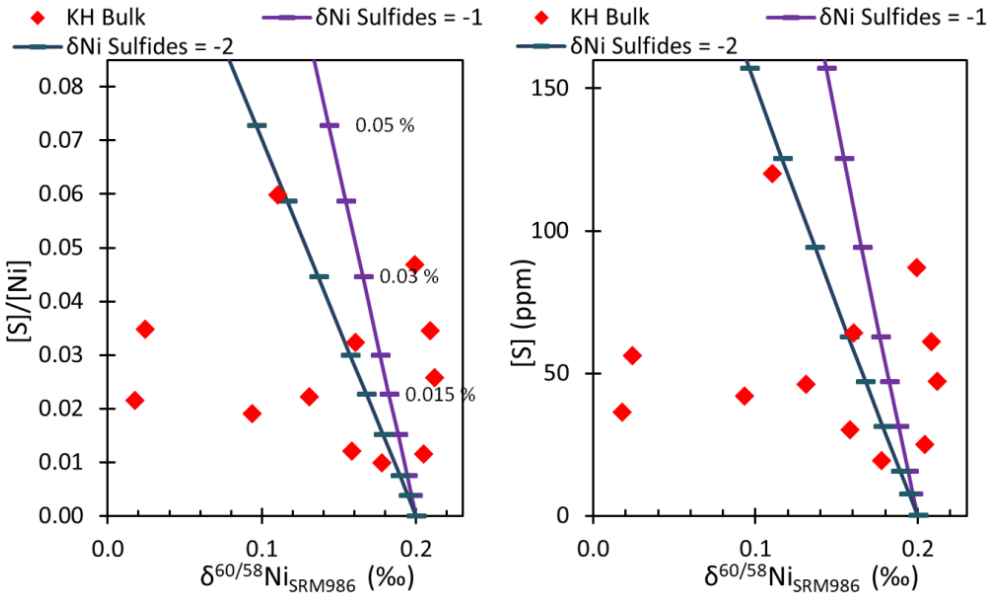

Figure 13 shows that the Kilbourne Hole xenoliths do not follow such a mixing line.

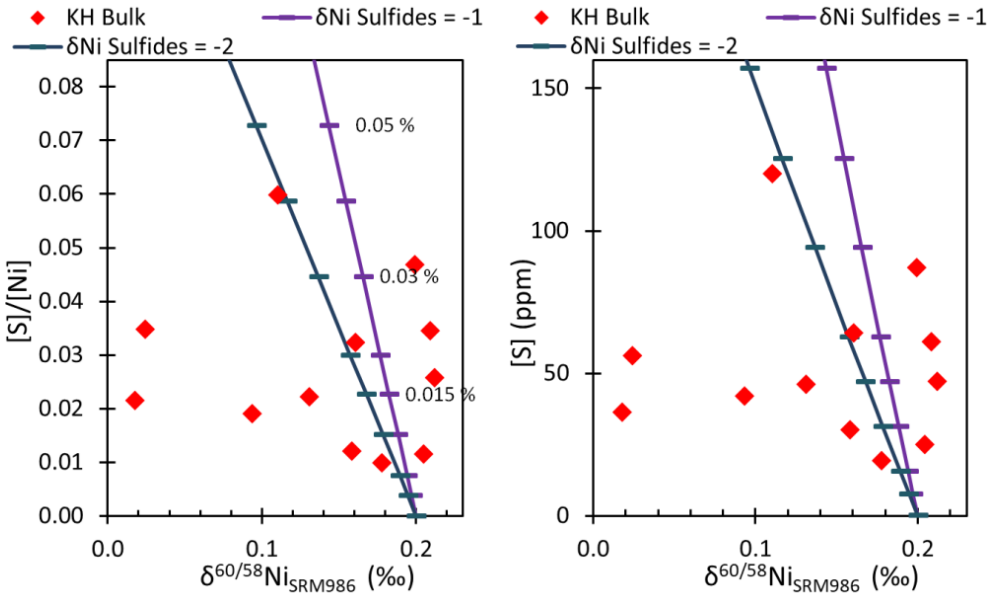

Figure 13

Plot showing the mixing lines from a simple mass-balance mixing model for different extreme negative Ni isotopic compositions for sulfide as a function of [S]/[Ni] (left) and [S] (right), modelled using [Ni] in sulfides as 21 wt%, and [S] sulfides as 32 wt%. Also shown are the actual Ni isotopic compositions for bulk Kilbourne Hole xenoliths, also as a function of [S]/[Ni] (left) and [S] (right) (data from (Harvey et al., 2012). These samples do not fall anywhere approximating the mixing lines.

The isotopic composition of websterites (-0.32‰) can be made using this model only by assuming no sulfide in the normal mantle, and ~0.3 wt% added sulfide with an isotopic

composition of -2‰. This is too extreme in amount and isotopic composition to be a reasonable explanation. The other samples that show light isotopic compositions average ~0.15‰ lighter than normal mantle (~0.06‰). This difference can only be accounted for with extreme isotopic composition or a relatively large volume of the mantle sulfides. With an isotopic composition of -2‰ there would need to be 0.075 wt% sulfide added, or 0.15 wt% for a more reasonable -1‰ isotopic composition.

Published Ni isotopic compositions for sulfides consists of 11 massive sulfides with Ni isotopic compositions from -0.38 to -1.05‰ (Gueguen et al., 2013; Hofmann et al., 2014; Tanimizu and Hirata, 2006). In this study, and the various works of Gall (Gall, 2011; Gall et al., 2017, 2013, 2012), two sulfides were analysed for internal reproducibility with isotopic compositions of -0.90‰ (Kambalda, magmatic origin, extreme light) and 0.76‰ (Sudbury, meteoritic origin, extreme heavy).

With the Ni isotopic compositions for sulfides being no lighter than -1.05‰, and reasonable concentration of sulfide in the mantle unlikely to be greater 0.075 wt%, it is not possible to reproduce a light Ni isotopic composition comparable to those found in the samples analysed in this study using this model. Therefore, fractionation of Ni by sulfides is dismissed as a mechanism for producing the observed heterogeneity in Ni isotopic compositions in the terrestrial mantle.

The minerals from ultramafic xenoliths that have been analysed in this work reconstruct to the bulk rock Ni isotopic composition analysed from bulk powder, where the modal mineralogy information is available, and all major phases have been analysed. Given these rocks often have sulfides as minor phases, which were not analysed as separates, the successful reconstruction provides further evidence that sulfides have no influence on the Ni isotopic composition of mantle rocks. This successful reconstruction also supports that Ni isotopic composition of bulk rocks is not perturbed by surficial alteration, interstitial glass, or minor secondary phases.

Table 3-3

Nickel isotopic composition of mineral phases and modal mineralogy used for reconstruction of bulk composition

2SD on delta	0.06‰	Actual		Reconstruction	
	Modal % (ppm)	Ni conc (ppm)	$\delta^{60/58}Ni_{SRM986}$ (‰)	Ni conc (ppm)	$\delta^{60/58}Ni_{SRM986}$ (‰)
Sample KH03-24		**1680**	**0.018**	**1625**	**-0.023**
Olivine	56.4	2384	-0.021		
OPX	13.2	324	-0.082		
CPX	27.8	661	-0.041		
Spinel	2.6	2057	0.032		
Sample KH03-27		**2198**	**0.094**	**2453**	**0.093**
Olivine	79.1	2714	0.094		
OPX	2.2	243	0.036		
CPX	18.9	1590	0.083		
Spinel	0.0	2133	0.128		

Extra-terrestrial olivine has been investigated by Chernonozhkin and co-workers (2016), who analysed olivine from pallasites from 4 different meteorites, and found each was heavier than the associated metal phase (range 0.554 to 1.221‰, with $\Delta^{60/58}Ni_{olivine\text{-}metal}$ from 0.21 to 2.03‰). Evidently, fractionation of Ni isotopes between olivine and meteoritic metal is less consistent and produces significantly heavier olivine than seen in terrestrial mantle samples.

3.5.3 Isotopically light Ni in the terrestrial mantle

This study has shown that there are a mantle samples showing a range of Ni isotopic compositions lighter than observed for normal mantle, suggesting the mantle is heterogeneous in Ni isotopes. These variations away from the average mantle Ni isotopic composition are of significant interest. The terrestrial mantle is the largest reservoir of Ni in the BSE due to its volume and high Ni concentration. To perturb the Ni isotopic composition of such a large Ni reservoir requires a significant volume of material with a very different Ni isotopic composition to that of the normal bulk mantle.

The previous section has shown that this variation is not linked to mineralogy or fractionation between mineral phases. Either a particular process is enriching light or depleting heavy

isotopes in certain areas that are then sampled, or the reverse is occurring in an area not sampled leaving residual areas of the mantle that have been sampled comparatively light. It is possible that a combination of both effects is being observed, however given the number of samples and sampled localities the presence of an unsampled heavy reservoir is considered unlikely.

The anomalously light Ni isotopic compositions found in pyroxenites in particular, is indicative of domains of light Ni isotopic composition in the mantle. This presumably relates to either an input of isotopically light Ni that has not been homogenized (potentially through recycling and subduction), or a process within the mantle during the formation of these lithologies that causes enrichment in the lighter isotope. This is further explored below.

Other than pyroxenites, the samples with notably light Ni isotopic compositions relative to the average unmetasomatised fertile peridotite are four samples from Kilbourne Hole with metasomatic textures, KH03-21, KH03-24, KH03-27, and KH03-10. As demonstrated previously, constituent mineral phases of these rocks each show similarly lighter Ni isotopic compositions, and reconstruct to agree with the bulk composition if all major phases analysed. The minerals are lighter in variable degrees in these rocks, suggesting that although the processing producing fractionation towards light isotope enrichment is acting on all phases, it has gone to different levels of completion in each phase/rock. A small range is also seen in bulk rocks (ranging from 0.09 to 0.15‰ lighter).

The metasomatic features observed in thin section include ‘spongy’ clinopyroxene rims that record a reaction texture with a micrometre width overgrowth, illustrated in Figure 3 from Harvey and co-workers (2012). According to Harvey and co-workers (2012) the samples with this texture are KH03-10, KH03-15, KH03-24, and KH03-27, but other metasomatic features are also described including interstitial glass (KH03-15, KH03-16, and KH03-21), and evidence of “refertilisation in antiquity” in bulk rock geochemistry (KH96-8, KH96-18, KH03-03, and KH03-21). The fact that other samples from this locality have similar features to those seen in xenoliths with light Ni isotopic compositions, but are without similarly light Ni isotopic compositions, suggests the presence of these textures may have limited to no bearing on Ni

isotopic composition. Alternatively, there may be a resistance to change in the Ni isotope composition until a particular threshold is reached, or that the bulk xenolith has fewer metasomatic features than the thin section suggests, then potentially the fractionation process has not pervaded the sample sufficiently to alter the Ni isotope composition of the bulk xenolith.

It should be considered that the metasomatic features observed in some Kilbourne Hole samples, and in theory potentially present in the samples from Tanzania and Cameroon could also be involved in the fractionation of Ni isotopic compositions in the mantle towards lighter compositions. This may be especially relevant if the hypothesis of Harvey and co-workers (2012) that the visible features such as interstitial glass represent only one metasomatic event, and others are not physically observable. This would agree better with the fact that the unusually light Ni isotopic compositions of some Kilbourne Hole samples do not correlate exactly with these observable metasomatic features. In the case of fluids being responsible, either a fluid with a light Ni isotopic composition is interacting with the rock, imparting a lighter Ni isotopic composition by exchange, or an evolving fluid is passing through and preferentially extracting heavy Ni from the bulk rock.

Investigation of fluid based alteration of ultramafic rocks has been limited to surface occurrences including analysis of serpentinites, laterites, saprolites, and ultramafic soils. Serpentinites have been shown to have light Ni isotopic compositions (0.08‰ (Gall, 2011); -0.13‰ (Gueguen et al., 2013); -0.28‰ and -0.47‰ (Hofmann et al., 2014)). Laterites, produced from tropical surface weathering of ultramafic rocks, have also been analysed for Ni isotopic composition (-0.11‰ (Gall et al., 2013), 0.00 to 0.14‰ (Ratié et al., 2015), and -0.12 to 0.9‰ (Spivak-Birndorf et al., 2018). Saprolite, a more highly weathered rock than laterite, has been found to have heavy and light Ni isotopic compositions e.g. 0.30‰ (Gall et al., 2013), and -0.61‰ to 0.30‰ (Ratié et al., 2015). Soils formed from ultramafic bedrock have also been shown to be both light (-0.19 to -0.02‰ (Ratié et al., 2015), -0.30 to 0.11‰ (Ratié et al., 2016)) and heavy (0.32 to 0.72‰ (Estrade et al., 2015)). Alteration of basaltic samples from ODP hole 504B were analysed by Gall (2011) and average 0.08±0.12‰ (n=7). Gall (2011) suggested

that, relative to pure MORB glasses, the altered samples were heavier in Ni isotopic composition.

Spivak-Birndorf and co-workers (2018) investigated the mobile phase of metasomatism, and found that heavier isotopes of Ni are preferentially mobilized into the dissolved phase during the overall surface weathering and transport process. This has previously been suggested by Gall et al. (2013), Cameron and Vance (2014), and Ratié and co-workers (2015) without direct sampling. Spivak-Birndorf and co-workers (2018) also found no fractionation with leaching of pure olivine, suggesting that the susceptible phase during low temperature metasomatism is not olivine.

Fractionation of Ni isotopic compositions by metasomatic fluids, as described above, may be related to subduction. In the case of Kilbourne Hole the Farallon plate subducted beneath the North American plate between 30 and 20 Ma (e.g. Liu et al., 2008) to be followed by the Juan de Fuca plate. The xenoliths are estimated to sample mantle from less than 0.14 Ma. During subduction, metasomatic fluids are released and move into the mantle wedge beneath Western USA. Once rifting was initiated during the formation of the Rio Grande Rift System this altered mantle began to move up, and was then sampled as xenoliths by the basanite being erupted at the rift. If this were the case, we would expect to see correlations in Ni isotopic signature with geochemical indicators of subducted material, which can be investigated at Kilbourne Hole.

The Kilbourne Hole xenoliths, as a whole, highlight the link between Ni isotopic composition of the bulk rock and other geochemical characteristics. In Figure 14 it is evident that there is a relationship exists in this locality between the Ni isotopic composition of the bulk xenoliths and the major element chemistry – in particular the Fe content. The relationship in this example is a negative correlation with one outlier, which if removed produces an r^2 value of 0.53, indicating that the lightest Ni isotopic compositions are associated with the greatest Fe enrichment. This is significant in two main ways.

First, the light Ni isotopic compositions highlighted earlier in four samples that have metasomatic features, and the pyroxenites (with one outlier) are part of a complete trend with

other geochemical indicators rather than separate groups. This may indicate the superficial metasomatism is not related to Ni isotopic composition of the bulk sample, which is supported by major element chemistry being unlikely to be perturbed during such a process.

Second, the bulk rock Ni isotopic composition is related to the concentration of major elements in the bulk rock. A relationship between major element chemistry and the isotopic composition of a trace element such as Ni was not expected. This result is important because the controlling processes for these different scales of geochemical parameter are clearly linked. Major element variability due to recycling of oceanic crust has previously proposed as the dominant mechanism affecting mafic lavas at Hawaii (Hauri, 1996), with up to 5% pyroxenitic lithology in the source of these lavas. Pyroxenite from recycled oceanic crust has been also subsequently suggested to be the source of Hawaiian lavas based on Ni concentrations (Sobolev et al., 2005), which suggest Ni isotopes might be similarly affected by this process.

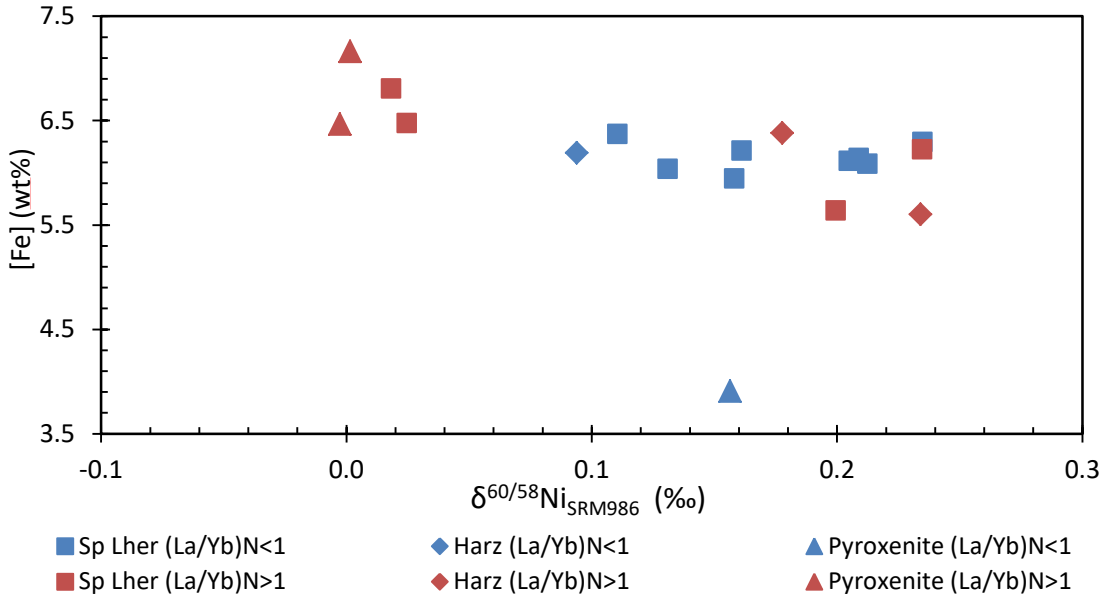

Figure 14

Plot of Ni isotopic composition of bulk rock Kilbourne Hole xenoliths and the bulk rock Fe content (wt%). Samples are separated into lithologies and whether the $(La/Yb)_N$ was >1 or <1. There is a negative correlation, when the pyroxenite with $(La/Yb)_N$<1 is excluded, where the r^2=0.53. External reproducibility of the Ni isotopic compositions is 0.06‰.

Another notable feature of the Kilbourne Hole dataset is a correlation between Ni isotopic compositions and bulk rock isotopic $^{143}Nd/^{144}Nd$ compositions (see Figure 15). There is a broad

positive correlation, with an r^2=0.47, with the lightest Ni isotopic compositions of the sample set associated with lower Nd isotopic compositions. This also supports that the pyroxenites and peridotites that have lighter Ni isotopic compositions are all part of a complete trend, with a common process or combination of processes controlling all the Ni isotopic compositions in the xenolith suite at this locality.

The significance of the correlation with Nd isotopic composition specifically, is that lower $^{143}Nd/^{144}Nd$ ratios are associated with more enriched lithologies with more incompatible elements (e.g. Haase et al. 2011). Therefore, the correlation of the lower $^{143}Nd/^{144}Nd$ with the light Ni isotopic composition is indicative of the connection between them, and strongly suggests that light Ni isotopic compositions in the mantle are related to the presence of enriched lithologies being entrained into the mantle. The Fe correlation discussed previously also agrees with this supposition.

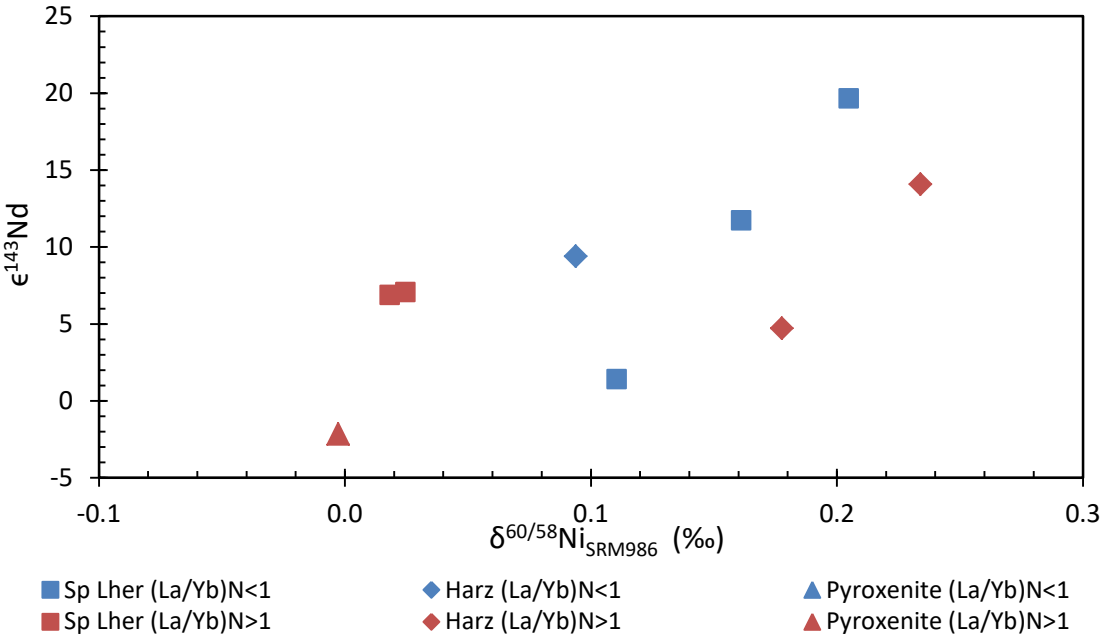

Figure 15

Plot of Ni isotopic composition of bulk rock Kilbourne Hole xenoliths and the bulk rock isotopic $^{143}Nd/^{144}Nd$ composition. Samples are separated into lithologies and whether the $(La/Yb)_N$ (chondrite normalised ratio of Light Rare Earth Element (REE) La to Heavy REE Yb was >1 or <1 indicating Light REE enrichment or depletion relative to chondrites). There is a positive correlation, with r^2=0.47. The conversion from raw Nd isotopic composition to $\epsilon^{143}Nd$ used a value for the Nd isotopic composition of the terrestrial BSE of 0.512630 (Bouvier et al., 2008). The heaviest Ni isotopic composition belongs to KH03-16, a sample that has a "difficult to account for Nd isotopic composition" (Harvey et al., 2012). An isochron produced from the Nd isotopic compositions and Sm/Nd suggests an age for last melt

depletion event of 702 Ma, with KH03-16 removed as an outlier (the heaviest Ni isotopic composition). External reproducibility of the Ni isotopic compositions is 0.06‰.

Earlier work on Kilbourne Hole Nd isotopic compositions by Roden and co-workers (1988) found a similar array, and identified two end member components a "MORB-related component" that is fertile in basaltic components with an unradiogenic Nd isotopic composition, and another component with radiogenic Nd isotopic composition. The "MORB-related component" is characterised by relatively high CaO, high Al_2O_3, and heavy REE enrichment, similar to the composition of the MORB source. These components are also separable based on their Nd model ages, with the MORB-related lherzolites identifiable from the pyroxenites, wall-rocks, and other lherzolites (Roden et al., 1988). Roden and co-workers (1988) identified some xenoliths as having been affected by a pyroxenite forming event, and the Nd model ages suggested an enrichment event. Complicated Sm-Nd systematics is suggested to typify metasomatised xenoliths.

Harvey and co-workers (2012) also categorised the samples into 2 groups but in this instance depending whether the primitive mantle normalised ratio of Light Rare Earth Element (REE) La to Heavy REE Yb was <1 (Group 1) or >1 (Group 2), indicating Light REE enrichment or depletion relative to primitive mantle. This categorisation has not shown any correlation with Ni isotopic composition. In each case the whole range of Ni isotopic compositions from this sample suite is spanned by samples of Group 1 (highlighted by red on Figure 14 and Figure 15), which are the samples that are LREE enriched.

Bussod and Williams (1991) described the lower crust and mantle underneath Kilbourne Hole as intraoceanic island arc and marginal basin lithologies that accreted to the continental margin between 1800 and 1600 Ma. Subsequent volcanism migrated Eastwards associated with subduction and accretion events, with increased magmatism between 75 and 50 Ma relating to either a change in convergence rate and/or a possible flattening of the sub-ducting slab (Bussod and Williams, 1991).

In the case of Kilbourne Hole subduction of the seismological studies that used travel-time tomography have revealed the existence of a low-velocity zone within the mantle wedge (Satsukawa et al., 2011). Roden and co-workers (1988) confirmed a component under Kilbourne Hole that is fertile, relatively LREE-depleted, and isotopically similar to MORB. They suggested this component was probably derived from the asthenosphere. Isotopic heterogeneity in Nd and Sr observed by Roden and co-workers (1988) was also said to require the addition of a second, enriched component characterized by relatively low and high ratios and unsupported ratios.

Roden and co-workers (1988) suggested that the association in Kilbourne Hole of the enriched or metasomatised peridotites, with alkaline basalts and the continental rift system, is formed from enriched continental lithosphere produced from the mixing and melting processes related to the ascending mantle beneath rifts. The Potrillo volcanic field, of which Kilbourne Hole is part, has been interpreted as representing the products of small-degree partial melting of a volatile enriched asthenosphere (Satsukawa et al., 2011). This suggests that the mantle that had previously been part of the mantle wedge could have been similarly enriched in fertile components as correlated with light Ni isotopic compositions.

The relationship between light Ni isotopic compositions in the bulk mantle as sampled by xenoliths with enriched lithologies corroborates with the pyroxenite xenoliths also having light Ni isotopic compositions. The extreme of this would be the Cameroon websterites compositions (P6 -0.26‰; P12 -0.38‰), which have the most extreme light Ni isotopic composition.

Pyroxenite has been suggested to form from silicate melts from subduction reacting with peridotite (Day et al., 2009; Sobolev et al., 2007). In the case of the Cameroon Line, no evidence for a recent subducting plate has been found, however potentially, another source of silicate melt could produce the same effect percolating through peridotite. In addition, Day and co-workers (2009) provided evidence that reservoirs enriched in recycled materials can be preserved long-term in the mantle, suggesting that the signature of enriched subducted material

could persist in the mantle. In addition, there is no reason for Ni isotopic composition to vary with time, apart from potential dilution effects.

If we assume these extreme light Ni isotopic compositions are part of the same process observed elsewhere relating to enriched lithologies then we must consider how, further to the specifics of Kilbourne Hole, we might produce this result. One previous pyroxenite sample analysed for Ni isotopic composition by Gall (Gall et al., 2017) had a heavy composition of 0.36‰, however this sample is described as having olivine as a major phase, unlike most pyroxenites. This does not fit into the pattern seen in samples from this study.

Materials that could be subducted have been analysed, including altered ocean basalts and serpentinites, and potentially ocean sediments and Fe-Mn crusts. Altered basalts samples analysed by Gall (2011) average $\delta^{60/58}Ni_{SRM986}$=0.08±0.12‰ (n=7), and compared with pure MORB glasses analysed in the same study that average of -0.07±0.20‰ (n=9). Serpentinised peridotites also have light values of 0.07‰ and 0.08‰ (Gall 2011), and -0.13‰ (Gueguen et al., 2013).

In contrast, heavy Ni isotopic compositions are found in Fe-Mn nodules and deep sea sediments (Ciscato et al., 2018; Porter et al., 2014). The latter study of organic rich shale sequences average Ni isotopic composition of 0.92±1.17‰, n=18, ranging from 0.28 to 2.5‰. The former marine sediment study averaged a comparable Ni isotopic composition 0.92±0.78‰ (range 0.04 to 1.33‰, n=32). Reference materials for shales have also been analysed and are also isotopically heavy (Chernonozhkin et al., 2016, 2015; Estrade et al., 2015; Gall, 2011; Gueguen et al., 2013; Ventura et al., 2015). Iron-manganese crusts have been analysed and found to be generally heavy. The USGS standards for Fe-Mn nodules have been analysed repeatedly: Nod-A-1 (1.07±0.05‰, n=7); and Nod-P-1 (0.37±0.06‰, n=7) (Gall, 2011; Gall et al., 2013; Gueguen et al., 2018, 2016, 2013; Ratié et al., 2015; Wang and Wasylenki, 2017). An in depth study of Fe-Mn crusts from Gall and co-workers (2013) averaged $\delta^{60/58}Ni_{SRM986}$=1.62±0.76‰ (n=24, ranging from 0.88 to 2.50‰). One time series of depth samples from a particular crust from north central Pacific ocean averaged $\delta^{60/58}Ni_{SRM986}$=1.85±0.35‰ (n=51, ranging from 1.14

to 2.27‰) (Gall et al., 2013). A similar study by Gueguen and co-workers (2016) analysed four depth profiles of Fe-Mn crusts averaging 1.76±0.16‰.

Recycling of oceanic crust has been suggested as the major process introducing variability in the Earth's interior, particularly in major element chemistry (Hauri, 1996). However, in Ni isotopes, altered oceanic crust is not sufficiently light in $\delta^{60/58}Ni_{SRM986}$ to compare to the lightest xenolith compositions and the sediments and Fe-Mn nodules are uniformly heavy in Ni isotopic composition, it is not direct input of this material producing the isotopically light $\delta^{60/58}Ni_{SRM986}$ found in some mantle samples.

An example of subduction altering the isotopic composition of the resulting magmas can be found in , König and co-workers' (2016) work on molybdenum isotopes. Molybdenum isotopes were found to fractionate in subduction environments, with heavier isotopes enriched in the more slab fluid dominated samples (König et al., 2016). For Mo isotopes, the isotopic composition of arc magmas with slab dominated signatures do not need to be produced directly from recycling of an input signature, but may instead be attributed to a slab-dehydration related fractionation process (König et al., 2016). Indeed, König and co-workers (2016) eliminated direct sediment recycling as the process controlling the Mo isotopic composition of the arc magmas. Proposed alternatives included a fractionation process in the mantle wedge during magma ascent; fractionation during melting of subducted sediment; or fractionation relating to the breakdown of a residual mineral phase that had previously scavenged light Mo (König et al., 2016).

Iron isotopes have lighter compositions in arc magmas than in MORB or OIB, and extreme light compositions have been interpreted to both oxidation and melt extraction following infiltration of the mantle wedge by slab-derived fluids (Williams et al., 2018). However, Williams and co-authors (2018) also suggested isotopically heavy Fe is preferentially removed during partial melting. Iron isotopes are also heavier in pyroxenites than in MORB and OIB (Williams and Bizimis, 2014). Gall and co-worker (Gall et al., 2017) found a correlation between Ni isotopic composition and the Fe isotopic composition in some xenoliths, potentially suggesting similar

controls on these isotope systems. However, given Fe isotopes respond strongly to changes in oxidation state, the similarity with Ni is limited.

The isotopic composition of Ni in the same environment is, as with Mo, unlikely to be directly related to sediment recycling, as analyses of ocean sediments have shown heavy Ni isotope compositions, and the majority of sediment does not entre the subduction zone itself. Melting of a residual mineral phases is also unlikely in the case of producing Ni isotope fractionation, as discussed previously. The Ni concentration in such phases and the analysed compositions of major minerals makes it implausible that major isotopic fractionation in Ni could be produced by this method. Fractionation in Ni isotopes during ascent of subducted material into mantle wedge remains a possibility.

König and co-workers (2016) used isotopes of molybdenum to examine the behaviour of elements in the presence of slab-derived fluids and –melts. They suggest that constraining this behaviour is essential to understand the contribution of subduction related magmas and the role of subduction zones in the evolution of the crust-mantle system. The investigation of Ni isotopes, such as in this work, moves to add towards this goal.

3.6 Conclusions

The Ni isotopic composition of the Bulk Silicate Earth is now better known than ever, with three estimates now published all within error (Steele et al. 2011; Gall et al. 2017, this work). The average of unmetasomatised fertile peridotites from this work, $\delta^{60/58}Ni_{SRM986}0.20\pm0.08$‰, includes no reference materials, and more bulk xenoliths than any previous estimate.

In addition, this study has shed light on areas of the mantle with Ni isotopic heterogeneity. Heterogeneity within the mantle in such a dominant and highly compatible element was unexpected and unpredicted. Prior to this study only with low temperature surface weathering had any major fractionation been observed in Ni isotopic composition of ultramafic rocks, during the formation of laterites and serpentinites.

Fractionation in the mantle has been previously thought to be related to mineralogy (Gall et al., 2017). This work has showed that mineralogy has no relationship with Ni isotope fractionation in the mantle and the isotopic composition of minerals is in equilibrium within a particular xenolith. The isotopic composition of minerals reconstructs to produce the bulk Ni isotopic composition, showing that minor phases and interstitial alteration products do not influence the bulk Ni isotopic composition of the mantle.

Correlation with Ni isotopic composition and Fe content in bulk xenoliths suggests a relationship between the process fractionating major elements in the rock that was not expected. A correlation between Ni isotopic composition and Nd isotopic composition indicates a common control on both parameters. A lower Nd isotopic composition is associated with enriched material, and with lighter Ni isotopic compositions. Varying proportions of enriched material therefore likely creates a range of Ni isotopic compositions, with a more normal mantle represented by lesser proportions of enriched basaltic melt. Pyroxenites represent the extreme of enriched material in the mantle, and have the extreme lightest Ni isotopic compositions. In a particular locality, the xenoliths show a continuum of Ni isotopic compositions in relation to the degree of contribution of enriched mantle. Enriched mantle is usually produced by the subduction of basaltic oceanic material, and has been suggested to be present in discrete areas of the mantle (Hauri, 1996; Sobolev et al., 2005). In some instances, enriched mantle could potentially be formed by percolation of a silicate melt through a peridotite produced through another method.

Input of enriched material is suggested to be related to subduction leading to input of basalt-enriched melt into the mantle wedge. This has been suggested to induce Mo isotope fractionation (heavier isotopes enriched) (König et al., 2016), and potentially also Fe (lighter isotopes enriched) (Williams et al., 2018).

König and co-workers (2016) suggested that constraining the presence of slab-derived fluids and –melts in the mantle is essential to understand the contribution of subduction related magmas and the role of subduction zones in the evolution of the crust-mantle system. This work

on Ni isotopes in the mantle has shown that Ni isotopic composition of an ultramafic xenolith can be indicative of enrichment in the mantle source.

3.7 References

Aigner-Torres, M., Blundy, J., Ulmer, P., Pettke, T., 2007. Laser Ablation ICPMS study of trace element partitioning between plagioclase and basaltic melts: an experimental approach. Contrib Miner. Pet. 153, 647–667. https://doi.org/10.1007/s00410-006-0168-2

Arai, T., Maruyama, S., 2017. Formation of anorthosite on the Moon through magma ocean fractional crystallization. Geosci. Front. 8, 299–308. https://doi.org/10.1016/j.gsf.2016.11.007

Armytage, R.M.G., Georg, R.B., Williams, H.M., Halliday, A.N., 2012. Silicon isotopes in lunar rocks : Implications for the Moon's formation and the early history of the Earth. Geochim. Cosmochim. Acta 77, 504–514. https://doi.org/10.1016/j.gca.2011.10.032

Aulbach, S., Rudnick, R.L., McDonough, W.F., 2008. Li-Sr-Nd isotope signatures of the plume and cratonic lithospheric mantle beneath the margin of the rifted Tanzanian craton (Labait). Contrib. to Mineral. Petrol. 155, 79–92. https://doi.org/10.1007/s00410-007-0226-4

Becker, J.S., 2007. Inorganic mass spectrometry : principles and applications. John Wiley & Sons.

Bédard, J.H., 2005. Trace element partitioning in plagioclase feldspar. Geochim. Cosmochim. Acta 70, 3717–3742. https://doi.org/10.1016/j.gca.2006.05.003

Bindeman, I.N., Davis, A.M., 2000. Trace element partitioning between plagioclase and melt: Investigation of dopant influence on partition behavior.

Birck, J.L., Lugmair, G.W., 1988. Nickel and chromium isotopes in Allende inclusions. Earth Planet. Sci. Lett. 90, 131–143. https://doi.org/10.1016/0012-821X(88)90096-9

Bizzarro, M., Ulfbeck, D., Thrane, K., 2006. Nickel isotopes in meteorites: evidence for live 60Fe and distinct 62Ni isotope reservoirs in the early solar system. Lunar Planet. Sci. XXXVII 37.

Bizzarro, M., Ulfbeck, D., Trinquier, A., Thrane, K., Connelly, J.N., Meyer, B.S., 2007. Evidence for a late supernova injection of 60Fe into the protoplanetary disk. Science 316, 1178–81. https://doi.org/10.1126/science.1141040

Bourdon, B., Langmuir, C.H., Zindler, A., 1996. Ridge-hotspot interaction along the Mid-Atlantic Ridge between 37'30' and 40'30'N: the U-Th disequilibrium evidence, Earth and Planetary Science Letters.

Bouvier, A., Vervoort, J.D., Patchett, P.J., 2008. The Lu-Hf and Sm-Nd isotopic composition of CHUR: Constraints from unequilibrated chondrites and implications for the bulk composition of terrestrial planets. Earth Planet. Sci. Lett. 273, 48–57. https://doi.org/10.1016/j.epsl.2008.06.010

Burton, K.W., Schiano, P., Birck, J.-L., Allègre, C.J., Rehkämper, M., Halliday, A.N., Dawson, J.B., 2000. The distribution and behaviour of rhenium and osmium amongst mantle minerals and the age of the lithospheric mantle beneath Tanzania. Earth Planet. Sci. Lett. 183, 93–106. https://doi.org/10.1016/S0012-821X(00)00259-4

Bussod, G.Y.A., Williams, D.R., 1991. Thermal and kinematic model of the southern Rio Grande rift: inferences from crustal and mantle xenoliths from Kilboume Hole, New Mexico. Tectonophysics 197, 373–389.

Cameron, V., Vance, D., 2014. Heavy nickel isotope compositions in rivers and the oceans. Geochim. Cosmochim. Acta 128, 195–211. https://doi.org/10.1016/j.gca.2013.12.007

Cameron, V., Vance, D., Archer, C., House, C.H., 2009. A biomarker based on the stable isotopes of nickel. Proc. Natl. Acad. Sci. U. S. A. 106, 10944–10948. https://doi.org/10.1073/pnas.0900726106

Canil, D., Pearson RL Rudnick, N.D., McDonough Carswell, W. DA, 1994. Ferric iron in peridotites and mantle oxidation states. Earth Planet. Sci. Lett. 123, 205–220.

Canup, R.M., 2012. Forming a Moon with an Earth-like Composition via a Giant Impact. Science 338, 1052–1055. https://doi.org/10.1126/science.1106818

Canup, R.M., Asphaug, E., 2001. Origin of the Moon in a giant impact near the end of the Earth's formation. Nature 412, 708–712. https://doi.org/10.1038/35089010

Canup, R.M., Barr, A.C., Crawford, D.A., 2013. Lunar-forming impacts: High-resolution SPH and AMR-CTH simulations. Icarus 222, 200–219. https://doi.org/10.1016/J.ICARUS.2012.10.011

Capobianco, C.J., Amelin, A.A., 1994. Metal-silicate partitioning of nickel and cobalt: The influence of temperature and oxygen fugacity. Geochim. Cosmochim. Acta 58, 125–140.

Chako Tchamabé, B., Youmen, D., Owona, S., Ohba, T., Németh, K., Nsangou Ngapna, M., E Asaah, A.N., Aka, F.T., Tanyileke, G., Hell, J. V, 2013. Eruptive history of the Barombi Mbo Maar, Cameroon Volcanic Line, Central Africa: Constraints from volcanic facies analysis. Cent. Eur. J. Geosci 5, 480–496. https://doi.org/10.2478/s13533-012-0147-2

Chen, J.H., Papanastassiou, D.A., 2006. NICKEL ISOTOPE INVESTIGATION BY MC-ICP-MS AND PTIMS, in: Lunar and Planetary Science XXXVII. pp. 61–62.

Chen, J.H., Papanastassiou, D.A., Wasserburg, G.J., 2009. A search for nickel isotopic anomalies in iron meteorites and chondrites. Geochim. Cosmochim. Acta 73, 1461–1471. https://doi.org/10.1016/j.gca.2008.11.040

Chernonozhkin, S.M., Goderis, S., Costas-Rodríguez, M., Claeys, P., Vanhaecke, F., 2016. Effect of parent body evolution on equilibrium and kinetic isotope fractionation: a combined Ni and Fe isotope study of iron and stony-iron meteorites. Geochim. Cosmochim. Acta 186, 168–188. https://doi.org/10.1016/j.gca.2016.04.050

Chernonozhkin, S.M., Goderis, S., Lobo, L., Claeys, P., Vanhaecke, F., 2015. Development of an isolation procedure and MC-ICP-MS measurement protocol for the study of stable isotope ratio variations of nickel. J. Anal. At. Spectrom. 30, 1518–1530. https://doi.org/10.1039/C5JA00080G

Chernonozhkin, S.M., Weyrauch, M., Goderis, S., Oeser, M., McKibbin, S.J., Horn, I., Hecht, L., Weyer, S., Claeys, P., Vanhaecke, F., 2017. Thermal equilibration of iron meteorite and pallasite parent bodies recorded at the mineral scale by Fe and Ni isotope systematics. Geochim. Cosmochim. Acta 217, 95–111. https://doi.org/10.1016/J.GCA.2017.08.022

Ciscato, E.R., Bontognali, T.R.R., Vance, D., 2018. Nickel and its isotopes in organic-rich sediments: implications for oceanic budgets and a potential record of ancient seawater. Earth Planet. Sci. Lett. 494, 239–250. https://doi.org/10.1016/j.epsl.2018.04.061

Cisowski, S.M., Collinson, D.W., Runcorn, S.K., Stephenson, A., Fuller, M., 1983. A REVIEW OF LUNAR PALEOINTENSITY DATA AND IMPLICATIONS FOR THE ORIGIN OF LUNAR MAGNETISM. J. Geophys. Res. 88, A691–A704.

Cook, D.L., Clayton, R.N., Wadhwa, M., Janney, P.E., Davis, A.M., 2008a. Nickel isotopic anomalies in troilite from iron meteorites. Geophys. Res. Lett. 35, 1–5. https://doi.org/10.1029/2007GL032431

Cook, D.L., Clayton, R.N., Wadhwa, M., Janney, P.E., Davis, A.M., 2008b. Nickel isotopic anomalies in troilite from iron meteorites. Geophys. Res. Lett. 35, L01203. https://doi.org/10.1029/2007GL032431

Cook, D.L., Wadhwa, M., Clayton, R.N., Dauphas, N., Janney, P.E., Davis, A.M., 2007. Mass-dependent fractionation of nickel isotopes in meteoritic metal. Meteorit. Planet. Sci. 42, 2067–2077. https://doi.org/10.1111/j.1945-5100.2007.tb01008.x

Cook, D.L., Wadhwa, M., Janney, P.E., Dauphas, N., Clayton, R.N., Davis, A.M., 2006. High precision measurements of non-mass-dependent effects in nickel isotopes in meteoritic

metal via multicollector ICPMS. Anal. Chem. 78, 8477–84. https://doi.org/10.1021/ac061285m

Cornen, G., Bandet, Y., Giresse, P., Maley, J., 1992. The nature and chronostratigraphy of Quaternary pyroclastic accumulations from Lake Barombi Mbo (West-Cameroon). J. Volcanol. Geotherm. Res. 51, 357–374.

Dauphas, N., Teng, F.-Z., Arndt, N.T., 2010. Magnesium and iron isotopes in 2.7 Ga Alexo komatiites: Mantle signatures, no evidence for Soret diffusion, and identification of diffusive transport in zoned olivine. Geochim. Cosmochim. Acta 74, 3274–3291. https://doi.org/10.1016/J.GCA.2010.02.031

Dauritria, J.M., Girod, M., 1987. Cenozoaic Volcanism associated with Swells and Rifts, in: Nixon, P.. (Ed.), Mantle Xenoliths. pp. 195–215.

Dawson, J.B., 2012. Nephelinite-melilitite-carbonatite relationships: Evidence from Pleistocene-recent volcanism in northern Tanzania. Lithos 152, 3–10. https://doi.org/10.1016/j.lithos.2012.01.008

Dawson, J.B., 2002. Metasomatism and Partial Melting in Upper-Mantle Peridotite Xenoliths from the Lashaine Volcano, Northern Tanzania. J. Petrol. 43, 1749–1777. https://doi.org/10.1093/petrology/43.9.1749

Dawson, J.B., 1992. Neogene tectonics and volcanicity in the North Tanzania sector of the Gregory Rift Valley: contrasts with the Kenya sector. Tectonophysics 204, 81–92. https://doi.org/10.1016/0040-1951(92)90271-7

Dawson, J.B., 1964a. Carbonate Tuff Cones in Northern Tanganyika. Geol. Mag. 101, 129. https://doi.org/10.1017/S0016756800048561

Dawson, J.B., 1964b. Carbonatitic volcanic ashes in Northern Tanganyika. Bull. Volcanol. 27, 81–91. https://doi.org/10.1007/BF02597513

Dawson, J.B., Powell, D.G., Reid, A.M., 1970. Ultrabasic Xenoliths and Lava from the Lashaine Volcano, Northern Tanzania. J. Petrol. 11, 519–548. https://doi.org/10.1093/petrology/11.3.519

Day, J.M.D., Pearson, D.G., Macpherson, C.G., Lowry, D., Carracedo, J.-C., 2009. Pyroxenite-rich mantle formed by recycled oceanic lithosphere: Oxygen-osmium isotope evidence from Canary Island lavas. Geology 37, 555–558. https://doi.org/10.1130/G25613A.1

Delano, J.W., 1985. Mare Volcanic Glasses, II: Abundances of Trace Ni and the Composition of the Moon.

Dingwell, D.B., O'Neill, H.S.C., Ertel, W., Spettel, B., 1994. The solubility and oxidation state of nickel in silicate melt at low oxygen fugacities: Results using a mechanically assisted equilibration technique. Geochim. Cosmochim. Acta 58, 1967–1974. https://doi.org/10.1016/0016-7037(94)90428-6

Dosso, L., Bougault, H., Langmuir, C., Bollinger, C., Bonnier, O., Etoubleau, J., 1999. The age and distribution of mantle heterogeneity along the Mid-Atlantic ridge (31-41°N). Earth Planet. Sci. Lett. 170, 269–286. https://doi.org/10.1016/S0012-821X(99)00109-0

Dziewonski, A.M., Anderson, D.L., 1981. Preliminary reference Earth model. Phys. Earth Planet. Inter. 25, 297–356. https://doi.org/10.1016/0031-9201(81)90046-7

Eberhardt, P., Geiss, J., Graf, H., Grögler, N., Krähenbühl, U., Schwaller, H., Schwarzmüller, J., Stettler, A., 1970. Correlation between rock type and irradiation history of Apollo 11 igneous rocks. Earth Planet. Sci. Lett. 10, 67–72. https://doi.org/10.1016/0012-821X(70)90065-8

Ehlers, K., Grove, T.L., Sisson, T.W., Recca, S.I., Zervas, D.A., 1992. The effect of oxygen fugacity on the partitioning of nickel and cobalt between olivine, silicate melt, and metal. Geochim. Cosmochim. Acta 56, 3733–3743. https://doi.org/10.1016/0016-7037(92)90166-G

El Goresy, A., Ramdohr, P., Taylor, L.A., 1971. The opaque minerals in the lunar rocks from Oceanus Procellarum, in: 2ns Lunar Science Conference. The M.I.T. Press, pp. 219–235.

Elliott, T., Steele, R.C.J., 2017. The Isotope Geochemistry of Ni, in: Reviews in Mineralogy and Geochemistry.

Estrade, N., Cloquet, C., Echevarria, G., Sterckeman, T., Deng, T., Tang, Y., Morel, J.-L., 2015. Weathering and vegetation controls on nickel isotope fractionation in surface ultramafic environments (Albania). Earth Planet. Sci. Lett. 423, 24–35. https://doi.org/10.1016/j.epsl.2015.04.018

Faure, G., Mensing, T.M., Faure, G., 2005. Isotopes : principles and applications. Wiley.

Feigenson, M.D., 1986. Continental alkali basalts as mixtures of kimberlite and depleted mantle: Evidence from Kilbourne Hole Maar, New Mexico. Geophys. Res. Lett. 13, 965–968. https://doi.org/10.1029/GL013i009p00965

Finnerty, A.A., Boyd, F.R., 1987. Thermobarometry for Garnet Peridotites, in: Nixon, P.H. (Ed.), Mantle Xenoltihs. Wiley, pp. 381–402.

Fischer, R.A., Nakajima, Y., Campbell, A.J., Frost, D.J., Harries, D., Langenhorst, F., Miyajima, N., Pollok, K., Rubie, D.C., 2015. High pressure metal-silicate partitioning of Ni, Co, V, Cr, Si, and O. Geochim. Cosmochim. Acta 167, 177–194. https://doi.org/10.1016/j.gca.2015.06.026

Fitton, J.G., 2007. The OIB Paradox, in: Foulger, G.R., Jurdy, D.M. (Eds.), Plates, Plumes, and Planetary Processes. The Geological Society of America, pp. 387–409.

Fitton, J.G., 1987. The Cameroon line, West Africa: a comparison between oceanic and continental alkaline volcanism. Geol. Soc. London, Spec. Publ. 30, 273–291. https://doi.org/10.1144/GSL.SP.1987.030.01.13

Fitton, J.G., Dunlop, H.M., 1985. The Cameroon line, West Africa, and its bearing on the origin of oceanic and continental alkali basalt. Earth Planet. Sci. Lett. 72, 23–38. https://doi.org/10.1016/0012-821X(85)90114-1

Fitton, J.G., Saunders, A.D., Kempton, P.D., Hardarson, B.S., 2003. Does depleted mantle form an intrinsic part of the Iceland plume? Geochemistry, Geophys. Geosystems 4. https://doi.org/10.1029/2002GC000424

Freeth, S.J., 1979. Deformation of the African plate as a consequence of membrane stress domains generated by post-Jurassic drift. Earth Planet. Sci. Lett. 45, 93–104. https://doi.org/10.1016/0012-821X(79)90111-0

Frost, D.J., Liebske, C., Langenhorst, F., McCammon, C.A., Trønnes, R.G., Rubie, D.C., 2004. Experimental evidence for the existence of iron-rich metal in the Earth's lower mantle. Nature 428, 409–412. https://doi.org/10.1038/nature02413

Gale, A., Dalton, C.A., Langmuir, C.H., Su, Y., Schilling, J.-G., 2013. The mean composition of ocean ridge basalts. Geochemistry, Geophys. Geosystems 14, 489–518. https://doi.org/10.1029/2012GC004334

Gall, L., 2011. Development and Application of Nickel Stable Isotopes as a New Geochemical Tracer. University Of Oxford.

Gall, L., Williams, H., Siebert, C., Halliday, A.N., 2012. Determination of mass-dependent variations in nickel isotope compositions using double spiking and MC-ICPMS. J. Anal. At. Spectrom. 27, 137. https://doi.org/10.1039/c1ja10209e

Gall, L., Williams, H.M., Halliday, A.N., Kerr, A.C., 2017. Nickel isotopic composition of the mantle. Geochim. Cosmochim. Acta 199, 196–209. https://doi.org/10.1016/j.gca.2016.11.016

Gall, L., Williams, H.M., Siebert, C., Halliday, A.N., Herrington, R.J., Hein, J.R., 2013. Nickel isotopic compositions of ferromanganese crusts and the constancy of deep ocean inputs

and continental weathering effects over the Cenozoic. Earth Planet. Sci. Lett. 375, 148–155. https://doi.org/10.1016/j.epsl.2013.05.019

Garcia, R.F., Gagnepain-Beyneix, J., Chevrot, S., Lognonné, P., 2011. Very preliminary reference Moon model. Phys. Earth Planet. Inter. 188, 96–113. https://doi.org/10.1016/J.PEPI.2011.06.015

Gessmann, C.K., Rubie, D.C., 2000. The origin of the depletions of V, Cr and Mn in the mantles of the Earth and Moon. Earth Planet. Sci. Lett. 184, 95–107. https://doi.org/10.1016/S0012-821X(00)00323-X

Gibson, S.A., McMahon, S.C., Day, J.A., Dawson, J.B., 2013. Highly Refractory Lithospheric Mantle beneath the Tanzanian Craton: Evidence from Lashaine Pre-metasomatic Garnet-bearing Peridotites. J. Petrol. 54, 1503–1546. https://doi.org/10.1093/petrology/egt020

Gramlich, J.W., Machlan, L.A., Barnes, I.L., Paulsen, P.J., 1989. Absolute isotopic abundance ratios and atomic weight of a reference sample of nickel. J. Res. Natl. Inst. Stand. Technol. 94, 347. https://doi.org/10.6028/jres.094.034

Guan, Y., Huss, G.R., Leshin, L.A., 2004. SIMS analyses of Mg, Cr, and Ni isotopes in primitive meteorites and short-lived radionuclides in the early solar system. Appl. Surf. Sci. 231–232, 899–902. https://doi.org/10.1016/j.apsusc.2004.03.163

Gueguen, B., Rouxel, O., Ponzevera, E., Bekker, A., Fouquet, Y., 2013. Nickel Isotope Variations in Terrestrial Silicate Rocks and Geological Reference Materials Measured by MC-ICP-MS. Geostand. Geoanalytical Res. 37, 297–317. https://doi.org/10.1111/j.1751-908X.2013.00209.x

Gueguen, B., Rouxel, O., Rouget, M.-L., Bollinger, C., Ponzevera, E., Germain, Y., Fouquet, Y., 2016. Comparative geochemistry of four ferromanganese crusts from the Pacific Ocean and significance for the use of Ni isotopes as paleoceanographic tracers. Geochim. Cosmochim. Acta 189, 214–235. https://doi.org/10.1016/J.GCA.2016.06.005

Gueguen, B., Sorensen, J. V., Lalonde, S. V., Peña, J., Toner, B.M., Rouxel, O., 2018. Variable Ni isotope fractionation between Fe-oxyhydroxides and implications for the use of Ni isotopes as geochemical tracers. Chem. Geol. 481, 38–52. https://doi.org/10.1016/J.CHEMGEO.2018.01.023

Haase, K.M., Regelous, M., Duncan, R.A., Brandl, P.A., Stroncik, N., Grevemeyer, I., 2011. Insights into mantle composition and mantle melting beneath mid-ocean ridges from postspreading volcanism on the fossil Galapagos Rise Theme: Geochemical Heterogeneities in Oceanic Island Basalt and Mid-ocean Ridge Basalt Sources: Implications for Melting. Geochem. Geophys. Geosyst 12. https://doi.org/10.1029/2010GC003482

Haase, K.M., Regelous, M., Duncan, R.A., Brandl, P.A., Stroncik, N., Grevemeyer, I., 2011. Insights into mantle composition and mantle melting beneath mid-ocean ridges from postspreading volcanism on the fossil Galapagos Rise. Geochemistry, Geophys. Geosystems 12, 1–21. https://doi.org/10.1029/2010GC003482

Halliday, A.N., 2000. Terrestrial accretion rates and the origin of the Moon. Earth Planet. Sci. Lett. 176, 17–30. https://doi.org/10.1016/S0012-821X(99)00317-9

Halliday, A.N., Davidson, J.P., Holden, P., DeWolf, C., Lee, D.-C., Fitton, J.G., 1990. Trace-element fractionation in plumes and the origin of HIMU mantle beneather the Cameroon line. Nature 346, 523–528. https://doi.org/10.1038/346183a0

Halliday, A.N., Davies, G.R., Lee, D.-C., Tommasini, S., Paslick, C.R., Fitton, J.G., James, D.E., 1992a. Lead isotope evidence for young trace element enrichment in the oceanic upper mantle. Nature 359, 623–627. https://doi.org/10.1038/359623a0

Halliday, A.N., Davies, G.R., Lee, D.-C., Tommasini, S., Paslick, C.R., Fitton, J.G., James, D.E., 1992b. Lead isotope evidence for young trace element enrichment in the oceanic upper mantle. Nature 359, 623–627. https://doi.org/10.1038/359623a0

Halliday, A.N., Davies, G.R., Lee, D.C., 1992. Lead isotope evidence for young trace-element enrichment in the oceanic upper mantle. Nature 359, 623–627.

Halliday, A.N., Dickin, A.P., Fallick, A.E., Fitton, J.G., 1988. Mantle dynamics: A Nd, Sr, Pb and O isotopic study of the Cameroon line volcanic chain. J. Petrol. 29, 181–211. https://doi.org/10.1093/petrology/29.1.181

Halliday, A.N., Lee, D.-C., Christensen, J.N., Rehkämper, M., Yi, W., Luo, X., Hall, C.M., Ballentine, C.J., Pettke, T., Stirling, C., 1998. Applications of Multiple Collector-ICPMS to Cosmochemistry, Geochemistry, and Paleoceanography. Geochim. Cosmochim. Acta 62, 919–940. https://doi.org/10.1016/S0016-7037(98)00057-X

Halliday, A.N., Lee, D.-C., Tommasini, S., Davies, G.R., Paslick, C.R., Godfrey Fitton, J., James, D.E., 1995. Incompatible trace elements in OIB and MORB and source enrichment in the sub-oceanic mantle. Earth Planet. Sci. Lett. 133, 379–395. https://doi.org/10.1016/0012-821X(95)00097-V

Hardarson, B.S., Fitton, J.G., 1997. Mechanisms of crustal accretion in Iceland. Geology 25, 1043–1046.

Harpp, K.S., White, W.M., 2001a. Tracing a mantle plume: Isotopic and trace element variations of Galápagos seamounts. Geochemistry, Geophys. Geosystems 2, n/a-n/a. https://doi.org/10.1029/2000GC000137

Harpp, K.S., White, W.M., 2001b. Tracing a mantle plume: Isotopic and trace element variations of Galápagos seamounts. Geochemistry, Geophys. Geosystems 2, n/a-n/a. https://doi.org/10.1029/2000GC000137

Hart, S.R., 1988. Heterogeneous mantle domains: signatures, genesis and mixing chronologies. Earth Planet. Sci. Lett. 90, 273–296. https://doi.org/10.1016/0012-821X(88)90131-8

Hart, S.R., Davis, K.E., 1978. Nickel partitioning between olivine and silicate melt. Earth Planet. Sci. Lett. 40, 203–219.

Hartmann, W.K., Davis, D.R., 1975. Satellite-Sized Planetesimals and Lunar Origin, ICARUS.

Harvey, J., Dale, C.W., Gannoun, A., Burton, K.W., 2011. Osmium mass balance in peridotite and the effects of mantle-derived sulfides on basalt petrogenesis. Geochim. Cosmochim. Acta 75, 5574–5596. https://doi.org/10.1016/j.gca.2011.07.001

Harvey, J., Konig, S., Luguet, A., 2015. The effects of melt depletion and metasomatism on highly siderophile and strongly chalcophile elements: S-Se-Te-Re-PGE systematics of peridotite xenoliths from Kilbourne Hole, New Mexico. Geochim. Cosmochim. Acta 166, 210–233. https://doi.org/10.1016/j.gca.2015.06.028

Harvey, J., Yoshikawa, M., Hammond, S.J., Burton, K.W., 2012. Deciphering the trace element characteristics in kilbourne hole peridotite xenoliths: Melt-rock interaction and metasomatism beneath the Rio Grande Rift, SW USA. J. Petrol. 53, 1709–1742. https://doi.org/10.1093/petrology/egs030

Hauri, E.H., 1996. Major-element variability in the Hawaiian mantle plume. Nature 382, 415–419. https://doi.org/10.1038/382415a0

Henderson, P., Henderson, G., 2009. The Cambridge Handbook of Earth Science Data. Cambridge University Press.

Herzberg, C., Vidito, C., Starkey, N.A., 2016. Nickel–cobalt contents of olivine record origins of mantle peridotite and related rocks. Am. Mineral. 101, 1952–1966. https://doi.org/10.2138/am-2016-5538

Hiesinger, H., Head III, J.W., 2006. New Views of Lunar Geoscience: An Introduction and Overview, in: Reviews in Mineralogy & Geochemistry Volume 60: New Views of the Moon. pp. 1–67.

Hofmann, A., Bekker, A., Dirks, P., Gueguen, B., Rumble, D., Rouxel, O.J., 2014. Comparing

orthomagmatic and hydrothermal mineralization models for komatiite-hosted nickel deposits in Zimbabwe using multiple-sulfur, iron, and nickel isotope data. Miner. Depos. 49, 75–100. https://doi.org/10.1007/s00126-013-0476-1

Holzheid, A., Palme, H., Chakraborty, S., 1997. The activities of NiO, CoO and FeO in silicate melts. Chem. Geol. 139, 21–38.

Irving, A.J., 1980. Petrology and geochemistry of composite ultramafic xenoliths in alkalic basalts and implications for magmatic processes within the mantle. Am. J. Sci. 280–A, 389–426.

James, D.E., Padovani, E.R., Hart, S.R., 1980. Preliminary results on the oxygen isotopic composition of the lower crust, Kilbourne Hole Maar, New Mexico. Geophys. Res. Lett. 7, 321–324. https://doi.org/10.1029/GL007i005p00321

Jana, D., Walker, D., 1997. The influence of silicate melt composition on distribution of siderophile elements among metal and silicate liquids. Earth Planet. Sci. Lett. 150, 463–472. https://doi.org/10.1016/S0012-821X(97)00079-4

Kegler, P., Holzheid, A., Frost, D.J., Rubie, D.C., Dohmen, R., Palme, H., 2008. New Ni and Co metal-silicate partitioning data and their relevance for an early terrestrial magma ocean. Earth Planet. Sci. Lett. 268. https://doi.org/10.1016/j.epsl.2007.12.020

Keller, G.R., Morgan, P., Seager, W.R., 1990. Crustal structure, gravity anomalies and heat flow in the southern Rio Grande rift and their relationship to extensional tectonics. Tectonophysics 174, 21–37.

Kempton, P.D., Fitton, J.G., Saunders, A.D., Nowell, G.M., Taylor, R.N., Hardarson, B.S., Pearson, G., 2000. The Iceland plume in space and time: a Sr–Nd–Pb–Hf study of the North Atlantic rifted margin, Earth and Planetary Science Letters. Elsevier. https://doi.org/10.1016/S0012-821X(00)00047-9

Kirsten, T., Deubner, J., Horn, P., Kaneoka, I., Kiko, J., Schaeffer, O.A., Thio, S.K., 1972. The rare gas record of Apollo 14 and 15 samples. Proc. Third Lunar Sci. Conf. vol. 3, p. 1865 - 1889 3, 1865–1889.

Kodolányi, J., Stephan, T., Trappitsch, R., Pignatari, M., Davis, A.M., Pellin, M.J., 2018. Iron and nickel isotope compositions of presolar silicon carbide grains from supernovae. Geochim. Cosmochim. Acta 221, 127–144. https://doi.org/10.1016/J.GCA.2017.05.029

König, S., Wille, M., Voegelin, A., Schoenberg, R., 2016. Molybdenum isotope systematics in subduction zones. Earth Planet. Sci. Lett. 447, 95–102. https://doi.org/10.1016/j.epsl.2016.04.033

Koornneef, J.M., Davies, G.R., Döpp, S.P., Vukmanovic, Z., Nikogosian, I.K., Mason, P.R.D., 2009. Nature and timing of multiple metasomatic events in the sub-cratonic lithosphere beneath Labait, Tanzania. Lithos 112, 896–912. https://doi.org/10.1016/J.LITHOS.2009.04.039

Korotev, R.L., 2018. List of Lunar Meteorites [WWW Document]. http://meteorites.wustl.edu/lunar/moon_meteorites_list_alpha.htm.

Krawczynski, M.J., Grove, T.L., 2012. Experimental investigation of the influence of oxygen fugacity on the source depths for high titanium lunar ultramafic magmas. Geochim. Cosmochim. Acta 79, 1–19. https://doi.org/10.1016/j.gca.2011.10.043

Langmuir, C.H., Klein, E.M., Plank, T., 1992. Petrological Systematics of Mid-Ocean Ridge Basalts: Constraints on Melt Generation Beneath Ocean Ridges, in: Phipps Morgan, J., Blackman, D.K., Sinton, J.M. (Eds.), Mantle Flow and Melt Generation at Mantle Ridges. American Geophysical Union (AGU), pp. 183–280. https://doi.org/10.1029/GM071p0183

Lazar, C., Young, E.D., Manning, C.E., 2012. Experimental determination of equilibrium nickel isotope fractionation between metal and silicate from 500 °C to 950 °C. Geochim. Cosmochim. Acta 86, 276–295. https://doi.org/10.1016/J.GCA.2012.02.024

Lee, D.-C., 1994. A Chemical, Isotopic, and Geochronological Study of the Cameroon Line, West Africa. University of Michigan.

Lee, D.-C., Halliday, A.N., Davies, G.R., Essene, E.J., Fitton, J.G., Temdjim, R., 1996. Melt Enrichment of Shallow Depleted Mantle: a Detailed Petrological, Trace Element and Isotopic Study of Mantle- Derived Xenoliths and Megacrysts from the Cameroon Line. J. Petrol. 37, 15–441.

Lee, D., Halliday, A.N., Davies, G.R., Essene, E.J., Fitton, J.G., Temdjim, R., 1996. Melt Enrichment of Shallow Depleted Mantle: a Detailed Petrological, Trace Element and Isotopic Study of Mantle- Derived Xenoliths and Megacrysts from the Cameroon Line. J. Petrol. 37, 415–441.

Liang, Y.-H., Halliday, A.N., Siebert, C., Fitton, J.G., Burton, K.W., Wang, K.-L., Harvey, J., 2017. Molybdenum isotope fractionation in the mantle. Geochim. Cosmochim. Acta 199, 91–111. https://doi.org/10.1016/J.GCA.2016.11.023

Liu, L., Spasojević, S., Gurnis, M., 2008. Reconstructing Farallon Plate Subduction Beneath North America Back to the Late Cretaceous. Science (80-.). 322. https://doi.org/10.1126/science.1164170

Liu, S., Li, Y., Ju, Y., Liu, J., Liu, J., Shi, Y., 2018. Equilibrium nickel isotope fractionation in nickel sulfide minerals. Geochim. Cosmochim. Acta 222, 1–16. https://doi.org/10.1016/J.GCA.2017.10.018

Lodders, K., 2003. Solar System Abundances and Condensation Temperatures of the Elements. Astrophys. Journal, 591, 1220–1247.

Ma, Z., Thompson, R.N., Lykke, K.R., Pellin, M.J., Davis, A.M., 1995. Time-of-Flight Mass Spectrometer with Improved Resolution Review of. Cit. Rev. Sci. Instruments 66, 1150. https://doi.org/10.1063/1.1145546

Maley, J., Livingstone, D.A., Giresse, P., Thouveny, N., Brenac, P., Kelts, K., Kling, G., Stager, C., Haag, M., Fournier, M., Bandet, Y., Williamson, D., Zogning, A., 1990. Lithostratigraphy, volcanism, paleomagnetism and palynology of Quaternary lacustrine deposits from Barombi Mbo (West Cameroon): preliminary results. J. Volcanol. Geotherm. Res. 42, 319–335.

McCammon, C., 2005. The Paradox of Mantle Redox. Science (80-.). 308. https://doi.org/10.1126/science.1108162

McDonough, W.F., Sun, S. s., 1995. The composition of the Earth. Chem. Geol. 120, 223–253. https://doi.org/10.1016/0009-2541(94)00140-4

Menzies, M.A., Arculus, R.J., G, B.M., Bergman, S.C., Ehrenberg, S.N., Irving, A.J., Roden, M.F., Schulze, D.J., 1987. A record of subduction processes and within-plate volcanism in lithospheric xenoliths of southwestern USA, in: Nixon, P.. (Ed.), Mantle Xenoliths. pp. 59–74.

Meyer, C., 2011. Lunar Sample Compendium.

Meyer, C., 2003. Lunar Regolith - NASA Lunar Petrographic Educational Thin Section Set.

Moorbath, S., Sigurdsson, H., Goodwin, R., 1968. K-Ar ages of the oldest exposed rocks in Iceland. Earth Planet. Sci. Lett. 4, 197–205. https://doi.org/10.1016/0012-821X(68)90035-6

Morand, P., Allègre, C.J., 1983. Nickel isotopic studies in meteorites. Earth Planet. Sci. Lett. 63, 167–176. https://doi.org/10.1016/0012-821X(83)90034-1

Morand, P., Audouze, J., Allègre, C.J., 1980. Search for nickel isotopic anomaly of meteorites, in: 43rd Annual Meeting of the Meteoritical Society.

Moreau, C., Regnoult, J.-M., Déruelle, B., Robineau, B., 1987. A new tectonic model for the Cameroon Line, Central Africa. Tectonophysics 141, 317–334.

https://doi.org/10.1016/0040-1951(87)90206-X

Morgan, W.J., 1983. Hotspot tracks and the early rifting of the Atlantic. Tectonophysics 94, 123–139. https://doi.org/10.1016/0040-1951(83)90013-6

Mostefaoui, S., Lugmair, G.W., Hoppe, P., 2005. 60 Fe: A Heat Source for Planetary Differentiation from a Nearby Supernova Explosion. Astrophys. J. 625, 271–277. https://doi.org/10.1086/429555

Moynier, F., Agranier, A., Hezel, D.C., Bouvier, A., 2010. Sr stable isotope composition of Earth, the Moon, Mars, Vesta and meteorites, Earth and Planetary Science Letters. https://doi.org/10.1016/j.epsl.2010.10.017

Moynier, F., Albarède, F., Herzog, G.F., 2006. Isotopic composition of zinc, copper, and iron in lunar samples. Geochim. Cosmochim. Acta 70, 6103–6117. https://doi.org/10.1016/j.gca.2006.02.030

Moynier, F., Blichert-Toft, J., Telouk, P., Luck, J.-M., Albarède, F., 2007. Comparative stable isotope geochemistry of Ni, Cu, Zn, and Fe in chondrites and iron meteorites. Geochim. Cosmochim. Acta 71, 4365–4379. https://doi.org/10.1016/j.gca.2007.06.049

Moynier, F., Blichert-Toft, J.F., Telouk, P., Albarede, F., 2005. Excesses of 60Ni in chondrites and iron meteorites, in: Lunar and Planetary Science XXXVI.

Neal, C.R., 2001. The Interior of the Moon: The presence of garnet in the primitive deep lunar mantle. J. Geophys. Res. 106, 27865–27885.

Neal, C.R., Taylor, L.A., 1992. Petrogenesis of mare basalts: A record of lunar volcanism*. Geochim. Cosmochim. Acta 56, 2177–2211.

Neal, C.R., Taylor, L.A., 1991. Evidence for metasomatism of the lunar highlands and the origin of whitlockite. Geochim. Cosmochim. Acta 55, 2965–2980.

Newsom, H.E., 1986. Constraints on the Origin of the Moon from the Abundance of Molybdenum and Other Siderophile Elements.

Nicholls, D., 1974. Complexes and First Row Transition Elements. Macmillan, London.

Nier, A.O., 1940. A Mass Spectrometer for Routine Isotope Abundance Measurements. Rev. Sci. Instrum. 11. https://doi.org/10.1063/1.1751688

Niu, Y., Batiza, R., 1997. Trace element evidence from seamounts for recycled oceanic crust in the Eastern Pacific mantle. Earth Planet. Sci. Lett. 148, 471–483. https://doi.org/10.1016/S0012-821X(97)00048-4

Nixon, P.., 1987. Introduction, in: Mantle Xenoliths. pp. 1–3.

Norton, I.O., 2007. Speculations on Cretaceous tectonic history of the northwest Pacific and a tectonic origin for the Hawaii hotspot, in: Plates, Plumes, and Planetary Processes. pp. 451–470.

O'Neill, H.S.C., 1981. The transition between spinel lherzolite and garnet lherzolite, and its use as a Geobarometer. Contrib. to Mineral. Petrol. 77, 185–194. https://doi.org/10.1007/BF00636522

Palme, H., Spettel, B., Bischoff, A., St6ffler, D., 1984. Early Differentiation of the Moon' Evidence from Trace Elements in Plagioclase, in: PROCEEDINGS OF THE FIFTEENTH LUNAR AND PLANETARY SCIENCE CONFERENCE, PART 1 JOURNAL OF GEOPHYSICAL RESEARCH. https://doi.org/10.1029/JB089iS01p000C3

Paniello, R.C., Day, J.M.D., Moynier, F., 2012. Zinc isotopic evidence for the origin of the Moon. Nature 490, 376–379. https://doi.org/10.1038/nature11507

Papanastassiou, D.A., Wasserburg, G.J., 1971. Rb-Sr AGES OF IGNEOUS ROCKS FROM THE APOLLO 14 MISSION AND THE AGE OF THE FRA MAURO FORMATION. Earth Planet. Sci. Lett. 12, 36–48.

Papike, J.J., Fowler, G.W., Adcock, C.T., Shearer, C.K., 1999. Systematics of Ni and Co in olivine from planetary melt systems: Lunar mare basalts. Am. Mineral. 84, 392–399. https://doi.org/10.2138/am-1999-0324

Paslick, C., Halliday, A.N., James, D., Dawson, J.B., 1995. Enrichment of the continental lithosphere by OIB melts: Isotopic evidence from the volcanic province of northern Tanzania. Earth Planet. Sci. Lett. 130, 109–126.

Paslick, C.R., 1995. A Geochemical Study of Volcanism associated with the early stages of Continental Rifting in Northern Tanzanian. University of Michigan.

Paslick, C.R., Halliday, A.N., Lange, R.A., James, D., Dawson, J.B., 1996. Indirect crustal contamination: evidence from isotopic and chemical disequilibria in minerals from alkali basalts and nephelinites from northern Tanzania. Contrib. to Mineral. Petrol. 125, 277–292. https://doi.org/10.1007/s004100050222

Peale, S.J., Cassen, P., 1978. Contribution of tidal dissipation to lunar thermal history. Icarus 36, 245–269. https://doi.org/10.1016/0019-1035(78)90109-4

Perkins, D., Anthony, E.Y., 2011. The evolution of spinel lherzolite xenoliths and the nature of the mantle at Kilbourne Hole, New Mexico. Contrib. to Mineral. Petrol. 162, 1139–1157. https://doi.org/10.1007/s00410-011-0644-1

Pike, J.E.N., Meyer, C.E., Wilshire, H.G., 1980. Petrography and Chemical Composition of a Suite of Ultramafic Xenoliths from Lashaine, Tanzania. J. Geol. 88, 343–352. https://doi.org/10.1086/628512

Pinter, Z., Patko, L., Djoukam, F.T.J., Kovacs, I., Tchouankoue, J.P., Falus, G., Konc, Z., Tommasi, A., Barou, F., Mihaly, J., Nemeth, C., Jeffries, T., 2015. Characterization of the sub-continental lithospheric mantle beneath the Cameroon volcanic line inferred from alkaline basalt hosted peridotite xenoliths from Barombi Mbo and Nyos Lakes. J. African Earth Sci. 111, 170–193. https://doi.org/10.1016/j.jafrearsci.2015.07.006

Porter, S.J., Selby, D., Cameron, V., 2014. Characterising the nickel isotopic composition of organic-rich marine sediments. Chem. Geol. 387, 12–21. https://doi.org/10.1016/j.chemgeo.2014.07.017

Quitte, G., Halliday, A.N., Meyer, B.S., Markowski, A., Latkoczy, C., Gunther, D., 2007. Correlated Iron 60, Nickel 62, and Zirconium 96 in Refractory Inclusions and the Origin of the Solar System. Astrophys. J. 655, 678–684. https://doi.org/10.1086/509771

Quitté, G., Meier, M., Latkoczy, C., Halliday, A.N., Günther, D., Gunther, D., Günther, D., Gunther, D., Günther, D., 2006. Nickel isotopes in iron meteorites–nucleosynthetic anomalies in sulfides with no effects in metals and no trace of 60Fe. Earth Planet. Sci. Lett. 242, 16–25. https://doi.org/10.1016/j.epsl.2005.11.053

Quitté, G., Oberli, F., 2006. Quantitative extraction and high precision isotope measurements of nickel by MC-ICPMS. J. Anal. At. Spectrom. 21, 1249. https://doi.org/10.1039/b607569j

Rai, N., Westrenen, W. Van, 2014. Lunar core formation : New constraints from metal – silicate partitioning of siderophile elements. Earth Planet. Sci. Lett. 388, 343–352. https://doi.org/10.1016/j.epsl.2013.12.001

Ratié, G., Jouvin, D., Garnier, J., Rouxel, O., Miska, S., Guimaraes, E., Cruz Vieira, L., Sivry, Y., Zelano, I., Montarges-Pelletier, E., Thil, F., Quantin, C., 2015. Nickel isotope fractionation during tropical weathering of ultramafic rocks. Chem. Geol. 402, 68–76. https://doi.org/10.1016/j.chemgeo.2015.02.039

Ratié, G., Quantin, C., Jouvin, D., Calmels, D., Ettler, V., Sivry, Y., Vieira, L.C., Ponzevera, E., Garnier, J., Cruz Vieira, L., Ponzevera, E., Garnier, J., 2016. Nickel isotope fractionation during laterite Ni ore smelting and refining : Implications for tracing the sources of Ni in smelter-affected soils. Appl. Geochemistry 64, 136–145. https://doi.org/10.1016/j.apgeochem.2015.09.005

Reedy, R.C., Englert, P., 1986. Workshop on COSMOGENIC NUCLIDES.

Regelous, M., Elliott, T., Coath, C.D., 2008. Nickel isotope heterogeneity in the early Solar System. Earth Planet. Sci. Lett. 272, 330–338. https://doi.org/10.1016/j.epsl.2008.05.001

Reid, A.M., Donaldson, C.H., Brown, R.W., Ridley, W.I., Dawson, J.B., 1975. Mineral chemistry of peridotite xenoliths from the Lashaine volcano, Tanzania. Phys. Chem. Earth 9, 525–543. https://doi.org/10.1016/0079-1946(75)90037-3

Rhodes, J.M., Dawson, J.B., 1975. Major and trace element chemistry of peridotite inclusions from the Lashaine volcano, Tanzania. Phys. Chem. Earth 9, 545–557. https://doi.org/10.1016/0079-1946(75)90038-5

Righter, K., 2002. Does the Moon Have a Metallic Core? Constraints from Giant Impact Modeling and Siderophile Elements. Icarus 158, 1–13. https://doi.org/10.1006/icar.2002.6859

Righter, K., Drake, M.J., Yaxley, G., 1997. Prediction of siderophile element metal-silicate partition coefficients to 20 GPa and 2800°C: the effects of pressure, temperature, oxygen fugacity, and silicate and metallic melt compositions. Phys. Earth Planet. Inter. 100, 115–134. https://doi.org/10.1016/S0031-9201(96)03235-9

Righter, K., Pando, K.M., Danielson, L., Lee, C.-T., 2010. Partitioning of Mo, P and other siderophile elements (Cu, Ga, Sn, Ni, Co, Cr, Mn, V, and W) between metal and silicate melt as a function of temperature and silicate melt composition. Earth Planet. Sci. Lett. 291, 1–9. https://doi.org/10.1016/J.EPSL.2009.12.018

Roden, M.F., Irving, A.J., Murthy, V.R., 1988. Isotopic and trace element composition of the upper mantle beneath a young continental rift: Results from Kilbourne Hole, New Mexico. Geochim. Cosmochim. Acta 52, 461–473. https://doi.org/10.1016/0016-7037(88)90101-9

Rugel, G., Faestermann, T., Knie, K., Korschinek, G., Poutivtsev, M., Schumann, D., Kivel, N., Günther-Leopold, I., Weinreich, R., Wohlmuther, M., 2009. New Measurement of the ^{60}Fe Half-Life. Phys. Rev. Lett. 103, 072502. https://doi.org/10.1103/PhysRevLett.103.072502

Sato, M., Hickling, N.L., McLane, J.E., 1973. Oxygen fugacity values of Apollo 12, 14, and 15 lunar samples and reduced state of lunar magmas, in: Proceedings of the Fourth Lunar Science Conference. pp. 1061–1079.

Satsukawa, T., Michibayashi, K., Anthony, E.Y., Stern, R.J., Gao, S.S., Liu, K.H., 2011. Seismic anisotropy of the uppermost mantle beneath the Rio Grande rift: Evidence from Kilbourne Hole peridotite xenoliths, New Mexico. Earth Planet. Sci. Lett. 311, 172–181. https://doi.org/10.1016/J.EPSL.2011.09.013

Sedaghatpour, F., Teng, F.Z., Liu, Y., Sears, D.W.G., Taylor, L.A., 2013. Magnesium isotopic composition of the Moon. Geochim. Cosmochim. Acta 120, 1–16. https://doi.org/10.1016/j.gca.2013.06.026

Sharp, Z.D., Shearer, C.K., McKeegan, K.D., Barnes, J.D., Wang, Y.Q., 2010. The Chlorine Isotope Composition of the Moon and Implications for an Anhydrous Mantle. Science (80-.). 329. https://doi.org/10.1126/science.1191349

Shearer, C.K., Hess, P.C., Wieczorek, M.A., Pritchard, M.E., Parmentier, E.M., Borg, L.E., Longhi, J., Elkins-Tanton, L.T., Neal, C.R., Antonenko, I., Canup, R.M., Halliday, A.N., Grove, T.L., Hager, B.H., Lee, D.C., Wiechert, U., 2006. Thermal and Magmatic Evolution of the Moon, in: Reviews in Mineralogy & Geochemistry Volume 60: New Views of the Moon. pp. 365–502.

Shimamura, T., Lugmair, G.W., 1983. Ni isotopic compositions in Allende and other meteorites. Earth Planet. Sci. Lett. 63, 177–188. https://doi.org/10.1016/0012-821X(83)90035-3

Shukolyukov, A., Lugmair, G.W., 1993a. 60Fe in eucrites. Earth Planet. Sci. Lett. 119, 159–

166. https://doi.org/10.1016/0012-821X(93)90013-Y

Shukolyukov, A., Lugmair, G.W., 1993b. Live Iron-60 in the Early Solar System. Science (80-.). 259, 1138–1142.

Siebert, C., Nägler, T.F., Kramers, J.D., 2001. Determination of molybdenum isotope fractionation by double-spike multicollector inductively coupled plasma mass spectrometry. Geochemistry, Geophys. Geosystems 2, n/a-n/a. https://doi.org/10.1029/2000GC000124

Silveira, G., Stutzmann, E., Davaille, A., Montagner, J.-P., Mendes-Victor, L., Sebai, A., 2006. Azores hotspot signature in the upper mantle. J. Volcanol. Geotherm. Res. 156, 23–34. https://doi.org/10.1016/J.JVOLGEORES.2006.03.022

Simon, J.I., DePaolo, D.J., 2010. Stable calcium isotopic composition of meteorites and rocky planets, Earth and Planetary Science Letters. https://doi.org/10.1016/j.epsl.2009.11.035

Sobolev, A. V, Hofmann, A.W., Kuzmin, D. V, Yaxley, G.M., Arndt, N.T., Chung, S.-L., Danyushevsky, L. V, Elliott, T., Frey, F.A., Garcia, M.O., Gurenko, A.A., Kamenetsky, V.S., Kerr, A.C., Krivolutskaya, N.A., Matvienkov, V. V, Nikogosian, I.K., Rocholl, A., Sigurdsson, I.A., Sushchevskaya, N.M., Teklay, M., 2007. The Amount of Recycled Crust in Sources of Mantle-Derived Melts. Science (80-.). 316.

Sobolev, A. V, Hofmann, A.W., Sobolev, S. V, Nikogosian, I.K., 2005. An olivine-free mantle source of Hawaiian shield basalts. Nature 434.

Spivak-Birndorf, L.J., Wang, S.-J., Bish, D.L., Wasylenki, L.E., 2018. Nickel isotope fractionation during continental weathering. Chem. Geol. 476, 316–326. https://doi.org/10.1016/J.CHEMGEO.2017.11.028

Steele, A.M., Colson, R.O., Haskin, L.A., 1991. Co and Ni as Incompatible elements in the Lunar Mantle: Implications for fO2 and the Petrogenesis of Apollo 15 Green Glass, in: LPSC XXII.

Steele, R.C.J., Coath, C.D., Regelous, M., Russell, S., Elliott, T., 2012. Neutron-poor nickel isotope anomalies in meteorites. Astrophys. J. 758, 59. https://doi.org/10.1088/0004-637X/758/1/59

Steele, R.C.J., Elliott, T., Coath, C.D., Regelous, M., 2011. Confirmation of mass-independent Ni isotopic variability in iron meteorites. Geochim. Cosmochim. Acta 75, 7906–7925. https://doi.org/10.1016/J.GCA.2011.08.030

Steenstra, E.S., Rai, N., Knibbe, J.S., Lin, Y.H., Van Westrenen, W., 2016. New geochemical models of core formation in the Moon from metal-silicate partitioning of 15 siderophile elements. Earth Planet. Sci. Lett. 441, 1–9. https://doi.org/10.1016/j.epsl.2016.02.028

Strelow, F.W.E., 1990. Distribution coefficients and cation-exchange behaviour of some ammines and aquo complexes of metallic elements in ammonium nitrate solution. Anal. Chim. Acta 233, 129–134. https://doi.org/10.1016/S0003-2670(00)83468-6

Strelow, F.W.E., Weinert, C.H.S.W., Eloff, C., 1972. Distribution coefficients and anion exchange behavior of elements in oxalic acid-hydrochloric acid mixtures. Anal. Chem. 44, 2352–2356. https://doi.org/10.1021/ac60322a001

Sun, C., Graff, M., Liang, Y., 2017. Trace element partitioning between plagioclase and silicate melt: The importance of temperature and plagioclase composition, with implications for terrestrial and lunar magmatism. Geochim. Cosmochim. Acta 206, 273–295. https://doi.org/10.1016/j.gca.2017.03.003

Tachibana, S., Huss, G.R., 2003. The Initial Abundance of 60 Fe in the Solar System. Astrophys. J. 588, L41–L44. https://doi.org/10.1086/375362

Tachibana, S., Huss, G.R., Kita, N.T., Shimoda, G., Morishita, Y., 2006. 60 Fe in Chondrites: Debris from a Nearby Supernova in the Early Solar System? Astrophys. J. 639, L87–L90. https://doi.org/10.1086/503201

Tanimizu, M., Hirata, T., 2006. Determination of natural isotopic variation in nickel using inductively coupled plasma mass spectrometry. J. Anal. At. Spectrom. 21, 1423. https://doi.org/10.1039/b609543g

Taylor, S.R., 1982. A Lunar Perspective. Lunar and Planetary Institute.

Taylor, S.R., 1975. Lunar Science: A Post-Apollo View.

Teng, F.-Z., Dauphas, N., Huang, S., Marty, B., 2013. Iron isotopic systematics of oceanic basalts. Geochim. Cosmochim. Acta 107, 12–26. https://doi.org/10.1016/J.GCA.2012.12.027

Thompson, G., Bryan, W.B., Humphris, S.E., 1989. Axial volcanism on the East Pacific Rise, in: Magmatism in the Ocean Basins. pp. 181–200.

Trappitsch, R., Stephan, T., Savina, M.R., Davis, A.M., Pellin, M.J., Rost, D., Gyngard, F., Gallino, R., Bisterzo, S., Cristallo, S., Dauphas, N., 2018. Simultaneous iron and nickel isotopic analyses of presolar silicon carbide grains. Geochim. Cosmochim. Acta 221, 87–108. https://doi.org/10.1016/J.GCA.2017.05.031

van Kan Parker, M., Sanloup, C., Sator, N., Guillot, B., Tronche, E.J., Perrillat, J.-P., Mezouar, M., Rai, N., van Westrenen, W., 2012. Neutral buoyancy of titanium-rich melts in the deep lunar interior. Nat. Geosci. 5, 186–189. https://doi.org/10.1038/ngeo1402

Vance, D., Little, S.H., Archer, C., Cameron, V., Andersen, M.B., Rijkenberg, M.J.A., Lyons, T.W., 2016. The oceanic budgets of nickel and zinc isotopes: the importance of sulfidic environments as illustrated by the Black Sea. Philos. Trans. A. Math. Phys. Eng. Sci. 374, 20150294. https://doi.org/10.1098/rsta.2015.0294

Vauchez, A., Dineur, F., Rudnick, R., 2005. Microstructure, texture and seismic anisotropy of the lithospheric mantle above a mantle plume: Insights from the Labait volcano xenoliths (Tanzania). Earth Planet. Sci. Lett. 232, 295–314. https://doi.org/10.1016/J.EPSL.2005.01.024

Ventura, G.T., Gall, L., Siebert, C., Prytulak, J., Szatmari, P., Hürlimann, M., Halliday, A.N., 2015. The stable isotope composition of vanadium, nickel, and molybdenum in crude oils. Appl. Geochemistry 59, 104–117. https://doi.org/10.1016/j.apgeochem.2015.04.009

Victor, A.H., 1986. Selective separation of Nickel from other elements by cation-exchange chromatography in dimethylglyoxime/hydrochloric acid/acetone media. Anal. Chim. Acta 183, 155–161.

Wadhwa, M., 2008. Redox Conditions on Small Bodies, the Moon and Mars, in: Reviews in Mineralogy and Geochemistry. GeoScienceWorld, pp. 493–510. https://doi.org/10.2138/rmg.2008.68.17

Walter, L.S., French, B.M., Heinrich, K.F.J., Lowman, P.D., Doan, A.S., Adler, I., 1971. Mineralogical studies of Apollo 12 samples, in: 2nd Lunar Science Conference. M.I.T. Press, pp. 343–358.

Wang, K., Jacobsen, S.B., Sedaghatpour, F., Chen, H., Korotev, R.L., 2015. The earliest Lunar Magma Ocean differentiation recorded in Fe isotopes. Earth Planet. Sci. Lett. 430, 202–208. https://doi.org/10.1016/j.epsl.2015.08.019

Wang, S.-J., Wasylenki, L.E., 2017. Experimental constraints on reconstruction of Archean seawater Ni isotopic composition from banded iron formations. Geochim. Cosmochim. Acta 206, 137–150. https://doi.org/10.1016/J.GCA.2017.02.023

Warren, P.H., 1985. THE MAGMA OCEAN CONCEPT AND LUNAR EVOLUTION. Ann. Rev. Earth planet. Sci 13, 201–241.

Warren, P.H., Wasson, J.T., 1979. The Origin of KREEP. Rev. Geophys. Sp. Phys. 17.

Wasylenki, L.E., Howe, H.D., Spivak-Birndorf, L.J., Bish, D.L., 2015. Ni isotope fractionation during sorption to ferrihydrite: Implications for Ni in banded iron formations. Chem. Geol.

400, 56–64. https://doi.org/10.1016/j.chemgeo.2015.02.007

Weber, R.C., Lin, P., Garnero, E.J., Williams, Q., Lognonné, P., 2011. Seismic Detection of the Lunar Core 331, 309–312.

Wedepohl, K.H., 1974. Nickel, in: Wedepohl, K.H. (Ed.), Handbook of Geochemistry. Springer.

Weis, D., Kieffer, B., Maerschalk, C., Barling, J., de Jong, J., Williams, G.A., Hanano, D., Pretorius, W., Mattielli, N., Scoates, J.S., Goolaerts, A., Friedman, R.M., Mahoney, J.B., 2006. High-precision isotopic characterization of USGS reference materials by TIMS and MC-ICP-MS. Geochemistry, Geophys. Geosystems 7, n/a-n/a. https://doi.org/10.1029/2006GC001283

Weyer, S., Anbar, A.D., Brey, G.P., Münker, C., Mezger, K., Woodland, A.B., 2007. Fe-isotope fractionation during partial melting on Earth and the current view on the Fe-isotope budgets of the planets (reply to the comment of F. Poitrasson and to the comment of B.L. Beard and C.M. Johnson on "Iron isotope fractionation during planetary differentiation" by S. Weyer, A.D. Anbar, G.P. Brey, C. Münker, K. Mezger and A.B. Woodland). Earth Planet. Sci. Lett. 256, 638–646. https://doi.org/10.1016/J.EPSL.2007.01.038

White, W.M., 1985. Sources of oceanic basalts: Radiogenic isotopic evidence. Geology 13, 115. https://doi.org/10.1130/0091-7613(1985)13<115:SOOBRI>2.0.CO;2

White, W.M., McBirney, A.R., Duncan, R.A., 1993. Petrology and geochemistry of the Galápagos Islands: Portrait of a pathological mantle plume. J. Geophys. Res. Solid Earth 98, 19533–19563. https://doi.org/10.1029/93JB02018

White, W.M., Tapia, M.D.M., Schilling, J.-G., 1979. The petrology and geochemistry of the Azores Islands. Contrib. to Mineral. Petrol. 69, 201–213. https://doi.org/10.1007/BF00372322

Wiechert, U., Halliday, A.N., Lee, D.-C., Snyder, G.A., Taylor, L.A., Rumble, D., 2001. Oxygen Isotopes and the Moon-Forming Giant Impact. Science (80-.). 294, 345–348.

Wieczorek, M.A., Jolliff, B.L., Khan, A., Pritchard, M.E., Weiss, B.P., Williams, J.G., Hood, L.L., Righter, K., Neal, C.R., Shearer, C.K., McCallum, I.S., Tompkins, S., Hawke, B.R., Peterson, C., Gillis, J.J., Bussey, B., 2006. The Constitution and Structure of the Lunar Interior, in: Reviews in Mineralogy & Geochemistry Volume 60: New Views of the Moon. pp. 221–343.

Willbold, M., Stracke, A., 2006. Trace element composition of mantle end-members: Implications for recycling of oceanic and upper and lower continental crust. Geochemistry, Geophys. Geosystems 7, 1–30. https://doi.org/10.1029/2005GC001005

Williams, H.M., Bizimis, M., 2014. Iron isotope tracing of mantle heterogeneity within the source regions of oceanic basalts. Earth Planet. Sci. Lett. 404, 396–407. https://doi.org/10.1016/J.EPSL.2014.07.033

Williams, H.M., Mccammon, C.A., Peslier, A.H., Halliday, A.N., Teutsch, N., Levasseur, S., Burg, J.-P., 2004. Iron Isotope Fractionation and the Oxygen Fugacity of the Mantle. Source Sci. New Ser. 304, 1656–1659.

Williams, H.M., Nielsen, S.G., Renac, C., Griffin, W.L., O'Reilly, S.Y., Mccammon, C.A., Pearson, N., Viljoen, F., Alt, J.C., Halliday, A.N., 2009. Fractionation of oxygen and iron isotopes by partial melting processes: Implications for the interpretation of stable isotope signatures in mafic rocks. Earth Planet. Sci. Lett. 283, 156–166. https://doi.org/10.1016/j.epsl.2009.04.011

Williams, H.M., Peslier, A.H., Mccammon, C., Halliday, A.N., 2005. Systematic iron isotope variations in mantle rocks and minerals : The effects of partial melting and oxygen fugacity. Earth Planet. Sci. Lett. 235, 435–452. https://doi.org/10.1016/j.epsl.2005.04.020

Williams, H.M., Prytulak, J., Woodhead, J.D., Kelley, K.A., Brounce, M., Plank, T., 2018.

Interplay of crystal fractionation, sulfide saturation and oxygen fugacity on the iron isotope composition of arc lavas: An example from the Marianas. Geochim. Cosmochim. Acta 226, 224–243. https://doi.org/10.1016/J.GCA.2018.02.008

Wing, B.A., Farquhar, J., 2015. Sulfur isotope homogeneity of lunar mare basalts. https://doi.org/10.1016/j.gca.2015.09.003

Wood, B.J., Bryndzia, L.T., Johnson, K., 1990. Mantle Oxidation State and Its Relationship to Tectonic Environment and Fluid Speciation. Science (80-.). 248.

Wood, B.J., Kiseeva, E.S., Mirolo, F.J., 2014. Accretion and core formation: The effects of sulfur on metal-silicate partition coefficients. Geochim. Cosmochim. Acta 145, 248–267. https://doi.org/10.1016/j.gca.2014.09.002

Yi, W., Halliday, A.N., Alt, J.C., Lee, D.-C., Rehkämper, M., Garcia, M.O. 0, Langmuir, C.H., Su, Y., Rehkämper, M., Garcia, M.O. 0, Langmuir, C.H., Su, Y., 2000. Cadmium, indium, tin, tellurium, and sulfur in oceanic basalts: Implications for chalcophile element fractionation in the Earth. J. Geophys. Res. 105, 18,927-18,948. https://doi.org/10.1029/2000JB900152

Yi, W., Halliday, A.N., Lee, D.-C., Christensen, J.N., 1995a. Indium and tin in basalts, sulfides, and the mantle. Geochim. Cosmochim. Acta 59, 5081–5090.

Yi, W., Halliday, A.N., Lee, D.-C., Christensen, J.N., 1995b. Indium and tin in basalts, sulfides, and the mantle. Geochim. Cosmochim. Acta 59, 5081–5090. https://doi.org/10.1016/0016-7037(95)00342-8

Zhao, Y., Xue, C., Liu, S.-A., Symons, D.T.A., Zhao, X., Yang, Y., Ke, J., 2017. Copper isotope fractionation during sulfide-magma differentiation in the Tulaergen magmatic Ni–Cu deposit, NW China. Lithos 286–287, 206–215. https://doi.org/10.1016/J.LITHOS.2017.06.007

Zindler, A., Hart, S., 1986. CHEMICAL GEODYNAMICS, Ann. Rev. Earth Planet. Sci.

4. Nickel isotopic fractionation in terrestrial mafic rocks

4.1. Introduction

Nickel in mafic rocks

Nickel has a similar ionic radius and charge to magnesium; the radii of Mg^{2+} and Ni^{2+} are 0.072 nm and 0.069 nm respectively (Henderson and Henderson, 2009). Therefore, the Ni^{2+} ion partitions readily into the octahedral metal sites in olivine, usually in place of the Mg^{2+} ion. For this reason, Ni is highly concentrated in olivine, and to a lesser degree in other ferromagnesian silicates, and is highly compatible during mantle melting. The strongly compatible behaviour means that Ni concentrations are highly variable as a result of olivine fractionation in particular. Over geological time, a relatively small proportion of Ni has been added to the crust, estimated at 0.03% the total Earth's Ni (McDonough and Sun, 1995). The partitioning of Ni does not depend on the Ni concentration in the system, although melt composition does play a strong role (Hart and Davis, 1978). Nickel concentrations in basaltic magmas and their partially melted mantle residues, depend on the partitioning between liquid and residual solid or cumulate phases, temperature and pressure conditions of fractional crystallization and partial melting, the Ni contents of the sources, and melt-rock reaction (Herzberg et al., 2016).

Unlike Fe, which is also in solid solution with Mg in mantle silicates, Ni is only divalent under mantle oxidation conditions. Iron can be in the +2 or +3 form depending on the oxygen fugacity. Stable Fe isotopes are fractionated during partial melting, as shown by Williams and co-workers (Williams et al., 2009, 2005, 2004), Weyer and co-workers (2007), and Teng and co-workers (Teng et al., 2013), with iron isotope compositions of samples of the terrestrial upper mantle systematically lighter than basalts. However, Fe isotopic differences can be a function of parameters such as oxidation state. Copper, which behaves similarly to Ni under some conditions, also shows significant isotopic variation during redox reactions but insignificant fractionation during mantle partial melting and magmatic differentiation, with the exception of sulfide liquid-silicate segregation (Zhao et al., 2017).

Investigation of Ni provides the opportunity to investigate mantle processes without the complication of effects associated with changes in oxidation state. Investigation of the stable Ni isotopic compositions of products of partial melting has been limited (Figure 16). Published data exists for eight samples for komatiite (Gall, 2011; Gall et al., 2017; Gueguen et al., 2013), one sample of picrite (Gall, 2011), twelve samples of MORB (Cameron et al., 2009; Gall, 2011; Gueguen et al., 2013), and five samples of granite (Gall, 2011).

Komatiites and picrites are formed from high degree partial melts, which represent more the mantle at the time and location of formation then they do the partial melting process. Komatiites have been found to have variable $\delta^{60/58}Ni_{SRM986}$, apparently depending on the presence of associated sulfide. Archean komatiites with disseminated sulfide mineralisation exhibit a large range in Ni isotopic compositions all significantly lighter than the estimates for BSE (Gall, 2011; Gueguen et al., 2013). Gall and co-workers (Gall et al., 2017) also analysed 5 Phanerozoic komatiites from Gorgona and found them to be in agreement with the BSE estimate in the same work. A picrite sample analysed by Gall (2011) also had a similar composition to the BSE (Figure 16).

The analyses of MORB showed variation in Ni isotopic composition, despite MORB being a relatively homogeneous rock type. Cameron and co-workers (2009) analysed three samples of MORB, which showed a range in Ni isotopic composition for 0.01 to 0.24‰. Gall (2011) analysed 8 samples of MORB, from the Atlantic, Indian, and East Pacific Rise spreading ridges, that ranged in Ni isotopic composition from -0.22 to 0.04‰ (Figure 16). Gall (2011), showed that MORB samples were, on average, significantly lighter than the estimate for BSE, and hence it was suggested that Ni isotopes fractionate with partial melting, with lighter isotopes preferentially enriched in the melt phase during melting. A relationship was also found between ridge spreading rate and Ni isotopic composition of the MORB, with slow ridges having heavier compositions than fast-spreading ones (Gall, 2011).

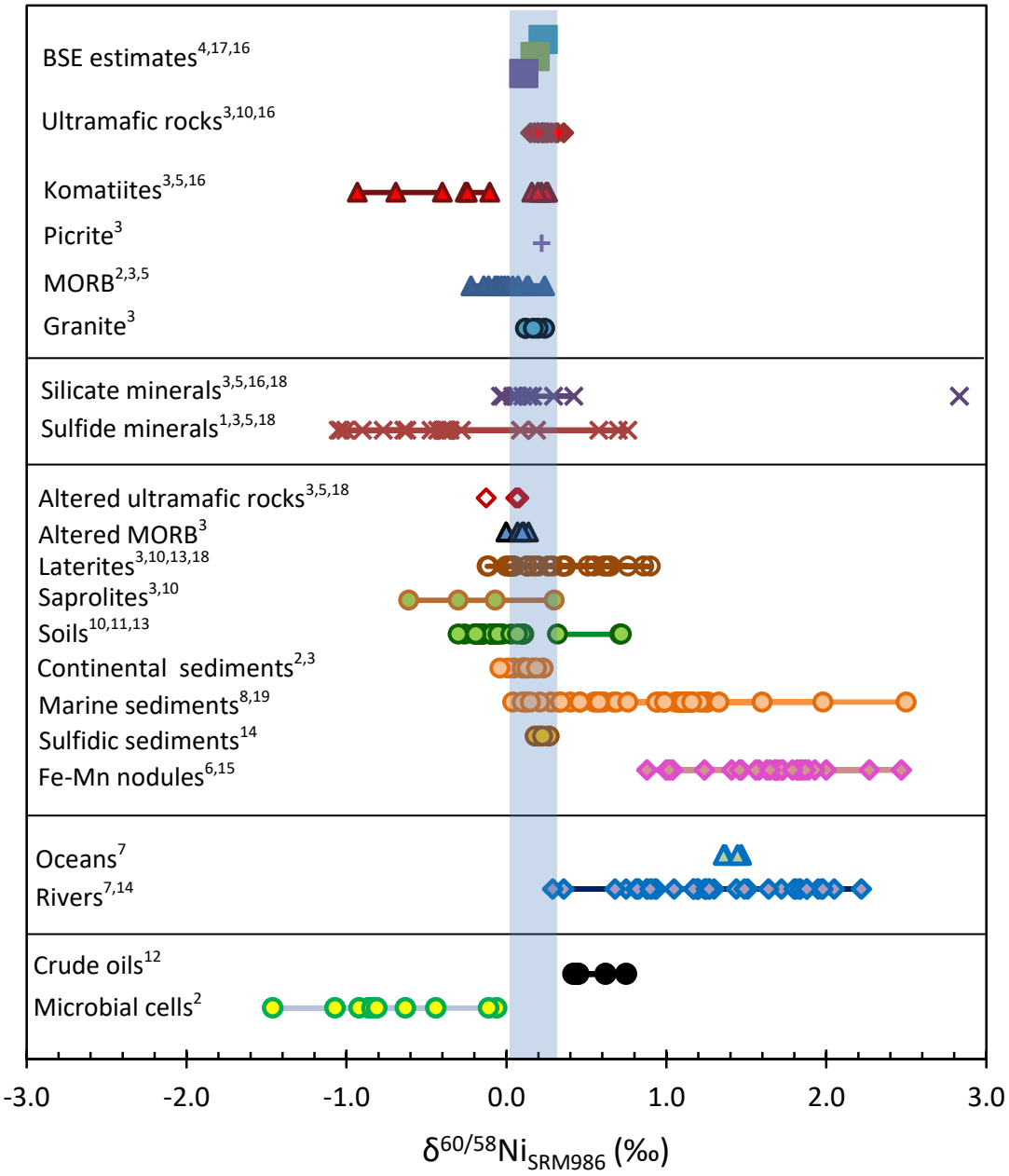

Figure 16

Published $\delta^{60/58}Ni_{SRM986}$ data for terrestrial samples. BSE estimates for comparison, from (Gall et al., 2017; Steele et al., 2011) and with the estimate of Gueguen and co-workers (2013) recalculated by (Elliott and Steele, 2017) to remove sediments.
[1](Tanimizu and Hirata, 2006); [2](Cameron et al., 2009); [3](Gall, 2011); [4](Steele et al., 2011); [5](Gueguen et al., 2013); [6](Gall et al., 2013); [7](Cameron and Vance, 2014); [8](Porter et al., 2014); [9](Hofmann et al., 2014); [10](Ratié et al., 2015); [11](Estrade et al., 2015); [12](Ventura et al., 2015); [13](Ratié et al., 2016); [14](Vance et al., 2016); [15](Gueguen et al., 2016); [16](Gall et al., 2017); [17](Elliott and Steele, 2017); [18](Spivak-Birndorf et al., 2018); [19](Ciscato et al., 2018)

No Ni isotopic data have so far been published on OIB samples with the exception of reference materials. Intraplate ocean islands are often associated with hotspots, which are considered the surface expression of a mantle plume. Analyses of potential temperatures of the material at OIBs has shown temperatures that olivines crystallised early in the life of the OIB are hotter

than the potential temperatures of MORB and this has suggested that for these OIBs formation in the deep mantle is likely.

In addition to the published sample data, crustal igneous rock standards have been analysed, primarily for inter-laboratory comparison. These include dolerite DNC-1 (Chernonozhkin et al., 2015; Gueguen et al., 2013), and basalts BIR1 (Chernonozhkin et al., 2015; Gall, 2011; Gueguen et al., 2013), BHVO2 (Chernonozhkin et al., 2015; Gall, 2011; Gueguen et al., 2013; Ratié et al., 2015), and JB-2 (Cameron et al., 2009; Chernonozhkin et al., 2015). Crustal igneous reference materials yet to be analysed by more than one lab include komatiite OKUM (Chernonozhkin et al., 2016, 2015), rhyolite JR-1 (Cameron et al., 2009), granites JG-2 (Cameron et al., 2009) and G-1 (Gueguen et al., 2013), granodiorite GSP-2 (Gall, 2011), andesites JA-1 (Cameron et al., 2009) and AGV-2 (Gall, 2011), and basalts BHVO1 (Chernonozhkin et al., 2016, 2015), and BCR-1 (Gall, 2011).

Geological setting of mafic rock production

Mid ocean ridge basalts are formed from adiabatic decompression melting of the upper mantle beneath spreading ridges. Chemical compositions of basalts at mid-ocean ridges depend on the composition and mineralogy of the source, degree of partial melting, depth of magma segregation, extent of fractional crystallization, and magma mixing processes during storage of magmas. Despite this, there is apparent compositional uniformity in the major element chemistry of MORB. Geochemically, normal mid-ocean ridge basalt (N-MORB) has relatively low K_2O and other incompatible elements, relative to primitive mantle, as well as unfractionated HREE and strongly depleted LREE (e.g. Langmuir et al., 1992).

In contrast, there are also examples of MORB with a more enriched concentration of highly incompatible elements (E-MORB), leading some authors to suggest they form by mixing with hot-spot sources. However, in many ridges both N-MORB and E-MORB are found, and the ratio in any specific ridge system can vary with ridge spreading rate. These are endmember compositions, but in practice the distinction is made based on primitive mantle normalised La/Sm being >1 (in enriched) or <1 (in normal) (e.g. Gale et al., 2013).

Oceanic volcanism has been attributed to being mixtures of five end-member components based on Nd, Sr, and Pb radiogenic isotopic compositions viz. depleted MORB source mantle (DMM), enriched mantle 1 (EM1), enriched mantle 2 (EM2), prevalent mantle (PREMA), and a magma source with high $^{238}U/^{204}Pb$ ratio (HIMU) e.g. (Hart, 1988; White, 1985; Zindler and Hart, 1986). Willbold and Stracke (2006) suggested that the enriched basalts cannot be grouped into merely two components by trace element systematics. Ocean island basalts (OIB) are thought to sample various mixtures of these components. They are more variable than MORB in terms of major elements, and with different trace element profiles. Ocean Island basalts have concentrations of incompatible elements that are enriched by a factor of ten compared to MORB, which is evidence that they originate from different mantle sources. Other evidence includes Nd, Sr, and Pb radiogenic isotopic compositions that are distinct from MORB values. The mantle under these ocean islands has higher mantle temperatures.

With the published variability in Ni isotopic compositions for MORB, and no published data for OIB this study has targeted additional MORB samples and compared these compositions to basalts from a selection of different ocean islands, and to mantle samples. A sub-set of samples has been targeted to address potential fractionation in Ni isotopes during partial melting and fractional crystallisation. This would permit determination of whether Ni isotopic heterogeneity in basalts relates to potential heterogeneity in basalt sources or if during melt related processes introduce isotope fractionation. Information that can be gained on mantle source regions from the Ni isotopic composition of the melt could be used, in principle, to estimate planetary mantles including that of the Moon if the same processes are thought to apply.

4.2. Sample strategy

Twelve samples from spreading ridges from the Atlantic and Pacific Oceans, and twelve sample from a total of four ocean islands were analysed in this work. MORB samples included examples of N-type and E-type tholeiites. In addition, a suite of 15 intraplate samples from both the oceanic and continental sectors of the Cameroon Line was also investigated. All the samples

with radiogenic isotopic data (Dosso et al., 1999; A. N. Halliday et al., 1992; Halliday et al., 1990; Harpp and White, 2001a) plot within a relatively small compositional range, between HIMU, PREMA, and DMM. Only MORB sample A127 D26-5 truly plots within the DMM field, but as it is the least La/Sm enriched E-MORB sample ($(La/Sm)_N$=1.06), it may be considered likely that the N-MORB samples, that do not have published radiogenic data, would show dominantly a DMM source.

The Cameroon Line basalts were analysed in order to investigate whether degree of partial melting has any effect on $\delta^{60/58}Ni_{SRM986}$. Analysed samples range from hypersthene-normative basalt, through alkali basalt and basanite, to nephelinite. The nephelinite samples also provided the ideal samples to investigate potential contamination in Ni through mechanical processing, as the very low Ni concentrations provide the potential for greatest perturbation.

4.2.1. Mid Ocean Ridge Basalts

Samples from two mid-ocean ridges were analysed in this study from the Pacific and Atlantic Ocean. Samples cover both E-MORB and N-MORB type tholeiites.

The Mid Atlantic Ridge

The Mid Atlantic Ridge (MAR) is a slow-spreading ridge. The area of MAR studied in this work was between 36 and 37°N, around the Azores hotspot. Samples were dredged using a manned submersible during the FAZAR expedition (1992). This part of the ridge is within the area of North MAR that shows a geochemical anomaly associated with the proximity of the Azores hotspot (Dosso et al., 1999). The region is characterized by large excesses in $^{230}Th/^{238}U$ and latitudinal variations in radiogenic isotopic ratios and trace element data (Dosso et al., 1999).

The majority of samples in this work have been previously studied by Bourdon and co-workers (1996) for U systematics, Dosso and co-workers for Sr, Nd, and Pb systematics (1999), and Yi and co-workers (2000) for Cd, In, Sn, Te, and S. The latter is the only study to include examples of N-MORB.

The East Pacific Rise

The East Pacific Rise (EPR) is, in places, the fastest-spreading ridge on the planet. There has been a range of primitive and evolved lava types extruded along the ridge. Much of the compositional variation has been attributed to low-pressure equilibrium crystallization for within distinct magma batches, and in part to variable degrees of high- and medium- pressure fractional crystallization between distinct magma batches (Thompson et al., 1989). The latter may also be attributed to different degrees of melting or melting at greater depths due to proximity of cold lithosphere (Thompson et al., 1989).

This work uses a subset of samples from Niu and Batiza (1997), who dredged samples from seamounts near the EPR between 5° and 15°N, to investigate the melting of the mantle. The results were consistent with two components, one enriched and the other depleted in incompatible elements, estimated to be physically small mantle domains to explain heterogeneity in lavas of single seamounts (Niu and Batiza, 1997). The enriched component was constrained with relative enrichments of high-field strength elements (HFSE), such as Nb, Ta, Zr, and Ti (Niu and Batiza, 1997). In contrast, the depleted component is constrained as exhibiting highly variable but correlated differences in ratios such as Zr/Hf, Nb/Ta, Th/U, Rb/Cs, which generally show little variation between MORB and OIB (Niu and Batiza, 1997).

The samples analysed in this work were initially analysed by Niu and Batiza (1997). R82-1 originates from 11.51°N 103.56°W, and a depth of 2174 metres below sea level (mbsl). R93-7 originates from 12.29°N 103.64°W, and a depth of 2721mbsl. R94-2 originates from 12.33°N 103.72°W, and a depth of 2694 mbsl. These samples have also been analysed for Mo isotopic composition (Liang et al., 2017)

4.2.2. Ocean Island Basalts

Samples from four Ocean Islands were analysed in this study; however, only one of them is not complicated by association with a nearby mid ocean ridge. Samples cover a range of lithologies including alkali basalts, transitional basalts, and tholeiites.

Loihi

Loihi is a seamount in the Hawaiian-Emperor seamount chain, associated with the most recent volcanism at the Hawaiian hotspot. The age-progressive island chain is made of massive basaltic shields, 3,000 to 40,000 km^3, dominated by highly alkaline and very mafic rocks. The basalt samples from the oldest end of the Emperor seamount chain are geochemically like N-MORB and not enriched like OIB (Norton, 2007). This is a submarine basaltic glass previously been studied by Yi and co-workers (2000) for Cd, In, Sn, Te, and S. The sample has also been studied for Mo isotopes (Liang et al., 2017).

Iceland

Iceland is the largest island associated with a mid ocean ridge. It is associated with a hotspot as well as straddling the northern Mid-Atlantic Ridge. The oldest Icelandic basalts are approximately 16 Ma (Moorbath et al., 1968) and are found in NW and SE extremities of the island.

The variation in the geochemical signatures of Icelandic basalts has been attributed to the mixing of two endmembers: N-MORB; and an enriched plume-derived OIB magma (Fitton, 2007). However, evidence from Pb-isotopes and trace elements has suggested the depleted component is intrinsic to the plume and not related to the MAR (Fitton et al., 2003). Generally, the most enriched basalts are from off the ridge axis and from the propagating tip of the eastern rift. Icelandic extrusions of E-MORB are the most voluminous in the world (Fitton, 2007).

The SNB series were collected from Snaefellsnes, one of the neo-volcanic zones, in central west Iceland (Kempton et al., 2000). Snaefellsnes lavas are of Quaternary age, relative to the Tertiary lavas of the other sites sampled. Other samples originate from North and East Iceland (Hardarson and Fitton, 1997). The samples in this work have been previously studied by Kempton and co-workers (2000) for Nd, Sr, Pb, and Hf isotopic composition (SNB19 only), and Hardarson and Fitton (1997) (others excluding SNB series) for trace elements and Nd isotopic composition. These samples have also been studied for Mo isotopes (Liang et al., 2017).

Galápagos

The Galápagos (officially Archipiélago de Colón, and part of Ecuador) is a series of Pleistocene to Recent islands in the equatorial East Pacific. The islands formed over a hotspot, which like Iceland, is complicated by proximity to a spreading ridge. At Galápagos there is a triple junction of the Nazca and Cocos plates with the Pacific Plate. The Galápagos Rift is also an extremely fast spreading ridge, and is currently north of the archipelago. Volcanism has been continuous for the last 20 Ma, and consists almost entirely of basaltic lavas and pyroclastics.

Geochemical studies of Galápagos basalts suggest the plume has a depleted N-MORB-like component (White et al., 1993). For this reason Galápagos has been excluded from some OIB data compilations (Fitton, 2007). Harpp and White (2001b) proposed four isotopically distinct end-members, three geographically restricted plume components and DMM.

Both samples analysed in this work were dredged from the north west of the island cluster, PL02 30-1 (tholeiite) from between Darwin island and Wolf island (01°16.3′S 91°46.9′W) and PL02 25-1 (alkali basalt) from the NW coast of Fernandina (01°35.5′N 91°55.6′W) (Harpp and White, 2001a).

The samples in this work have also been previously studied by Yi and co-workers (2000) for Cd, In, Sn, Te, and S and by Harpp and White (2001b) for Sr, Nd, Pb, and He isotopic data. These samples have also been studied for Mo isotopes (Liang et al., 2017).

Azores

The Azores are a chain of 9 major volcanic islands, some of which are still active. They are all volcanic in origin, with the plateau dated at ~20 Ma, and the archipelago itself volcanically active from 7 Ma to present (Silveira et al., 2006). The islands spread over 600 km of the central Atlantic, off the coast of Portugal.

The Azores form from a hot spot on the Mid Atlantic Ridge (MAR), like Iceland. The volcano on Pico achieves the highest elevation on the MAR. In contrast to Iceland, the Azores are part of a triple junction between the North American, European (Eurasian), and African (Nubian) plate.

The rocks of the Azores plateau are dominantly alkali basalts and differentiation products of alkali basalts (White et al., 1979), contrasting with the thoeliite dominated MAR.

The three samples examined here each come from a different island, two from the central group (Pico, Fayal) and one from the western group (Flores). All of the lavas are <10 Ma in age, and are petrographically relatively fresh (Halliday et al., 1995).

The samples studied in this work have been studied by Halliday and co-workers (1992; 1995; Yi et al., 1995a). These samples have also been studied more recently for Mo isotopes (Liang et al., 2017).

4.2.3. Cameroon Line

The Cameroon Line is a 1600 km long linear series of volcanoes and volcanic islands (Tertiary to Recent), which consists of volcanoes in Nigeria, Cameroon, Equatorial Guinea, and São Tomé and Príncipe. Four volcanic islands make up the oceanic section of the Line: Pagalú (formerly known as Annobon), São Tomé, Príncipe, and Bioko (formerly known as Fernando Pó). There are four main volcanic centres in Cameroon; Mount Cameroon, Manengouba, Bambouto, and Oku. There are also 2 extensive lava plateaux: Biu Plataeu in Nigeria; and Ngaoundéré Plateau in Cameroon.

The Cameroon Line has disputed origins with theories including a mega-shear zone, a continental rift, membrane tectonics (Freeth, 1979), and rifting associated with a hotspot (Morgan, 1983). The Cameroon Line is a unique geological situation, as it is the only known intra-plate alkaline volcanic province to transect the oceanic to continental boundary (Fitton, 1987). The chemical compositions of comparable basalts in both continental and oceanic sectors are similar to almost indistinguishable (Fitton, 1987; Fitton and Dunlop, 1985). Halliday and co-workers (1990), identified high $^{206}Pb/^{204}Pb$ ratios in lavas from the continent-ocean-boundary of the Cameroon Line characteristic of the HIMU mantle endmember, suggesting a fossil mantle plume with diminishing lateral effects. Fitton and Dunlop (1985) suggested explanation involving a laterally displaced (by movement of the African plate) region of volcanism

previously related to upwelling under the Benue Trough. The volcanism does not progress in a correlation with age, suggesting there is no migrating hotspot.

The Cameroon Line produces principally alkali volcanic rocks including transitional basalts, nephelinites, phonolites, and alkali rhyolites. Phonolites are the dominant evolved rock type in the oceanic sector, with increasing continental crustal contamination and crystal fractionation producing the alkali rhyolites as the dominant evolved rock type in the continental sector (Fitton, 1987). The volcano Etinde produces entirely nephelinites unlike the other volcanic centres in the Cameroon Line where mafic lavas always range from basanite to hy-normative basalts (D. Lee et al., 1996).

The Cameroon Line mafic samples analysed in this study come from numerous volcanic centres, selected to range across the oceanic sector and the continental. The island of Príncipe (P18) samples the oceanic sector, and the ocean-continental boundary is sampled by sites from the island Bioko (FP44), and volcanoes on the mainland: Etinde (C20, C22, C134, C150, C151, C152), and Mount Cameroon (C30, 192). The continental sector includes samples from the most northerly site in this study, Mandara Mountains (C146), as well as two sites NW of Mount Cameroon: Manengouba (C51, C65, C72), and Bambouto (C112).

Dating of the Cameroon Line volcanism by Ar-Ar dating has proved problematic due to excess Ar in feldspathoids (Lee, 1994). Mount Cameroon is a composite volcano that has erupted a range of basalts (over the last 10 Ma) from alkali basalts to basanites (Lee, 1994). The volcano at Manengouba has erupted a complete compositional continuum over the last 1.5 Ma (including ne- normative basalts, hy- normative basalts, trachyte, and rare rhyolite) (Lee, 1994). Bambouto is a large dissected volcanic centre, with a bimodal basalt-trachyte suite of erupted lavas dating from 43 to 1 Ma (Lee, 1994). The volcanism range from Bambouto has been suggested to be linked to a crustal contamination contribution to the evolved rocks (Lee, 1994). The Mandara Mountains are made of granite and gneiss covered in 33-20 Ma alkali basalt lava flows (Lee, 1994).

The samples in this work have also been studied extensively by Halliday and coworkers (1995, 1990, 1988). These samples have also been studied more recently for Mo isotopes (Liang et al., 2017)

4.2.4. Other mafic samples

Two further samples were analysed from Tanzania to add other samples formed by low degree partial melting to complement the nephelinite samples from the Cameroon Line. They are both foidites, with one having olivine and melilite as major phases. These were analysed to test whether nephelinite lithologies had uniform Ni isotopic compositions from different localities. These samples were H93-3 from Kwaraha, a mountain of volcanic origin about 120 km SW of Monduli (Paslick et al., 1995) and BD105 from Oldoinyo, Loolmurwak, 60 miles NW of Lashaine (Dawson, 1964a).

4.3. Sample preparation

The Atlantic OIB and African continental samples used in this study were either provided by Godfrey Fitton, Edinburgh University, or collected during fieldwork by teams including Alex Halliday and Cassi Paslick. These, along with the submarine basaltic glass samples from Galápagos and Loihi were originally chosen for the study of Yi et al (2000).

Samples were dominantly archived powders, with the exception of the MORB samples, which were glass chips. The glass chips were optically examined to be clean of surface alteration. To check that archive powders had not been contaminated during crushing, fresh chips from the Etinde nephelinite samples were obtained from Godfrey Fitton. The nephelinites have the lowest [Ni] of all the studied samples and would have been the most vulnerable to possible Ni contamination during preparation of the archived powders. The fresh chips had weathered surfaces removed, before hand crushing in agate and compared with data for powders (see section 4.4.1).

Details of purification and analysis are described in Chapter 2, a short summary is provided here. Acids used were distilled in house by sub-boiling and diluted by volume with ultrapure 18MΩ MQ water. Samples were accurately weighed into Teflon vials and dissolved using 1 part HF and 3 parts HNO3 (2 ml total) followed by dissolution in 6M HCl (up to 5 ml), usually by hotplate dissolution. The double spike was applied before dissolution in a ratio of 2.5 part double spike Ni to 1 part sample Ni, unless the sample required determination of Ni concentrations by ICP-MS, to allow accurate spiking. Samples with lower Ni concentrations required larger volumes of acid to dissolve and to load onto the first column, and sometimes were split across multiple columns. Purification of Ni is completed by three ion exchange Teflon microcloumns of diminishing size with a method adapted from (Gall et al., 2012). Analysis was performed in pseudo-high resolution on a Nu Plasma HR MC-ICPMS.

4.4. Results

Results are presented in Table 4-1, and plotted in Figure 17. The average $\delta^{60/58}Ni_{SRM986}$ for the mafic samples analysed in this study is 0.07±0.17‰ (2SD, n=41). Despite the spread in each case, the average for ocean island basalts (OIB) is 0.05±0.25‰ (2SD, n=12), is identical to the mean of mid ocean ridge basalts (MORB) of 0.06±0.17‰ (2SD, n=12). Both in turn are identical to the average of 0.08±0.05‰ (2SD, n=15) for the Cameroon Line, which despite the range in lithologies has limited variation in Ni isotopic composition. These identical averages for basaltic rocks are offset to lighter $\delta^{60/58}Ni_{SRM986}$ values relative to the mean for unmetasomatised mantle peridotite of 0.20±0.08‰, discussed in Chapter 3.

Table 4-1

Nickel concentration and isotopic composition for mafic samples analysed in this study

Nickel concentrations from isotope dilution, and n is the number of separate analyses of the sample (>3 means the sample was analysed more than once from separate chemistries). The MAR samples are sometimes referred to in the literature with AIII127 DR as prefix. Lithological designations from (Alex N. Halliday et al., 1992a; Halliday et al., 1990; Hardarson and Fitton, 1997; Harpp and White, 2001b; Kempton et al., 2000; Niu and Batiza, 1997; Yi et al., 1995b) as well as Fitton (pers. comm.) and Halliday (pers. comm.). External reproducibility in Ni isotopic composition is 0.06‰.

	Sample Code	Lithology	Locality	Ni (ppm)	$\delta^{60/58}$Ni	2sd	n
Ocean Island Basalts	AZF3	Transitional basalt	Flores, Azores	374.3	-0.035	0.023	4
	AZP6	Alkali basalt	Pico, Azores	47.94	-0.160	0.001	2
	AZFY2	Alkali basalt	Fayal, Azores	167.4	-0.111	0.065	3
	PL02 25-1	Alkali basalt	Galápagos	77.55	-0.030	0.018	7
	PL02 30-1	Tholeiite	Galápagos	118.4	0.008	0.066	2
	D4-6G	Alkali basalt	Loihi, seamount nr Hawaii	238.5	0.170	0.000	7
	ST38	Tholeiite	N, Iceland	86.00	0.189	0.055	4
	GS18	Tholeiite	N, Iceland	57.00	0.217	0.016	4
	CX11	Tholeiite	E, Iceland	49.48	0.231	0.028	4
	CX19	Tholeiite	E, Iceland	76.73	0.106	0.019	2
	SNB19	Tholeiite	W, Iceland	197.3	0.012	0.034	2
	SNB40	Tholeiite	W, Iceland	167.9	0.033	0.034	4
Mid Ocean Ridge Basalts	R82-1	N type MORB	East Pacific Ridge	125.0	0.192	0.000	4
	R94-2	N type MORB	East Pacific Ridge	43.62	0.193	0.051	4
	R93-7	E type MORB	East Pacific Ridge	121.1	0.045	0.029	2
	A127 D5-5	N type MORB	Mid Atlantic Ridge	156.6	0.151	0.011	2
	A127 D8-2	N type MORB	Mid Atlantic Ridge	138.5	0.056	0.006	3
	A127 D10-2A	MORB	Mid Atlantic Ridge	81.20	0.123	0.028	3
	A127 D15-1	E type MORB	Mid Atlantic Ridge	61.46	0.028	0.000	2
	A127 D17-3	E type MORB	Mid Atlantic Ridge	90.86	-0.041	0.028	4
	A127 D21-3	E type MORB	Mid Atlantic Ridge	54.48	-0.017	0.037	4
	A127 D22-5	E type MORB	Mid Atlantic Ridge	38.07	0.021	0.008	2
	A127 D26-5	E type MORB	Mid Atlantic Ridge	84.67	-0.023	0.073	3
	A127 D27-5	E type MORB	Mid Atlantic Ridge	116.5	-0.038	0.018	2

Cameroon Line	P18	Olivine nephelinite	Príncipe, Island in Cameroon Line	184.1	0.030	0.070	3
	C134	Mafic nephelinite	Etinde, Cameroon	42.67	0.117	0.049	3
	C151	Mafic nephelinite	Etinde, Cameroon	92.16	0.063	0.033	5
	C22	Nephelinite	Etinde, Cameroon	12.58	0.075	0.036	6
	C20	Nephelinite	Etinde, Cameroon	12.17	0.069	0.043	4
	C152	Hauyne nephelinite	Etinde, Cameroon	7.76	0.105	0.072	5
	C150	Olivine melanephelinite	Etinde, Cameroon	43.04	0.069	0.080	6
	C65	Hy-normative basalt	Manengouba, Cameroon	228.2	0.060	0.044	3
	C192	Basanite	Mt Cameroon, Cameroon	52.88	0.066	0.000	3
	C30	Basanite	Mt Cameroon, Cameroon	213.8	0.113	0.006	3
	C112	Basanite	Bambouto, Cameroon	133.9	0.098	0.022	3
	C51	Alkali basalt	Manengouba, Cameroon	158.4	0.063	0.032	4
	C72	Alkali basalt	Manengouba, Cameroon	150.8	0.073	0.066	2
	C146	Alkali basalt	Mandara Mts, Cameroon	150.3	0.017	0.000	4
	FP44	Alkali basalt	Bioko, Island in Cameroon Line	75.02	0.101	0.044	3
Continent Volcanis	H93-3	Foidite	Kwaraha, N Tanzania	149.2	0.156	0.049	3
	BD105	Olivine-melilite nephelinite	Oldoinyo, Loolmurwak, Tanzania	359.3	0.127	0.055	3

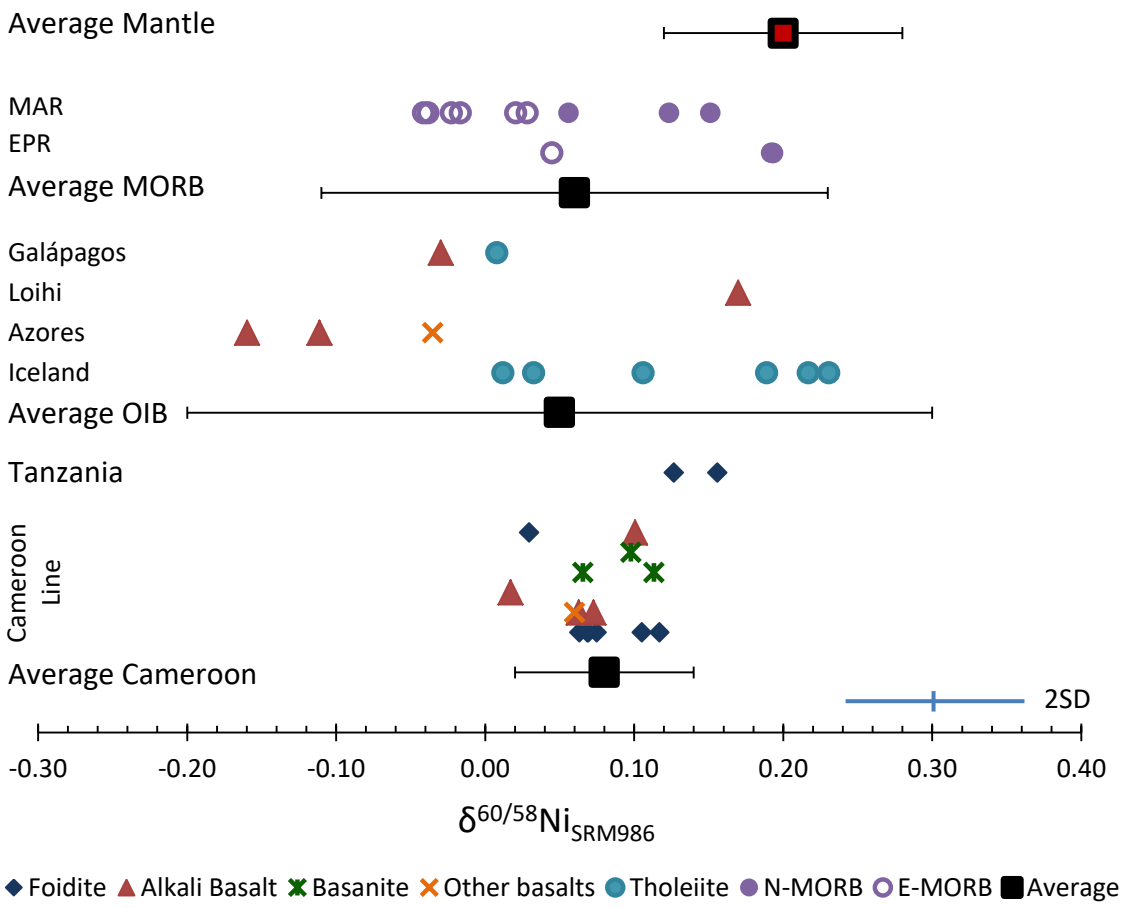

Figure 17

Nickel isotopic compositions for MORB, OIB, Tanzania, and Cameroon Line samples, separated by geographical locality and lithology, relative to the average for unmetasomatised peridotite $\delta^{60/58}Ni_{SRM986}$=0.20±0.08‰ (representative of BSE). The Cameroon Line includes different volcanic centres, separated on the y-axis: Islands, Bambouto, Mt Cameroon, Mandaras Mountains, Manengouba, and EtideExternal reproducibility (2SD) in Ni isotopic composition is 0.06‰.

4.4.1. Comparison between sample processing methods

Before discussing whole rock Ni isotopic compositions analysed in this work, it is necessary to test the validity of results from archive powders, relative to those from fresh preparations. The nephelinite samples from Etinde volcano in Cameroon had extremely low Ni concentrations, which were likely to make any perturbation in Ni isotopic composition by the processing method significant and easily observable in the results. Therefore, part of the Cameroon Line project was looking to test for any difference in the Ni isotopic composition, or Ni concentration, between the original rock powders prepared by Prof G. Fitton in the 1970s and

1980s, and duplicates prepared from original hand specimens to current geochemistry standards. Samples were stored in MQ washed glass bottles until ready for weighing and dissolution, as described in Chapter 2 (section 1.2.2).

Results are presented in Table 4-2. All but one sample had Ni isotopic composition within error in both preparations, with external reproducibility of 0.06‰. The Ni concentration (calculated from isotope dilution) was always fractionally greater in the new preparation, suggesting no Ni was added during the original preparation. This suggests that it is highly unlikely that any perturbation of the Ni was introduced through old preparation methods, and that use of archive powders for investigation of Ni isotopes is effective.

Table 4-2

Comparison between Ni isotopic composition analysed in this study for nephelinites from Etinde, Cameroon prepared from archive powders or fresh preparation

Nickel concentrations from isotope dilution, and n is the number of separate analyses of the sample (>3 means the sample was analysed more than once from separate chemistries). External reproducibility for Ni isotopic composition is 0.06‰.

		ORIGINAL POWDER				NEW PREPARATION			
Sample Code	**Lithology**	**Ni (ppm)**	**$\delta^{60/58}$Ni**	**2sd**	**n**	**Ni (ppm)**	**$\delta^{60/58}$Ni**	**2sd**	**n**
C20	Nephelinite	11.8	**0.080**		1	12.6	**0.066**	0.047	3
C22	Nephelinite	9.95	**0.077**	0.030	3	13.17	**0.073**	0.040	3
C150	Olivine melanephelinite	41.7	**0.038**	0.069	3	44.4	**0.100**	0.019	3
C151	Mafic nephelinite	91.8	**0.054**	0.030	3	92.5	**0.078**	0.006	2
C152	Hauyne nephelinite	7.2	**0.145**	0.048	2	8.37	**0.078**	0.008	3

4.4.2. Localities

Mid Ocean Ridge Basalts

The 12 Mid Ocean Ridge Basalt (MORB) samples include nine from part of the Mid Atlantic Ridge (MAR), and three from the East Pacific Rise (EPR) ridge. The samples can be divided based on incompatible trace element ratios (e.g. Gale et al., 2013) into N-MORB (normal, $La/Sm_n < 1$) and E-MORB (enriched, $La/Sm_n > 1$).

The MAR samples average $\delta^{60/58}Ni_{SRM986}$=0.03±0.13‰ (n=9), whereas the EPR samples average 0.14±0.14‰ (n=3). The N-type MORB are heavier (0.15±0.11‰, n=4) than the E-type MORB (-0.00±0.06‰, n=7). Both N-MORB and E-MORB lithologies are found in both ridges analysed in this work. One sample (A127 D10-2A) lacks published La and Sm data, but based on the Ni isotopic composition it would be expected to be N-MORB.

Ocean Island Basalts

The Azores samples average $\delta^{60/58}Ni_{SRM986}$=-0.10±0.10‰ (n=3), which is the most negative mafic sample set composition. The lightest sample (-0.16‰), AZP6, is an alkali basalt, from the most south-easterly island sampled Pico. The heaviest is AZF3, a transitional basalt, from the most westerly island Flores (-0.04‰). Sample AZFY2 (alkali basalt, from Fayal) falls in the middle at (-0.11‰).

The two samples from the Galápagos average $\delta^{60/58}Ni_{SRM986}$=-0.01±0.04‰, making this locality the second lightest on average for the OIBs. Both samples were dredged from the north west of the island cluster.

The single sample from Loihi (D4-6) has a Ni isotopic composition $\delta^{60/58}Ni_{SRM986}$=0.17‰. It is an alkali basalt that was sampled as a quench glass.

The six Iceland samples average $\delta^{60/58}Ni_{SRM986}$=0.13±0.17‰. Two of the samples are from Snaefellsnes and these have the lightest Ni isotopic compositions (SNB19 0.01‰; SNB40 0.03‰). The other four samples average 0.19±0.10‰ and are from North and East Iceland.

Cameroon Line

The Cameroon Line samples are very similar to each other ranging from $\delta^{60/58}Ni_{SRM986}$=0.02‰ (C146, Mandara Mountains, alkali basalt), to 0.12‰ (C134, Etinde, mafic nephelinite). The overall average is 0.08±0.05‰ (n=15). There is no resolvable difference between oceanic and continental sectors.

In addition, there is no resolvable difference between alkali basalts (0.06±0.06‰, n=4), hy-normative basalt (0.06‰, n=1), nephelinites (0.08‰±0.05, n=7) and basanites (0.09±0.04‰, n=3).

Continental Rift Setting

The two samples analysed from Tanzania have Ni isotopic compositions identical within error (H93-3 0.16‰, BD105 0.13‰). These are heavier than the nephelinite samples of the Cameroon Line.

4.5. Discussion

4.5.1. Nickel isotopes and geological setting

The OIB dataset analysed in this study ($\delta^{60/58}Ni_{SRM986}$=0.05±0.25‰ (n=12)) shows an indistinguishable average Ni isotopic composition to the MORB dataset ($\delta^{60/58}Ni_{SRM986}$=0.06±0.17‰ (n=12)). Therefore, OIB and MORB both have Ni isotopic compositions on average lighter than BSE estimates, and within error of each other. This suggests that Ni isotopic composition of a mafic sample is not affected by the geological setting, and is invariant to the process that causes the production of mafic igneous rocks at the Earth's surface. However, the radiogenic compositions of these lithologies are from a relatively restricted range, for example Nd isotopic compositions ranging from $\epsilon^{143}Nd$ =2.3 (H93-3) to 10.0 (A127 D26-5).

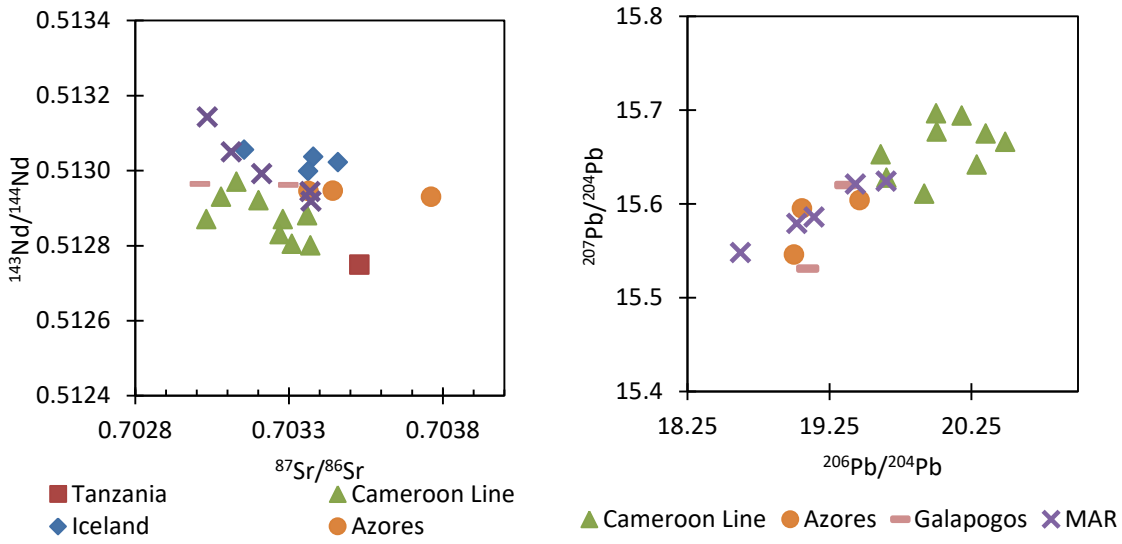

Figure 18

Available radiogenic isotopic compositions for mafic samples analysed for Ni isotopic composition in this work. Data from (Dosso et al., 1999; Alex N. Halliday et al., 1992b; Halliday et al., 1990; Hardarson and Fitton, 1997; Harpp and White, 2001b; Paslick et al., 1996) and Halliday (pers. comm.).

It is noteworthy that the MORB compositions between comparable lithologies (N-MORB vs E-MORB) have relatively invariant compositions between geographically separate spreading ridges. This is also suggested by the continuum created with data from both two ridges seen in Figure 26. Different spreading rates and proximity to other geological features that can complicate geochemistry of basalts from a particular ridge also do not appear to influence bulk rock Ni isotopic composition.

There is also heterogeneity in OIBs from different geographical settings, with averages for the different OIBs ranging from -0.10‰ (Azores, n=3) to 0.17‰ (Loihi, n=1). The Iceland samples (n=6) show the largest variation between different samples from the same hotspot, with samples ranging from 0.01 to 0.23‰, a range that extends nearly two thirds of the range seen in all OIB samples. This again supports that heterogeneity in OIB samples is not controlled by factors relating to geographical location, such as proximity to a ridge. Molybdenum isotopic composition has been similarly shown to be equally variable within and between OIBs (Liang et al., 2017).

4.5.2. Nickel isotopes and partial melting

The study of the Cameroon Line facilitates investigation of Ni isotopic compositions from a range of basalts from the same volcanic system, which reflect different degrees of partial melting. There is thought to be no source variation because the radiogenic isotope systems show limited variation (eg ϵ^{143}Nd ranges from 3.32 to 5.85).

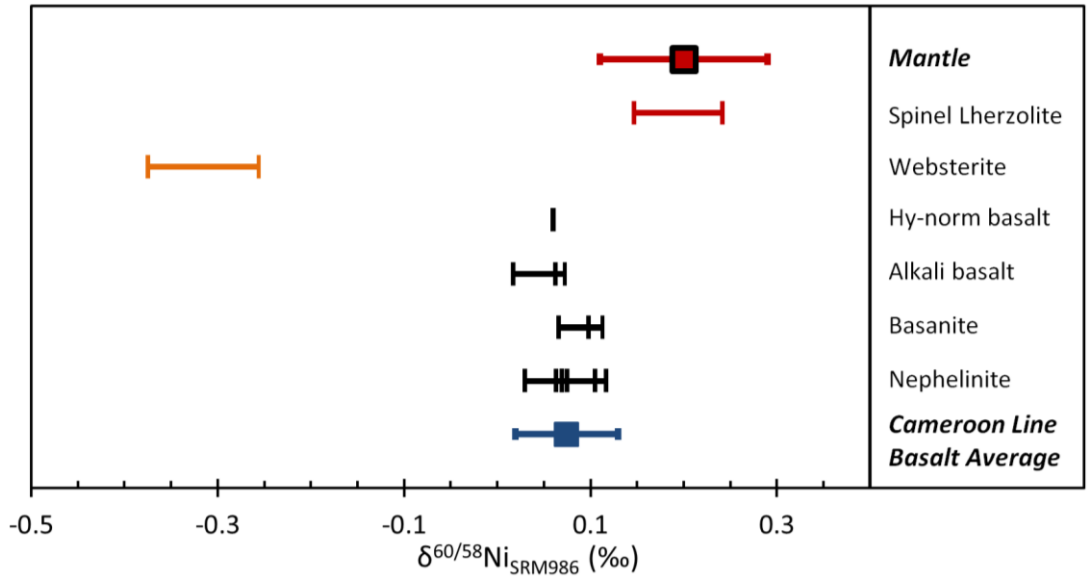

Figure 19

Nickel isotopic compositions for bulk ultramafic and mafic rocks from the Cameroon Line compared to the average for unmetasomatised fertile peridotite $\delta^{60/58}Ni_{SRM986}$=0.20±0.08‰ (representative of the BSE or 'normal mantle'). The mafic rocks cover a range of degrees of partial melting and show no variation in Ni isotopic composition throughout the range, highlighting that Ni isotopic compositions do not fractionate with degree of melting. The error on the average for the mafic rocks from this volcanic system is less than that of the external reproducibility in Ni isotopic composition (0.06‰).

Nephelinites have a very low degree of partial melting, hence the low Ni concentration in these rocks. Alkali basalts and hypersthene normative basalts have larger degrees of partial melting, and basanites are formed by an intermediate degree of partial melting. The averages for the hy-normative basalt ($\delta^{60/58}Ni_{SRM986}$=0.06‰), alkali basalts (0.06‰), basanites (0.09‰) and nephelinites (0.08‰) are identical and span half the long-term reproducibility of this work. All the samples are within error of each other and average 0.08±0.06‰ (n=15). Therefore, it is evident that Ni isotopic compositions do not fractionate with degree of melting.

Incompatible trace element ratios have also been used as an indicator of partial melting. Lanthanum is more incompatible than Nd therefore the ratio of these elements fractionates with

partial melting. Figure 20 shows Ni composition relative to La/Nd, for the Cameroon Line as an example of a single volcanic system. Figure 21 shows the entire mafic Ni isotope dataset, for which there is La and Nd data. No correlation is seen, in either case, indicating a lack in partial melting control on Ni isotopic composition.

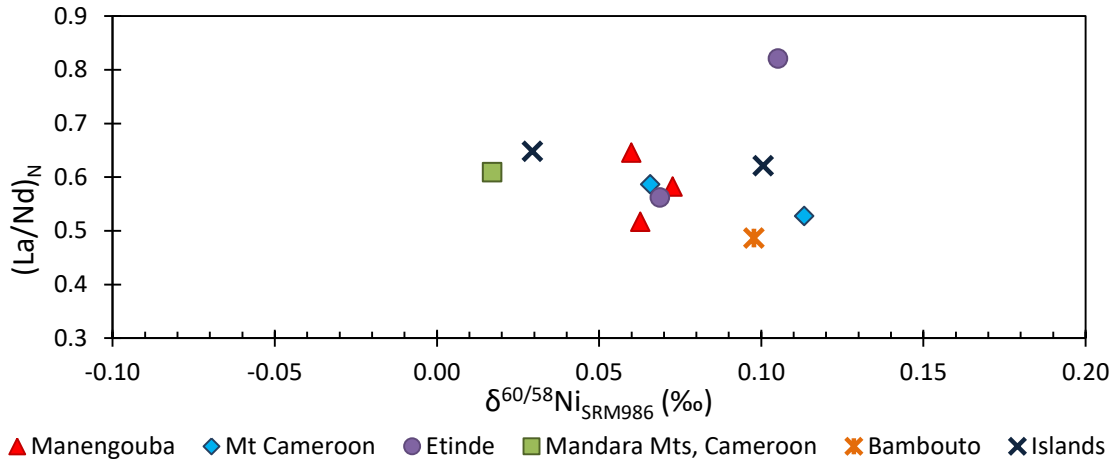

Figure 20

Nickel isotopic composition for bulk mafic rocks from the Cameroon Line, by geographical locality, vs chondrite normalised ratio of La (LREE) to Nd (MREE) as analysed by J. G. Fitton (pers comm). Not all samples for which Ni isotopes have been analysed have trace element data, hence some samples are missing from the above plot. Low degree melts have LREE enrichment, and if there was a partial melting control on Ni isotopic composition some correlation would be expected. No correlation is seen in the dataset. External reproducibility in Ni isotopic composition is 0.06‰.

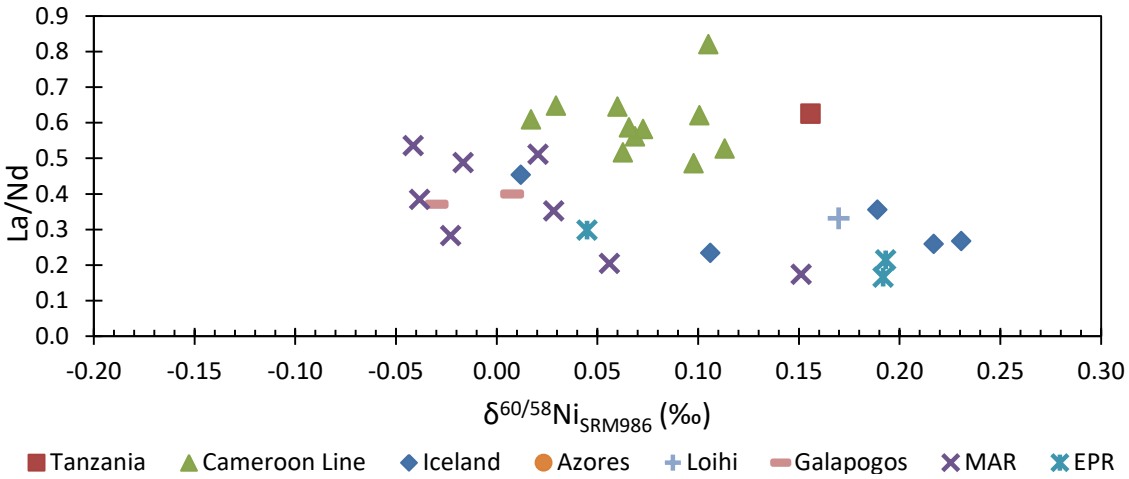

Figure 21

Nickel isotopic composition for mafic samples against La/Nd (incompatible elemental ratio). Data for La and Nd from (Halliday et al., 1995, 1990; Hardarson and Fitton, 1997; Kempton et al., 2000; Niu and Batiza, 1997; Paslick et al., 1995; Yi et al., 2000) and Halliday (pers. comm) and Fitton (pers. comm.) Ni concentration analysed by isotope dilution. Some samples with Ni isotopic composition but no La and/or Nd data are excluded. No single correlation is observable. The external reproducibility on the Ni isotopic compositions is 0.06‰.

4.5.3. Nickel isotopes and fractional crystallisation

The major element MgO (plotted in Figure 22 for the Cameroon Line), shows correlations with Ni concentration, within separate volcanic systems. This is interpreted as magmatic differentiation due to olivine fractionation, which is a major host of Ni and MgO in basalts and the mantle. However, MgO shows no correlation with Ni isotopic compositions (Figure 23, left), within a single volcanic system. Nickel concentration also shows no correlation with Ni isotopic composition within the volcanic systems analysed (Figure 23, right). This suggests that Ni isotopes do not fractionate with basalt differentiation.

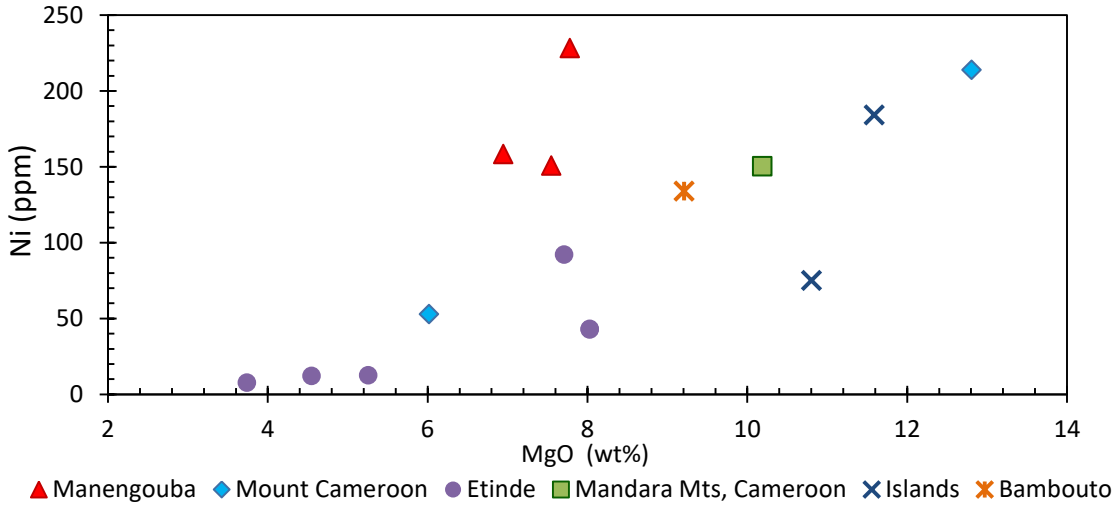

Figure 22

Nickel concentration as analysed by isotope dilution vs MgO content as analysed by J. G. Fitton (pers comm). Individual correlations are seen within samples from the same volcanic system, showing that the samples are showing magmatic differentiation. External reproducibility in Ni isotopic composition is 0.06‰.

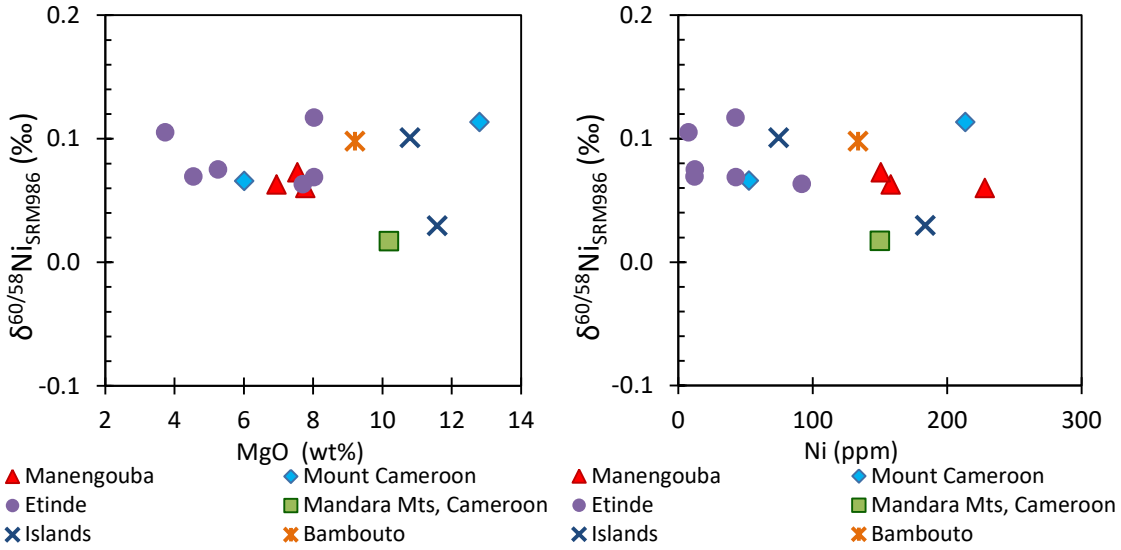

Figure 23

Left: Nickel isotopic composition for bulk mafic rocks from the Cameroon Line vs MgO as analysed by J. G. Fitton (pers comm); Right: Ni isotopic composition vs Ni concentration as analysed by isotope dilution. No correlation is seen with Ni isotopic composition and either indicator, even within any single volcanic system. External reproducibility in Ni isotopic composition is 0.06‰.

The Ni isotope composition of the entire suite of mafic samples shows no relationship with, for example, Ni/Cr as a compatible trace element ratio (Figure 24). Compatible trace element ratios also reflect crystal fractionation, in the case of Ni/Cr the Ni in olivine, and Cr in clinopyroxene. The lack of correlation with Ni/Cr therefore is further evidence that fractional crystallisation does not influence the Ni isotopic composition. This is also consistent with the lack of significant isotopic fractionation between the main Ni bearing mineral phases in ultramafic rocks (Chapter 3), where the largest fractionation between mineral phases in a xenolith was consistently ~0.12‰.

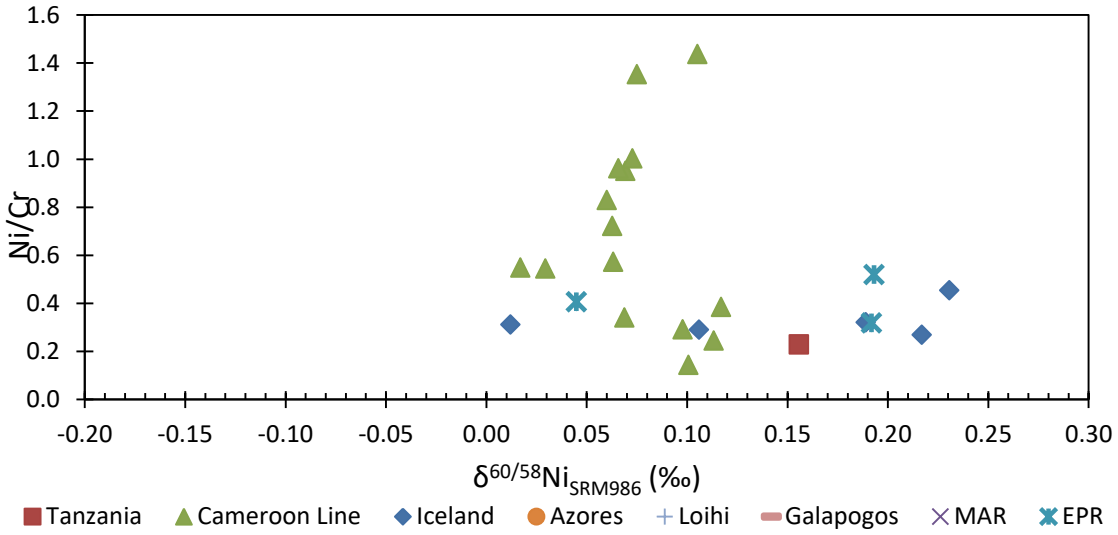

Figure 24

Nickel isotopic composition for mafic samples against Ni/Cr (compatible elemental ratio). No correlations are found in the data. Data for Cr from (Halliday et al., 1995, 1990; Hardarson and Fitton, 1997; Kempton et al., 2000; Niu and Batiza, 1997; Paslick et al., 1995; Yi et al., 2000), Halliday (pers. comm) and Fitton (pers. comm.) Ni concentration analysed by isotope dilution. Some samples with Ni isotopic composition but no Cr data are excluded. No single correlation is observable. The external reproducibility on the Ni isotopic compositions is 0.06 ‰.

Despite the lack of correlation between Ni isotopic composition and Ni concentration in both xenoliths, xenolith mineral separates, MORB, and Cameroon Line OIB, some other individual OIBs appear to show such correlations (Figure 25). A strong negative correlation exists in the Iceland dataset (three separate volcanic areas) with an r^2=0.863. The Azores sample set (3 different volcanic islands), in contrast, shows a strong positive correlation with r^2=0.999. The other OIBs have fewer than three analysed samples and cannot be compared.

The correlation in Ni concentration seen in Iceland and the Azores is not comparable in direction, as would be expected for fractional crystallisation, which affects Ni concentration by removal of Ni-rich olivine. Indeed, both Iceland and the Azores have positive correlations between Ni concentration and MgO (Figure 26, right), which is suggestive of fractional crystallisation. Figure 26 (left) shows the Ni isotopic composition has the same correlation with MgO that Figure 25 showed with Ni concentration.

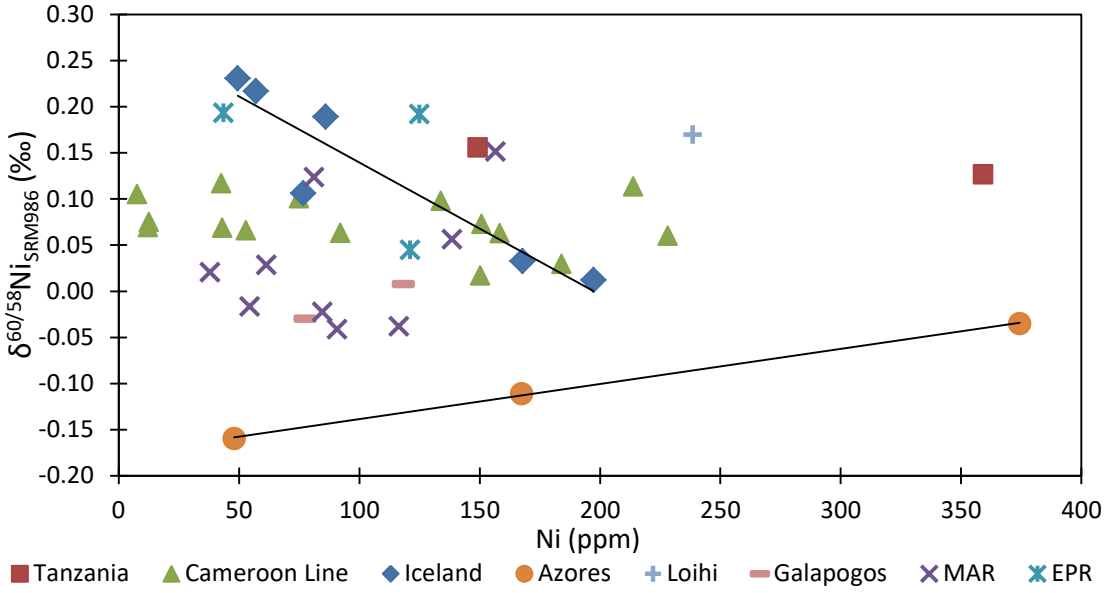

Figure 25

Nickel isotopic composition for bulk mafic whole rock samples against Ni concentration analysed by isotope dilution. Correlations appear to exist, with limited data, within individual OIB systems, but in contrasting directions. A strong negative correlation exists in the Iceland dataset with r^2=0.863. The Azores sample set, in contrast, shows a strong positive correlation with r^2=0.999. The other OIBs have fewer than 3 samples and cannot be compared. There are no relationships in MORB or Cameroon Line samples. The external reproducibility of the Ni isotopic composition is 0.06‰.

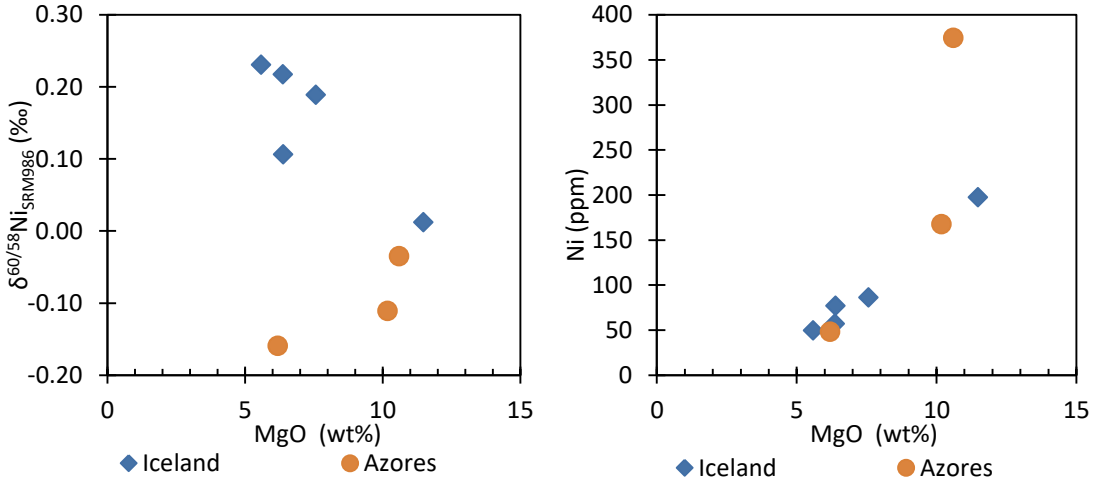

Figure 26

Left: Nickel isotopic compositions against MgO. The Azores data has a positive correlation r^2=0.980. The Iceland data has a negative correlation, with r^2=0.690. Right: Nickel concentrations against MgO for the Azores and Iceland. The Azores data has a positive correlation r^2=0.690. The Iceland data also has a positive correlation, although stronger, with r^2=0.980.

MgO data from (Hardarson and Fitton, 1997; Kempton et al., 2000) and Halliday (pers. comm.), Ni concentration from isotope dilution. External reproducibility on Ni isotopic composition is 0.06‰

The correlations in Ni concentration, in these 2 OIBs, which is unlikely to be related to fractional crystallisation, given that the samples are not from the same volcanic system, nor is the relationship comparable between these OIBs, and not present in other volcanic systems. The reason for this correlation has not yet been deduced .

4.5.4. Nickel isotopes and recycling signatures in mafic samples

In Chapter 3, the Ni isotopic composition of Kilbourne Hole mantle xenoliths showed a broad positive correlation with Nd isotopic composition, suggesting that light Ni isotopic compositions are associated with less radiogenic Nd isotopic compositions, and therefore mantle enrichment by recycled material (e.g. Haase et al., 2011). As Ni isotopic compositions in mafic samples are heterogeneous but also unaffected by partial melting and fractional crystallisation, it may be that a recycling signature is being preserved in these samples.

There is limited Nd isotopic data on any single volcanic system analysed for $\delta^{60/58}Ni_{SRM986}$ in this work, to compare with the Kilbourne Hole data. Neodymium isotopic ratios have been analysed on only 5 of the MAR samples, all of which were E-type tholeiites ($(La/Sm)_N$=1.06 to 2.94). Shown in Figure 27, there is a very weak positive correlation (r^2=0.33), which may be supportive of a similar relationship between Ni isotopic composition and Nd isotopic composition as observed in Chapter 3, although the Ni isotopic compositions of these samples are all within the error of external reproducibility. Figure 27 also shows no trends within any of the other volcanic systems with Nd isotopic composition, although the range in Nd observed in these samples is very limited, especially compared to the range of 25 epsilon units in the Kilbourne Hole xenoliths. It may be suggested that the Cameroon Line exhibits a very weak negative trend (r^2=0.26), however, as with the MAR, all Ni isotopic compositions are within error, as well as the range in Nd being very small.

Neodymium isotopic compositions are complicated by processes that affect the parent daughter ratio, as well as the length of time since the enriched material was introduced to the mantle source regions. This time period and the parent daughter ratio are both generally different between localities, making it likely that any relationship with Ni isotopic composition and Nd

isotopic composition would be relatively site specific. The same is true for other radiogenic systems, which have been used to argue for endmember domains in the mantle of different radiogenic compositions. The samples in this work all have $\epsilon^{143}Nd$ >2.3, showing that all the mafic samples are more radiogenic in Nd than CHUR ($^{143}Nd/^{144}Nd_{CHUR}$=0.512630 (Bouvier et al., 2008)).

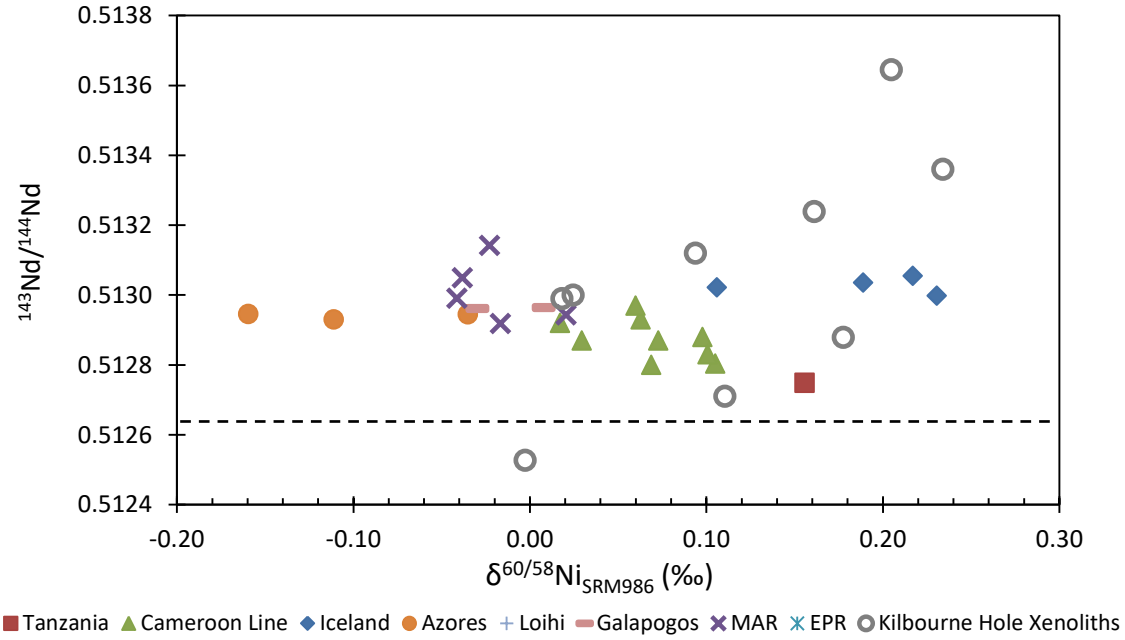

Figure 27

Bulk rock mafic Ni isotopic compositions plotted relative to Nd isotopic ratios for the same samples. Nd data from (A. N. Halliday et al., 1992; Halliday et al., 1990; Hardarson and Fitton, 1997; Harpp and White, 2001b; Paslick et al., 1996) and Halliday (pers. comm.). No Nd isotopic compositions exist for some MORB, Loihi, one Tanzanian sample, two Iceland samples, and some Cameroon Line samples; hence, these samples are excluded from this plot. Plotted for comparison are the data for Kilbourne Hole xenoliths, grey circles, described in Chapter 3. CHUR shown as dashed line at 0.512630. External reproducibility in Ni isotopic composition is 0.06‰.

This work has suggested that only source composition affects resulting Ni isotopic compositions, which is in turn controlled by the presence and distribution of recycled components in the mantle. This allows a signature from enriched recycled material to be observable in the Ni isotopic composition of rocks mantle and mantle derived rocks, no matter how recently the event took place.

The Nd isotopic evidence for light Ni isotopic compositions with enriched lithologies is supported directly by the average Ni isotopic composition for E-MORB samples from both sampled ridges being resolvably lighter than the average of N-MORB. Figure 28 shows that the

Ni isotopic composition of E-MORB and N-MORB (as defined by chondrite normalised La/Sm) is a continuum, as the negative correlation shows. A similar continuum in Ni isotopic composition with an indicator of enrichment was also seen in (Chapter 3) in the xenoliths of Kilbourne Hole (with Nd isotopic ratios, plotted in grey on Figure 27).

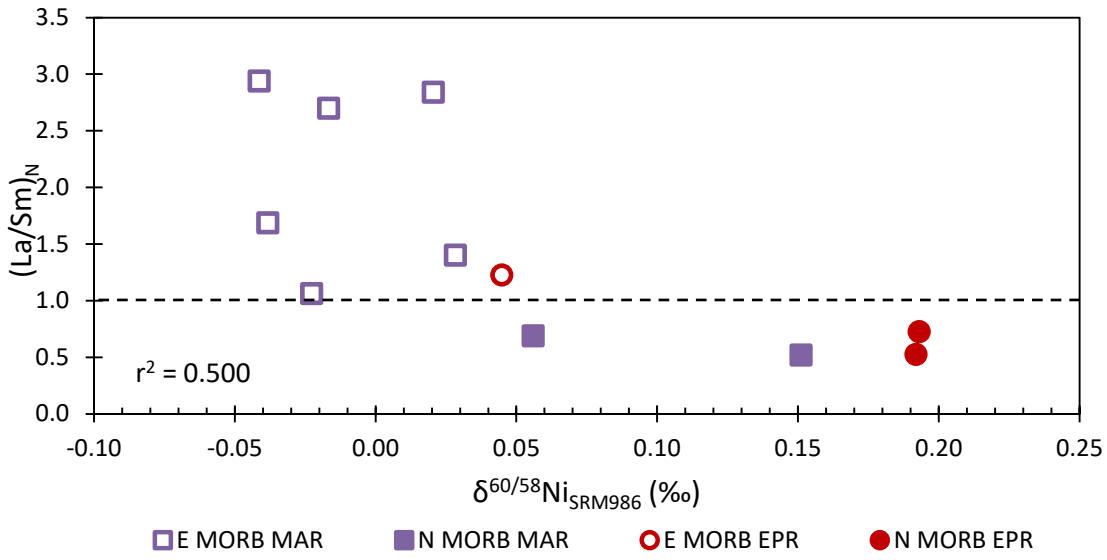

Figure 28

Nickel isotopic composition for MORB against chondrite normalised La/Sm, showing a negative correlation with r^2=0.500 on the entire dataset. Mid Atlantic Ridge alone has r^2=0.393, and EPR r^2=0.920 if taken separately. Circles indicate the East Pacific Rise, and squares indicate the Mid Atlantic Ridge, with E-MORB shown by open symbols and N-MORB by solid symbols. Data for La and Sm from Yi and co-workers (2000) and Niu and Batiza (1997). One sample with Ni isotopic composition but no La and Sm data is excluded. The external reproducibility on the Ni isotopic compositions is 0.06‰.

A subduction component in E-MORB has been specifically proposed for these EPR samples (Niu and Batiza, 1997) to explain trace element concentrations. As previously stated, light Ni isotopic compositions have been observed in all analysed E-MORB samples. This further supports the conclusion of Chapter 3, that light Ni isotopic compositions are produced in the mantle during subduction. It also supports that these light Ni isotopic compositions are preserved as heterogeneous mantle domains. These lighter domains may be transported by physical mixing on long timescales with the Ni isotopic composition unaltered by time, mantle melting and differentiation and then entrained with the upper mantle under mid-ocean ridges.

As can be seen in Figure 19, Cameroon Line basalts (average $\delta^{60/58}Ni_{SRM986}$=0.08±0.06‰, n=15) are approximately 0.12‰ lighter than the composition of average mantle (0.20±0.09‰, n=19)

and the average of spinel lherzolites from the same volcanic system (0.19±0.10‰, n=2). The average $\delta^{60/58}Ni_{SRM986}$ of the Cameroon Line basalts is identical within error to the averages for MORB (0.06±0.17‰) and OIB (0.05±0.25‰) (see section 4.5.1) although the MORB and other OIB show significantly wider ranges in $\delta^{60/58}Ni_{SRM986}$. Most, but not all of the mafic lavas analysed in this study are lighter than the average Ni isotopic composition for unmetasomatised fertile peridotite (assumed in this work to be equivalent to the average upper mantle) suggesting that melting involves components other than unmetasomatised peridotite. A small amount of mixing of a Ni isotopic composition as light as the Cameroon Line websterites (Figure 29) would produce partial melts lighter than average mantle. A mass balance calculation shows that between 23-29% of websterite (average composition -0.32‰) is required to achieve the average basalt $\delta^{60/58}Ni_{SRM986}$=0.08‰, when mixed with a bulk upper mantle of 0.20‰.

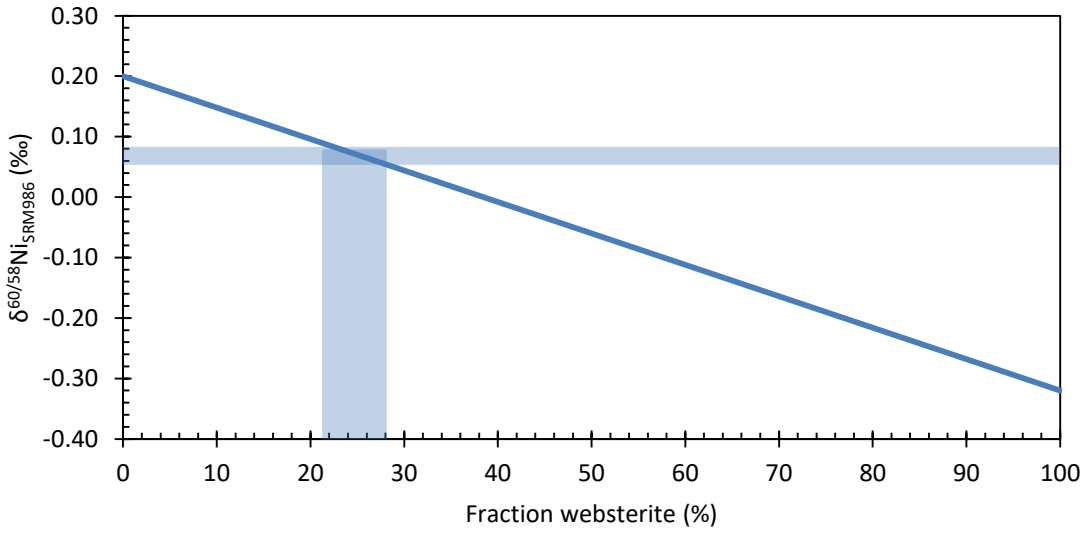

Figure 29

Nickel isotopic composition of a mixed mantle with changing fraction of websterite component (-0.32‰), representing the extreme light Ni isotopic composition of the enriched recycled material mixing with normal unmetasomatised fertile upper mantle (0.20‰). Between 23 and 29% websterite can reproduce the basaltic Ni isotopic compositions (0.05-0.08‰).

Expanding this, the entire analysed $\delta^{60/58}Ni_{SRM986}$ of the mafic samples could be recreated by mixing of the average composition of websterites (-0.32‰) with a mantle composition equal to the heaviest mantle sample (0.26‰). This implies that even the average upper mantle composition (0.20‰) has some small amount of websterite component. This may in fact be

likely given that recycling has been introducing enriched material into the mantle over long timescales that would be potentially sufficient to mix into the majority of the upper mantle sampled by xenoliths. The average composition of fertile upper mantle peridotites could be produced with only 10% websterite material. The majority of mafic samples could be produced by adding between 20-35% websterite material. The whole mafic suite can be produced by mixing 5-72% websterite material (see Appendix 7.6).

Many of the samples analysed in this work have also been analysed for Mo isotopic composition (Liang et al., 2017) and the data are plotted together in Figure 30. A similarly large range in isotopic compositions is found in both isotopic systems, although extremes are not found in the same OIB samples in both systems. No correlation is observable in the entire dataset, however the possibility of several endmember mixing correlations is possible. Ocean Island basalts appear to follow a negative correlation from Azores, through Loihi, Galápagos and Western Iceland, to Northern Iceland with r^2=0.54. Of the MORB samples only 2 samples have been analysed for both systems consisting of 1 N-MORB and 1 E-MORB from EPR.

As shown here for Ni isotopic compositions, molybdenum isotopic compositions have been shown to vary within OIBs as well as between OIBs and MORB (Liang et al., 2017). However, Cameroon line samples, specifically, show a large range in Mo isotopic composition, including from a single volcano (Etinde) (Liang et al., 2017) where there is only limited variation in Ni isotopic composition. No correlations were found with Mo isotopic composition and radiogenic Pb, Sr, and Nd (Liang et al., 2017). Liang and co-workers (2017) considered this to mean source effects on Mo isotopic composition are minor and the variations in Mo isotopic composition reflect a difference in magmatic processes associated with production and differentiation of MORB and OIB, potentially relating to partial melting of sulfide. This contrasts with the conclusions of this work on Ni isotopic compositions.

The OIB correlation (excluding Cameroon Line) with Ni and Mo isotopic compositions may relate to the suggested control on Mo isotopic composition of subduction zone processes, as suggested by Konig and co-workers (2016). Molybdenum isotopes were found to fractionate in

subduction environments, with heavier isotopes enriched in the more slab fluid dominated samples, because light Mo isotopes were locked in secondary phases (König et al., 2016). A negative correlation with the heaviest Mo isotopic compositions associated with the lightest Ni isotopic compositions would be expected if a similar subduction related process was producing the light Ni and to that enriching heavy Mo in the mantle wedge. The lack of correlation when all the samples are included, does not support that the two isotopic systems co-vary, suggesting that there is no common process connecting the fractionation of Mo and Ni isotopes.

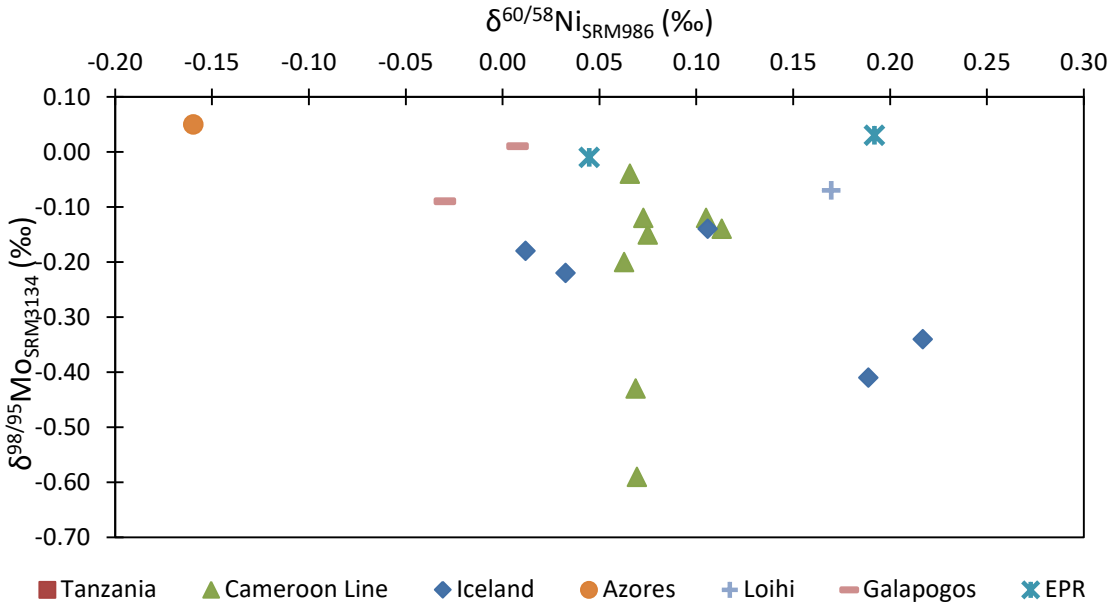

Figure 30

Bulk mafic samples Ni isotopic composition of mafic samples plotted against Mo isotopic composition from (Liang et al., 2017). Not all samples for which Ni isotopes have been analysed have Mo isotopic compositions, hence some samples are missing from the above plot. No correlation is observable in the entire dataset, however the possibility of several endmember mixing correlations is possible. OIBs appear to follow a negative correlation from Azores to Northern Iceland with and r^2=0.54. In contrast, Cameroon line samples show a correlation in Mo with limited variation in Ni. MORB samples appear to correlation towards BSE estimates for both Mo (-0.15‰) and Ni (0.20‰). External reproducibility on Mo isotopic compositions is 0.04 to 0.09‰, and for Ni isotopic composition is 0.06‰.

4.6. Conclusions

Nickel isotopic composition in mafic samples have been shown not to vary with degree of partial melting, because Cameroon Line mafic rocks derived by different degrees of partial melting have identical Ni isotopic compositions. Incompatible trace element ratios lack correlation with Ni isotopic compositions, also supporting this conclusion. The lack of

significant fractionation between major mantle mineral phases, shown in Chapter 3, also implied that partial melting could not induce a large fractionation in Ni isotopic composition. Lack of correlation with compatible trace element ratios, and MgO even within a particular volcanic system, suggest that Ni isotopes are also invariant during fractional crystallisation.

This study has shown that although the average of the Ni isotopic composition in MORB and OIB are identical, showing geological setting does not affect Ni isotopes. Within each setting there is a large range in Ni isotopic compositions, which suggests that there is a process fractionating Ni isotopes in the mantle that is ubiquitous and highly variable. The majority of samples in this range are lighter than the average for unmetasomatised fertile peridotite. Given the lack of fractionation in Ni isotopes with melting, this may suggest that the mafic samples more accurately represent the average upper mantle composition.

The conclusion from Chapter 3 that lighter Ni isotopic compositions were associated with enriched lithologies is further supported by this work, with E-type MORB with high chondrite normalised La/Sm (indicator of LREE enrichment) is associated with lighter Ni isotopic composition. This negative E-type MORB to N-MORB correlation was evident with two different mid-ocean ridges. The correlation forms a continuum, similar to the continuum in Kilbourne Hole xenoliths and Nd isotopic ratio, and E-MORB and N-MORB do not form separate groups or extremes.

Analysis of the Ni isotopic composition of the mafic samples has shed further light on the heterogeneity in the mantle by virtue of sampling the mantle sources of basalts. With Ni isotopes invariant to partial melting and magmatic differentiation, the basaltic Ni isotopic composition reflects the mantle source region of the volcanic system. This mantle source region has a Ni isotopic composition that is suggested by this study to be controlled by the amount of recycled pyroxenitic material incorporated into that region.

As Ni isotopic composition is not affected by time from the input of recycled material, unlike radiogenic isotopic composition, Ni isotopes have the potential to isolate the degree of enriched recycled component in the source regardless of the time since that material was input and

fractionated in Ni isotopes. A mass balance calculation has suggested that 23-29% websterite (-0.32‰) into the mantle (0.20‰) could produce the basaltic signature in Ni isotopic compositions, that average between 0.05 and 0.08‰ for the different mafic suites.

4.7. References

Aigner-Torres, M., Blundy, J., Ulmer, P., Pettke, T., 2007. Laser Ablation ICPMS study of trace element partitioning between plagioclase and basaltic melts: an experimental approach. Contrib Miner. Pet. 153, 647–667. https://doi.org/10.1007/s00410-006-0168-2

Arai, T., Maruyama, S., 2017. Formation of anorthosite on the Moon through magma ocean fractional crystallization. Geosci. Front. 8, 299–308. https://doi.org/10.1016/j.gsf.2016.11.007

Armytage, R.M.G., Georg, R.B., Williams, H.M., Halliday, A.N., 2012. Silicon isotopes in lunar rocks : Implications for the Moon's formation and the early history of the Earth. Geochim. Cosmochim. Acta 77, 504–514. https://doi.org/10.1016/j.gca.2011.10.032

Aulbach, S., Rudnick, R.L., McDonough, W.F., 2008. Li-Sr-Nd isotope signatures of the plume and cratonic lithospheric mantle beneath the margin of the rifted Tanzanian craton (Labait). Contrib. to Mineral. Petrol. 155, 79–92. https://doi.org/10.1007/s00410-007-0226-4

Becker, J.S., 2007. Inorganic mass spectrometry : principles and applications. John Wiley & Sons.

Bédard, J.H., 2005. Trace element partitioning in plagioclase feldspar. Geochim. Cosmochim. Acta 70, 3717–3742. https://doi.org/10.1016/j.gca.2006.05.003

Bindeman, I.N., Davis, A.M., 2000. Trace element partitioning between plagioclase and melt: Investigation of dopant influence on partition behavior.

Birck, J.L., Lugmair, G.W., 1988. Nickel and chromium isotopes in Allende inclusions. Earth Planet. Sci. Lett. 90, 131–143. https://doi.org/10.1016/0012-821X(88)90096-9

Bizzarro, M., Ulfbeck, D., Thrane, K., 2006. Nickel isotopes in meteorites: evidence for live 60Fe and distinct 62Ni isotope reservoirs in the early solar system. Lunar Planet. Sci. XXXVII 37.

Bizzarro, M., Ulfbeck, D., Trinquier, A., Thrane, K., Connelly, J.N., Meyer, B.S., 2007. Evidence for a late supernova injection of 60Fe into the protoplanetary disk. Science 316, 1178–81. https://doi.org/10.1126/science.1141040

Bourdon, B., Langmuir, C.H., Zindler, A., 1996. Ridge-hotspot interaction along the Mid-Atlantic Ridge between 37'30' and 40'30'N: the U-Th disequilibrium evidence, Earth and Planetary Science Letters.

Bouvier, A., Vervoort, J.D., Patchett, P.J., 2008. The Lu-Hf and Sm-Nd isotopic composition of CHUR: Constraints from unequilibrated chondrites and implications for the bulk composition of terrestrial planets. Earth Planet. Sci. Lett. 273, 48–57. https://doi.org/10.1016/j.epsl.2008.06.010

Burton, K.W., Schiano, P., Birck, J.-L., Allègre, C.J., Rehkämper, M., Halliday, A.N., Dawson, J.B., 2000. The distribution and behaviour of rhenium and osmium amongst mantle minerals and the age of the lithospheric mantle beneath Tanzania. Earth Planet. Sci. Lett. 183, 93–106. https://doi.org/10.1016/S0012-821X(00)00259-4

Bussod, G.Y.A., Williams, D.R., 1991. Thermal and kinematic model of the southern Rio Grande rift: inferences from crustal and mantle xenoliths from Kilboume Hole, New Mexico. Tectonophysics 197, 373–389.

Cameron, V., Vance, D., 2014. Heavy nickel isotope compositions in rivers and the oceans. Geochim. Cosmochim. Acta 128, 195–211. https://doi.org/10.1016/j.gca.2013.12.007

Cameron, V., Vance, D., Archer, C., House, C.H., 2009. A biomarker based on the stable isotopes of nickel. Proc. Natl. Acad. Sci. U. S. A. 106, 10944–10948. https://doi.org/10.1073/pnas.0900726106

Canil, D., Pearson RL Rudnick, N.D., McDonough Carswell, W. DA, 1994. Ferric iron in peridotites and mantle oxidation states. Earth Planet. Sci. Lett. 123, 205–220.

Canup, R.M., 2012. Forming a Moon with an Earth-like Composition via a Giant Impact. Science 338, 1052–1055. https://doi.org/10.1126/science.1106818

Canup, R.M., Asphaug, E., 2001. Origin of the Moon in a giant impact near the end of the Earth's formation. Nature 412, 708–712. https://doi.org/10.1038/35089010

Canup, R.M., Barr, A.C., Crawford, D.A., 2013. Lunar-forming impacts: High-resolution SPH and AMR-CTH simulations. Icarus 222, 200–219. https://doi.org/10.1016/J.ICARUS.2012.10.011

Capobianco, C.J., Amelin, A.A., 1994. Metal-silicate partitioning of nickel and cobalt: The influence of temperature and oxygen fugacity. Geochim. Cosmochim. Acta 58, 125–140.

Chako Tchamabé, B., Youmen, D., Owona, S., Ohba, T., Németh, K., Nsangou Ngapna, M., E Asaah, A.N., Aka, F.T., Tanyileke, G., Hell, J. V, 2013. Eruptive history of the Barombi Mbo Maar, Cameroon Volcanic Line, Central Africa: Constraints from volcanic facies analysis. Cent. Eur. J. Geosci 5, 480–496. https://doi.org/10.2478/s13533-012-0147-2

Chen, J.H., Papanastassiou, D.A., 2006. NICKEL ISOTOPE INVESTIGATION BY MC-ICP-MS AND PTIMS, in: Lunar and Planetary Science XXXVII. pp. 61–62.

Chen, J.H., Papanastassiou, D.A., Wasserburg, G.J., 2009. A search for nickel isotopic anomalies in iron meteorites and chondrites. Geochim. Cosmochim. Acta 73, 1461–1471. https://doi.org/10.1016/j.gca.2008.11.040

Chernonozhkin, S.M., Goderis, S., Costas-Rodríguez, M., Claeys, P., Vanhaecke, F., 2016. Effect of parent body evolution on equilibrium and kinetic isotope fractionation: a combined Ni and Fe isotope study of iron and stony-iron meteorites. Geochim. Cosmochim. Acta 186, 168–188. https://doi.org/10.1016/j.gca.2016.04.050

Chernonozhkin, S.M., Goderis, S., Lobo, L., Claeys, P., Vanhaecke, F., 2015. Development of an isolation procedure and MC-ICP-MS measurement protocol for the study of stable isotope ratio variations of nickel. J. Anal. At. Spectrom. 30, 1518–1530. https://doi.org/10.1039/C5JA00080G

Chernonozhkin, S.M., Weyrauch, M., Goderis, S., Oeser, M., McKibbin, S.J., Horn, I., Hecht, L., Weyer, S., Claeys, P., Vanhaecke, F., 2017. Thermal equilibration of iron meteorite and pallasite parent bodies recorded at the mineral scale by Fe and Ni isotope systematics. Geochim. Cosmochim. Acta 217, 95–111. https://doi.org/10.1016/J.GCA.2017.08.022

Ciscato, E.R., Bontognali, T.R.R., Vance, D., 2018. Nickel and its isotopes in organic-rich sediments: implications for oceanic budgets and a potential record of ancient seawater. Earth Planet. Sci. Lett. 494, 239–250. https://doi.org/10.1016/j.epsl.2018.04.061

Cisowski, S.M., Collinson, D.W., Runcorn, S.K., Stephenson, A., Fuller, M., 1983. A REVIEW OF LUNAR PALEOINTENSITY DATA AND IMPLICATIONS FOR THE ORIGIN OF LUNAR MAGNETISM. J. Geophys. Res. 88, A691–A704.

Cook, D.L., Clayton, R.N., Wadhwa, M., Janney, P.E., Davis, A.M., 2008a. Nickel isotopic anomalies in troilite from iron meteorites. Geophys. Res. Lett. 35, 1–5. https://doi.org/10.1029/2007GL032431

Cook, D.L., Clayton, R.N., Wadhwa, M., Janney, P.E., Davis, A.M., 2008b. Nickel isotopic anomalies in troilite from iron meteorites. Geophys. Res. Lett. 35, L01203. https://doi.org/10.1029/2007GL032431

Cook, D.L., Wadhwa, M., Clayton, R.N., Dauphas, N., Janney, P.E., Davis, A.M., 2007. Mass-dependent fractionation of nickel isotopes in meteoritic metal. Meteorit. Planet. Sci. 42, 2067–2077. https://doi.org/10.1111/j.1945-5100.2007.tb01008.x

Cook, D.L., Wadhwa, M., Janney, P.E., Dauphas, N., Clayton, R.N., Davis, A.M., 2006. High precision measurements of non-mass-dependent effects in nickel isotopes in meteoritic

metal via multicollector ICPMS. Anal. Chem. 78, 8477–84. https://doi.org/10.1021/ac061285m

Cornen, G., Bandet, Y., Giresse, P., Maley, J., 1992. The nature and chronostratigraphy of Quaternary pyroclastic accumulations from Lake Barombi Mbo (West-Cameroon). J. Volcanol. Geotherm. Res. 51, 357–374.

Dauphas, N., Teng, F.-Z., Arndt, N.T., 2010. Magnesium and iron isotopes in 2.7 Ga Alexo komatiites: Mantle signatures, no evidence for Soret diffusion, and identification of diffusive transport in zoned olivine. Geochim. Cosmochim. Acta 74, 3274–3291. https://doi.org/10.1016/J.GCA.2010.02.031

Dauritria, J.M., Girod, M., 1987. Cenozoaic Volcanism associated with Swells and Rifts, in: Nixon, P.. (Ed.), Mantle Xenoliths. pp. 195–215.

Dawson, J.B., 2012. Nephelinite-melilitite-carbonatite relationships: Evidence from Pleistocene-recent volcanism in northern Tanzania. Lithos 152, 3–10. https://doi.org/10.1016/j.lithos.2012.01.008

Dawson, J.B., 2002. Metasomatism and Partial Melting in Upper-Mantle Peridotite Xenoliths from the Lashaine Volcano, Northern Tanzania. J. Petrol. 43, 1749–1777. https://doi.org/10.1093/petrology/43.9.1749

Dawson, J.B., 1992. Neogene tectonics and volcanicity in the North Tanzania sector of the Gregory Rift Valley: contrasts with the Kenya sector. Tectonophysics 204, 81–92. https://doi.org/10.1016/0040-1951(92)90271-7

Dawson, J.B., 1964a. Carbonate Tuff Cones in Northern Tanganyika. Geol. Mag. 101, 129. https://doi.org/10.1017/S0016756800048561

Dawson, J.B., 1964b. Carbonatitic volcanic ashes in Northern Tanganyika. Bull. Volcanol. 27, 81–91. https://doi.org/10.1007/BF02597513

Dawson, J.B., Powell, D.G., Reid, A.M., 1970. Ultrabasic Xenoliths and Lava from the Lashaine Volcano, Northern Tanzania. J. Petrol. 11, 519–548. https://doi.org/10.1093/petrology/11.3.519

Day, J.M.D., Pearson, D.G., Macpherson, C.G., Lowry, D., Carracedo, J.-C., 2009. Pyroxenite-rich mantle formed by recycled oceanic lithosphere: Oxygen-osmium isotope evidence from Canary Island lavas. Geology 37, 555–558. https://doi.org/10.1130/G25613A.1

Delano, J.W., 1985. Mare Volcanic Glasses, II: Abundances of Trace Ni and the Composition of the Moon.

Dingwell, D.B., O'Neill, H.S.C., Ertel, W., Spettel, B., 1994. The solubility and oxidation state of nickel in silicate melt at low oxygen fugacities: Results using a mechanically assisted equilibration technique. Geochim. Cosmochim. Acta 58, 1967–1974. https://doi.org/10.1016/0016-7037(94)90428-6

Dosso, L., Bougault, H., Langmuir, C., Bollinger, C., Bonnier, O., Etoubleau, J., 1999. The age and distribution of mantle heterogeneity along the Mid-Atlantic ridge (31-41°N). Earth Planet. Sci. Lett. 170, 269–286. https://doi.org/10.1016/S0012-821X(99)00109-0

Dziewonski, A.M., Anderson, D.L., 1981. Preliminary reference Earth model. Phys. Earth Planet. Inter. 25, 297–356. https://doi.org/10.1016/0031-9201(81)90046-7

Eberhardt, P., Geiss, J., Graf, H., Grögler, N., Krähenbühl, U., Schwaller, H., Schwarzmüller, J., Stettler, A., 1970. Correlation between rock type and irradiation history of Apollo 11 igneous rocks. Earth Planet. Sci. Lett. 10, 67–72. https://doi.org/10.1016/0012-821X(70)90065-8

Ehlers, K., Grove, T.L., Sisson, T.W., Recca, S.I., Zervas, D.A., 1992. The effect of oxygen fugacity on the partitioning of nickel and cobalt between olivine, silicate melt, and metal. Geochim. Cosmochim. Acta 56, 3733–3743. https://doi.org/10.1016/0016-7037(92)90166-G

El Goresy, A., Ramdohr, P., Taylor, L.A., 1971. The opaque minerals in the lunar rocks from Oceanus Procellarum, in: 2ns Lunar Science Conference. The M.I.T. Press, pp. 219–235.

Elliott, T., Steele, R.C.J., 2017. The Isotope Geochemistry of Ni, in: Reviews in Mineralogy and Geochemistry.

Estrade, N., Cloquet, C., Echevarria, G., Sterckeman, T., Deng, T., Tang, Y., Morel, J.-L., 2015. Weathering and vegetation controls on nickel isotope fractionation in surface ultramafic environments (Albania). Earth Planet. Sci. Lett. 423, 24–35. https://doi.org/10.1016/j.epsl.2015.04.018

Faure, G., Mensing, T.M., Faure, G., 2005. Isotopes : principles and applications. Wiley.

Feigenson, M.D., 1986. Continental alkali basalts as mixtures of kimberlite and depleted mantle: Evidence from Kilbourne Hole Maar, New Mexico. Geophys. Res. Lett. 13, 965–968. https://doi.org/10.1029/GL013i009p00965

Finnerty, A.A., Boyd, F.R., 1987. Thermobarometry for Garnet Peridotites, in: Nixon, P.H. (Ed.), Mantle Xenoltihs. Wiley, pp. 381–402.

Fischer, R.A., Nakajima, Y., Campbell, A.J., Frost, D.J., Harries, D., Langenhorst, F., Miyajima, N., Pollok, K., Rubie, D.C., 2015. High pressure metal-silicate partitioning of Ni, Co, V, Cr, Si, and O. Geochim. Cosmochim. Acta 167, 177–194. https://doi.org/10.1016/j.gca.2015.06.026

Fitton, J.G., 2007. The OIB Paradox, in: Foulger, G.R., Jurdy, D.M. (Eds.), Plates, Plumes, and Planetary Processes. The Geological Society of America, pp. 387–409.

Fitton, J.G., 1987. The Cameroon line, West Africa: a comparison between oceanic and continental alkaline volcanism. Geol. Soc. London, Spec. Publ. 30, 273–291. https://doi.org/10.1144/GSL.SP.1987.030.01.13

Fitton, J.G., Dunlop, H.M., 1985. The Cameroon line, West Africa, and its bearing on the origin of oceanic and continental alkali basalt. Earth Planet. Sci. Lett. 72, 23–38. https://doi.org/10.1016/0012-821X(85)90114-1

Fitton, J.G., Saunders, A.D., Kempton, P.D., Hardarson, B.S., 2003. Does depleted mantle form an intrinsic part of the Iceland plume? Geochemistry, Geophys. Geosystems 4. https://doi.org/10.1029/2002GC000424

Freeth, S.J., 1979. Deformation of the African plate as a consequence of membrane stress domains generated by post-Jurassic drift. Earth Planet. Sci. Lett. 45, 93–104. https://doi.org/10.1016/0012-821X(79)90111-0

Frost, D.J., Liebske, C., Langenhorst, F., McCammon, C.A., Trønnes, R.G., Rubie, D.C., 2004. Experimental evidence for the existence of iron-rich metal in the Earth's lower mantle. Nature 428, 409–412. https://doi.org/10.1038/nature02413

Gale, A., Dalton, C.A., Langmuir, C.H., Su, Y., Schilling, J.-G., 2013. The mean composition of ocean ridge basalts. Geochemistry, Geophys. Geosystems 14, 489–518. https://doi.org/10.1029/2012GC004334

Gall, L., 2011. Development and Application of Nickel Stable Isotopes as a New Geochemical Tracer. University Of Oxford.

Gall, L., Williams, H., Siebert, C., Halliday, A.N., 2012. Determination of mass-dependent variations in nickel isotope compositions using double spiking and MC-ICPMS. J. Anal. At. Spectrom. 27, 137. https://doi.org/10.1039/c1ja10209e

Gall, L., Williams, H.M., Halliday, A.N., Kerr, A.C., 2017. Nickel isotopic composition of the mantle. Geochim. Cosmochim. Acta 199, 196–209. https://doi.org/10.1016/j.gca.2016.11.016

Gall, L., Williams, H.M., Siebert, C., Halliday, A.N., Herrington, R.J., Hein, J.R., 2013. Nickel isotopic compositions of ferromanganese crusts and the constancy of deep ocean inputs

and continental weathering effects over the Cenozoic. Earth Planet. Sci. Lett. 375, 148–155. https://doi.org/10.1016/j.epsl.2013.05.019

Garcia, R.F., Gagnepain-Beyneix, J., Chevrot, S., Lognonné, P., 2011. Very preliminary reference Moon model. Phys. Earth Planet. Inter. 188, 96–113. https://doi.org/10.1016/J.PEPI.2011.06.015

Gessmann, C.K., Rubie, D.C., 2000. The origin of the depletions of V, Cr and Mn in the mantles of the Earth and Moon. Earth Planet. Sci. Lett. 184, 95–107. https://doi.org/10.1016/S0012-821X(00)00323-X

Gibson, S.A., McMahon, S.C., Day, J.A., Dawson, J.B., 2013. Highly Refractory Lithospheric Mantle beneath the Tanzanian Craton: Evidence from Lashaine Pre-metasomatic Garnet-bearing Peridotites. J. Petrol. 54, 1503–1546. https://doi.org/10.1093/petrology/egt020

Gramlich, J.W., Machlan, L.A., Barnes, I.L., Paulsen, P.J., 1989. Absolute isotopic abundance ratios and atomic weight of a reference sample of nickel. J. Res. Natl. Inst. Stand. Technol. 94, 347. https://doi.org/10.6028/jres.094.034

Guan, Y., Huss, G.R., Leshin, L.A., 2004. SIMS analyses of Mg, Cr, and Ni isotopes in primitive meteorites and short-lived radionuclides in the early solar system. Appl. Surf. Sci. 231–232, 899–902. https://doi.org/10.1016/j.apsusc.2004.03.163

Gueguen, B., Rouxel, O., Ponzevera, E., Bekker, A., Fouquet, Y., 2013. Nickel Isotope Variations in Terrestrial Silicate Rocks and Geological Reference Materials Measured by MC-ICP-MS. Geostand. Geoanalytical Res. 37, 297–317. https://doi.org/10.1111/j.1751-908X.2013.00209.x

Gueguen, B., Rouxel, O., Rouget, M.-L., Bollinger, C., Ponzevera, E., Germain, Y., Fouquet, Y., 2016. Comparative geochemistry of four ferromanganese crusts from the Pacific Ocean and significance for the use of Ni isotopes as paleoceanographic tracers. Geochim. Cosmochim. Acta 189, 214–235. https://doi.org/10.1016/J.GCA.2016.06.005

Gueguen, B., Sorensen, J. V., Lalonde, S. V., Peña, J., Toner, B.M., Rouxel, O., 2018. Variable Ni isotope fractionation between Fe-oxyhydroxides and implications for the use of Ni isotopes as geochemical tracers. Chem. Geol. 481, 38–52. https://doi.org/10.1016/J.CHEMGEO.2018.01.023

Haase, K.M., Regelous, M., Duncan, R.A., Brandl, P.A., Stroncik, N., Grevemeyer, I., 2011. Insights into mantle composition and mantle melting beneath mid-ocean ridges from postspreading volcanism on the fossil Galapagos Rise Theme: Geochemical Heterogeneities in Oceanic Island Basalt and Mid-ocean Ridge Basalt Sources: Implications for Melting. Geochem. Geophys. Geosyst 12. https://doi.org/10.1029/2010GC003482

Haase, K.M., Regelous, M., Duncan, R.A., Brandl, P.A., Stroncik, N., Grevemeyer, I., 2011. Insights into mantle composition and mantle melting beneath mid-ocean ridges from postspreading volcanism on the fossil Galapagos Rise. Geochemistry, Geophys. Geosystems 12, 1–21. https://doi.org/10.1029/2010GC003482

Halliday, A.N., 2000. Terrestrial accretion rates and the origin of the Moon. Earth Planet. Sci. Lett. 176, 17–30. https://doi.org/10.1016/S0012-821X(99)00317-9

Halliday, A.N., Davidson, J.P., Holden, P., DeWolf, C., Lee, D.-C., Fitton, J.G., 1990. Trace-element fractionation in plumes and the origin of HIMU mantle beneather the Cameroon line. Nature 346, 523–528. https://doi.org/10.1038/346183a0

Halliday, A.N., Davies, G.R., Lee, D.-C., Tommasini, S., Paslick, C.R., Fitton, J.G., James, D.E., 1992a. Lead isotope evidence for young trace element enrichment in the oceanic upper mantle. Nature 359, 623–627. https://doi.org/10.1038/359623a0

Halliday, A.N., Davies, G.R., Lee, D.-C., Tommasini, S., Paslick, C.R., Fitton, J.G., James, D.E., 1992b. Lead isotope evidence for young trace element enrichment in the oceanic upper mantle. Nature 359, 623–627. https://doi.org/10.1038/359623a0

Halliday, A.N., Davies, G.R., Lee, D.C., 1992. Lead isotope evidence for young trace-element enrichment in the oceanic upper mantle. Nature 359, 623–627.

Halliday, A.N., Dickin, A.P., Fallick, A.E., Fitton, J.G., 1988. Mantle dynamics: A Nd, Sr, Pb and O isotopic study of the Cameroon line volcanic chain. J. Petrol. 29, 181–211. https://doi.org/10.1093/petrology/29.1.181

Halliday, A.N., Lee, D.-C., Christensen, J.N., Rehkämper, M., Yi, W., Luo, X., Hall, C.M., Ballentine, C.J., Pettke, T., Stirling, C., 1998. Applications of Multiple Collector-ICPMS to Cosmochemistry, Geochemistry, and Paleoceanography. Geochim. Cosmochim. Acta 62, 919–940. https://doi.org/10.1016/S0016-7037(98)00057-X

Halliday, A.N., Lee, D.-C., Tommasini, S., Davies, G.R., Paslick, C.R., Godfrey Fitton, J., James, D.E., 1995. Incompatible trace elements in OIB and MORB and source enrichment in the sub-oceanic mantle. Earth Planet. Sci. Lett. 133, 379–395. https://doi.org/10.1016/0012-821X(95)00097-V

Hardarson, B.S., Fitton, J.G., 1997. Mechanisms of crustal accretion in Iceland. Geology 25, 1043–1046.

Harpp, K.S., White, W.M., 2001a. Tracing a mantle plume: Isotopic and trace element variations of Galápagos seamounts. Geochemistry, Geophys. Geosystems 2, n/a-n/a. https://doi.org/10.1029/2000GC000137

Harpp, K.S., White, W.M., 2001b. Tracing a mantle plume: Isotopic and trace element variations of Galápagos seamounts. Geochemistry, Geophys. Geosystems 2, n/a-n/a. https://doi.org/10.1029/2000GC000137

Hart, S.R., 1988. Heterogeneous mantle domains: signatures, genesis and mixing chronologies. Earth Planet. Sci. Lett. 90, 273–296. https://doi.org/10.1016/0012-821X(88)90131-8

Hart, S.R., Davis, K.E., 1978. Nickel partitioning between olivine and silicate melt. Earth Planet. Sci. Lett. 40, 203–219.

Hartmann, W.K., Davis, D.R., 1975. Satellite-Sized Planetesimals and Lunar Origin, ICARUS.

Harvey, J., Dale, C.W., Gannoun, A., Burton, K.W., 2011. Osmium mass balance in peridotite and the effects of mantle-derived sulfides on basalt petrogenesis. Geochim. Cosmochim. Acta 75, 5574–5596. https://doi.org/10.1016/j.gca.2011.07.001

Harvey, J., Konig, S., Luguet, A., 2015. The effects of melt depletion and metasomatism on highly siderophile and strongly chalcophile elements: S-Se-Te-Re-PGE systematics of peridotite xenoliths from Kilbourne Hole, New Mexico. Geochim. Cosmochim. Acta 166, 210–233. https://doi.org/10.1016/j.gca.2015.06.028

Harvey, J., Yoshikawa, M., Hammond, S.J., Burton, K.W., 2012. Deciphering the trace element characteristics in kilbourne hole peridotite xenoliths: Melt-rock interaction and metasomatism beneath the Rio Grande Rift, SW USA. J. Petrol. 53, 1709–1742. https://doi.org/10.1093/petrology/egs030

Hauri, E.H., 1996. Major-element variability in the Hawaiian mantle plume. Nature 382, 415–419. https://doi.org/10.1038/382415a0

Henderson, P., Henderson, G., 2009. The Cambridge Handbook of Earth Science Data. Cambridge University Press.

Herzberg, C., Vidito, C., Starkey, N.A., 2016. Nickel–cobalt contents of olivine record origins of mantle peridotite and related rocks. Am. Mineral. 101, 1952–1966. https://doi.org/10.2138/am-2016-5538

Hiesinger, H., Head III, J.W., 2006. New Views of Lunar Geoscience: An Introduction and Overview, in: Reviews in Mineralogy & Geochemistry Volume 60: New Views of the Moon. pp. 1–67.

Hofmann, A., Bekker, A., Dirks, P., Gueguen, B., Rumble, D., Rouxel, O.J., 2014. Comparing

orthomagmatic and hydrothermal mineralization models for komatiite-hosted nickel deposits in Zimbabwe using multiple-sulfur, iron, and nickel isotope data. Miner. Depos. 49, 75–100. https://doi.org/10.1007/s00126-013-0476-1

Holzheid, A., Palme, H., Chakraborty, S., 1997. The activities of NiO, CoO and FeO in silicate melts. Chem. Geol. 139, 21–38.

Irving, A.J., 1980. Petrology and geochemistry of composite ultramafic xenoliths in alkalic basalts and implications for magmatic processes within the mantle. Am. J. Sci. 280–A, 389–426.

James, D.E., Padovani, E.R., Hart, S.R., 1980. Preliminary results on the oxygen isotopic composition of the lower crust, Kilbourne Hole Maar, New Mexico. Geophys. Res. Lett. 7, 321–324. https://doi.org/10.1029/GL007i005p00321

Jana, D., Walker, D., 1997. The influence of silicate melt composition on distribution of siderophile elements among metal and silicate liquids. Earth Planet. Sci. Lett. 150, 463–472. https://doi.org/10.1016/S0012-821X(97)00079-4

Kegler, P., Holzheid, A., Frost, D.J., Rubie, D.C., Dohmen, R., Palme, H., 2008. New Ni and Co metal-silicate partitioning data and their relevance for an early terrestrial magma ocean. Earth Planet. Sci. Lett. 268. https://doi.org/10.1016/j.epsl.2007.12.020

Keller, G.R., Morgan, P., Seager, W.R., 1990. Crustal structure, gravity anomalies and heat flow in the southern Rio Grande rift and their relationship to extensional tectonics. Tectonophysics 174, 21–37.

Kempton, P.D., Fitton, J.G., Saunders, A.D., Nowell, G.M., Taylor, R.N., Hardarson, B.S., Pearson, G., 2000. The Iceland plume in space and time: a Sr–Nd–Pb–Hf study of the North Atlantic rifted margin, Earth and Planetary Science Letters. Elsevier. https://doi.org/10.1016/S0012-821X(00)00047-9

Kirsten, T., Deubner, J., Horn, P., Kaneoka, I., Kiko, J., Schaeffer, O.A., Thio, S.K., 1972. The rare gas record of Apollo 14 and 15 samples. Proc. Third Lunar Sci. Conf. vol. 3, p. 1865 - 1889 3, 1865–1889.

Kodolányi, J., Stephan, T., Trappitsch, R., Pignatari, M., Davis, A.M., Pellin, M.J., 2018. Iron and nickel isotope compositions of presolar silicon carbide grains from supernovae. Geochim. Cosmochim. Acta 221, 127–144. https://doi.org/10.1016/J.GCA.2017.05.029

König, S., Wille, M., Voegelin, A., Schoenberg, R., 2016. Molybdenum isotope systematics in subduction zones. Earth Planet. Sci. Lett. 447, 95–102. https://doi.org/10.1016/j.epsl.2016.04.033

Koornneef, J.M., Davies, G.R., Döpp, S.P., Vukmanovic, Z., Nikogosian, I.K., Mason, P.R.D., 2009. Nature and timing of multiple metasomatic events in the sub-cratonic lithosphere beneath Labait, Tanzania. Lithos 112, 896–912. https://doi.org/10.1016/J.LITHOS.2009.04.039

Korotev, R.L., 2018. List of Lunar Meteorites [WWW Document]. http://meteorites.wustl.edu/lunar/moon_meteorites_list_alpha.htm.

Krawczynski, M.J., Grove, T.L., 2012. Experimental investigation of the influence of oxygen fugacity on the source depths for high titanium lunar ultramafic magmas. Geochim. Cosmochim. Acta 79, 1–19. https://doi.org/10.1016/j.gca.2011.10.043

Langmuir, C.H., Klein, E.M., Plank, T., 1992. Petrological Systematics of Mid-Ocean Ridge Basalts: Constraints on Melt Generation Beneath Ocean Ridges, in: Phipps Morgan, J., Blackman, D.K., Sinton, J.M. (Eds.), Mantle Flow and Melt Generation at Mantle Ridges. American Geophysical Union (AGU), pp. 183–280. https://doi.org/10.1029/GM071p0183

Lazar, C., Young, E.D., Manning, C.E., 2012. Experimental determination of equilibrium nickel isotope fractionation between metal and silicate from 500 °C to 950 °C. Geochim. Cosmochim. Acta 86, 276–295. https://doi.org/10.1016/J.GCA.2012.02.024

Lee, D.-C., 1994. A Chemical, Isotopic, and Geochronological Study of the Cameroon Line, West Africa. University of Michigan.

Lee, D.-C., Halliday, A.N., Davies, G.R., Essene, E.J., Fitton, J.G., Temdjim, R., 1996. Melt Enrichment of Shallow Depleted Mantle: a Detailed Petrological, Trace Element and Isotopic Study of Mantle- Derived Xenoliths and Megacrysts from the Cameroon Line. J. Petrol. 37, 15–441.

Lee, D., Halliday, A.N., Davies, G.R., Essene, E.J., Fitton, J.G., Temdjim, R., 1996. Melt Enrichment of Shallow Depleted Mantle: a Detailed Petrological, Trace Element and Isotopic Study of Mantle- Derived Xenoliths and Megacrysts from the Cameroon Line. J. Petrol. 37, 415–441.

Liang, Y.-H., Halliday, A.N., Siebert, C., Fitton, J.G., Burton, K.W., Wang, K.-L., Harvey, J., 2017. Molybdenum isotope fractionation in the mantle. Geochim. Cosmochim. Acta 199, 91–111. https://doi.org/10.1016/J.GCA.2016.11.023

Liu, L., Spasojević, S., Gurnis, M., 2008. Reconstructing Farallon Plate Subduction Beneath North America Back to the Late Cretaceous. Science (80-.). 322. https://doi.org/10.1126/science.1164170

Liu, S., Li, Y., Ju, Y., Liu, J., Liu, J., Shi, Y., 2018. Equilibrium nickel isotope fractionation in nickel sulfide minerals. Geochim. Cosmochim. Acta 222, 1–16. https://doi.org/10.1016/J.GCA.2017.10.018

Lodders, K., 2003. Solar System Abundances and Condensation Temperatures of the Elements. Astrophys. Journal, 591, 1220–1247.

Ma, Z., Thompson, R.N., Lykke, K.R., Pellin, M.J., Davis, A.M., 1995. Time-of-Flight Mass Spectrometer with Improved Resolution Review of. Cit. Rev. Sci. Instruments 66, 1150. https://doi.org/10.1063/1.1145546

Maley, J., Livingstone, D.A., Giresse, P., Thouveny, N., Brenac, P., Kelts, K., Kling, G., Stager, C., Haag, M., Fournier, M., Bandet, Y., Williamson, D., Zogning, A., 1990. Lithostratigraphy, volcanism, paleomagnetism and palynology of Quaternary lacustrine deposits from Barombi Mbo (West Cameroon): preliminary results. J. Volcanol. Geotherm. Res. 42, 319–335.

McCammon, C., 2005. The Paradox of Mantle Redox. Science (80-.). 308. https://doi.org/10.1126/science.1108162

McDonough, W.F., Sun, S. s., 1995. The composition of the Earth. Chem. Geol. 120, 223–253. https://doi.org/10.1016/0009-2541(94)00140-4

Menzies, M.A., Arculus, R.J., G, B.M., Bergman, S.C., Ehrenberg, S.N., Irving, A.J., Roden, M.F., Schulze, D.J., 1987. A record of subduction processes and within-plate volcanism in lithospheric xenoliths of southwestern USA, in: Nixon, P.. (Ed.), Mantle Xenoliths. pp. 59–74.

Meyer, C., 2011. Lunar Sample Compendium.

Meyer, C., 2003. Lunar Regolith - NASA Lunar Petrographic Educational Thin Section Set.

Moorbath, S., Sigurdsson, H., Goodwin, R., 1968. K-Ar ages of the oldest exposed rocks in Iceland. Earth Planet. Sci. Lett. 4, 197–205. https://doi.org/10.1016/0012-821X(68)90035-6

Morand, P., Allègre, C.J., 1983. Nickel isotopic studies in meteorites. Earth Planet. Sci. Lett. 63, 167–176. https://doi.org/10.1016/0012-821X(83)90034-1

Morand, P., Audouze, J., Allègre, C.J., 1980. Search for nickel isotopic anomaly of meteorites, in: 43rd Annual Meeting of the Meteoritical Society.

Moreau, C., Regnoult, J.-M., Déruelle, B., Robineau, B., 1987. A new tectonic model for the Cameroon Line, Central Africa. Tectonophysics 141, 317–334.

https://doi.org/10.1016/0040-1951(87)90206-X

Morgan, W.J., 1983. Hotspot tracks and the early rifting of the Atlantic. Tectonophysics 94, 123–139. https://doi.org/10.1016/0040-1951(83)90013-6

Mostefaoui, S., Lugmair, G.W., Hoppe, P., 2005. 60 Fe: A Heat Source for Planetary Differentiation from a Nearby Supernova Explosion. Astrophys. J. 625, 271–277. https://doi.org/10.1086/429555

Moynier, F., Agranier, A., Hezel, D.C., Bouvier, A., 2010. Sr stable isotope composition of Earth, the Moon, Mars, Vesta and meteorites, Earth and Planetary Science Letters. https://doi.org/10.1016/j.epsl.2010.10.017

Moynier, F., Albarède, F., Herzog, G.F., 2006. Isotopic composition of zinc, copper, and iron in lunar samples. Geochim. Cosmochim. Acta 70, 6103–6117. https://doi.org/10.1016/j.gca.2006.02.030

Moynier, F., Blichert-Toft, J., Telouk, P., Luck, J.-M., Albarède, F., 2007. Comparative stable isotope geochemistry of Ni, Cu, Zn, and Fe in chondrites and iron meteorites. Geochim. Cosmochim. Acta 71, 4365–4379. https://doi.org/10.1016/j.gca.2007.06.049

Moynier, F., Blichert-Toft, J.F., Telouk, P., Albarede, F., 2005. Excesses of 60Ni in chondrites and iron meteorites, in: Lunar and Planetary Science XXXVI.

Neal, C.R., 2001. The Interior of the Moon: The presence of garnet in the primitive deep lunar mantle. J. Geophys. Res. 106, 27865–27885.

Neal, C.R., Taylor, L.A., 1992. Petrogenesis of mare basalts: A record of lunar volcanism*. Geochim. Cosmochim. Acta 56, 2177–2211.

Neal, C.R., Taylor, L.A., 1991. Evidence for metasomatism of the lunar highlands and the origin of whitlockite. Geochim. Cosmochim. Acta 55, 2965–2980.

Newsom, H.E., 1986. Constraints on the Origin of the Moon from the Abundance of Molybdenum and Other Siderophile Elements.

Nicholls, D., 1974. Complexes and First Row Transition Elements. Macmillan, London.

Nier, A.O., 1940. A Mass Spectrometer for Routine Isotope Abundance Measurements. Rev. Sci. Instrum. 11. https://doi.org/10.1063/1.1751688

Niu, Y., Batiza, R., 1997. Trace element evidence from seamounts for recycled oceanic crust in the Eastern Pacific mantle. Earth Planet. Sci. Lett. 148, 471–483. https://doi.org/10.1016/S0012-821X(97)00048-4

Nixon, P.., 1987. Introduction, in: Mantle Xenoliths. pp. 1–3.

Norton, I.O., 2007. Speculations on Cretaceous tectonic history of the northwest Pacific and a tectonic origin for the Hawaii hotspot, in: Plates, Plumes, and Planetary Processes. pp. 451–470.

O'Neill, H.S.C., 1981. The transition between spinel lherzolite and garnet lherzolite, and its use as a Geobarometer. Contrib. to Mineral. Petrol. 77, 185–194. https://doi.org/10.1007/BF00636522

Palme, H., Spettel, B., Bischoff, A., St6ffler, D., 1984. Early Differentiation of the Moon' Evidence from Trace Elements in Plagioclase, in: PROCEEDINGS OF THE FIFTEENTH LUNAR AND PLANETARY SCIENCE CONFERENCE, PART 1 JOURNAL OF GEOPHYSICAL RESEARCH. https://doi.org/10.1029/JB089iS01p000C3

Paniello, R.C., Day, J.M.D., Moynier, F., 2012. Zinc isotopic evidence for the origin of the Moon. Nature 490, 376–379. https://doi.org/10.1038/nature11507

Papanastassiou, D.A., Wasserburg, G.J., 1971. Rb-Sr AGES OF IGNEOUS ROCKS FROM THE APOLLO 14 MISSION AND THE AGE OF THE FRA MAURO FORMATION. Earth Planet. Sci. Lett. 12, 36–48.

Papike, J.J., Fowler, G.W., Adcock, C.T., Shearer, C.K., 1999. Systematics of Ni and Co in olivine from planetary melt systems: Lunar mare basalts. Am. Mineral. 84, 392–399. https://doi.org/10.2138/am-1999-0324

Paslick, C., Halliday, A.N., James, D., Dawson, J.B., 1995. Enrichment of the continental lithosphere by OIB melts: Isotopic evidence from the volcanic province of northern Tanzania. Earth Planet. Sci. Lett. 130, 109–126.

Paslick, C.R., 1995. A Geochemical Study of Volcanism associated with the early stages of Continental Rifting in Northern Tanzanian. University of Michigan.

Paslick, C.R., Halliday, A.N., Lange, R.A., James, D., Dawson, J.B., 1996. Indirect crustal contamination: evidence from isotopic and chemical disequilibria in minerals from alkali basalts and nephelinites from northern Tanzania. Contrib. to Mineral. Petrol. 125, 277–292. https://doi.org/10.1007/s004100050222

Peale, S.J., Cassen, P., 1978. Contribution of tidal dissipation to lunar thermal history. Icarus 36, 245–269. https://doi.org/10.1016/0019-1035(78)90109-4

Perkins, D., Anthony, E.Y., 2011. The evolution of spinel lherzolite xenoliths and the nature of the mantle at Kilbourne Hole, New Mexico. Contrib. to Mineral. Petrol. 162, 1139–1157. https://doi.org/10.1007/s00410-011-0644-1

Pike, J.E.N., Meyer, C.E., Wilshire, H.G., 1980. Petrography and Chemical Composition of a Suite of Ultramafic Xenoliths from Lashaine, Tanzania. J. Geol. 88, 343–352. https://doi.org/10.1086/628512

Pinter, Z., Patko, L., Djoukam, F.T.J., Kovacs, I., Tchouankoue, J.P., Falus, G., Konc, Z., Tommasi, A., Barou, F., Mihaly, J., Nemeth, C., Jeffries, T., 2015. Characterization of the sub-continental lithospheric mantle beneath the Cameroon volcanic line inferred from alkaline basalt hosted peridotite xenoliths from Barombi Mbo and Nyos Lakes. J. African Earth Sci. 111, 170–193. https://doi.org/10.1016/j.jafrearsci.2015.07.006

Porter, S.J., Selby, D., Cameron, V., 2014. Characterising the nickel isotopic composition of organic-rich marine sediments. Chem. Geol. 387, 12–21. https://doi.org/10.1016/j.chemgeo.2014.07.017

Quitte, G., Halliday, A.N., Meyer, B.S., Markowski, A., Latkoczy, C., Gunther, D., 2007. Correlated Iron 60, Nickel 62, and Zirconium 96 in Refractory Inclusions and the Origin of the Solar System. Astrophys. J. 655, 678–684. https://doi.org/10.1086/509771

Quitté, G., Meier, M., Latkoczy, C., Halliday, A.N., Günther, D., Gunther, D., Günther, D., Gunther, D., Günther, D., 2006. Nickel isotopes in iron meteorites–nucleosynthetic anomalies in sulfides with no effects in metals and no trace of 60Fe. Earth Planet. Sci. Lett. 242, 16–25. https://doi.org/10.1016/j.epsl.2005.11.053

Quitté, G., Oberli, F., 2006. Quantitative extraction and high precision isotope measurements of nickel by MC-ICPMS. J. Anal. At. Spectrom. 21, 1249. https://doi.org/10.1039/b607569j

Rai, N., Westrenen, W. Van, 2014. Lunar core formation : New constraints from metal – silicate partitioning of siderophile elements. Earth Planet. Sci. Lett. 388, 343–352. https://doi.org/10.1016/j.epsl.2013.12.001

Ratié, G., Jouvin, D., Garnier, J., Rouxel, O., Miska, S., Guimaraes, E., Cruz Vieira, L., Sivry, Y., Zelano, I., Montarges-Pelletier, E., Thil, F., Quantin, C., 2015. Nickel isotope fractionation during tropical weathering of ultramafic rocks. Chem. Geol. 402, 68–76. https://doi.org/10.1016/j.chemgeo.2015.02.039

Ratié, G., Quantin, C., Jouvin, D., Calmels, D., Ettler, V., Sivry, Y., Vieira, L.C., Ponzevera, E., Garnier, J., Cruz Vieira, L., Ponzevera, E., Garnier, J., 2016. Nickel isotope fractionation during laterite Ni ore smelting and refining : Implications for tracing the sources of Ni in smelter-affected soils. Appl. Geochemistry 64, 136–145. https://doi.org/10.1016/j.apgeochem.2015.09.005

Reedy, R.C., Englert, P., 1986. Workshop on COSMOGENIC NUCLIDES.

Regelous, M., Elliott, T., Coath, C.D., 2008. Nickel isotope heterogeneity in the early Solar System. Earth Planet. Sci. Lett. 272, 330–338. https://doi.org/10.1016/j.epsl.2008.05.001

Reid, A.M., Donaldson, C.H., Brown, R.W., Ridley, W.I., Dawson, J.B., 1975. Mineral chemistry of peridotite xenoliths from the Lashaine volcano, Tanzania. Phys. Chem. Earth 9, 525–543. https://doi.org/10.1016/0079-1946(75)90037-3

Rhodes, J.M., Dawson, J.B., 1975. Major and trace element chemistry of peridotite inclusions from the Lashaine volcano, Tanzania. Phys. Chem. Earth 9, 545–557. https://doi.org/10.1016/0079-1946(75)90038-5

Righter, K., 2002. Does the Moon Have a Metallic Core? Constraints from Giant Impact Modeling and Siderophile Elements. Icarus 158, 1–13. https://doi.org/10.1006/icar.2002.6859

Righter, K., Drake, M.J., Yaxley, G., 1997. Prediction of siderophile element metal-silicate partition coefficients to 20 GPa and 2800°C: the effects of pressure, temperature, oxygen fugacity, and silicate and metallic melt compositions. Phys. Earth Planet. Inter. 100, 115–134. https://doi.org/10.1016/S0031-9201(96)03235-9

Righter, K., Pando, K.M., Danielson, L., Lee, C.-T., 2010. Partitioning of Mo, P and other siderophile elements (Cu, Ga, Sn, Ni, Co, Cr, Mn, V, and W) between metal and silicate melt as a function of temperature and silicate melt composition. Earth Planet. Sci. Lett. 291, 1–9. https://doi.org/10.1016/J.EPSL.2009.12.018

Roden, M.F., Irving, A.J., Murthy, V.R., 1988. Isotopic and trace element composition of the upper mantle beneath a young continental rift: Results from Kilbourne Hole, New Mexico. Geochim. Cosmochim. Acta 52, 461–473. https://doi.org/10.1016/0016-7037(88)90101-9

Rugel, G., Faestermann, T., Knie, K., Korschinek, G., Poutivtsev, M., Schumann, D., Kivel, N., Günther-Leopold, I., Weinreich, R., Wohlmuther, M., 2009. New Measurement of the ^{60}Fe Half-Life. Phys. Rev. Lett. 103, 072502. https://doi.org/10.1103/PhysRevLett.103.072502

Sato, M., Hickling, N.L., McLane, J.E., 1973. Oxygen fugacity values of Apollo 12, 14, and 15 lunar samples and reduced state of lunar magmas, in: Proceedings of the Fourth Lunar Science Conference. pp. 1061–1079.

Satsukawa, T., Michibayashi, K., Anthony, E.Y., Stern, R.J., Gao, S.S., Liu, K.H., 2011. Seismic anisotropy of the uppermost mantle beneath the Rio Grande rift: Evidence from Kilbourne Hole peridotite xenoliths, New Mexico. Earth Planet. Sci. Lett. 311, 172–181. https://doi.org/10.1016/J.EPSL.2011.09.013

Sedaghatpour, F., Teng, F.Z., Liu, Y., Sears, D.W.G., Taylor, L.A., 2013. Magnesium isotopic composition of the Moon. Geochim. Cosmochim. Acta 120, 1–16. https://doi.org/10.1016/j.gca.2013.06.026

Sharp, Z.D., Shearer, C.K., McKeegan, K.D., Barnes, J.D., Wang, Y.Q., 2010. The Chlorine Isotope Composition of the Moon and Implications for an Anhydrous Mantle. Science (80-.). 329. https://doi.org/10.1126/science.1191349

Shearer, C.K., Hess, P.C., Wieczorek, M.A., Pritchard, M.E., Parmentier, E.M., Borg, L.E., Longhi, J., Elkins-Tanton, L.T., Neal, C.R., Antonenko, I., Canup, R.M., Halliday, A.N., Grove, T.L., Hager, B.H., Lee, D.C., Wiechert, U., 2006. Thermal and Magmatic Evolution of the Moon, in: Reviews in Mineralogy & Geochemistry Volume 60: New Views of the Moon. pp. 365–502.

Shimamura, T., Lugmair, G.W., 1983. Ni isotopic compositions in Allende and other meteorites. Earth Planet. Sci. Lett. 63, 177–188. https://doi.org/10.1016/0012-821X(83)90035-3

Shukolyukov, A., Lugmair, G.W., 1993a. 60Fe in eucrites. Earth Planet. Sci. Lett. 119, 159–

166. https://doi.org/10.1016/0012-821X(93)90013-Y

Shukolyukov, A., Lugmair, G.W., 1993b. Live Iron-60 in the Early Solar System. Science (80-.). 259, 1138–1142.

Siebert, C., Nägler, T.F., Kramers, J.D., 2001. Determination of molybdenum isotope fractionation by double-spike multicollector inductively coupled plasma mass spectrometry. Geochemistry, Geophys. Geosystems 2, n/a-n/a. https://doi.org/10.1029/2000GC000124

Silveira, G., Stutzmann, E., Davaille, A., Montagner, J.-P., Mendes-Victor, L., Sebai, A., 2006. Azores hotspot signature in the upper mantle. J. Volcanol. Geotherm. Res. 156, 23–34. https://doi.org/10.1016/J.JVOLGEORES.2006.03.022

Simon, J.I., DePaolo, D.J., 2010. Stable calcium isotopic composition of meteorites and rocky planets, Earth and Planetary Science Letters. https://doi.org/10.1016/j.epsl.2009.11.035

Sobolev, A. V, Hofmann, A.W., Kuzmin, D. V, Yaxley, G.M., Arndt, N.T., Chung, S.-L., Danyushevsky, L. V, Elliott, T., Frey, F.A., Garcia, M.O., Gurenko, A.A., Kamenetsky, V.S., Kerr, A.C., Krivolutskaya, N.A., Matvienkov, V. V, Nikogosian, I.K., Rocholl, A., Sigurdsson, I.A., Sushchevskaya, N.M., Teklay, M., 2007. The Amount of Recycled Crust in Sources of Mantle-Derived Melts. Science (80-.). 316.

Sobolev, A. V, Hofmann, A.W., Sobolev, S. V, Nikogosian, I.K., 2005. An olivine-free mantle source of Hawaiian shield basalts. Nature 434.

Spivak-Birndorf, L.J., Wang, S.-J., Bish, D.L., Wasylenki, L.E., 2018. Nickel isotope fractionation during continental weathering. Chem. Geol. 476, 316–326. https://doi.org/10.1016/J.CHEMGEO.2017.11.028

Steele, A.M., Colson, R.O., Haskin, L.A., 1991. Co and Ni as Incompatible elements in the Lunar Mantle: Implications for fO2 and the Petrogenesis of Apollo 15 Green Glass, in: LPSC XXII.

Steele, R.C.J., Coath, C.D., Regelous, M., Russell, S., Elliott, T., 2012. Neutron-poor nickel isotope anomalies in meteorites. Astrophys. J. 758, 59. https://doi.org/10.1088/0004-637X/758/1/59

Steele, R.C.J., Elliott, T., Coath, C.D., Regelous, M., 2011. Confirmation of mass-independent Ni isotopic variability in iron meteorites. Geochim. Cosmochim. Acta 75, 7906–7925. https://doi.org/10.1016/J.GCA.2011.08.030

Steenstra, E.S., Rai, N., Knibbe, J.S., Lin, Y.H., Van Westrenen, W., 2016. New geochemical models of core formation in the Moon from metal-silicate partitioning of 15 siderophile elements. Earth Planet. Sci. Lett. 441, 1–9. https://doi.org/10.1016/j.epsl.2016.02.028

Strelow, F.W.E., 1990. Distribution coefficients and cation-exchange behaviour of some ammines and aquo complexes of metallic elements in ammonium nitrate solution. Anal. Chim. Acta 233, 129–134. https://doi.org/10.1016/S0003-2670(00)83468-6

Strelow, F.W.E., Weinert, C.H.S.W., Eloff, C., 1972. Distribution coefficients and anion exchange behavior of elements in oxalic acid-hydrochloric acid mixtures. Anal. Chem. 44, 2352–2356. https://doi.org/10.1021/ac60322a001

Sun, C., Graff, M., Liang, Y., 2017. Trace element partitioning between plagioclase and silicate melt: The importance of temperature and plagioclase composition, with implications for terrestrial and lunar magmatism. Geochim. Cosmochim. Acta 206, 273–295. https://doi.org/10.1016/j.gca.2017.03.003

Tachibana, S., Huss, G.R., 2003. The Initial Abundance of 60 Fe in the Solar System. Astrophys. J. 588, L41–L44. https://doi.org/10.1086/375362

Tachibana, S., Huss, G.R., Kita, N.T., Shimoda, G., Morishita, Y., 2006. 60 Fe in Chondrites: Debris from a Nearby Supernova in the Early Solar System? Astrophys. J. 639, L87–L90. https://doi.org/10.1086/503201

Tanimizu, M., Hirata, T., 2006. Determination of natural isotopic variation in nickel using inductively coupled plasma mass spectrometry. J. Anal. At. Spectrom. 21, 1423. https://doi.org/10.1039/b609543g

Taylor, S.R., 1982. A Lunar Perspective. Lunar and Planetary Institute.

Taylor, S.R., 1975. Lunar Science: A Post-Apollo View.

Teng, F.-Z., Dauphas, N., Huang, S., Marty, B., 2013. Iron isotopic systematics of oceanic basalts. Geochim. Cosmochim. Acta 107, 12–26. https://doi.org/10.1016/J.GCA.2012.12.027

Thompson, G., Bryan, W.B., Humphris, S.E., 1989. Axial volcanism on the East Pacific Rise, in: Magmatism in the Ocean Basins. pp. 181–200.

Trappitsch, R., Stephan, T., Savina, M.R., Davis, A.M., Pellin, M.J., Rost, D., Gyngard, F., Gallino, R., Bisterzo, S., Cristallo, S., Dauphas, N., 2018. Simultaneous iron and nickel isotopic analyses of presolar silicon carbide grains. Geochim. Cosmochim. Acta 221, 87–108. https://doi.org/10.1016/J.GCA.2017.05.031

van Kan Parker, M., Sanloup, C., Sator, N., Guillot, B., Tronche, E.J., Perrillat, J.-P., Mezouar, M., Rai, N., van Westrenen, W., 2012. Neutral buoyancy of titanium-rich melts in the deep lunar interior. Nat. Geosci. 5, 186–189. https://doi.org/10.1038/ngeo1402

Vance, D., Little, S.H., Archer, C., Cameron, V., Andersen, M.B., Rijkenberg, M.J.A., Lyons, T.W., 2016. The oceanic budgets of nickel and zinc isotopes: the importance of sulfidic environments as illustrated by the Black Sea. Philos. Trans. A. Math. Phys. Eng. Sci. 374, 20150294. https://doi.org/10.1098/rsta.2015.0294

Vauchez, A., Dineur, F., Rudnick, R., 2005. Microstructure, texture and seismic anisotropy of the lithospheric mantle above a mantle plume: Insights from the Labait volcano xenoliths (Tanzania). Earth Planet. Sci. Lett. 232, 295–314. https://doi.org/10.1016/J.EPSL.2005.01.024

Ventura, G.T., Gall, L., Siebert, C., Prytulak, J., Szatmari, P., Hürlimann, M., Halliday, A.N., 2015. The stable isotope composition of vanadium, nickel, and molybdenum in crude oils. Appl. Geochemistry 59, 104–117. https://doi.org/10.1016/j.apgeochem.2015.04.009

Victor, A.H., 1986. Selective separation of Nickel from other elements by cation-exchange chromatography in dimethylglyoxime/hydrochloric acid/acetone media. Anal. Chim. Acta 183, 155–161.

Wadhwa, M., 2008. Redox Conditions on Small Bodies, the Moon and Mars, in: Reviews in Mineralogy and Geochemistry. GeoScienceWorld, pp. 493–510. https://doi.org/10.2138/rmg.2008.68.17

Walter, L.S., French, B.M., Heinrich, K.F.J., Lowman, P.D., Doan, A.S., Adler, I., 1971. Mineralogical studies of Apollo 12 samples, in: 2nd Lunar Science Conference. M.I.T. Press, pp. 343–358.

Wang, K., Jacobsen, S.B., Sedaghatpour, F., Chen, H., Korotev, R.L., 2015. The earliest Lunar Magma Ocean differentiation recorded in Fe isotopes. Earth Planet. Sci. Lett. 430, 202–208. https://doi.org/10.1016/j.epsl.2015.08.019

Wang, S.-J., Wasylenki, L.E., 2017. Experimental constraints on reconstruction of Archean seawater Ni isotopic composition from banded iron formations. Geochim. Cosmochim. Acta 206, 137–150. https://doi.org/10.1016/J.GCA.2017.02.023

Warren, P.H., 1985. THE MAGMA OCEAN CONCEPT AND LUNAR EVOLUTION. Ann. Rev. Earth planet. Sci 13, 201–241.

Warren, P.H., Wasson, J.T., 1979. The Origin of KREEP. Rev. Geophys. Sp. Phys. 17.

Wasylenki, L.E., Howe, H.D., Spivak-Birndorf, L.J., Bish, D.L., 2015. Ni isotope fractionation during sorption to ferrihydrite: Implications for Ni in banded iron formations. Chem. Geol.

400, 56–64. https://doi.org/10.1016/j.chemgeo.2015.02.007

Weber, R.C., Lin, P., Garnero, E.J., Williams, Q., Lognonné, P., 2011. Seismic Detection of the Lunar Core 331, 309–312.

Wedepohl, K.H., 1974. Nickel, in: Wedepohl, K.H. (Ed.), Handbook of Geochemistry. Springer.

Weis, D., Kieffer, B., Maerschalk, C., Barling, J., de Jong, J., Williams, G.A., Hanano, D., Pretorius, W., Mattielli, N., Scoates, J.S., Goolaerts, A., Friedman, R.M., Mahoney, J.B., 2006. High-precision isotopic characterization of USGS reference materials by TIMS and MC-ICP-MS. Geochemistry, Geophys. Geosystems 7, n/a-n/a. https://doi.org/10.1029/2006GC001283

Weyer, S., Anbar, A.D., Brey, G.P., Münker, C., Mezger, K., Woodland, A.B., 2007. Fe-isotope fractionation during partial melting on Earth and the current view on the Fe-isotope budgets of the planets (reply to the comment of F. Poitrasson and to the comment of B.L. Beard and C.M. Johnson on "Iron isotope fractionation during planetary differentiation" by S. Weyer, A.D. Anbar, G.P. Brey, C. Münker, K. Mezger and A.B. Woodland). Earth Planet. Sci. Lett. 256, 638–646. https://doi.org/10.1016/J.EPSL.2007.01.038

White, W.M., 1985. Sources of oceanic basalts: Radiogenic isotopic evidence. Geology 13, 115. https://doi.org/10.1130/0091-7613(1985)13<115:SOOBRI>2.0.CO;2

White, W.M., McBirney, A.R., Duncan, R.A., 1993. Petrology and geochemistry of the Galápagos Islands: Portrait of a pathological mantle plume. J. Geophys. Res. Solid Earth 98, 19533–19563. https://doi.org/10.1029/93JB02018

White, W.M., Tapia, M.D.M., Schilling, J.-G., 1979. The petrology and geochemistry of the Azores Islands. Contrib. to Mineral. Petrol. 69, 201–213. https://doi.org/10.1007/BF00372322

Wiechert, U., Halliday, A.N., Lee, D.-C., Snyder, G.A., Taylor, L.A., Rumble, D., 2001. Oxygen Isotopes and the Moon-Forming Giant Impact. Science (80-.). 294, 345–348.

Wieczorek, M.A., Jolliff, B.L., Khan, A., Pritchard, M.E., Weiss, B.P., Williams, J.G., Hood, L.L., Righter, K., Neal, C.R., Shearer, C.K., McCallum, I.S., Tompkins, S., Hawke, B.R., Peterson, C., Gillis, J.J., Bussey, B., 2006. The Constitution and Structure of the Lunar Interior, in: Reviews in Mineralogy & Geochemistry Volume 60: New Views of the Moon. pp. 221–343.

Willbold, M., Stracke, A., 2006. Trace element composition of mantle end-members: Implications for recycling of oceanic and upper and lower continental crust. Geochemistry, Geophys. Geosystems 7, 1–30. https://doi.org/10.1029/2005GC001005

Williams, H.M., Bizimis, M., 2014. Iron isotope tracing of mantle heterogeneity within the source regions of oceanic basalts. Earth Planet. Sci. Lett. 404, 396–407. https://doi.org/10.1016/J.EPSL.2014.07.033

Williams, H.M., Mccammon, C.A., Peslier, A.H., Halliday, A.N., Teutsch, N., Levasseur, S., Burg, J.-P., 2004. Iron Isotope Fractionation and the Oxygen Fugacity of the Mantle. Source Sci. New Ser. 304, 1656–1659.

Williams, H.M., Nielsen, S.G., Renac, C., Griffin, W.L., O'Reilly, S.Y., Mccammon, C.A., Pearson, N., Viljoen, F., Alt, J.C., Halliday, A.N., 2009. Fractionation of oxygen and iron isotopes by partial melting processes: Implications for the interpretation of stable isotope signatures in mafic rocks. Earth Planet. Sci. Lett. 283, 156–166. https://doi.org/10.1016/j.epsl.2009.04.011

Williams, H.M., Peslier, A.H., Mccammon, C., Halliday, A.N., 2005. Systematic iron isotope variations in mantle rocks and minerals : The effects of partial melting and oxygen fugacity. Earth Planet. Sci. Lett. 235, 435–452. https://doi.org/10.1016/j.epsl.2005.04.020

Williams, H.M., Prytulak, J., Woodhead, J.D., Kelley, K.A., Brounce, M., Plank, T., 2018.

Interplay of crystal fractionation, sulfide saturation and oxygen fugacity on the iron isotope composition of arc lavas: An example from the Marianas. Geochim. Cosmochim. Acta 226, 224–243. https://doi.org/10.1016/J.GCA.2018.02.008

Wing, B.A., Farquhar, J., 2015. Sulfur isotope homogeneity of lunar mare basalts. https://doi.org/10.1016/j.gca.2015.09.003

Wood, B.J., Bryndzia, L.T., Johnson, K., 1990. Mantle Oxidation State and Its Relationship to Tectonic Environment and Fluid Speciation. Science (80-.). 248.

Wood, B.J., Kiseeva, E.S., Mirolo, F.J., 2014. Accretion and core formation: The effects of sulfur on metal-silicate partition coefficients. Geochim. Cosmochim. Acta 145, 248–267. https://doi.org/10.1016/j.gca.2014.09.002

Yi, W., Halliday, A.N., Alt, J.C., Lee, D.-C., Rehkämper, M., Garcia, M.O. 0, Langmuir, C.H., Su, Y., Rehkämper, M., Garcia, M.O. 0, Langmuir, C.H., Su, Y., 2000. Cadmium, indium, tin, tellurium, and sulfur in oceanic basalts: Implications for chalcophile element fractionation in the Earth. J. Geophys. Res. 105, 18,927-18,948. https://doi.org/10.1029/2000JB900152

Yi, W., Halliday, A.N., Lee, D.-C., Christensen, J.N., 1995a. Indium and tin in basalts, sulfides, and the mantle. Geochim. Cosmochim. Acta 59, 5081–5090.

Yi, W., Halliday, A.N., Lee, D.-C., Christensen, J.N., 1995b. Indium and tin in basalts, sulfides, and the mantle. Geochim. Cosmochim. Acta 59, 5081–5090. https://doi.org/10.1016/0016-7037(95)00342-8

Zhao, Y., Xue, C., Liu, S.-A., Symons, D.T.A., Zhao, X., Yang, Y., Ke, J., 2017. Copper isotope fractionation during sulfide-magma differentiation in the Tulaergen magmatic Ni–Cu deposit, NW China. Lithos 286–287, 206–215. https://doi.org/10.1016/J.LITHOS.2017.06.007

Zindler, A., Hart, S., 1986. CHEMICAL GEODYNAMICS, Ann. Rev. Earth Planet. Sci.

5. Nickel isotopic composition of the silicate Moon

5.1. Introduction

The Moon is the only permanent natural satellite of the Earth, and has the largest size relative to its planet of any Solar System satellite. The surface of the Moon is dominated by anorthositic lunar highlands and mafic lunar mare, forming the lowlands. The lunar surface is largely covered by 5-10 m of lunar regolith, a loose layer of heterogeneous material including soils, breccia, and glasses associated with impact and pyroclastic events (e.g. (Meyer, 2003)).

There are several hypotheses for the formation of the Moon, but the most commonly accepted model is that of the Giant Impact. The Giant Impact model was proposed in a different form by Hartmann and Davis (1975), and has been developed and interrogated over the following decades including ever more sophisticated computer simulations (for example see the many works by Canup on this subject e.g. (Canup, 2012; Canup et al., 2013; Canup and Asphaug, 2001). In the Giant Impact model the moon accreted from ejected material after a high energy collision between the proto-Earth and a large planetesimal, named Theia (Halliday, 2000).

The high energy of the Giant Impact collision may potentially have led to a lunar magma ocean (LMO), the presence of which is supported by existence of KREEP and the widespread distribution, chemical composition, mineralogy and ancient isotopic ages of the lunar highland anorthosites (Warren, 1985). The lunar anorthosites indicate a large differentiation event must have occurred in the early evolution of the Moon (Warren, 1985). KREEP rocks are rocks highly enriched in incompatible elements (particularly potassium, rare earth elements, and phosphorus), which are thought to relate to the final product of the fractional crystallisation of a large magma body (Warren and Wasson, 1979). In some literature the final residue of the LMO are termed urKREEP, and basalts contaminated with this material are the KREEP basalts (Neal and Taylor, 1992). No urKREEP has been directly sampled, whereas KREEP basalts have been returned from almost all lunar landing sites, as either basaltic impact melts or pristine basalts of

magmatic origin (Neal and Taylor, 1992). KREEP basalts are generally more enriched in Mg than can be readily explained (Wieczorek et al., 2006).

The lunar crust is feldspathic, and it is thought it was formed as a flotation of plagioclase-rich cumulates from the lunar magma ocean (e.g. Warren, 1985). This is often thought to explain the positive europium anomaly of the highland anorthosites. The feldspathic crust was later overlain in the lowlands by the lunar mare basalts, which all have a complementary negative europium anomaly. Neal (2001) proposed overturn as necessary to introduce the negative Eu anomaly into lunar basalts. Basalts are largely formed from phases that crystallised early, therefore would not be affected by the subsequent Eu fractionation caused by plagioclase crystallisation.

Mare basalts have lower viscosity than comparable terrestrial basalts, causing the lack of relief of the maria, and they are more common on the nearside of the Moon (Neal and Taylor, 1992). Mare basalts are higher in total iron and Fe/Mg, than terrestrial basalts, and have Al_2O_3 <15 wt% (Neal and Taylor, 1992). Mare basalts demonstrate an almost continuous distribution of radiometric ages from 4.3 to 3.0 Ga (Taylor, 1982), suggesting their formation does not relate to impacts, which would produce a more discrete grouping.

The structure of the Moon has been inferred from seismic data and geochemistry. The crust of the Moon is thicker on the farside of the moon compared to the nearside (80-90 km vs 60-70 km) (Neal and Taylor, 1992). Weber and co-workers (2011) used reanalysed Apollo-era lunar seismograms to suggest the Moon had a solid inner and fluid outer core of 1.7% of the lunar mass, overlain by a partially molten silicate layer in the lower mantle. Estimates of siderophile element abundances in the lunar mantle have also been used to argue for the existence of a small lunar metal core comprising 0.1–5.5 wt% of the total lunar mass, depending on the siderophile concentration of the proto-Moon being chondritic or equivalent to the Earth's mantle (e.g. (Newsom, 1986; Righter, 2002)). Without ultramafic lunar xenoliths, mantle geochemistry is estimated from the trace element data of lunar basalt samples that are thought to be partial melts of the lunar mantle (Rai and Westrenen, 2014). The lunar mantle is thought to be heterogeneous in composition, as suggested by the differences in major and trace element chemistry between otherwise similar lunar basalts (Neal and Taylor, 1992). Palaeomagnetic data

on lunar samples has provided evidence for a magnetic field on the Moon from 3.9 to 3.6 Ga (Cisowski et al., 1983).

The Moon has been sampled by a small number of sample return missions (1969 – 1976), and by meteorites. Lunar sample return has been dominated by the NASA Apollo missions, and also Soviet Luna missions, which largely returned samples dominated by soils and small pieces of basalt (generally <1 g). This has led to some problems with representative sample sizes for lunar whole rock analyses (Neal and Taylor, 1992). Samples of lunar material fall into two main categories: crystalline rocks, and pulverized material (soil, breccia, regolith etc), and the crystalline samples generally have lower Ni concentration (Wedepohl, 1974). Lunar meteorites were excavated during impact of the lunar surface, which results in random sampling of unknown areas of the lunar surface. The first lunar meteorite was found in 1979 and the accepted total is now over 385 (Korotev, 2018).

Lunar samples are often classified in three levels, based first on TiO_2 content (<1 wt% = very low-Ti, 1-6 wt% = low-Ti, >6% = high-Ti) second, on Al_2O_3 (<11 wt% = low-Al, >11wt% = high-Al) and thirdly on K contents (<2000 ppm = low-K, >2000 ppm = high-K) as described in Neal and Taylor (1992). This study has followed the example of Neal and Taylor (1992) to look at lunar samples by rock type rather than sample site. Historically, studies classified samples from a single site, but often the classifications were non-transferable when samples from other sites were returned and analysed. This has resulted in at least 21 different types of basalt identified in the literature (Neal and Taylor, 1992).

Nickel concentrations vary between different lithologies and landing sites. The majority of lowland basalts have Ni concentrations <55 ppm, whereas highland rocks have higher Ni concentrations including 110 ppm in gabbroic anorthosite (Wedepohl, 1974). Terrestrial anorthosite ranges from 9 to 23 ppm, with gabbroic anorthosite having concentrations up to 90 ppm (Wedepohl, 1974). This suggests that the Ni concentration is similar in highland lunar rocks to equivalent terrestrial rocks, whereas terrestrial tholeiitic basalts average 134 ppm (Wedepohl, 1974), which is significantly higher in Ni than lowland lunar basalts.

Isotopically the Moon has been shown to be extremely similar to the Earth. The vast majority of elements that have so far been measured show no resolvable difference between the Moon and Earth (examples: O (Wiechert et al., 2001) Si (Armytage et al., 2012), Sr (Moynier et al., 2010), Ca (Simon and DePaolo, 2010), Cu (Moynier et al., 2006), Fe (Wang et al., 2015), Mg (Sedaghatpour et al., 2013) etc.). Some evidence for differences between the isotopic composition of the Earth and Moon has been found in Zn (e.g (Paniello et al., 2012) and (Hopkins et al., in prep), in contrast to earlier work (Moynier et al., 2006).

Nickel, as a non-volatile element, is expected to show a lunar isotopic composition identical to Earth. This, however, has yet to be tested. Nickel is depleted in the lunar mantle relative to CI chondrites (Rai and Westrenen, 2014), and the Moon has much lower basalt Ni concentrations compared with terrestrial basalts. Volcanic glass from the Moon has a higher Ni concentration than the mare basalts, which has been suggested to imply low-pressure fractionation of trace elements during emplacement of the mare basalts (Delano, 1985). The formation of a small core may have fractionated Ni isotopes, but there is no evidence for this process of having occurred during the segregation of the terrestrial core (Gall et al., 2017; Steele et al., 2011).

The process of basalt formation on the Moon occurs without water, other volatiles, and plate tectonics, which contribute to the process on the Earth. Fractional crystallization, assimilation, and source heterogeneity are thought to account for the majority of compositional heterogeneity in low-Ti basalts (Neal and Taylor, 1992).

Nickel isotopes in terrestrial environments have been shown not to fractionate with degree of partial melting or fractional crystallisation (Chapters 3 and 4), and these processes have been suggested to largely affect the composition of basalts at the lunar surface (Neal and Taylor, 1992). Therefore, source heterogeneity and wall-rock assimilation effects, which have been invoked to account for the compositional heterogeneity in lunar basalts, may be isolated by the study of Ni isotopic compositions.

Analysis of Ni isotopic compositions of lunar samples could provide further evidence for the formation mechanism for the Moon and the development of the layered solid body we have

today. Nickel concentration is lower in lunar relative to terrestrial, which investigation of isotopes may further elucidate.

Before evaluating Ni isotopes in lunar samples it is necessary ensure that lunar Ni isotopic compositions are related by mass dependent fractionation. A number of isotopic systems have shown evidence of cosmogenic reactions that produced isotopic anomalies in lunar samples, including vanadium (Hopkins., in prep). For this reason, unspiked samples were analysed and corrected by internal normalisation (results presented in section 5.5).

5.2. Sample background

The samples in this work include low-Ti basalts (specific TiO_2 2 to 5%) and a single example of high-Ti basalt (11.7% TiO_2). One low-Ti basalt is an Al-rich basalt from Apollo 14. The Apollo 14 samples have had their composition explained as fractional crystallisation combined with assimilation of KREEP, as they are rich in K as well as Al. Top surfaces of the majority of the samples have been determined by ^{58}Co (Meyer, 2011).

All the lunar samples studied during this work were collected by NASA Apollo missions, and obtained through NASA CAPTEM. They were collected during Apollo missions 11, 12, 14, and 15, largely from locations along the nearside equator, with the site of Apollo 15 further North. The samples are mare basalts, which have revealed considerable information about lunar volcanism and the nature of the lunar mantle (Neal and Taylor, 1992). These samples were therefore ideal to study these aspects of the Moon through Ni isotopes.

Samples were chosen to test a range of lithologies and localities on the lunar surface. Often the limiting factor in analysis of lunar samples is the amount of Ni in the samples relative to average terrestrial basalts and the amount of material there was available.

Sample 10017 is a fine grained and vesicular ilmenite basalt, with a high K and high-Ti signature (Meyer, 2011). This was the largest sample returned by Apollo 11, and had a rounded surface pitted with micro-meteorite craters prior to breaking, indicating that it had been tumbled on the lunar surface (Meyer, 2011). Numerous groups published detailed petrography of this

sample in 1970, and all described a sample lacking alteration. The mineralogy consists largely of 50-150 μm clinopyroxene, equant 50-150 μm ilmenite, and 2-3 mm plagioclase, with high K glass (Meyer, 2011). There is no olivine in this sample. Neal (2001) showed that Ni was particularly low in this sample. The absolute radiometric age of this sample is between 3.65 and 3.59 Ga (Meyer, 2011). The exposure age has been determined to be distinctly different in the high K basalts relative to the low K (Eberhardt et al., 1970). This sample has published exposure ages of 308 to 510 Ma (see references in Meyer, 2011).

Sample 12002 is a medium grained and porphyritic olivine basalt, with a low-Ti signature (Meyer, 2011). It has not tumbled on the lunar surface (Meyer, 2011). The mineralogy consists largely of phenocrysts of olivine and sector zoned clinopyroxene with plagioclase and ilmenite (Meyer, 2011). The absolute radiometric age of this sample is 3.36 Ga (Papanastassiou and Wasserburg, 1971). This sample has published exposure ages of 92 to 161 Ma (see references in Meyer, 2011).

Sample 12018 is a medium grained olivine basalt, with a low-Ti signature and apparent accumulation of mafic minerals (producing relatively high MgO content) (Meyer, 2011). It has not tumbled on the lunar surface (Meyer, 2011). The mineralogy consists largely of phenocrysts of olivine and pyroxene with plagioclase and ilmenite (Meyer, 2011). It has been described as virtually undeformed and with no observable shock-metamorphic effects (Walter et al., 1971). The average grain size ranges from 0.4 to 1.0 mm (Meyer, 2011). This sample also contains fayalite-K-rich glass-phosphate that has been interpreted as residual melt (El Goresy et al., 1971). This sample has published exposure ages of 170 to 210 Ma (see references in Meyer, 2011).

Sample 12054 is a medium grained ilmenite basalt, with a low-Ti signature and a glass splash covering much of the sample (Meyer, 2011). Three cuts were analysed in this work: interior, exterior, and glass splash. Sample 12054 has not tumbled on the lunar surface (Meyer, 2011). The mineralogy consists largely of lath-shaped plagioclase, and largely equant pyroxene with elongate ilmenite (Meyer, 2011). The sample has been described as equigranular and having a

simple history (Meyer, 2011). The glass coating is a flowed vesicular basaltic melt, which thermally modified the main sample along the contact (Meyer, 2011). This sample has published exposure ages of 0.15 to 0.175 Ma (see references in Meyer, 2011).

Sample 12063 is a medium grained and porphyritic ilmenite basalt, with a low-Ti signature and is the largest sample of lunar material (Meyer, 2011). It had been turned over at least once on the lunar surface (Meyer, 2011). The mineralogy consists largely of phenocrysts of olivine and pyroxene, with ilmenite (Meyer, 2011). The average grain sizes are olivine 0.6-0.8 mm, pyroxene 0.3-1.5 mm, and ilmenite 0.1-0.3 mm (Meyer, 2011). This sample has published exposure ages of 65 to 95 Ma (see references in Meyer, 2011). This sample has been radiometrically dated to 3.3±0.1 Ga (see references in Meyer, 2011). It is believed to have been collected at Bench Crater, but was not identified in surface photography (Meyer, 2011).

Sample 14053 is a medium grained and ophytic Al-rich mare basalt, with a low-Ti signature (Meyer, 2011). It has a low siderophile element content, and is highly reduced (Meyer, 2011). The mineralogy consists largely of large zoned pyroxene, with laths of plagioclase (Meyer, 2011). This sample has published exposure ages of 21 to 25 Ma (see references in Meyer, 2011). It has also been radiometrically dated to 3.9 Ga (see references in Meyer, 2011). It was collected at station C2 at Cone Crater, perched on a boulder, with breccia attached to a flat side of the sample (Meyer, 2011).

Sample 15016 is a medium grained and highly vesicular olivine normative basalt, with a low-Ti signature and high Mg (Meyer, 2011). The mineralogy consists largely of phenocrysts of zoned pyroxene, and olivine, with plagioclase, spinel, and metal (Meyer, 2011). Vesicles make up 50% of the volume (Meyer, 2011). This sample has published exposure ages of 285-315 Ma, and Aluminium 26 is saturated. (see references in Meyer, 2011). It has also been radiometrically dated to 3.34 Ga (see references in Meyer, 2011). It was collected at the Hadley Rille site, where the regolith is very thin (Meyer, 2011). The volcanic magma depth has been experimentally determined to be from > 250 km (Meyer, 2011).

Sample 15535 is a medium grained olivine normative basalt, with a low-Ti signature (Meyer, 2011). The mineralogy consists largely of small equant crystals of pyroxene and olivine, in poikilitic plagioclase, with patches of mafic minerals and opaques (Meyer, 2011). This sample has published exposure ages of 110 Ma (see references in Meyer, 2011). It was collected from a small boulder at the Hadley Rille site, where the regolith is very thin (Meyer, 2011).

Sample 15556 is a fine grained and highly vesicular olivine normative basalt, with a low-Ti signature and high Mg (Meyer, 2011). The grain size is constant in this sample and the mineralogy consists largely of pyroxene, plagioclase, and ilmenite, with minor olivine (Meyer, 2011). Vesicles make up 50% of the volume (Meyer, 2011). This sample has no published exposure ages. It has also been radiometrically dated to 3.4 Ga (Kirsten et al., 1972). It was collected from an area called The Terrace at the Hadley Rille site, where the regolith is very thin (Meyer, 2011).

The samples include examples from pristine powders, and additional samples from the matrix column cut of a Zn purification column, with sufficient overlap to compare for lack of Zn column related Ni fractionation. The same powders have been analysed in the same lab for zinc and vanadium isotopic composition by Sean Hopkins (in. prep). Different cuts of the same samples have been analysed by the Sharp group for Cl, and Farquhar group for S isotopic compositions (pers. comm.).

The concentration of many elements in these samples was determined by separate dissolutions of the same powders analysed on the Perkin Elmer NexION 350D Quadrupole ICP-MS, at the Department of Earth Sciences, University of Oxford.

5.3. Sample preparation

All details of purification and analysis are described in Chapter 2, and summarised below.

Homogenous lunar powder was produced in house by Sean Hopkins by grinding 0.25 g of sample chip in agate, in the lunar lab at the department of Earth Sciences, University of Oxford.

Additional lunar samples were sourced from matrix cuts of a Zn purification column completed by Sean Hopkins, as these cuts contain all the Ni of those samples. Samples from the matrix cuts of the Zn purification column were prepared for column purification by Sean Hopkins, using 60-120 mg from the identical homogenous powder.

All acids used were distilled in house by sub-boiling and diluted by volume with ultrapure 18MΩ MQ water. Powdered samples (10 to 80 mg) were accurately weighed into Teflon vials and dissolved using 1 part HF and 3 parts HNO_3 (2 ml total) followed by dissolution in 6M HCl (up to 5 ml), and the latter by hotplate dissolution. The samples for the mass dependent investigation had the double spike added directly to powder before dissolution. The Zn separation column matrix cut samples weighed as aliquots and dried. For the mass dependent investigation these samples were spiked after the matrix cut was dried, and equilibrated before purification.

Purification of Ni is completed by three ion exchange Teflon microcolumns of diminishing size, based on the procedure of Gall and co-workers (2012). Analysis was performed in pseudo-high resolution on a Nu Instruments Nu Plasma HR MC-ICPMS and measurements reported relative to data for SRM986.

Samples for investigation of potential cosmogenic effects were processed entirely separately to mass dependent samples, without contact with double spike.

Investigation for cosmogenic effects requires more natural Ni than samples that are to be analysed with addition of Ni from double spike. The total Ni was calculated to ensure >200 mV signal on the lowest mass peak 61, resulting in ~ 20V total signal. The equivalent amount of lunar material used was between 20 and 140 mg, depending on Ni concentration.

The MC-ICP-MS used was the same as used throughout this project, although it was cleaned and had many consumables replaced. These included a new torch, new cones, and new nebuliser, and a DSN replacement that had never seen double spike. The bracketing standard of unspiked SRM986 did not go through chemistry, but an in-house standard (Sudbury NiS) and a

USGS sample (BHVO2) were purified with the samples. The results comprise of 18-20 replicates, repeated 3 or 4 times with a fresh baseline between each analysis. The reported composition is the average and reproducibility (2SD) of the 3 or 4 analyses of the sample. The correction for instrumental mass bias (which also corrects for natural mass dependent isotope fractionation in the sample) used in this work uses an exponential fractionation law.

In the cosmogenic work we investigated different normalisation ratios including 61/58 (Quitté and Oberli, 2006) and 62/58 (Chen et al., 2009; Cook et al., 2006; Quitté et al., 2006; Quitté and Oberli, 2006), and 58/61 (Regelous et al., 2008; Steele et al., 2012, 2011) and 62/61 (Steele et al., 2012). In general, normalisations involving ^{61}Ni isotope have greater errors due to the lower voltage on this smallest beam. Normalisations involving 58, are vulnerable to any error in the Fe correction propagating into the isotopic ratio, particularly if 58 is the denominator, causing errors to propagate into all isotopic ratios. The most commonly used normalising and reported ratios were reported here (Table 5-2).

5.4. Results

5.4.1 Mass dependent isotopic fractionation determined using double spiking

Stable nickel isotopic compositions of 11 lunar basalts comprising olivine basalts, ilmenite basalts, Al-rich basalt, and a sample of glass splash are presented in Table 5-1. The replication corresponds to replicate mass spectrometry analyses of the separated solutions. Results are shown for preparations from powder and Zn matrix cuts. A comparison between the data for 5 samples measured both ways to evaluate consistency is shown in Figure 32. It can be seen that four out of the five show excellent agreement and lend confidence to the expectation that, given the near quantitative separation of Ni in the aliquot associated with Zn chemical separation, there should be no isotopic fractionation associated with this stage of treatment. However, one matrix aliquot is significantly heavier than the data for the corresponding powder. No obvious source of contamination could generate this difference. It is unlikely that the difference originates from fractionation on the Zn purification column, as this would be expected to be

observable in all samples. However, if one Zn column had incomplete Ni separation, this might result in a fractionation, such as is observed.

Table 5-1

Table of mass dependent Ni isotopic compositions from lunar samples measured relative to SRM986.
Lithological designations taken from (Meyer, 2011). Sample numbers include sample (5 digits) and cut (3 digits). Nickel concentrations from isotope dilution, and n is the number of separate analyses of the sample. External reproducibility on Ni isotopic composition measurements = 0.06‰.

			Powder				ZnMatrix			
Sample	**Rock Type**		**Ni / ppm**	**$\delta^{60/58}$Ni (‰)**	**2sd**	**n**	**Ni / ppm**	**$\delta^{60/58}$Ni (‰)**	**2sd**	**n**
High-Ti basalt										
10017 405	High K Ilmenite basalt	Interior	5.52	**0.288**	0.001	2				
Low-Ti basalt										
12002 598	Olivine basalt		102	**0.095**	0.048	4				
12018 277	Olivine basalt						63.4	**0.320**	0.011	2
12054 13	Glass splash of an ilmenite basalt	Glass splash	18.9	**0.348**	0.026	4	17.6	**0.334**	0.047	2
12054 146	Glass-coated ilmenite basalt	Interior					9.61	**-0.003**	0.069	2
12054 150	Glass-coated ilmenite basalt	Exterior					5.83	**0.187**	0.000	2
12063 343	Ilmenite basalt		31.1	***0.210***	0.030	4	27.0	***0.443***	0.007	2
14053 305	Al-rich basalt		11.2	**-0.203**	0.017	4	9.92			
15016 240	Vesicular olivine-normative basalt		67.4	**0.254**	0.030	4	49.3	**0.227**		
15535 165	Olivine normative basalt		66.8	**0.260**	0.039	4	57.3	**0.297**		
15556 258	Vesicular olivine-normative basalt		45.2	**0.203**	0.018	4	43.1	**0.175**		

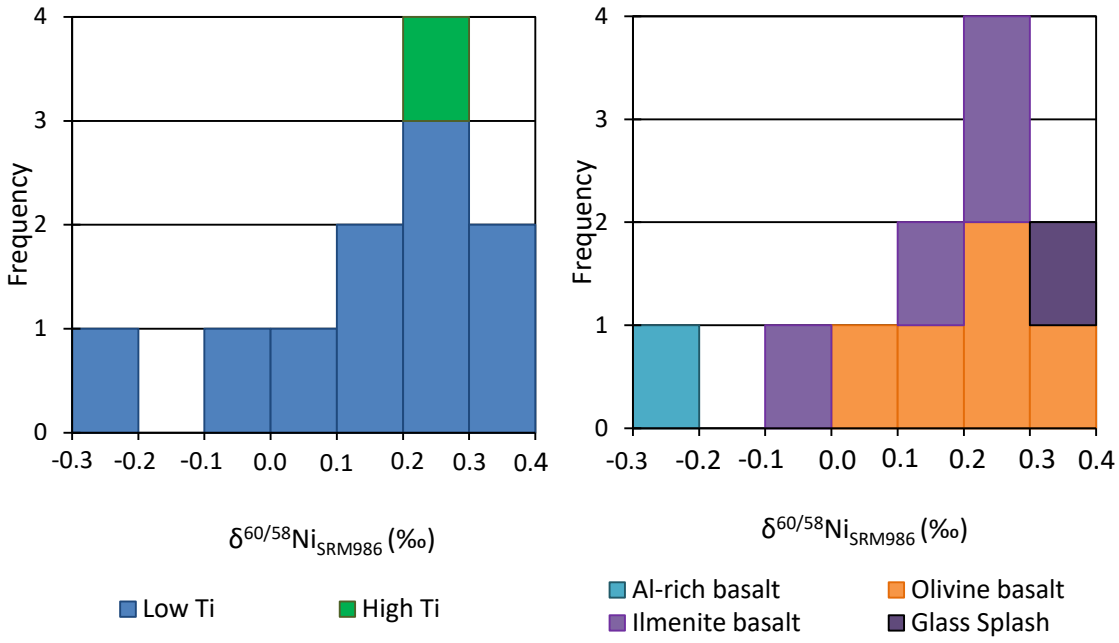

Figure 31

Histograms of Ni isotopic compositions for samples analysed in this work, averaged from results from Zn matrix cuts and powdered samples (see Appendix 7.7) and subdivided by (a) Ti classification and (b) lithological classification. External reproducibility in Ni isotopic composition is 0.06‰.

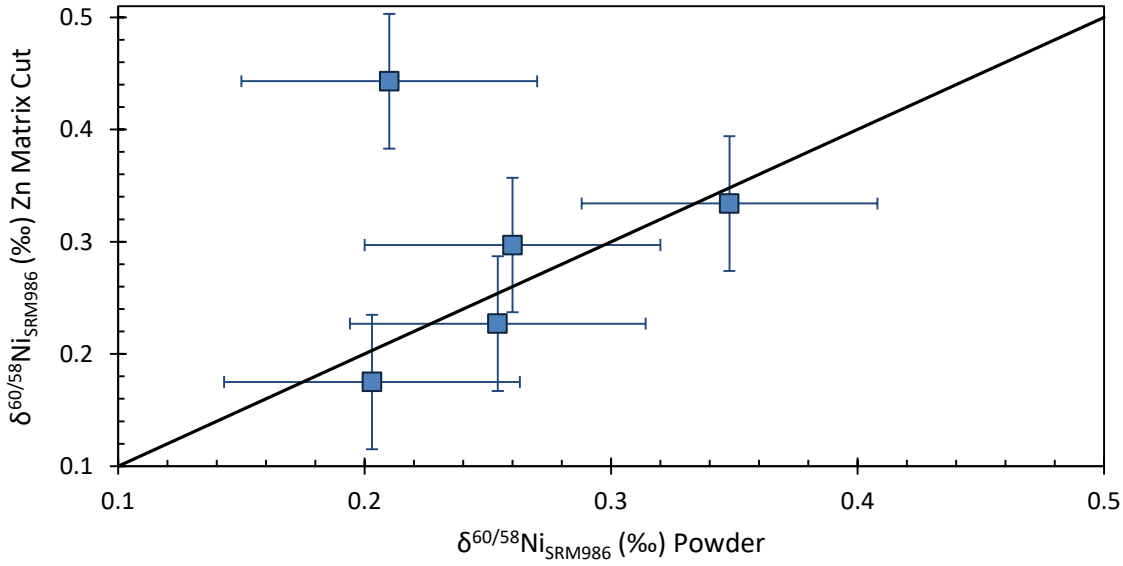

Figure 32

Plot comparing Ni isotopic composition of the lunar samples analysed from pristine powder and from matrix cuts from the Zn column, with a 1:1 line for comparison. Error bars are 0.06‰ representing the external reproducibility of the analyses. Four of the five samples are within error of the 1:1 line, with one outlier with a heavy Ni isotopic composition in the Zn matrix cut sample.

Ten low-Ti basalts were sampled over a range of lithologies and they show a large range in Ni isotopic composition from -0.20 to 0.34‰ (excluding the outlier of 12063 analysed from Zn matrix cut). The heaviest Ni isotopic composition is found in the glass splash that covered one ilmenite basalt sample. This sample is thought to be produced from a nearby impact showering the melt over the adjacent material. The lightest lunar Ni isotopic composition is the sole example of aluminium rich basalt. The only example of high-Ti basalt has a Ni isotopic composition of 0.29‰, which is approximately the same as the modal average of all lunar compositions.

Ilmenite basalts (excluding the glass splash) average $\delta^{60/58}Ni_{SRM986}$=0.17±0.21‰ (n=4) and have a range of 0.29‰. If the high-Ti basalt sample is excluded, because the genesis of high-Ti basalts is thought to be separate to the low-Ti, the average becomes 0.13±0.19‰ (n=3) with a range of 0.21‰. A similar range of 0.23‰ is found in olivine basalts, which average 0.23±0.15‰ (n=5).

5.5. Potential cosmogenic effects

Cosmogenic effects are the result of cosmic ray bombardment of the lunar surface. Isotopes of an element are enriched or depleted relative to their natural abundance as a result of irradiation. This is a major complication for deciphering the original magmatic composition of a lava on the lunar surface. Indeed, for some transition metals with extreme atomic abundances, such as vanadium, cosmogenic effects can entirely dominate the isotopic variability (Hopkins et al., in prep).

The Ni isotopic compositions of the lunar samples do not form a correlation with the exposure ages of the samples (Meyer, 2011) as seen in the left panel of Figure 33. This supports the view that the Ni isotopic composition is not affected by cosmogenic processes. Cosmogenic effects have induced apparent isotopic fractionations in other isotope systems for example the production of ^{182}W from ^{181}Ta by neutron capture (Leya et al., 2000). However, as exposure age controls the magnitude of such effects, and Ni isotopic composition does not trend with

exposure age, it is unlikely that Ni is affected by these processes. The lack of correlation with Ni isotopic composition and exposure age is further evidence that the analysed compositions are the result of intrinsic mass-dependent fractionation. Cosmogenic effects have been suggested to dominate V isotopic compositions analysed on the same sample aliquots by Sean Hopkins (in prep.) are shown in Figure 33 (right) plotted against the Ni isotopic composition. No correlation is observed in this data, also supporting that cosmogenic effects are not affecting Ni isotopic compositions.

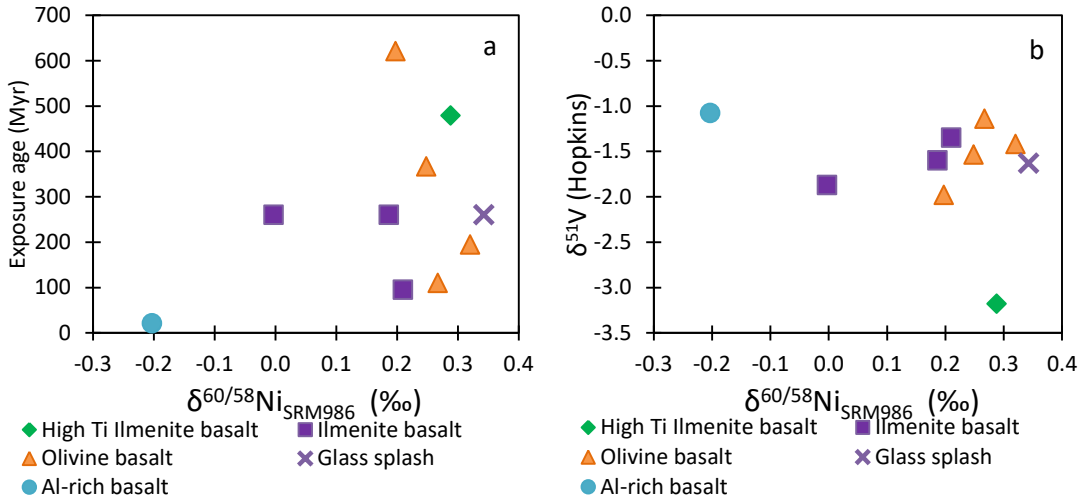

Figure 33

a: Nickel isotopic composition of lunar basalt samples plotted against the exposure age for the same samples (Meyer, 2011). No single trend is found within the data. External reproducibility on Ni isotopic composition is 0.06‰.
b: Nickel isotopic composition of lunar basalt samples plotted against V isotopic composition from Hopkins and co-workers (in prep.) on the same sample cuts. External reproducibility on Ni isotopic composition is 0.06‰, and on V data is 0.2 to 0.58‰..

Cosmogenic effects can be evaluated more comprehensively by measuring the unspiked Ni isotopic composition. The effects should not be as extreme in Ni as in, for example, V but can be evaluated by using an unspiked aliquot and internal normalisation to correct for mass discrimination during processing and mass spectrometry, as previously conducted for studying Ni nucleosynthetic and radiogenic effects (e.g. (Quitté et al., 2006)). They are expressed in epsilon units (ϵ, 10^4) relative to a terrestrial standard composition. Therefore, an epsilon value of zero within uncertainty relative to a terrestrial rock standard processed the same way would indicate no resolvable effect in the sample.

Nucleosynthetic effects have been identified on isotope ^{62}Ni, as it is overproduced in type Ia supernovae (Steele et al., 2011). Isotope ^{60}Ni has a contribution from decay of short lived radioactive isotope ^{60}Fe (half-life= 2.6 Ma (Rugel et al., 2009)). Mass 61 is the least abundant Ni isotope, which if used in the normalisation process can propagate the increased error associated with low signal into all the isotopes. The isotope ^{58}Ni also has an Fe interference correction, which if used in the normalisation process can propagate any error in the correction into all the isotopes. Here we present the ratios and normalisations most commonly used in the literature $\epsilon^{62/61}Ni_{58/61}$, $\epsilon^{61/58}Ni_{62/58}$, $\epsilon^{60/58}Ni_{62/58}$, and $\epsilon^{60/61}Ni_{58/61}$.

Results are presented in Table 5-2. All lunar samples except 15556 were analysed from material separated from the matrix from the Zn column. All samples (lunar, and standards) were analysed at the same total signal (18.5-20.8 V). Samples and standards were analysed in 4 blocks of 18-20 ratios, with the exception of 15016 and 15556 (P), which had sufficient sample for 3 blocks of 20 ratios only (at the same signal intensity), and two examples of standards which ran out of solution during the last of the 4 blocks.

The process used to produce SRM986 has previously been shown to have induced a mass dependent fractionation in Ni (Tanimizu and Hirata, 2006), and may also not truly represent terrestrial composition for cosmogenic analysis. The USGS basalt standard BHVO2 represents terrestrial Ni isotopic composition, and was processed with the samples, and analysed twice during the run (each at 3 or 4 blocks of 18 ratios). Therefore, BHVO2 should serve as a more reliable baseline for comparing lunar samples.

Secondary standard Sudbury was analysed multiple times during the analytical sessions. It has a resolvable different stable Ni isotopic composition relative to the BHVO2 terrestrial standard.

Table 5-2

Comparison of unspiked Ni isotopic ratios for lunar samples, and reference materials expressed in Epsilon
All lunar samples prepared from Zn matrix cuts and pristine powder (15556). Data reported for the most common reported and normalising ratios in the literature, relative to the analysed composition of BHVO2. Internal reproducibility is reported as 2SE.
The external reproducibility was taken as the larger value from repeated analyses of standards BHVO2 and Sudbury.

	Eps 62/61	2SE	Eps 61/58	2SE	Eps 60/58	2SE	Eps 60/61	2SE
Normalised to	58/61		62/58		62/58		58/61	
BHVO2	**0.000**	0.173	**0.000**	0.131	**0.000**	0.167	**0.000**	0.215
Sudbury	**0.446**	0.266	**-0.337**	0.201	**-0.656**	0.039	**-0.454**	0.156
12018	**-0.123**	0.166	**0.093**	0.125	**-0.810**	0.060	**-0.901**	0.097
12063	**0.197**	0.264	**-0.149**	0.200	**-0.163**	0.122	**-0.124**	0.233
15556	**0.087**	0.240	**-0.066**	0.181	**-0.400**	0.049	**-0.370**	0.165
15556 (P)	**0.131**	0.205	**0.251**	0.155	**-0.391**	0.066	**-0.584**	0.141
15016	**-0.254**	0.132	**0.192**	0.100	**-0.603**	0.028	**-0.737**	0.090

Run precision or internal reproducibility (2SE on the number of ratios in the calculate composition) never exceeds 0.3 epsilon units on any ratio for this work. External reproducibility can be estimated from the repeat analyses of BHVO2 and Sudbury (2SD on repeated analyses). Both internal and external reproducibility are reported in Table 5-3, and compared to those reported in the literature.

Table 5-3

External reproducibility for this work compared with published uncertainties
Published uncertainties from (Chen et al., 2009; Cook et al., 2006; Quitté et al., 2006; Quitté and Oberli, 2006; Regelous et al., 2008; Steele et al., 2012, 2011) relative to the maximum internal reproducibility of the analyses for this work, and the reproducibility of BHVO2 analysed twice during the analytical session

	Eps 62/61	Eps 61/58	Eps 60/58	Eps 60/61
Normalised to	58/61	62/58	62/58	58/61
Our study, max int rep	**0.293**	**0.222**	**0.259**	**0.277**
Our study, max ext rep (BHVO2)	**0.126**	**0.095**	**0.615**	**0.571**
Quitte&Oberlie 2006		1.2	0.5	
Quitte et al 2006		0.6	0.3	
Cook et al 2006		0.08	0.06	
Chen et al 2009		0.5	0.1	
Regelous et al 2008	0.1			0.05
Steele et al 2011	0.06			0.04
Steele et al 2012	0.05			0.03

Table 5-3 shows that the reported errors in the literature have improved with recent advances. Our data has similar internal reproducibility, or better, than the literature equivalents except for $\epsilon^{62/61}$Ni and $\epsilon^{60/61}$Ni (both normalised to 58/61). It is suspected that the large errors of this ratio relate to the low voltage isotope 61 being the denominator in both cases. With larger amounts of material, allowing more ratios and higher signal such as have been analysed in the literature, the internal reproducibility would be reduced. The external reproducibility could have been improved with further replicates, as one of the analyses of BHVO2 had an extreme composition for $\epsilon^{60/58}$Ni and $\epsilon^{60/61}$Ni, relative to SRM986, which is unlikely to be accurate to the true composition.

Further validation of the run can be obtained by comparing the epsilon/amu value for the samples to show no residual mass dependent fractionation in the resulting sample composition. There is a difference in epsilon/amu in this work that suggests the epsilon does not reflect uncorrected mass dependent fractionation.

The analysis of USGS standard BHVO2 may also be used to confirm the validity of the run, by comparing the resulting isotopic composition of with the published data. The error are the average of the internal precision of the analyses in this run. The BHVO2 sample analysed in this work has a Ni isotopic composition identical to BSE estimates in the literature and the SRM986 in $\epsilon^{60/61}Ni_{58/61}$ and $\epsilon^{61/58}Ni_{62/58}$. The other ratios are outside of error of SRM986 ($\epsilon^{60/61}Ni_{58/61}$ and $\epsilon^{60/58}Ni_{62/58}$).

One non mass dependent Ni analysis for BHVO2 has previously been published (Regelous et al., 2008), shown in Table 5-4. Comparing this with the analysed result for BHVO2, $\epsilon^{62/61}Ni_{58/61}$ overlaps with the value analysed in this work, although thee error is larger. The other comparable ratio, $\epsilon^{60/61}Ni_{58/61}$, has a much larger error in this study, but does not show any overlap in composition. This is suspected to relate to the small size of the voltage peaks on isotope 61, as the denominator in both parts of the composition, because of the limited material available for analysis.

Table 5-4

Compositions for unspiked Ni isotopic composition for BHVO2, with published equivalent
Published data from (Regelous et al., 2008), with errors reported as 2SE internal precision

	Eps 62/61	2SE	Eps 60/61	2SE
Normalise to	58/61		58/61	
Our study	**0.05**	0.17	**0.61**	0.21
Regelous et al, 2008	**0.00**	0.10	**0.00**	0.05

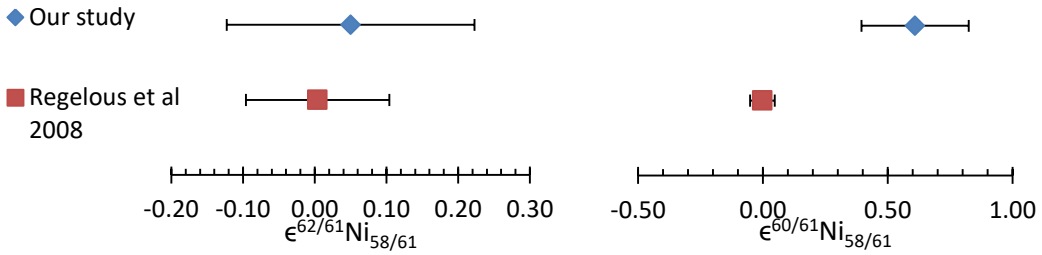

Figure 34

Nickel isotopic compositions analysed for cosmogenic effects as $\epsilon^{62/61}Ni_{58/61}$ and $\epsilon^{60/61}Ni_{58/61}$ for USGS basalt BHVO2, with results as analysed in this work and (Regelous et al., 2008). Error bars are 2SE (Regelous et al., 2008) internal reproducibility

5.5.1. Comparison between powdered sample and sample from Zn matrix column cut

Only one lunar sample was analysed both from powdered material and from material from the matrix of the Zn column. This sample showed variable epsilon values for each preparation (Figure 35), but are within error on the individual analyses (2SE internal reproducibility).

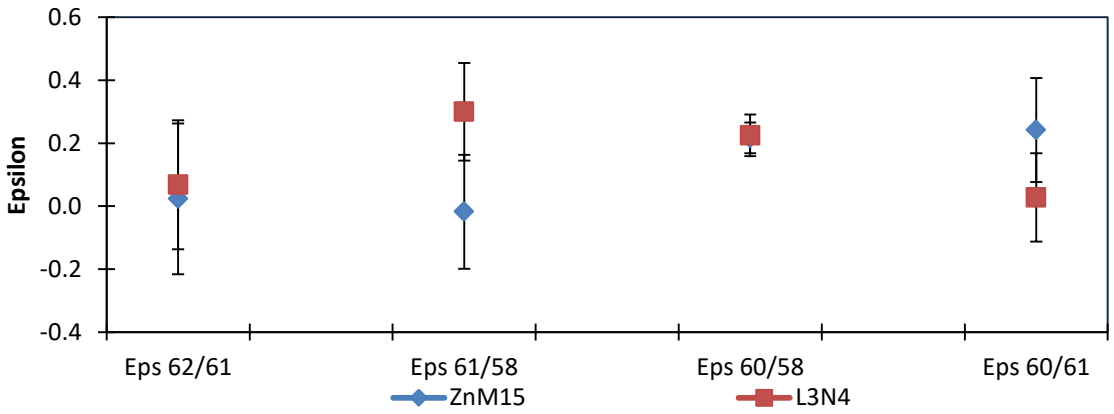

Figure 35

Comparison of 15556 analysed from Zn matrix cut (ZnM15) and from powder (L3N4). Error bars are 2SE internal reproducibility. The samples overlap for all reported ratios.

5.5.2. Cosmogenic effects

The analyses of potential cosmogenic effects in these samples were hampered by insufficient sample material, due to the low Ni concentration and limited source material in lunar basalts. Therefore, few samples were analysed to test for cosmogenic effects, and insufficient replicates lead to larger errors. However, a number of conclusions can still be drawn.

Secondary standard Sudbury (a NiS from an impact site, that may have meteoritic contribution), has a resolvable different Ni isotopic composition than the BHVO2 terrestrial standard. This may be indicative of meteoritic mass independent anomalies in Ni isotopes, such has been observed in earlier studies (e.g. Regelous et al., 2008).

The four main reported compositions in the literature are displayed in Figure 36, where all samples are reported relative to the analysed composition of BHVO2, representing the terrestrial Ni isotopic composition. For ‘a’ and ‘b’ the samples of lunar material are within error of zero and these are the isotopic ratios that had better reproducibility for BHVO2 and better agreement for BHVO2 and the literature (for BHVO2 and terrestrial earth). Both these ratios do not measure the isotope ^{60}Ni. Plots ‘c’ and ‘d’ show more variable compositions and poorer reproducibility of BHVO2. This suggests an analytical artefact in the measuring of these ratios, rather than an indication of cosmogenic reactions in the lunar samples. In both cases, however, the numerator of the sample is ^{60}Ni. Cosmogenic effects have been suggested to produce ^{60}Fe from Ni (Reedy and Englert, 1986). There is a possibility that this may be affecting the analysis of this isotope, if there is any residual Fe in the purified sample, which unlike ^{58}Fe is not corrected for in the maths. However, the fact that these isotopic ratios are the ones with the greatest deviation from terrestrial in BHVO2, which should not have any cosmogenic effects, suggests the variability is an artefact of the poor analysis of these ratios.

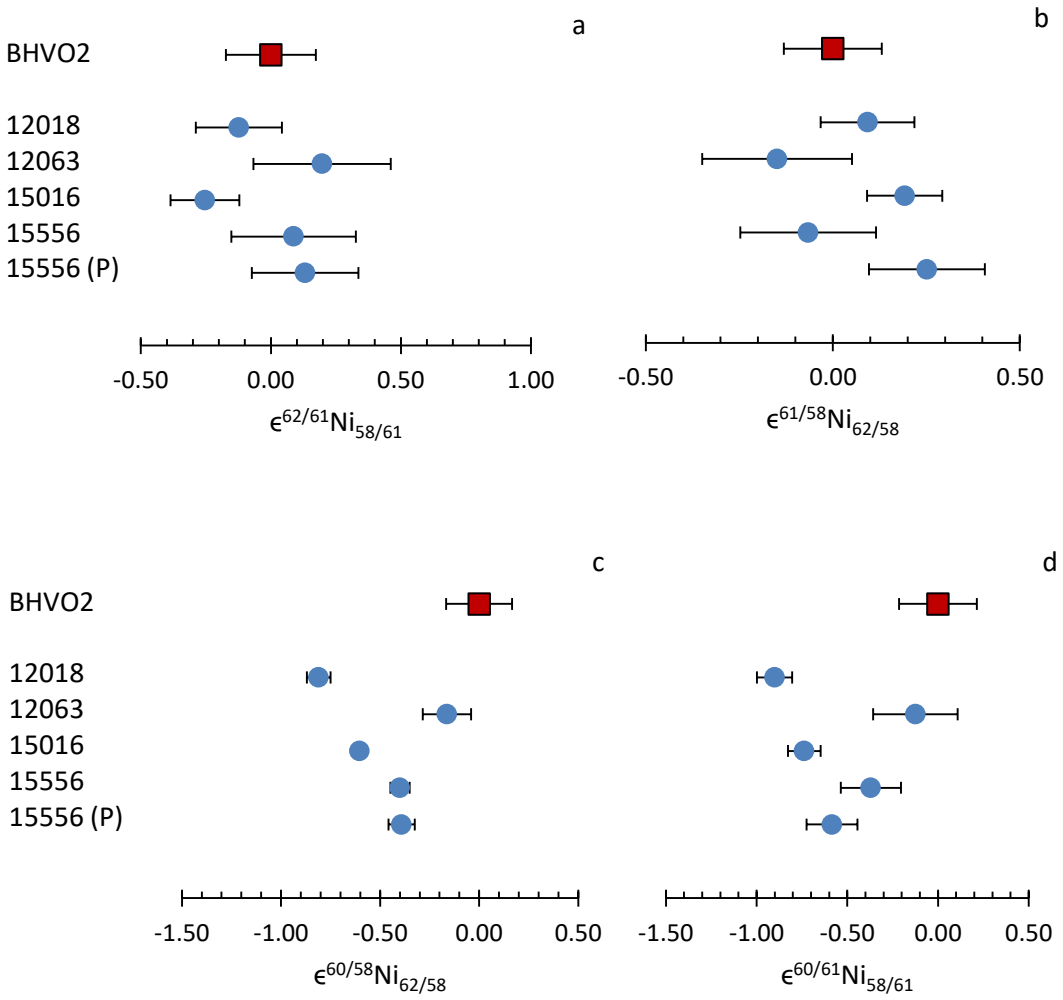

Figure 36

Nickel isotopic compositions for lunar samples normalised to the analysed composition of BHVO2 (terrestrial). Error bars are 2SE of the internal precision. All samples from Zn matrix cuts except suffix P.

In Figure 37, isotopic compositions for mass independent fractionation are plotted against $\delta^{60/58}Ni_{SRM986.}$ Plotted relative to the composition of BHVO2, the only sample in plots 'a' and 'b' with an extreme $\delta^{60/58}Ni_{SRM986}$ and extreme unspiked composition is Sudbury, which has suspected mass independent fractionation. Sample 12018 has one of the more extreme $\delta^{60/58}Ni_{SRM986}$ of the lunar suite, but Figure 37 'a' and 'b' shows this sample to be less extreme in unspiked ratio than other lunar samples. Plots 'c' and 'd' of Figure 37 represent unspiked ratios that have been previously suggested to have been poorly analysed. Indeed, in these plots the lunar compositions fall on an apparent negative correlation from BHVO2 to more extreme $\delta^{60/58}Ni_{SRM986.}$

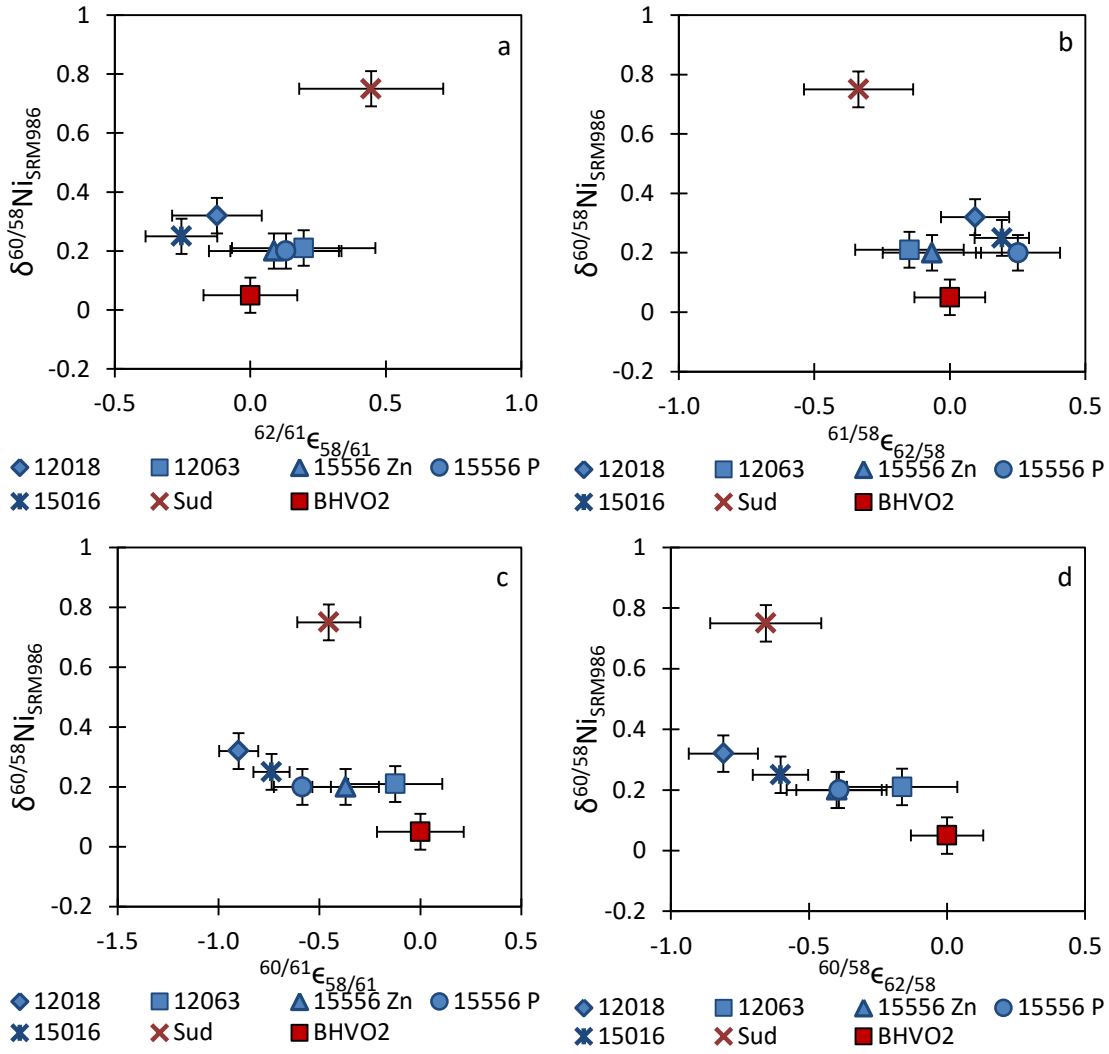

Figure 37

Nickel isotopic composition in epsilon relative to analysed BHVO2 value, plotted against mass dependent Ni isotopic composition in $\delta^{60/58}Ni_{SRM986}$. Error bars are 2SE of internal reproducibility, mass dependent error is 2SD of external reproducibility (0.06‰). All are analysed from Zn Matrix cut, except suffix 'P'.

The apparent negative correlation within the lunar samples between $\delta^{60/58}Ni_{SRM986}$ and both $\epsilon^{60/58}Ni_{62/58}$ and $\epsilon^{60/61}Ni_{58/61}$ (shown in 'c' and 'd' in Figure 37) may relate to the aforementioned analytical problem suspected on isotope ^{60}Ni, as this is the numerator in all the isotope ratios reported in these plots.

The results of this investigation of potential cosmogenic effects, suggest that there is no conclusive evidence of mass independent fractionation in the lunar samples. Without strong evidence of cosmogenic effects in the lunar samples, for further discussion the measured $\delta^{60/58}Ni_{SRM986}$ are entirely attributable to intrinsic mass dependent effects.

5.6. Discussion

5.6.1. Comparison between $\delta^{60/58}Ni_{SRM986}$ in lunar and terrestrial mafic samples

Terrestrial mafic samples average $\delta^{60/58}Ni_{SRM986}$=0.07±0.17‰ (n=41), with no difference in average isotopic composition of MORB and OIB. Lunar basalts have an average Ni isotopic composition 0.18±0.31‰ (n=11), which is heavier than the terrestrial equivalent, and with a larger spread. The distribution of these sample sets is plotted in Figure 38, normalised in terms of frequency relative to total analysed samples. The distribution with the lunar samples has a negative outlier due to the Al rich basalt with light $\delta^{60/58}Ni_{SRM986}$. The average composition for unmetasomatised fertile peridotite produced by this work is $\delta^{60/58}Ni_{SRM986}$=0.20±0.08‰ (n=18), which agrees with previous estimates (see Chapter 3). The modal average of terrestrial mafic samples is lighter than the BSE, whereas the modal average of the lunar samples is heavier than the BSE.

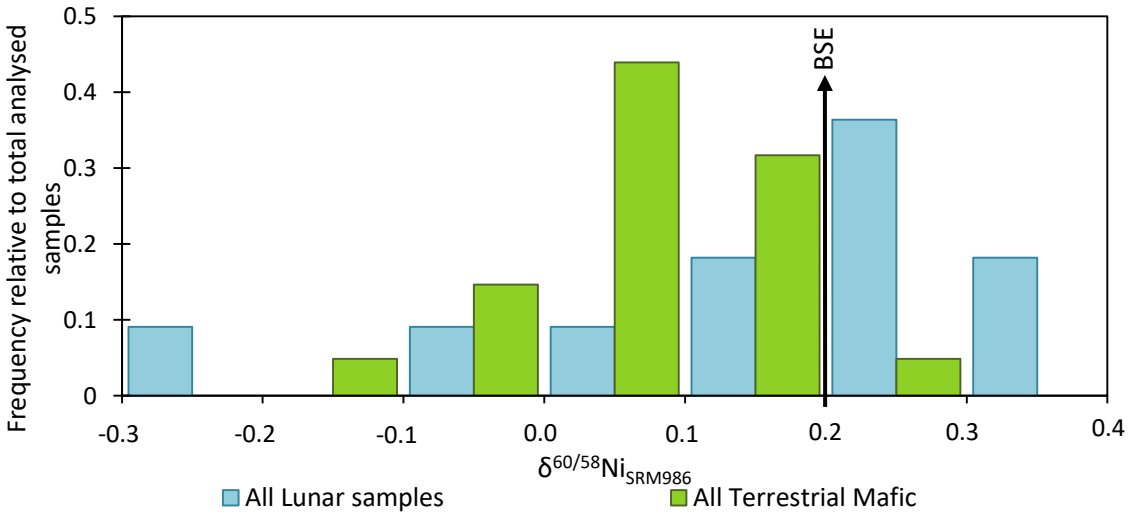

Figure 38

Comparison of the Ni isotopic composition of terrestrial mafic samples with lunar mafic samples, with frequency relative to total analysed samples for comparable scale. The lunar samples have a heavier distribution of Ni isotopic composition than the comparable terrestrial rocks, but also have the more extreme light Ni isotopic composition. The estimate of the unmetasomatised fertile peridotite from this work is depicted for reference. External reproducibility in Ni isotopic composition is 0.06‰.

The predominantly heavier Ni isotopic compositions of the lunar samples relative to the BSE and terrestrial mafic samples is suggestive of a major difference in the $\delta^{60/58}Ni_{SRM986}$ of the source regions or in fractionating processes. Terrestrial basalts display a variable signature of lighter Ni isotopic compositions thought to reflect different amounts recycled pyroxenitic material (Chapter 4). The moon lacks a method of recycling to produce domains of lighter Ni isotopic composition to mix with the lunar mantle in the source regions of magma generation. This would explain why the average lunar basalt composition is heavier in Ni isotopic composition than the equivalent terrestrial average.

There is significantly more variability in the compositions of the lunar samples than the terrestrial equivalents. The 2SD of the average of the lunar samples is nearly twice the value for terrestrial samples, even with a relatively small sample size (a quarter of the terrestrial). Without recycling of material on the Moon, there is evidently another process causing fractionation of $\delta^{60/58}Ni_{SRM986}$ on the Moon.

Magma generation on the Moon is less well understood than on Earth. Two main theories exist as summarised in (Taylor, 1975):

1. impact melting, with association of impact structures on the opposite side to areas of mare basalt
2. tidal melting (Peale and Cassen, 1978), suggested because areas of mare basalt are more extensive on the nearside, leading to suggestions of tidal forcing relating to proximity of the Earth.

Tidal melting provides a reason for cessation of lunar volcanism because the distance between the Moon and the Earth has been increasing with time. Over time, this would reduce the effect the tidal forcing could have of the Moon and eventually be insufficient to induce melting.

The theory of impact melting has been considered unlikely since the early days of lunar planetary science. Objections have included the distinct composition of the mare basalts to the highlands, the older age of the highland rocks, and the implication with impact melting of a

layered lunar structure at odds with geophysical data (Taylor, 1975). Individual impact sites may cause small scale localised melting but are not thought to be volumetrically significant (Taylor, 1975).

Partial melting in the lunar interior requires lunar melts to be less dense than the Moon overall (Taylor, 1975). This theory may well explain the chemistry, mineralogy, high pressure, and melting studies, but it needs to also explain the old age of the lunar basalts, with no rocks sampled with ages less than 3.16 Ga (Taylor, 1975), which is likely to be decaying of the power of the sources of heat for melting. The latter has been a line of potential evidence for tidal melting in the nearside, which ceased as the Moon moved sufficiently away from the Earth (Hiesinger and Head III, 2006). It is unlikely, given the lack of effect terrestrial melting processes have on Ni isotopic composition, that a melting process on the Moon could induce a fractionation in $\delta^{60/58}Ni_{SRM986}$.

Jana and Walker (1997) reported experimental data showing Ni partition coefficients were invariant to silicate melt polymerisation, as affected by compositional variation. Righter and co-workers (2010) showed limited but systematic change in the partitioning behaviour of Ni with increased temperature, with Ni becoming fractionally less compatible in metal with increased temperature, agreeing with earlier results (Gessmann and Rubie, 2000; Righter et al., 1997). This suggests that compositional differences between the Earth and Moon cannot introduce changes in partitioning of Ni, to cause potential isotopic fractionation.

A major difference between the basalts of the Earth and Moon is the oxidation state under which they were produced. Oxidation state, or oxygen fugacity, refers to the chemical potential of oxygen in an environment. Low oxygen fugacity is indicative of reducing conditions. Reducing conditions favour the formation of, for example, Fe^{2+} or Fe^{0} (metal) rather than Fe^{3+}. Indeed, the earliest samples returned showed metal as a primary igneous phase, which is not possible at terrestrial upper mantle oxidation states, and eary experimental work identified the oxygen fugacities of lunar basalts as up to 2 orders of magnitude lower in than terrestrial basalts (Sato et al., 1973).

Lunar basalts have recorded values for oxygen fugacity ranging from close to the Iron-Wüstite (IW) buffer to ~2 log units below it, and the current best estimate of the fO_2 of the lunar mantle is between 1.7 and 2.1 log units below the IW buffer (Rai and Westrenen, 2014). Ferric iron (Fe^{3+}) has been shown to be almost entirely absent in lunar basalts (Wadhwa, 2008). In contrast, terrestrial mantle rocks have shown that the oxygen fugacity of the upper mantle is relatively high (Wood et al., 1990), even though the abundance of oxidized iron (Fe^{3+}) is low (Canil et al., 1994), due to the aforementioned olivine preference for Fe^{2+}. Wood and co-workers (1990) report terrestrial upper mantle fO_2 ranging from -1.5 to +1.5 log units relative to the fayalite-magnetite-quartz buffer (FMQ, more oxidised than IW), with lower values from continental extension and higher values from active subduction zones.

Early work at low oxygen fugacities suggested that Ni could become incompatible in olivine and pyroxene, which was thought to relate to a change in oxidation state of Ni (Ehlers et al., 1992; Steele et al., 1991). In contrast, Capobianco and Amelin (1994) determined that, for their experiments, Ni remained divalent throughout. This was further supported by Holzheid and co-workers (1997) for log fO_2 = +1.5 to -3 (IW), and also by Dingwell and co-workers (1994) for log fO_2 = -8.5 to -13.75 (atm). Capobianco and Amelin (1994) also found that at low oxygen fugacities the solubility of Ni in silicate could not be fully accounted for by a simple oxidation-reduction equilibrium constant (Capobianco and Amelin, 1994). Holzheid and co-workers (1997) showed that Ni solubility increases with increasing fO_2, but is invariant to FeO and MgO content. Wood and co-workers (2014) showed that Ni partitioning is invariant to oxidation state but affected by high S content. Subsequent work showed this is unlikely to affect Ni in the Moon, as the bulk lunar S contents are insufficient to reach the realm where Ni partitioning could be affected (Steenstra et al., 2016).

Recent work on Ni partitioning has showed that there are two pressure regimes in the temperature and pressure dependences of Ni–Fe, with temperature becoming less significant at 5 GPa (Kegler et al., 2008). Different regimes in pressure dependence on Ni partitioning was supported by further experiments by Fischer and co-workers (2015), who showed that at low pressures, Ni becomes less siderophile relative to iron with increasing temperature, but as

pressure increases, Ni partitioning becomes less sensitive to temperature and at ~45 GPa the temperature dependence reverses.

With the Moon considerably smaller than the Earth, pressure dependence may affect partitioning of Ni differently under lunar conditions relative to terrestrial. In particular recent models have suggested the lunar core-mantle boundary is at approximately 5 GPa (Garcia et al., 2011; van Kan Parker et al., 2012). The core-mantle boundary pressure on Earth has been estimated at ~140 GPa (Dziewonski and Anderson, 1981). The maximum pressure on the Moon to affect Ni partitioning is therefore 28 times less than the equivalent on Earth. This implies, based on the conclusions of Fischer and co-workers (2015), that the proportion of Ni in the lunar core is less than on Earth. The proto-Moon formed largely from the mantle of the Earth, then formed a small lunar core, under much lower pressures than on Earth. This may have caused a fractionation of Ni isotopes during the segregation of Ni into the metal core, in a way that is not thought to have happened on Earth (Gall et al., 2017).

In addition, reducing conditions, such as found on the Moon, produce more Fe^{2+} or Fe^{0} (metal) than Fe^{3+}. Olivine rarely incorporates Fe^{3+}, even if the environment is oxidising like the terrestrial upper mantle, due to the easy substitution of Fe^{2+} and Mg^{2+} (McCammon, 2005). Other mantle minerals (spinel, garnet) are more readily able to favour incorporating the oxidised iron into their structures (McCammon, 2005). In contrast, perovskite, dominant mineral phase in the terrestrial lower mantle stabilizes 50% of the iron as Fe^{3+} (Frost et al., 2004). A proposed effect of the high Fe^{3+} in the lower terrestrial mantle perovskite is to increase the Fe^{0} content of the lower mantle to balance the charge (McCammon, 2005). Nickel (Ni^{2+}) substitutes easily for similar sized Mg^{2+}, but also for Fe^{2+}. With increased quantities of Fe^{2+} in the region of melt generation on the Moon relative to the Earth, increased competition for compatible mineral lattice spaces for Ni^{2+} may affect the behaviour of Ni. The partitioning of Ni into alternative mineral lattice sites may, therefore, induce an isotopic fractionation in lunar basalts that is absent on Earth.

5.6.2. Lunar nickel isotopes and time

Six out of 11 of the samples have radiometric ages (Meyer, 2011; Papanastassiou and Wasserburg, 1971) and it can be seen (Figure 39) that the lightest sample (Al rich basalt 14053), is the oldest sample. The next oldest sample, the high-Ti basalt (10017) is relatively heavy however, and there is no well-defined relationship between age and Ni isotopic composition. The apparent correlation with absolute age is dominated by a single sample, 14053. Without 14053, the other samples have heavier Ni isotopic compositions, and lack a correlation with absolute age.

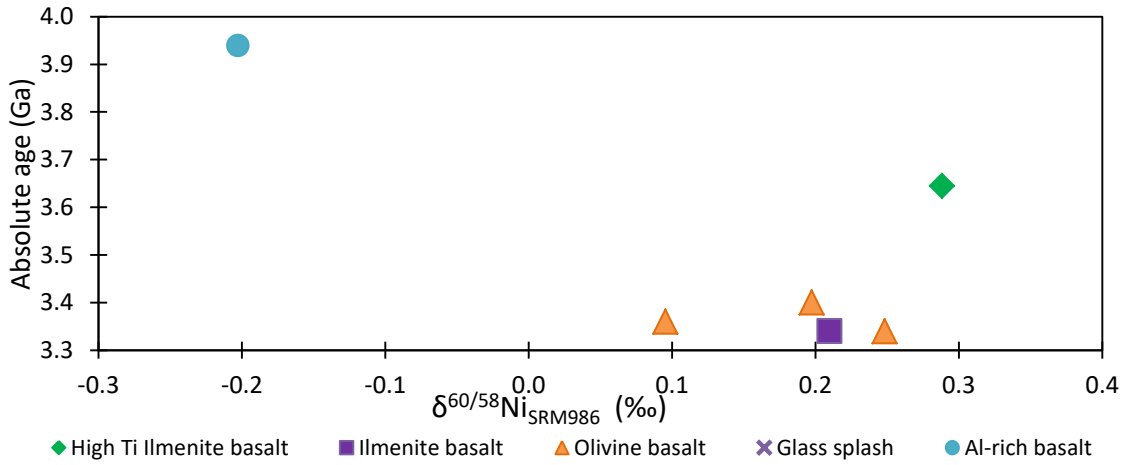

Figure 39

Nickel isotopic composition of lunar basalt samples plotted against the absolute age for the same samples (Meyer, 2011; Papanastassiou and Wasserburg, 1971). A negative trend is observed, dominated by a single sample, with r^2=0.633. If the Al-rich basalt is excluded a positive trend may be seen (r^2=0.520). Excluding the High-Ti basalt improves the negative trend (r^2= 0.910). External reproducibility on Ni isotopic composition is 0.06‰.

The age of the samples analysed is after any effects from core differentiation and the lunar magma ocean would have ceased. An evolution in mantle geochemistry between 3.9 and 3.3 Ga may relate to late-stage overturn of material after the separation of the plagioclase flotation crust. Overturn has been proposed to account for many geochemical characteristics of the lunar basalts, and could well account for the change in mantle composition with time, as the areas first overturned would be most enriched and the later areas sampled would have been more homogenised.

5.6.3. Lunar nickel isotopes and other isotopic systematics

Isotopic compositions for other elements have been measured on these lunar rocks, either on the same cut (Zn, V) or similar cuts from the same host sample (S, Cl). Of these, Zn and V were analysed in house by Sean Hopkins (in prep.), whereas S was analysed by the Farquhar group (pers. comm.), and Cl by the Sharp group (pers. comm.). These isotope systems are plotted with Ni isotopic composition in Figure 40, with $\delta^{50}V$ in Figure 33. In general these plots show that the samples with extreme elemental and Ni isotopic composition (Al rich basalt, high-Ti basalt) also have extreme isotopic systematics in the other systems (where analysed).

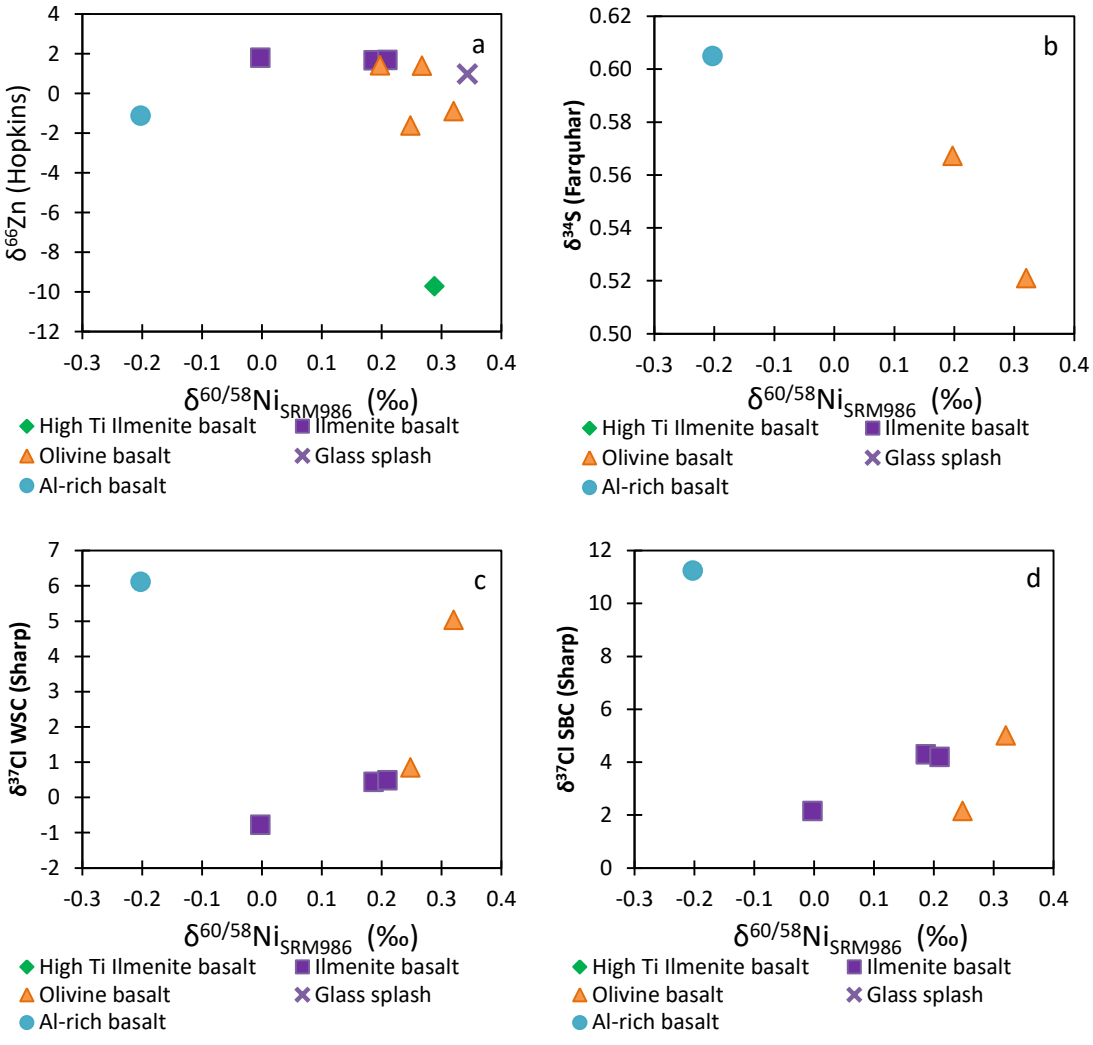

Figure 40

Top: Comparison of Ni isotopic composition with Zn (left) from Hopkins and co-workers (in prep.) on the same sample cuts and S (right) isotopic composition from Farquhar (pers. comm.) on the same sample numbers. No linear correlation is seen within the data for the former, whereas the latter has a strong negative correlation (r^2=0.879), although limited overlap of samples. The external reproducibility of the Ni isotopic compositions is 0.06‰. The 2SD error on Zn data is 0.02 to 0.19‰, and on S is 0.066‰.

Bottom: Comparison of Ni isotopic composition with Cl isotopic composition relative to WSC (left) and SBC (right) from Sharp (pers. comm.) on the same sample numbers. No linear trend is seen within the data, unless the Al-rich basalt (14053) is excluded as an outlier (r squared becomes 0.626 for WSC, and 0.371 for SBC). The external reproducibility of the Ni isotopic compositions is 0.06‰, and Cl is 0.50‰.

No linear correlations are seen with Ni isotopic composition and Zn isotopic composition. Sulphur isotopic composition shows a negative trend with Ni isotopes, but only three samples have been analysed for both systems. If the Al rich basalt is excluded, the chlorine isotopic compositions for the remaining 5 samples show a positive trend, particularly relative to WSC (r^2=0.626).

Chlorine and zinc isotopes have been shown to be affected by their volatility, which should not be a factor in the fractionation of the relatively refractory Ni. Therefore, the lack of correlation in these isotope systems is unsurprising. Sharp and co-workers (2010) suggested that variation in Cl isotopes is attributable to devolatilisation of anhydrous lunar basalts, and fractionation during degassing (Sharp et al., 2010). Light Cl has been suggested to be lost during devolatilisation, and this occurs less when there is an excess of H, such as on Earth (Sharp et al., 2010). Variation in Zn isotopes has also been attributed to volatilization of Zn in planetary rocks, with light Zn preferentially lost (Paniello et al., 2012). Zinc is more volatile than Cl, and can be extensively fractionated during high temperature evaporative processes (Paniello et al., 2012).

Variation in S isotopes has also been attributed to degassing, where ^{32}S would be preferentially evaporated as volatile species COS from a H-poor melt, with one exception that has been suggested to relate to cosmic ray spallation of ^{40}Ca (Wing and Farquhar, 2015). In contrast, extensive sulphur cycling and sulfide– sulphate speciation cause fractionation on the Earth, although the Δ^{33}S and Δ^{36}S values are comparable between Earth and Moon (Wing and Farquhar, 2015). However, as there is both a trend in S isotopic composition and Ni isotopic composition and with S content in the basalts (Figure 45), further investigation of a similar source for these isotopic fractionations may need investigation.

5.6.4. Lunar nickel isotopes and mineralogy

Nickel isotopic compositions in terrestrial rocks show no trends with mineralogy (Chapter 3); similar plots with lunar sample data are shown in Figure 41 and Figure 42, and Appendix 7.8. The only mineral that has a relatively strong correlation with Ni isotopic composition is plagioclase (shown in Figure 41, left), which has a negative trend (r^2=0.584). This is surprising given the low Ni concentration in plagioclase, and the lack of trend (r^2=0.087) with Ni concentration and plagioclase (Figure 41, right).

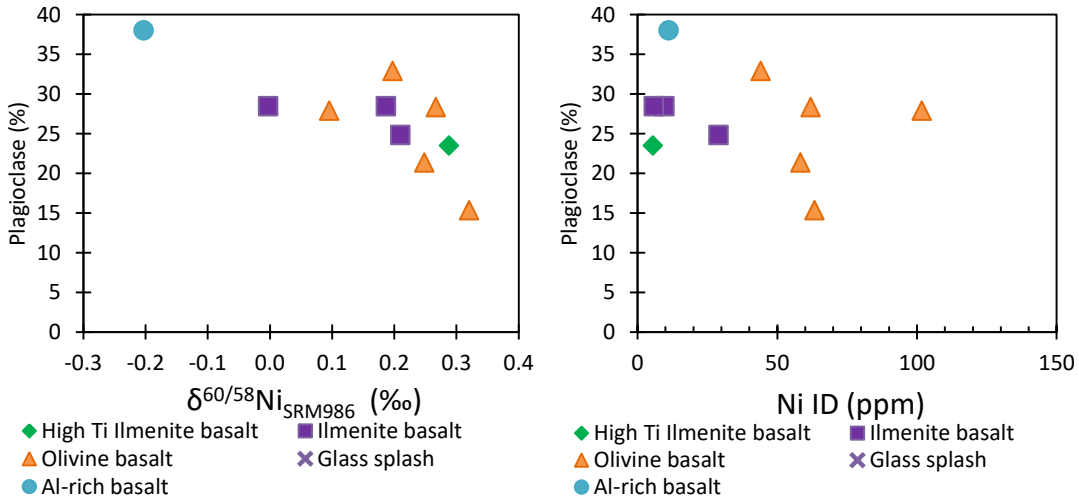

Figure 41

Nickel isotopic composition of the lunar samples plotted against the mineralogy in modal percent (Meyer, 2011). Limited data for spinel reflects the fewer data points for this plot. 12054 was analysed as an interior and exterior samples, plus the glass splash (mineralogy unknown) but mineralogy is assumed invariant between interior and exterior. Plagioclase shows a negative trend with Ni isotopic composition (r^2=0.584), but no trend with Ni concentration (r^2=0.087). In contrast, nickel isotopic compositions in terrestrial rocks show no trends with mineralogy. External reproducibility in Ni isotopic composition is 0.06‰.

Nickel isotopic composition of the lunar samples plotted relative to the reported modal percentage of other minerals, shows no linear trend (olivine, ilmenite, pyroxene, mesostasis, troilite, or Fe-metal). Spinel, excluding the Al rich sample, may have a weak negative trend with Ni isotopic composition (r^2=0.308).

A relationship with Fe-Ni metal, or troilite (FeS), might have been expected, given the concentration of Ni in these phases, as terrestrial Ni^{2+} readily substitutes for Mg^{2+} and Fe^{2+}, however, this is not observed (Figure 42). However, there is similarly no trend with Ni concentration in these samples, and there has previously been shown to be no Ni isotopic

difference between chondrites and the BSE, suggesting metal-silicate segregation cannot introduce significant fractionation under terrestrial conditions (Gall et al., 2017; Steele et al., 2011). This would be consistent with a lack of trend between Ni isotopic composition and modal percentage of metal. A trend in troilite, may be have been expected given the trend in S content of the basalts (Figure 45), and with S isotopic composition (Figure 40). A control on Ni partitioning with high S content has also been suggested (Wood et al., 2014), for high S contents, such as might be expected in areas in of the mantle with high concentrations of sulfide and iron metal. The lack of trend with basaltic metal and troilite abundance might relate to the low pressures of melting, which, as discussed above changes the partitioning behaviour.

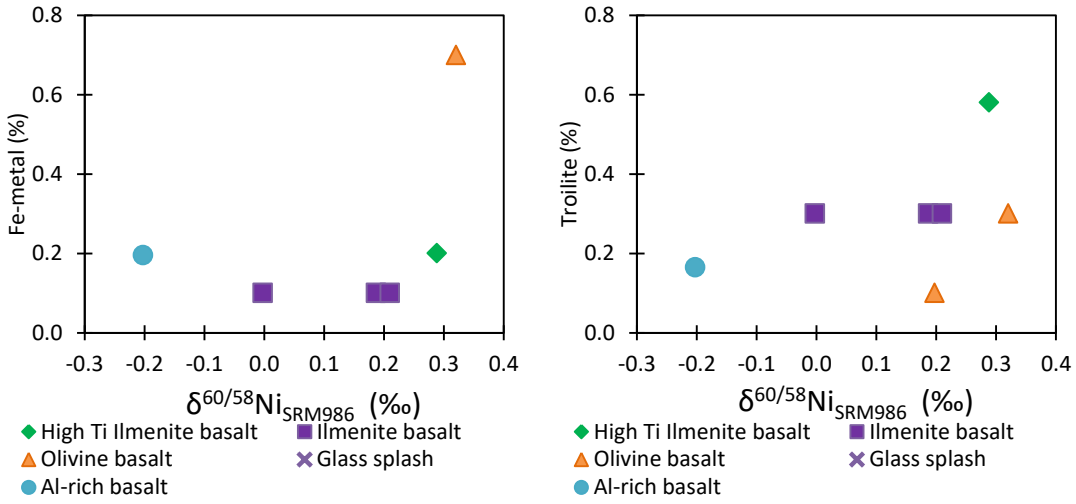

Figure 42

Nickel isotopic composition of the lunar samples plotted against the Fe-metal and troilite in modal percent (Meyer, 2011). 12054 was analysed as an interior and exterior samples, plus the glass splash (mineralogy unknown) but mineralogy is assumed invariant between interior and exterior. External reproducibility in Ni isotopic composition is 0.06‰.

The correlation between Ni isotopic composition and plagioclase may indicate that production of plagioclase and fractionation of Ni isotopes are controlled by the same large-scale process. Plagioclase ($NaAlSi_3O_8$ – $CaAl_2Si_2O_8$) does not host significant Fe or Mg, which are the sites that usually host Ni in terrestrial rocks. Palme and co-workers (1984) name Ni as one of the elements that is incompatible in plagioclase. Plagioclase sites are designed to hold Ca^{2+} (ionic radius 0.112 nm) or Na^{2+} (0.118 nm) in 8 fold coordination, and Al^{3+} (0.039 nm) and Si^{4+} (0.026 nm) in 4 fold coordination (Henderson and Henderson, 2009). In contrast, Ni^{2+} has ionic radius

of 0.049-0.055 nm in 4 fold coordination, and 0.069 nm in 6 fold coordination (Henderson and Henderson, 2009). These values do not correspond to either site in the plagioclase structure.

Compatibility of trace elements in plagioclase has also been shown to alter with oxygen fugacity, with some trace elements including Fe becoming more compatible in plagioclase with less negative fO_2 (Aigner-Torres et al., 2007). The partition coefficient for Ni in plagioclase in a lunar basalt is indeed less than an equivalent terrestrial MORB sample, in experimental tests (Sun et al., 2017). This is in agreement with the concentration measurements of Wedepohl (1974) and Palme and co-worker (1984), where the concentration of Ni in plagioclase is very low compared to basaltic melts and other Mg-Fe-silicates. Wedepohl (1974) quotes concentrations of Ni in plagioclase from terrestrial basaltic greenstone, at 8, 25 and 30 ppm. Estimates of Ni in lunar anorthosites, which consist of >95 % plagioclase (Arai and Maruyama, 2017), are similarly low in Ni concentration (<20 ppm (Palme et al., 1984)). Compared to the 1000s ppm Ni in olivine and spinel, and 100s ppm in pyroxenes, plagioclase does not host significant Ni. Papike and co-workers (1999) have showed that Ni in olivine in lunar mare basalts behaves as in terrestrial equivalents, suggesting that behaviour of Ni in lunar minerals is comparable to terrestrial equivalents.

Plagioclase-rich rocks are thought to be sampling the flotation cumulates of the lunar magma ocean, which are expected to have been isolated during LMO overturn. However, up to 15% plagioclase was not isolated from the regions of basalt formation (Neal and Taylor, 1991), potentially suggesting that the overturn may have included some plagioclase. This material plus the elements incompatible in plagioclase, may suggest the degree of enrichment by overturn into the region of mantle that became the source of the analysed basalts.

5.6.5. Lunar nickel isotopes and other geochemical characteristics

Geochemical data were collected on the exact aliquots of sample powder that was analysed for isotopic composition, excluding sample 12002 and the glass splash (12054, 13). For other elements an average of literature data has been taken, most of which was compiled in Meyer's Lunar Sample Compendium (2011). The glass splash sample is without data from either method

and cannot be conjectured about in this section. Some correlations are present regardless of the source of the data, others appear in the elements analysed in house, but not with literature data. The elemental concentrations on the exact cuts of sample analysed for isotopic composition should be more reliable, as heterogeneity of larger lunar samples may cause compositional variation between the part of the sample analysed for Ni isotopes and the part analysed for elemental composition in the literature. Indeed, in general the trends are stronger in the data obtained on the same sample aliquots. Niobium is the exception, as it shows a correlation with literature data if the high-Ti sample is excluded (r^2=0.559), but not with the Nb analysed in house (r^2=0.135).

In general, the samples with the most primitive compositions (high in Fe, low in incompatible elements, high in compatible elements e.g. Co) appear to have heavier Ni isotopic compositions. The samples trend towards lighter compositions in more evolved samples (high in incompatible elements).

Specifically, the analysed lunar Ni isotopic compositions correlate positively with some geochemical parameters including major element, FeO (r^2=0.517), and minor trace element Co (r^2=0.404, improving to 0.653 without the high-Ti sample). The single high-Ti sample has a KREEP component and therefore a very different chemistry that separates it from the processing that produced the other samples. If this sample is excluded then a number of further trends are observed with r^2>0.37. These include negative correlations with a number of incompatible elements, including major element K_2O (Figure 43, left). These also include the majority of the LREE, excluding Pm that was not analysed, and Eu and Sc that both had only a weak correlation with Ni isotopic composition (r^2=0.28).

There is strong negative correlation in low-Ti basalts between Ni isotopic composition and K_2O (Figure 43, left, r^2=0.823). Nickel concentration and K_2O (Figure 43, right) shows similar correlation (r^2=0.768), showing that Ni is still behaving compatibly in the lunar mafic environment (excluding the high-Ti sample).

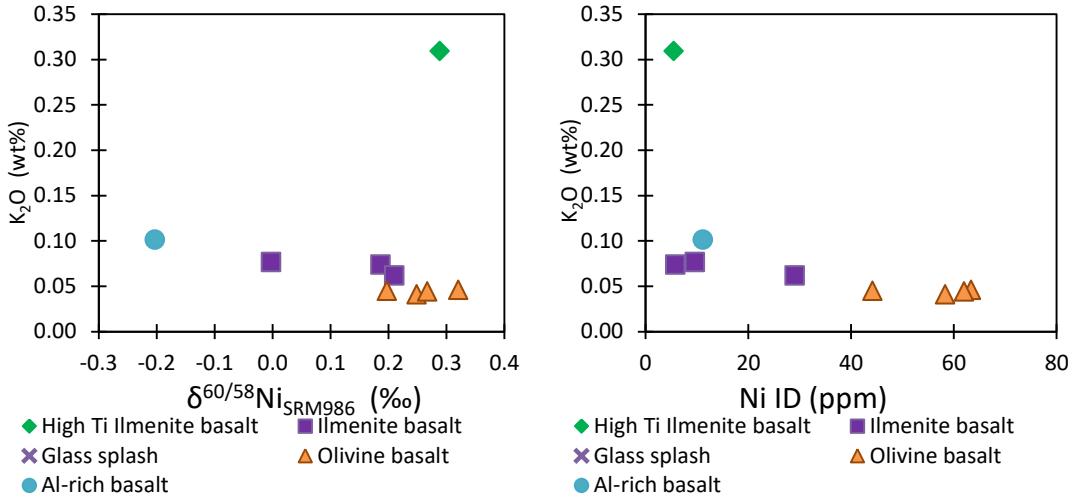

Figure 43

Left: Nickel isotopic composition against K_2O. Excluding the High-Ti sample, there is a strong correlation of r^2=0.823. Right: Nickel concentration against K_2O. Excluding the High-Ti sample, there is a strong correlation of r^2=0.768. External reproducibility of Ni isotopic composition 0.06‰. K_2O was analysed on the same aliquots via quadrupole single collector mass spectrometer in wt%, with detection limit 0.048 wt%.

Another similar strong negative trend with Ni isotopic composition and Al_2O_3 (Figure 44, left), which is likely in association with the trend with plagioclase, as seen in section 5.6.2 (Figure 42). The correlation is negative, similar to plagioclase, with high aluminium associated with light Ni isotopic compositions. However, there is a much weaker trend with Ni concentration (Figure 44, right) suggesting, as with plagioclase, that the process fractionating Ni isotopes in not similarly controlling Ni concentration. This decoupling between Ni concentrations and Ni isotopic compositions was also seen in the terrestrial samples (Chapters 3 and 4).

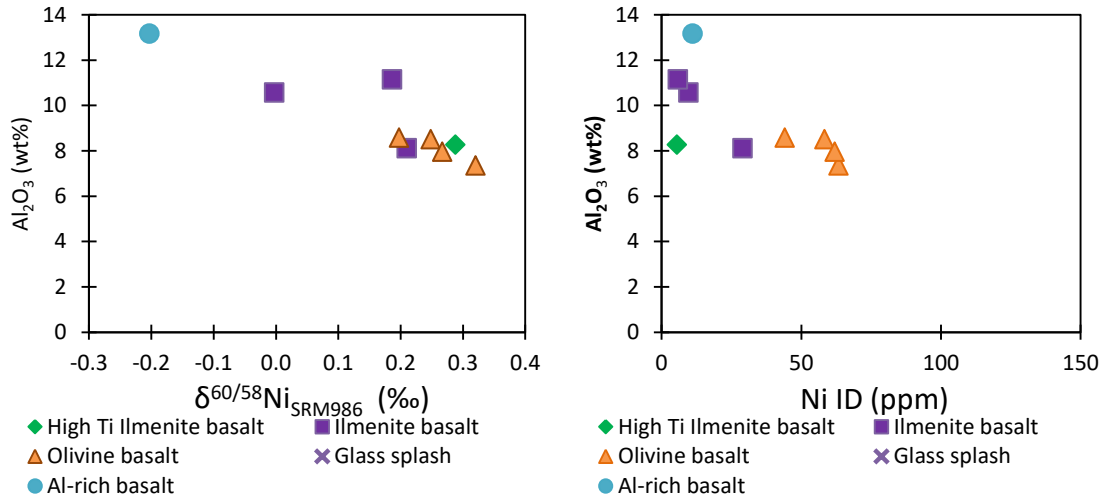

Figure 44

Right: Nickel concentration against Al_2O_3 analysed on the same aliquots via quadrupole single collector mass spectrometer. Excluding the High-Ti sample, there is a strong correlation of r^2=0.813. One sample, 12002, was not analysed for Al_2O_3 and is not plotted. Left: Right: Nickel concentration against Al_2O_3 analysed on the same aliquots via quadrupole single collector mass spectrometer. There is a correlation of r^2=0.449. One sample, 12002, was not analysed for Al_2O_3 and is not plotted. External reproducibility of Ni isotopic composition 0.06‰. Al_2O_3 in wt%, with detection limit 0.045 wt%.

The REE correlations (excluding the high-Ti sample) are strongest at the LREE end of the range: La (r^2=0.677), Ce (r^2=0.726), Pr (r^2=0.717). There are also correlations with Zr (r^2=0.804), Hf (r^2=0.713), U (r^2=0.693), Ba (r^2=0.672), Th (r^2=0.651), Pb (r^2=0.578), Li (r^2=0.420), and Cr (r^2=0.411). Examples of these plots are shown in Figure 45. With elements not analysed in house, some correlations were also found with Ir (r^2=0.660), Na_2O (r^2=0.659), S (r^2=0.616), and Ta (r^2=0.597).

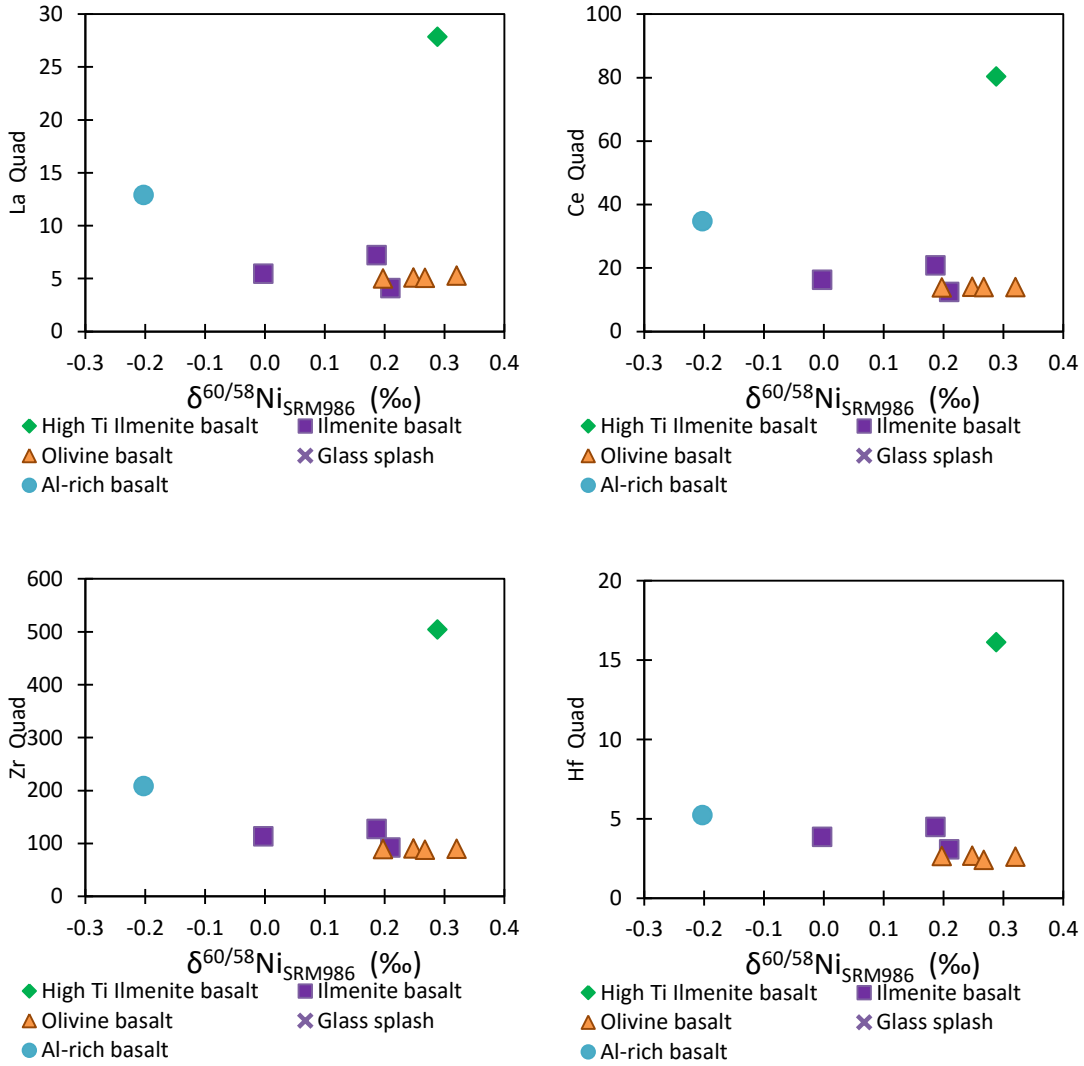

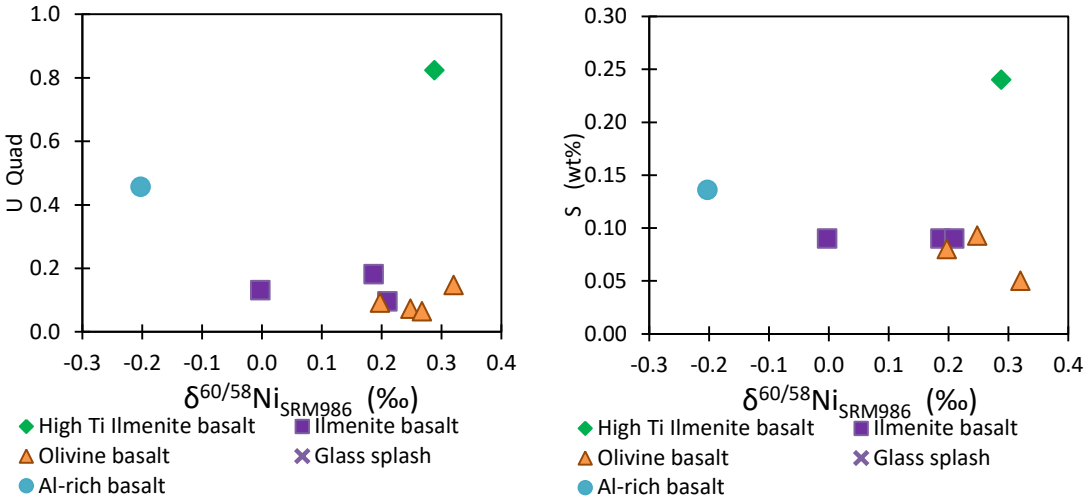

Figure 45

Ni isotopic composition plotted against various elemental concentrations. Correlations are seen in La (r^2=0.677), Ce (r^2=0.726), Zr (r2=0.804), Hf (r^2=0.713), U (r^2=0.693), and S (r^2=0.616).All but S analysed on of the same aliquots as the Ni isotopes were determined on, by quadrupole single collector mass spectrometer, data for S from an average of literature data. Unless otherwise stated elemental concentrations are in ppm.

The trend with sulphur has been previously mentioned, and suggested to relate to the proposed control on Ni partitioning with high S content (Wood et al., 2014), for high S contents, such as might be expected in areas in of the mantle with high concentrations of sulfide and iron metal. If this effect with Ni partitioning and S content requires the mantle pressures to occur, this would explain the lack of trend with basaltic sulfide abundance. The variation in Ni isotopic compositions may then be observed where the source region in the lunar mantle had both sulfide and metal, and sufficient [S] and pressure to affect partitioning of Ni between these phases, when melting begins. This partitioning change may affect Ni isotopic composition, and be preserved in the resulting basaltic rocks.

The majority of the trends with Ni isotopic composition and elemental concentrations are with elements that are incompatible in lunar basaltic systems (as seen in K above in Figure 43, and in some REE, and Zr, and U (see Figure 45), and (not shown) Ba, Th, etc.). These elements have generally low concentrations in lunar basalts because either the source regions are depleted in these elements, or that the source regions are cumulates of minerals that do not readily incorporate them (Wieczorek et al., 2006). The exception to this generality are the Apollo 14 high K basalts (also sampled by Luna 16), which are thought to indicate assimilation of some

trace element rich component, or a source region enriched in these incompatible elements. The Apollo 14 basalt analysed in this work had an extremely light Ni isotopic composition, which suggests that samples that are more enriched in incompatible elements host lighter Ni isotopic compositions, although generally lower Ni concentrations.

These elements (K, Zr, U, Ba, Th, etc.) are also specifically incompatible in plagioclase (e.g. Palme et al., 1984). The compatibility of trace elements in plagioclase often depends on the composition, or percent anorthosite of the mineral, such as with Ba, Fe, Ti, Zr and Sr (Bédard, 2005; Bindeman and Davis, 2000). Nickel, while generally compatible, is also incompatible in plagioclase, and plagioclase shows a similarly strong negative trend with Ni isotopic composition as the aforementioned elements (Figure 41). Mare basalts, as a whole, have been shown by petrologic experiments to be derived from an ultramafic source with pyroxene and olivine (Wieczorek et al., 2006), both of which host abundant Ni on Earth. Trace element geochemistry of lunar mare basalts, and especially the REE, have been used to show the ultramafic sources of the mare are complementary to the feldspathic crust (Wieczorek et al., 2006), which in turn lead to the LMO hypothesis. Variations in REE in mare basalts have been taken to reflect source variations (Wieczorek et al., 2006), which has also been the conclusion of this work on variations in Ni isotopic compositions. The strong trend between the different lunar REE and the Ni isotopic composition supports that source compositional variations are responsible for both characteristics. The elements that are incompatible in plagioclase, would be enriched in the mantle after plagioclase flotation, and overturn would have caused a reincorporation of these elements despite other mineral crystallisation. Other factors in variations in REE in lunar mare are degree of melting, fractionation during solidification, and assimilation of crustal material (Wieczorek et al., 2006). Of these, the two former have been shown in this work not to affect Ni isotopic composition, leaving only assimilation with the potential to complicate the Ni isotope signature further. Fractionation of Ni isotopes by assimilation requires a process to generate fractionated Ni compositions in the material being assimilated.

Late-stage overturn of the lunar mantle after the flotation of plagioclase has been suggested to reintroduce heat producing elements into the lunar interior, to provide an energy source for melting (Shearer et al., 2006). Overturn has also been invoked to introduce a negative Eu anomaly into the lunar mantle (Neal, 2001), and add Mg into the KREEP (Wieczorek et al., 2006), therefore it may potentially also redistribute isotopes of Ni. This could account for the correlations of Ni isotopic composition and other elements incompatible in plagioclase, as these are the elements not separated out of the LMO into plagioclase at the time of overturn.

The apparent relationships between Ni isotopic composition and these various geochemical indicators either relates to mixing of endmember sources (two for low-Ti basalts, potentially a third for high-Ti), or to magmatic fractionation. Magmatic fractionation usually requires the samples to be linked within a single volcanic system, of which there is no clear evidence. Regardless, there is no correlation between Ni isotopic composition and [Ni], nor with FeO/MgO (Figure 46).

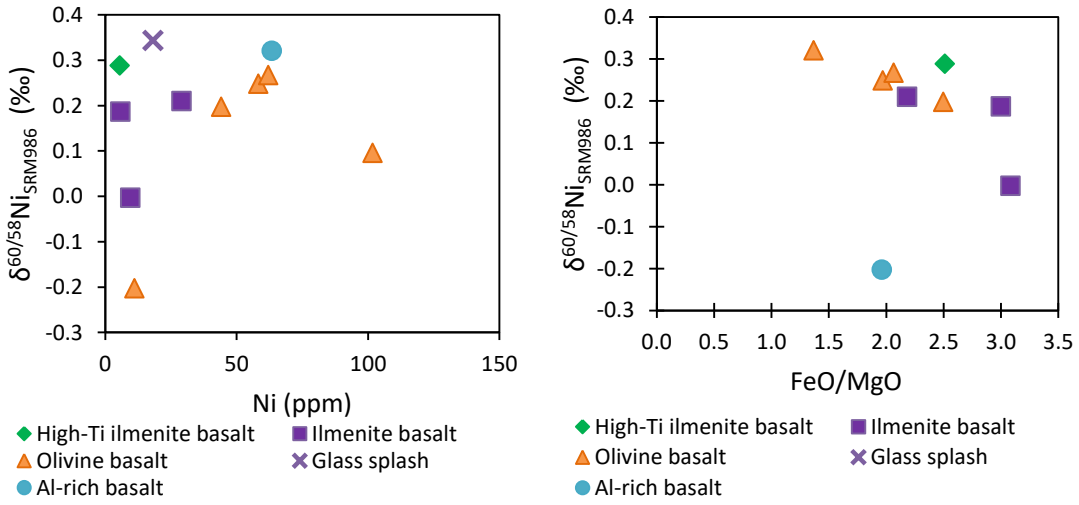

Figure 46

Nickel isotopic composition for lunar samples, by lithology, against indicators of magmatic differentiation: Nickel concentration (left); and FeO/MgO (right). [Ni] has r^2=0.039, FeO/MgO has r^2=0.049. Nickel concentration by isotope dilution, FeO and MgO by analysis by Quadrupole single collector mass spectrometry done on the same aliquots of samples. External reproducibility for Ni isotopic composition is 0.06‰.

Another compatible trace element ratio, which could represent magmatic differentiation if the samples have co-genetic origin, Ni/Cr, has a positive correlation if the high-Ti sample is excluded (Figure 47, right, r^2=0.500). With the High-Ti included, the r squared is reduced to

0.247. However, another compatible trace element ratio, Co/Ni (Figure 47, left) shows no trend with Ni isotopic composition, with or without the high-Ti sample. Papike and co-workers (1999) showed that Co behaviour in lunar mare basalts olivine was different compared to the terrestrial equivalents, which may suggest that Co/Ni is not a good ratio for representing degree of lunar magmatic differentiation, in lunar environments. However, with the lack of trends in Fe/Mg and [Ni] (Figure 46), it is likely that the apparent trends in lunar Ni isotopic composition do not relate to magmatic differentiation.

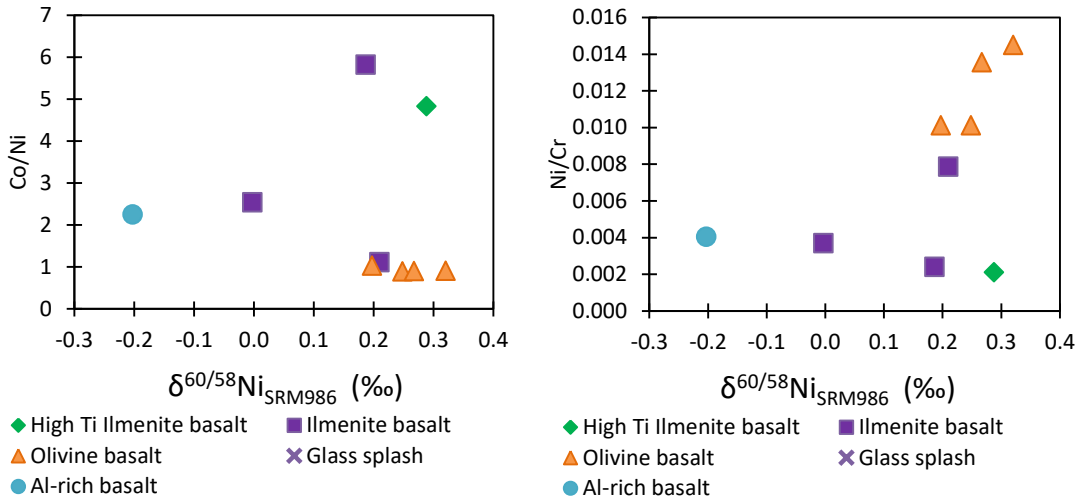

Figure 47

Nickel isotopic composition against compatible trace element ratios Co/Ni (left, r^2=0.007) and Ni/Cr (right, r^2= 0.247, or 0.500 without high-Ti sample). External reproducibility on Ni isotopic composition is 0.06‰. Nickel concentration measured by isotope dilution, other elements analysed by Quadrupole single collector mass spectrometry done on the same aliquots of samples.

A traditional indicator of partial melting, La/Sm (Figure 48, left) has a no clear trend (r^2=0.171), suggesting that, as with the terrestrial mafic samples, there is no control on Ni isotope composition with degree of partial melting. This is supported by the lack of correlation with other incompatible trace element ratios such as Ba/Nb (Figure 48, right).

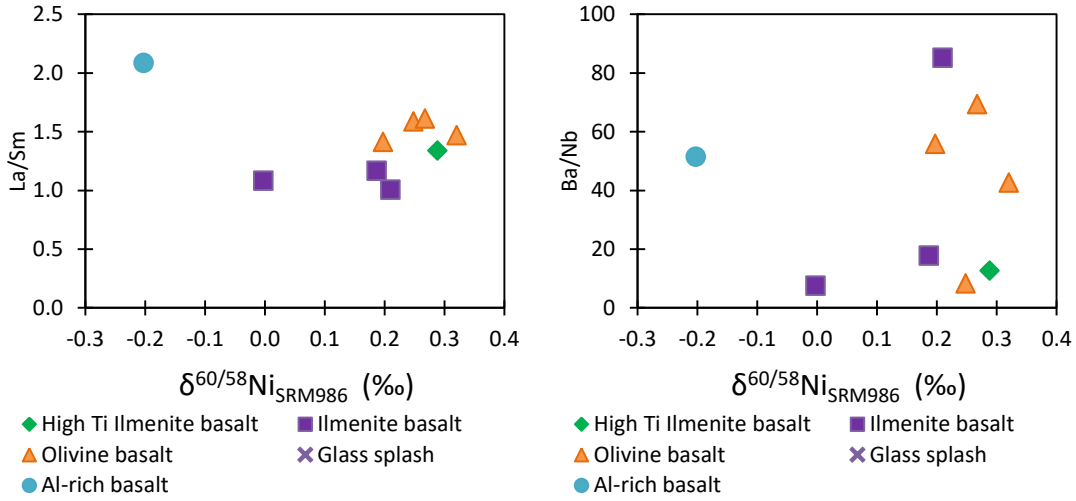

Figure 48

Nickel isotopic composition against incompatible trace element ratios La/Sm (left, r^2=0.171) and Ba/Nb (right, r^2= 0.0003). External reproducibility on Ni isotopic composition is 0.06‰. Elemental concentrations analysed by Quadrupole single collector mass spectrometry done on the same aliquots of samples.

Magmatic differentiation, and partial melting, are both therefore unlikely contributors to the observed trends, given trace element ratios (Figure 46, Figure 47, and Figure 48). Therefore, the likely mechanism for producing linear trends in element concentrations with Ni isotopic composition is mixing. Mixing between a high K source associated with a light Ni isotopic composition, and a more primitive mantle source with a Ni isotopic composition heavier than the BSE, could produce the observed trends.

Hafnium and lanthanum have been shown to correlate in lunar samples from Apollo 14, with a relationship from mafic cumulates to fractional crystallization (FC) and/or assimilation and fractional crystallisation with KREEP (AFC) at the other (Neal and Taylor, 1992). As previously shown, Ni isotopes appear not to be affected by fractional crystallisation, even in lunar environments, which suggests that the influence of KREEP, as a change in source geochemistry, is a controlling factor on lunar Ni isotope fractionation. However, KREEP is not concentrated in Ni, and forms after Ni in the LMO should have been contained in silicates with octahedral sites, and metal. However, higher than predicted Mg contents in KREEP (Wieczorek et al., 2006), which may relate to late stage overturn, may allow for substitution of Ni for Mg. Titanium is normally incompatible in olivine and pyroxene, but in the lunar environment did not become enriched in KREEP with other incompatible elements (Wieczorek et al., 2006). The Ni

isotope signatures may therefore provide evidence for the incorporation of more compatible elements into the KREEP basalts after differentiation, in a way that caused some fractionation of the isotopes. Alternatively, the influx of KREEP material into a mantle source region may have caused, or coincided with, melting and thereby triggered the process that fractionated the Ni isotopes.

The strongest trends with Ni isotope composition are with LREE, which are more strongly enriched in the liquid phases produced by partial melting, because they are more incompatible than HREE. However, elemental ratios have shown that degree of partial melting does not correlate with Ni isotopic composition in Earth (Chapter 4) or in the lunar samples (for example Figure 48). Therefore, the stronger trends with LREE are likely to be indicative of source variations, with the LREE enriched by a process bringing light Ni isotopic composition, prior to the melting that produced the sampled lunar basalts.

5.6.6. Comparison between $\delta^{60/58}Ni_{SRM986}$ for the high-Ti sample and low-Ti samples

Ten low-Ti basalts were sampled over a range of lithologies and they show a large range in Ni isotopic composition from $\delta^{60/58}Ni_{SRM986}$ = -0.20 to 0.34‰. The average Ni isotopic composition of these samples is 0.17±0.31‰. The only example of a high-Ti basalt has a Ni isotopic composition heavier than the BSE estimates at $\delta^{60/58}Ni_{SRM986}$ = 0.29‰, which is heavier than the average for low-Ti basalts. Only 2 samples of low-Ti basalts are heavier in Ni isotopic composition than the high-Ti sample, one of which is the atypical glass splash.

In many previously shown plots, a trend in Ni isotopic composition and the other variable, specifically absolute age (Figure 39), and the REE and many other elements referred to in section 5.6.5, has broken down with the addition of the high-Ti sample. This implies that there is no common relationship between the Ni isotopic compositions of the respective sources of low-Ti and high-Ti basalts.

Separation between the high-Ti and low-Ti basalts has been previously shown with major element chemistry, for example TiO_2 vs FeO+MgO (Krawczynski and Grove, 2012), and in

separate trends in ϵHf and ϵNd space (Shearer et al., 2006). High-Ti basalts have lower Ni concentrations than low-Ti, and non-chondritic ratios of high field strength elements (HFSE: Zr, Nb, Hf, Ta, Th) relative to the chondritic ratios seen in low-Ti basalts (Wieczorek et al., 2006). Models for formation of high-Ti basalts and low-Ti basalts also suggest that there is a separation in sources for these lithologies.

Source models for high-Ti basalts generally involve either early stage LMO cumulates, late stage LMO cumulates, and hybrids of both, with open-system fractional crystallisation thought to contribute heavily to the compositional range (Neal and Taylor, 1992). The general high-Ti source has been suggested to be formed from small-scale overturn of the LMO, which would introduce sufficient high Mg early formed cumulates to generate the Mg numbers of these samples, and allow fractional crystallisation to produce the observed compositional scatter (Neal and Taylor, 1992). That the high-Ti source may have been of different oxygen fugacity has been suggested, caused by a shift in the TiO_2:Ti_2O_3 ratio, because Ti is the only major element that could change valence state with reducing conditions (Krawczynski and Grove, 2012).

The high-Ti sample potentially has heavier Ni isotopic composition because the higher contribution of Ti-Fe oxides, which could host Ni in the octahedral Fe site. However, Ni concentration is not higher in the high-Ti sample, suggesting that the fractionation of Ni isotopes may be decoupled from concentration effects.

Low-Ti basalts are thought to be formed from heterogeneous source regions with contribution from fractional crystallisation. Particularly, consistent trends observed in Apollo 12 and 15 basalts with indicators of fractional crystallisation (Mg/Mg+Fe) (Neal and Taylor, 1992). Source models for Apollo 12 and 15 low-Ti basalts particularly almost all require multiple generally similar but distinct source regions, with intra-group variation suggested to be formed by closed-system fractional crystallization, which requires a storage magma chamber or flows of lava up to 30 m thick (Neal and Taylor, 1992). In the case of the low-Ti basalts the source region is more dominated by the early LMO cumulates (olivine and pyroxene) and lower abundance of Ti-Fe oxides than the high-Ti samples (Neal and Taylor, 1992). The high Al

basalts have a wide compositional range, suggesting KREEP involvement in their formation, either in the source or added after magma generation (Neal and Taylor, 1992). Plagioclase is also required (<15%) in models of formation of the high Al basalts, requiring incomplete separation of plagioclase into the flotation crust, or a shallow source for magma generation (Neal and Taylor, 1992).

However, the review by Neal and Taylor (1992) also suggests that there is no petrographic relationship between the olivine and pigeonite basalts from Apollo 12, and no fractional crystallisation connection between the quartz-normative basalts and olivine-normative basalts from Apollo 15. These factors suggest that, even within the low-Ti basalts, there may be other processes or that these samples are not as genetically linked as early work suggested.

5.7. Conclusions

Analysis of unspiked Ni isotopic compositions suggest that there are no cosmogenic effects perturbing the analysed mass dependent compositions.

The lunar mantle, without plate tectonics and subduction, cannot produce domains of light Ni isotopic compositions from recycling, as have been sampled on Earth. The average Ni isotopic composition of the lunar basalts is heavier than that of equivalent terrestrial rocks, leading further support to the fact that the lunar mantle is missing this major process producing lighter $\delta^{60/58}Ni_{SRM986}$.

Lunar Ni isotopic compositions have, like terrestrial, been shown in this work to be invariant to degree of partial melting and magmatic differentiation. However, as there are lunar samples with light Ni isotopic compositions, and trends in the geochemical characteristics of the sample with Ni isotopic composition, a process is occurring on the Moon to fractionate Ni isotopes in a way that is not seen, or is insignificant, on Earth. We have tested the samples to see if the $\delta^{60/58}Ni_{SRM986}$ variability is an artefact from cosmogenic effects but we have found no evidence of this. The unspiked isotopic compositions analysed are normal within uncertainty. No

relationship was found with Ni isotopic composition and exposure age. There is no correlation with the exposure related effects found in V, similarly removing cosmogenic effects from the potential cause.

There is also no correlation with Ni isotopic composition and Zn, thought to fractionate during devolatilisation. The few samples analysed for Cl do show a hint of a trend. Only two identical samples have been analysed for both Mg and Fe stable isotopic composition and Ni isotopic composition, which allows no conjecture for these isotopes. There may be a correlation with S isotopic composition, however only 3 samples have been analysed for both systems. There is also a correlation with Ni isotopic composition with S concentration, which may support a joint parent process producing both effects, perhaps linked to sulfides. Lack of clear correlation with Zn and Cl suggests that volatilisation is not a potential cause of lunar Ni isotopic fractionation.

Therefore, other mechanisms for Ni isotopic fractionation are required. With partial melting and magmatic differentiation also excluded, this leaves source variations as the most likely cause for variation in Ni isotopic composition, supported by extreme compositions being in lithologies with distinct chemistry, including the lightest $\delta^{60/58}Ni_{SRM986}$ in the Al-rich basalt, and the single high-Ti sample having one of the heaviest compositions observed. Source variations are proposed to have formed based on fractionation during Ni partitioning in the lower fO_2 and higher S conditions of the lunar mantle. This is potentially supported by the correlation between Ni isotopic composition and S content and S isotopic composition.

The fractionation process affecting lunar Ni may not occur on Earth, because the lower oxygen fugacity has forced Ni ions out of the most compatible sites, such as olivine, due to increased competition with Fe^{2+}. The redistribution of Ni between melt, and metal in the proximity of sulfide may fractionate Ni isotopes, and produce the observed variable Ni isotopic compositions, relating to source variations. In mantle sources with insufficient troilite and metal, this fractionation process may be less, or non-existent, and the resulting basaltic composition would be less significantly affected, or unaltered from bulk.

Similar to terrestrial samples, no correlation is seen with mineralogy and Ni isotopic composition, with the exception of plagioclase. Plagioclase does not host significant Ni in the mineral structure and has low Ni concentrations. No correlation with [Ni] is observed, compared to a correlation with r^2=0.584 with Ni isotopic composition. A similar correlation, with r^2=0.813, is observed in Al_2O_3, supporting that there is an influence on Ni isotopes with a process associated with plagioclase formation. Incomplete separation of plagioclase during the flotation of this mineral during the LMO is well known, and may leave some plagioclase to be vulnerable to reintroduction to the mantle during overturn.

The strong correlation between Ni isotopic composition and plagioclase, and with elements incompatible in plagioclase may relate to LMO overturn, after the flotation of the plagioclase crust that formed the lunar highlands. The reintroduction of material particularly incompatible elements, including heat producing elements, into the mantle, may be the trigger for melting and then the distribution of sulfides and metal in the mantle region may cause the fractionation of Ni isotopes, that persisted into the produced basalts. The sample with the lightest Ni isotopic composition has the highest amount of incompatible elements, Al, and plagioclase leading to the suggestion that the greatest Ni fractionation occurs when these factors are all in abundance in the same region of the mantle.

In summary, this data has showed that the behaviour of Ni isotopes is different in the lunar environment to the equivalent terrestrial environment, resulting in Ni isotopic fractionation by a process that does not occur on the Earth.

5.8. References

Aigner-Torres, M., Blundy, J., Ulmer, P., Pettke, T., 2007. Laser Ablation ICPMS study of trace element partitioning between plagioclase and basaltic melts: an experimental approach. Contrib Miner. Pet. 153, 647–667. https://doi.org/10.1007/s00410-006-0168-2

Arai, T., Maruyama, S., 2017. Formation of anorthosite on the Moon through magma ocean fractional crystallization. Geosci. Front. 8, 299–308. https://doi.org/10.1016/j.gsf.2016.11.007

Armytage, R.M.G., Georg, R.B., Williams, H.M., Halliday, A.N., 2012. Silicon isotopes in lunar rocks : Implications for the Moon's formation and the early history of the Earth. Geochim. Cosmochim. Acta 77, 504–514. https://doi.org/10.1016/j.gca.2011.10.032

Aulbach, S., Rudnick, R.L., McDonough, W.F., 2008. Li-Sr-Nd isotope signatures of the plume and cratonic lithospheric mantle beneath the margin of the rifted Tanzanian craton (Labait). Contrib. to Mineral. Petrol. 155, 79–92. https://doi.org/10.1007/s00410-007-0226-4

Becker, J.S., 2007. Inorganic mass spectrometry : principles and applications. John Wiley & Sons.

Bédard, J.H., 2005. Trace element partitioning in plagioclase feldspar. Geochim. Cosmochim. Acta 70, 3717–3742. https://doi.org/10.1016/j.gca.2006.05.003

Bindeman, I.N., Davis, A.M., 2000. Trace element partitioning between plagioclase and melt: Investigation of dopant influence on partition behavior.

Birck, J.L., Lugmair, G.W., 1988. Nickel and chromium isotopes in Allende inclusions. Earth Planet. Sci. Lett. 90, 131–143. https://doi.org/10.1016/0012-821X(88)90096-9

Bizzarro, M., Ulfbeck, D., Thrane, K., 2006. Nickel isotopes in meteorites: evidence for live 60Fe and distinct 62Ni isotope reservoirs in the early solar system. Lunar Planet. Sci. XXXVII 37.

Bizzarro, M., Ulfbeck, D., Trinquier, A., Thrane, K., Connelly, J.N., Meyer, B.S., 2007. Evidence for a late supernova injection of 60Fe into the protoplanetary disk. Science 316, 1178–81. https://doi.org/10.1126/science.1141040

Bourdon, B., Langmuir, C.H., Zindler, A., 1996. Ridge-hotspot interaction along the Mid-Atlantic Ridge between 37'30' and 40'30'N: the U-Th disequilibrium evidence, Earth and Planetary Science Letters.

Bouvier, A., Vervoort, J.D., Patchett, P.J., 2008. The Lu-Hf and Sm-Nd isotopic composition of CHUR: Constraints from unequilibrated chondrites and implications for the bulk composition of terrestrial planets. Earth Planet. Sci. Lett. 273, 48–57. https://doi.org/10.1016/j.epsl.2008.06.010

Burton, K.W., Schiano, P., Birck, J.-L., Allègre, C.J., Rehkämper, M., Halliday, A.N., Dawson, J.B., 2000. The distribution and behaviour of rhenium and osmium amongst mantle minerals and the age of the lithospheric mantle beneath Tanzania. Earth Planet. Sci. Lett. 183, 93–106. https://doi.org/10.1016/S0012-821X(00)00259-4

Bussod, G.Y.A., Williams, D.R., 1991. Thermal and kinematic model of the southern Rio Grande rift: inferences from crustal and mantle xenoliths from Kilboume Hole, New Mexico. Tectonophysics 197, 373–389.

Cameron, V., Vance, D., 2014. Heavy nickel isotope compositions in rivers and the oceans. Geochim. Cosmochim. Acta 128, 195–211. https://doi.org/10.1016/j.gca.2013.12.007

Cameron, V., Vance, D., Archer, C., House, C.H., 2009. A biomarker based on the stable isotopes of nickel. Proc. Natl. Acad. Sci. U. S. A. 106, 10944–10948. https://doi.org/10.1073/pnas.0900726106

Canil, D., Pearson RL Rudnick, N.D., McDonough Carswell, W. DA, 1994. Ferric iron in

peridotites and mantle oxidation states. Earth Planet. Sci. Lett. 123, 205–220.

Canup, R.M., 2012. Forming a Moon with an Earth-like Composition via a Giant Impact. Science 338, 1052–1055. https://doi.org/10.1126/science.1106818

Canup, R.M., Asphaug, E., 2001. Origin of the Moon in a giant impact near the end of the Earth's formation. Nature 412, 708–712. https://doi.org/10.1038/35089010

Canup, R.M., Barr, A.C., Crawford, D.A., 2013. Lunar-forming impacts: High-resolution SPH and AMR-CTH simulations. Icarus 222, 200–219. https://doi.org/10.1016/J.ICARUS.2012.10.011

Capobianco, C.J., Amelin, A.A., 1994. Metal-silicate partitioning of nickel and cobalt: The influence of temperature and oxygen fugacity. Geochim. Cosmochim. Acta 58, 125–140.

Chako Tchamabé, B., Youmen, D., Owona, S., Ohba, T., Németh, K., Nsangou Ngapna, M., E Asaah, A.N., Aka, F.T., Tanyileke, G., Hell, J. V, 2013. Eruptive history of the Barombi Mbo Maar, Cameroon Volcanic Line, Central Africa: Constraints from volcanic facies analysis. Cent. Eur. J. Geosci 5, 480–496. https://doi.org/10.2478/s13533-012-0147-2

Chen, J.H., Papanastassiou, D.A., 2006. NICKEL ISOTOPE INVESTIGATION BY MC-ICP-MS AND PTIMS, in: Lunar and Planetary Science XXXVII. pp. 61–62.

Chen, J.H., Papanastassiou, D.A., Wasserburg, G.J., 2009. A search for nickel isotopic anomalies in iron meteorites and chondrites. Geochim. Cosmochim. Acta 73, 1461–1471. https://doi.org/10.1016/j.gca.2008.11.040

Chernonozhkin, S.M., Goderis, S., Costas-Rodríguez, M., Claeys, P., Vanhaecke, F., 2016. Effect of parent body evolution on equilibrium and kinetic isotope fractionation: a combined Ni and Fe isotope study of iron and stony-iron meteorites. Geochim. Cosmochim. Acta 186, 168–188. https://doi.org/10.1016/j.gca.2016.04.050

Chernonozhkin, S.M., Goderis, S., Lobo, L., Claeys, P., Vanhaecke, F., 2015. Development of an isolation procedure and MC-ICP-MS measurement protocol for the study of stable isotope ratio variations of nickel. J. Anal. At. Spectrom. 30, 1518–1530. https://doi.org/10.1039/C5JA00080G

Chernonozhkin, S.M., Weyrauch, M., Goderis, S., Oeser, M., McKibbin, S.J., Horn, I., Hecht, L., Weyer, S., Claeys, P., Vanhaecke, F., 2017. Thermal equilibration of iron meteorite and pallasite parent bodies recorded at the mineral scale by Fe and Ni isotope systematics. Geochim. Cosmochim. Acta 217, 95–111. https://doi.org/10.1016/J.GCA.2017.08.022

Ciscato, E.R., Bontognali, T.R.R., Vance, D., 2018. Nickel and its isotopes in organic-rich sediments: implications for oceanic budgets and a potential record of ancient seawater. Earth Planet. Sci. Lett. 494, 239–250. https://doi.org/10.1016/j.epsl.2018.04.061

Cisowski, S.M., Collinson, D.W., Runcorn, S.K., Stephenson, A., Fuller, M., 1983. A REVIEW OF LUNAR PALEOINTENSITY DATA AND IMPLICATIONS FOR THE ORIGIN OF LUNAR MAGNETISM. J. Geophys. Res. 88, A691–A704.

Cook, D.L., Clayton, R.N., Wadhwa, M., Janney, P.E., Davis, A.M., 2008a. Nickel isotopic anomalies in troilite from iron meteorites. Geophys. Res. Lett. 35, 1–5. https://doi.org/10.1029/2007GL032431

Cook, D.L., Clayton, R.N., Wadhwa, M., Janney, P.E., Davis, A.M., 2008b. Nickel isotopic anomalies in troilite from iron meteorites. Geophys. Res. Lett. 35, L01203. https://doi.org/10.1029/2007GL032431

Cook, D.L., Wadhwa, M., Clayton, R.N., Dauphas, N., Janney, P.E., Davis, A.M., 2007. Mass-dependent fractionation of nickel isotopes in meteoritic metal. Meteorit. Planet. Sci. 42, 2067–2077. https://doi.org/10.1111/j.1945-5100.2007.tb01008.x

Cook, D.L., Wadhwa, M., Janney, P.E., Dauphas, N., Clayton, R.N., Davis, A.M., 2006. High precision measurements of non-mass-dependent effects in nickel isotopes in meteoritic metal via multicollector ICPMS. Anal. Chem. 78, 8477–84.

https://doi.org/10.1021/ac061285m

Cornen, G., Bandet, Y., Giresse, P., Maley, J., 1992. The nature and chronostratigraphy of Quaternary pyroclastic accumulations from Lake Barombi Mbo (West-Cameroon). J. Volcanol. Geotherm. Res. 51, 357–374.

Dauphas, N., Teng, F.-Z., Arndt, N.T., 2010. Magnesium and iron isotopes in 2.7 Ga Alexo komatiites: Mantle signatures, no evidence for Soret diffusion, and identification of diffusive transport in zoned olivine. Geochim. Cosmochim. Acta 74, 3274–3291. https://doi.org/10.1016/J.GCA.2010.02.031

Dauritria, J.M., Girod, M., 1987. Cenozoaic Volcanism associated with Swells and Rifts, in: Nixon, P.. (Ed.), Mantle Xenoliths. pp. 195–215.

Dawson, J.B., 2012. Nephelinite-melilitite-carbonatite relationships: Evidence from Pleistocene-recent volcanism in northern Tanzania. Lithos 152, 3–10. https://doi.org/10.1016/j.lithos.2012.01.008

Dawson, J.B., 2002. Metasomatism and Partial Melting in Upper-Mantle Peridotite Xenoliths from the Lashaine Volcano, Northern Tanzania. J. Petrol. 43, 1749–1777. https://doi.org/10.1093/petrology/43.9.1749

Dawson, J.B., 1992. Neogene tectonics and volcanicity in the North Tanzania sector of the Gregory Rift Valley: contrasts with the Kenya sector. Tectonophysics 204, 81–92. https://doi.org/10.1016/0040-1951(92)90271-7

Dawson, J.B., 1964a. Carbonate Tuff Cones in Northern Tanganyika. Geol. Mag. 101, 129. https://doi.org/10.1017/S0016756800048561

Dawson, J.B., 1964b. Carbonatitic volcanic ashes in Northern Tanganyika. Bull. Volcanol. 27, 81–91. https://doi.org/10.1007/BF02597513

Dawson, J.B., Powell, D.G., Reid, A.M., 1970. Ultrabasic Xenoliths and Lava from the Lashaine Volcano, Northern Tanzania. J. Petrol. 11, 519–548. https://doi.org/10.1093/petrology/11.3.519

Day, J.M.D., Pearson, D.G., Macpherson, C.G., Lowry, D., Carracedo, J.-C., 2009. Pyroxenite-rich mantle formed by recycled oceanic lithosphere: Oxygen-osmium isotope evidence from Canary Island lavas. Geology 37, 555–558. https://doi.org/10.1130/G25613A.1

Delano, J.W., 1985. Mare Volcanic Glasses, II: Abundances of Trace Ni and the Composition of the Moon.

Dingwell, D.B., O'Neill, H.S.C., Ertel, W., Spettel, B., 1994. The solubility and oxidation state of nickel in silicate melt at low oxygen fugacities: Results using a mechanically assisted equilibration technique. Geochim. Cosmochim. Acta 58, 1967–1974. https://doi.org/10.1016/0016-7037(94)90428-6

Dosso, L., Bougault, H., Langmuir, C., Bollinger, C., Bonnier, O., Etoubleau, J., 1999. The age and distribution of mantle heterogeneity along the Mid-Atlantic ridge (31-41°N). Earth Planet. Sci. Lett. 170, 269–286. https://doi.org/10.1016/S0012-821X(99)00109-0

Dziewonski, A.M., Anderson, D.L., 1981. Preliminary reference Earth model. Phys. Earth Planet. Inter. 25, 297–356. https://doi.org/10.1016/0031-9201(81)90046-7

Eberhardt, P., Geiss, J., Graf, H., Grögler, N., Krähenbühl, U., Schwaller, H., Schwarzmüller, J., Stettler, A., 1970. Correlation between rock type and irradiation history of Apollo 11 igneous rocks. Earth Planet. Sci. Lett. 10, 67–72. https://doi.org/10.1016/0012-821X(70)90065-8

Ehlers, K., Grove, T.L., Sisson, T.W., Recca, S.I., Zervas, D.A., 1992. The effect of oxygen fugacity on the partitioning of nickel and cobalt between olivine, silicate melt, and metal. Geochim. Cosmochim. Acta 56, 3733–3743. https://doi.org/10.1016/0016-7037(92)90166-G

El Goresy, A., Ramdohr, P., Taylor, L.A., 1971. The opaque minerals in the lunar rocks from Oceanus Procellarum, in: 2ns Lunar Science Conference. The M.I.T. Press, pp. 219–235.

Elliott, T., Steele, R.C.J., 2017. The Isotope Geochemistry of Ni, in: Reviews in Mineralogy and Geochemistry.

Estrade, N., Cloquet, C., Echevarria, G., Sterckeman, T., Deng, T., Tang, Y., Morel, J.-L., 2015. Weathering and vegetation controls on nickel isotope fractionation in surface ultramafic environments (Albania). Earth Planet. Sci. Lett. 423, 24–35. https://doi.org/10.1016/j.epsl.2015.04.018

Faure, G., Mensing, T.M., Faure, G., 2005. Isotopes : principles and applications. Wiley.

Feigenson, M.D., 1986. Continental alkali basalts as mixtures of kimberlite and depleted mantle: Evidence from Kilbourne Hole Maar, New Mexico. Geophys. Res. Lett. 13, 965–968. https://doi.org/10.1029/GL013i009p00965

Finnerty, A.A., Boyd, F.R., 1987. Thermobarometry for Garnet Peridotites, in: Nixon, P.H. (Ed.), Mantle Xenoltihs. Wiley, pp. 381–402.

Fischer, R.A., Nakajima, Y., Campbell, A.J., Frost, D.J., Harries, D., Langenhorst, F., Miyajima, N., Pollok, K., Rubie, D.C., 2015. High pressure metal-silicate partitioning of Ni, Co, V, Cr, Si, and O. Geochim. Cosmochim. Acta 167, 177–194. https://doi.org/10.1016/j.gca.2015.06.026

Fitton, J.G., 2007. The OIB Paradox, in: Foulger, G.R., Jurdy, D.M. (Eds.), Plates, Plumes, and Planetary Processes. The Geological Society of America, pp. 387–409.

Fitton, J.G., 1987. The Cameroon line, West Africa: a comparison between oceanic and continental alkaline volcanism. Geol. Soc. London, Spec. Publ. 30, 273–291. https://doi.org/10.1144/GSL.SP.1987.030.01.13

Fitton, J.G., Dunlop, H.M., 1985. The Cameroon line, West Africa, and its bearing on the origin of oceanic and continental alkali basalt. Earth Planet. Sci. Lett. 72, 23–38. https://doi.org/10.1016/0012-821X(85)90114-1

Fitton, J.G., Saunders, A.D., Kempton, P.D., Hardarson, B.S., 2003. Does depleted mantle form an intrinsic part of the Iceland plume? Geochemistry, Geophys. Geosystems 4. https://doi.org/10.1029/2002GC000424

Freeth, S.J., 1979. Deformation of the African plate as a consequence of membrane stress domains generated by post-Jurassic drift. Earth Planet. Sci. Lett. 45, 93–104. https://doi.org/10.1016/0012-821X(79)90111-0

Frost, D.J., Liebske, C., Langenhorst, F., McCammon, C.A., Trønnes, R.G., Rubie, D.C., 2004. Experimental evidence for the existence of iron-rich metal in the Earth's lower mantle. Nature 428, 409–412. https://doi.org/10.1038/nature02413

Gale, A., Dalton, C.A., Langmuir, C.H., Su, Y., Schilling, J.-G., 2013. The mean composition of ocean ridge basalts. Geochemistry, Geophys. Geosystems 14, 489–518. https://doi.org/10.1029/2012GC004334

Gall, L., 2011. Development and Application of Nickel Stable Isotopes as a New Geochemical Tracer. University Of Oxford.

Gall, L., Williams, H., Siebert, C., Halliday, A.N., 2012. Determination of mass-dependent variations in nickel isotope compositions using double spiking and MC-ICPMS. J. Anal. At. Spectrom. 27, 137. https://doi.org/10.1039/c1ja10209e

Gall, L., Williams, H.M., Halliday, A.N., Kerr, A.C., 2017. Nickel isotopic composition of the mantle. Geochim. Cosmochim. Acta 199, 196–209. https://doi.org/10.1016/j.gca.2016.11.016

Gall, L., Williams, H.M., Siebert, C., Halliday, A.N., Herrington, R.J., Hein, J.R., 2013. Nickel isotopic compositions of ferromanganese crusts and the constancy of deep ocean inputs

and continental weathering effects over the Cenozoic. Earth Planet. Sci. Lett. 375, 148–155. https://doi.org/10.1016/j.epsl.2013.05.019

Garcia, R.F., Gagnepain-Beyneix, J., Chevrot, S., Lognonné, P., 2011. Very preliminary reference Moon model. Phys. Earth Planet. Inter. 188, 96–113. https://doi.org/10.1016/J.PEPI.2011.06.015

Gessmann, C.K., Rubie, D.C., 2000. The origin of the depletions of V, Cr and Mn in the mantles of the Earth and Moon. Earth Planet. Sci. Lett. 184, 95–107. https://doi.org/10.1016/S0012-821X(00)00323-X

Gibson, S.A., McMahon, S.C., Day, J.A., Dawson, J.B., 2013. Highly Refractory Lithospheric Mantle beneath the Tanzanian Craton: Evidence from Lashaine Pre-metasomatic Garnet-bearing Peridotites. J. Petrol. 54, 1503–1546. https://doi.org/10.1093/petrology/egt020

Gramlich, J.W., Machlan, L.A., Barnes, I.L., Paulsen, P.J., 1989. Absolute isotopic abundance ratios and atomic weight of a reference sample of nickel. J. Res. Natl. Inst. Stand. Technol. 94, 347. https://doi.org/10.6028/jres.094.034

Guan, Y., Huss, G.R., Leshin, L.A., 2004. SIMS analyses of Mg, Cr, and Ni isotopes in primitive meteorites and short-lived radionuclides in the early solar system. Appl. Surf. Sci. 231–232, 899–902. https://doi.org/10.1016/j.apsusc.2004.03.163

Gueguen, B., Rouxel, O., Ponzevera, E., Bekker, A., Fouquet, Y., 2013. Nickel Isotope Variations in Terrestrial Silicate Rocks and Geological Reference Materials Measured by MC-ICP-MS. Geostand. Geoanalytical Res. 37, 297–317. https://doi.org/10.1111/j.1751-908X.2013.00209.x

Gueguen, B., Rouxel, O., Rouget, M.-L., Bollinger, C., Ponzevera, E., Germain, Y., Fouquet, Y., 2016. Comparative geochemistry of four ferromanganese crusts from the Pacific Ocean and significance for the use of Ni isotopes as paleoceanographic tracers. Geochim. Cosmochim. Acta 189, 214–235. https://doi.org/10.1016/J.GCA.2016.06.005

Gueguen, B., Sorensen, J. V., Lalonde, S. V., Peña, J., Toner, B.M., Rouxel, O., 2018. Variable Ni isotope fractionation between Fe-oxyhydroxides and implications for the use of Ni isotopes as geochemical tracers. Chem. Geol. 481, 38–52. https://doi.org/10.1016/J.CHEMGEO.2018.01.023

Haase, K.M., Regelous, M., Duncan, R.A., Brandl, P.A., Stroncik, N., Grevemeyer, I., 2011. Insights into mantle composition and mantle melting beneath mid-ocean ridges from postspreading volcanism on the fossil Galapagos Rise Theme: Geochemical Heterogeneities in Oceanic Island Basalt and Mid-ocean Ridge Basalt Sources: Implications for Melting. Geochem. Geophys. Geosyst 12. https://doi.org/10.1029/2010GC003482

Haase, K.M., Regelous, M., Duncan, R.A., Brandl, P.A., Stroncik, N., Grevemeyer, I., 2011. Insights into mantle composition and mantle melting beneath mid-ocean ridges from postspreading volcanism on the fossil Galapagos Rise. Geochemistry, Geophys. Geosystems 12, 1–21. https://doi.org/10.1029/2010GC003482

Halliday, A.N., 2000. Terrestrial accretion rates and the origin of the Moon. Earth Planet. Sci. Lett. 176, 17–30. https://doi.org/10.1016/S0012-821X(99)00317-9

Halliday, A.N., Davidson, J.P., Holden, P., DeWolf, C., Lee, D.-C., Fitton, J.G., 1990. Trace-element fractionation in plumes and the origin of HIMU mantle beneather the Cameroon line. Nature 346, 523–528. https://doi.org/10.1038/346183a0

Halliday, A.N., Davies, G.R., Lee, D.-C., Tommasini, S., Paslick, C.R., Fitton, J.G., James, D.E., 1992a. Lead isotope evidence for young trace element enrichment in the oceanic upper mantle. Nature 359, 623–627. https://doi.org/10.1038/359623a0

Halliday, A.N., Davies, G.R., Lee, D.-C., Tommasini, S., Paslick, C.R., Fitton, J.G., James, D.E., 1992b. Lead isotope evidence for young trace element enrichment in the oceanic upper mantle. Nature 359, 623–627. https://doi.org/10.1038/359623a0

Halliday, A.N., Davies, G.R., Lee, D.C., 1992. Lead isotope evidence for young trace-element enrichment in the oceanic upper mantle. Nature 359, 623–627.

Halliday, A.N., Dickin, A.P., Fallick, A.E., Fitton, J.G., 1988. Mantle dynamics: A Nd, Sr, Pb and O isotopic study of the Cameroon line volcanic chain. J. Petrol. 29, 181–211. https://doi.org/10.1093/petrology/29.1.181

Halliday, A.N., Lee, D.-C., Christensen, J.N., Rehkämper, M., Yi, W., Luo, X., Hall, C.M., Ballentine, C.J., Pettke, T., Stirling, C., 1998. Applications of Multiple Collector-ICPMS to Cosmochemistry, Geochemistry, and Paleoceanography. Geochim. Cosmochim. Acta 62, 919–940. https://doi.org/10.1016/S0016-7037(98)00057-X

Halliday, A.N., Lee, D.-C., Tommasini, S., Davies, G.R., Paslick, C.R., Godfrey Fitton, J., James, D.E., 1995. Incompatible trace elements in OIB and MORB and source enrichment in the sub-oceanic mantle. Earth Planet. Sci. Lett. 133, 379–395. https://doi.org/10.1016/0012-821X(95)00097-V

Hardarson, B.S., Fitton, J.G., 1997. Mechanisms of crustal accretion in Iceland. Geology 25, 1043–1046.

Harpp, K.S., White, W.M., 2001a. Tracing a mantle plume: Isotopic and trace element variations of Galápagos seamounts. Geochemistry, Geophys. Geosystems 2, n/a-n/a. https://doi.org/10.1029/2000GC000137

Harpp, K.S., White, W.M., 2001b. Tracing a mantle plume: Isotopic and trace element variations of Galápagos seamounts. Geochemistry, Geophys. Geosystems 2, n/a-n/a. https://doi.org/10.1029/2000GC000137

Hart, S.R., 1988. Heterogeneous mantle domains: signatures, genesis and mixing chronologies. Earth Planet. Sci. Lett. 90, 273–296. https://doi.org/10.1016/0012-821X(88)90131-8

Hart, S.R., Davis, K.E., 1978. Nickel partitioning between olivine and silicate melt. Earth Planet. Sci. Lett. 40, 203–219.

Hartmann, W.K., Davis, D.R., 1975. Satellite-Sized Planetesimals and Lunar Origin, ICARUS.

Harvey, J., Dale, C.W., Gannoun, A., Burton, K.W., 2011. Osmium mass balance in peridotite and the effects of mantle-derived sulfides on basalt petrogenesis. Geochim. Cosmochim. Acta 75, 5574–5596. https://doi.org/10.1016/j.gca.2011.07.001

Harvey, J., Konig, S., Luguet, A., 2015. The effects of melt depletion and metasomatism on highly siderophile and strongly chalcophile elements: S-Se-Te-Re-PGE systematics of peridotite xenoliths from Kilbourne Hole, New Mexico. Geochim. Cosmochim. Acta 166, 210–233. https://doi.org/10.1016/j.gca.2015.06.028

Harvey, J., Yoshikawa, M., Hammond, S.J., Burton, K.W., 2012. Deciphering the trace element characteristics in kilbourne hole peridotite xenoliths: Melt-rock interaction and metasomatism beneath the Rio Grande Rift, SW USA. J. Petrol. 53, 1709–1742. https://doi.org/10.1093/petrology/egs030

Hauri, E.H., 1996. Major-element variability in the Hawaiian mantle plume. Nature 382, 415–419. https://doi.org/10.1038/382415a0

Henderson, P., Henderson, G., 2009. The Cambridge Handbook of Earth Science Data. Cambridge University Press.

Herzberg, C., Vidito, C., Starkey, N.A., 2016. Nickel–cobalt contents of olivine record origins of mantle peridotite and related rocks. Am. Mineral. 101, 1952–1966. https://doi.org/10.2138/am-2016-5538

Hiesinger, H., Head III, J.W., 2006. New Views of Lunar Geoscience: An Introduction and Overview, in: Reviews in Mineralogy & Geochemistry Volume 60: New Views of the Moon. pp. 1–67.

Hofmann, A., Bekker, A., Dirks, P., Gueguen, B., Rumble, D., Rouxel, O.J., 2014. Comparing

orthomagmatic and hydrothermal mineralization models for komatiite-hosted nickel deposits in Zimbabwe using multiple-sulfur, iron, and nickel isotope data. Miner. Depos. 49, 75–100. https://doi.org/10.1007/s00126-013-0476-1

Holzheid, A., Palme, H., Chakraborty, S., 1997. The activities of NiO, CoO and FeO in silicate melts. Chem. Geol. 139, 21–38.

Irving, A.J., 1980. Petrology and geochemistry of composite ultramafic xenoliths in alkalic basalts and implications for magmatic processes within the mantle. Am. J. Sci. 280–A, 389–426.

James, D.E., Padovani, E.R., Hart, S.R., 1980. Preliminary results on the oxygen isotopic composition of the lower crust, Kilbourne Hole Maar, New Mexico. Geophys. Res. Lett. 7, 321–324. https://doi.org/10.1029/GL007i005p00321

Jana, D., Walker, D., 1997. The influence of silicate melt composition on distribution of siderophile elements among metal and silicate liquids. Earth Planet. Sci. Lett. 150, 463–472. https://doi.org/10.1016/S0012-821X(97)00079-4

Kegler, P., Holzheid, A., Frost, D.J., Rubie, D.C., Dohmen, R., Palme, H., 2008. New Ni and Co metal-silicate partitioning data and their relevance for an early terrestrial magma ocean. Earth Planet. Sci. Lett. 268. https://doi.org/10.1016/j.epsl.2007.12.020

Keller, G.R., Morgan, P., Seager, W.R., 1990. Crustal structure, gravity anomalies and heat flow in the southern Rio Grande rift and their relationship to extensional tectonics. Tectonophysics 174, 21–37.

Kempton, P.D., Fitton, J.G., Saunders, A.D., Nowell, G.M., Taylor, R.N., Hardarson, B.S., Pearson, G., 2000. The Iceland plume in space and time: a Sr–Nd–Pb–Hf study of the North Atlantic rifted margin, Earth and Planetary Science Letters. Elsevier. https://doi.org/10.1016/S0012-821X(00)00047-9

Kirsten, T., Deubner, J., Horn, P., Kaneoka, I., Kiko, J., Schaeffer, O.A., Thio, S.K., 1972. The rare gas record of Apollo 14 and 15 samples. Proc. Third Lunar Sci. Conf. vol. 3, p. 1865 - 1889 3, 1865–1889.

Kodolányi, J., Stephan, T., Trappitsch, R., Pignatari, M., Davis, A.M., Pellin, M.J., 2018. Iron and nickel isotope compositions of presolar silicon carbide grains from supernovae. Geochim. Cosmochim. Acta 221, 127–144. https://doi.org/10.1016/J.GCA.2017.05.029

König, S., Wille, M., Voegelin, A., Schoenberg, R., 2016. Molybdenum isotope systematics in subduction zones. Earth Planet. Sci. Lett. 447, 95–102. https://doi.org/10.1016/j.epsl.2016.04.033

Koornneef, J.M., Davies, G.R., Döpp, S.P., Vukmanovic, Z., Nikogosian, I.K., Mason, P.R.D., 2009. Nature and timing of multiple metasomatic events in the sub-cratonic lithosphere beneath Labait, Tanzania. Lithos 112, 896–912. https://doi.org/10.1016/J.LITHOS.2009.04.039

Korotev, R.L., 2018. List of Lunar Meteorites [WWW Document]. http://meteorites.wustl.edu/lunar/moon_meteorites_list_alpha.htm.

Krawczynski, M.J., Grove, T.L., 2012. Experimental investigation of the influence of oxygen fugacity on the source depths for high titanium lunar ultramafic magmas. Geochim. Cosmochim. Acta 79, 1–19. https://doi.org/10.1016/j.gca.2011.10.043

Langmuir, C.H., Klein, E.M., Plank, T., 1992. Petrological Systematics of Mid-Ocean Ridge Basalts: Constraints on Melt Generation Beneath Ocean Ridges, in: Phipps Morgan, J., Blackman, D.K., Sinton, J.M. (Eds.), Mantle Flow and Melt Generation at Mantle Ridges. American Geophysical Union (AGU), pp. 183–280. https://doi.org/10.1029/GM071p0183

Lazar, C., Young, E.D., Manning, C.E., 2012. Experimental determination of equilibrium nickel isotope fractionation between metal and silicate from 500 °C to 950 °C. Geochim. Cosmochim. Acta 86, 276–295. https://doi.org/10.1016/J.GCA.2012.02.024

Lee, D.-C., 1994. A Chemical, Isotopic, and Geochronological Study of the Cameroon Line, West Africa. University of Michigan.

Lee, D.-C., Halliday, A.N., Davies, G.R., Essene, E.J., Fitton, J.G., Temdjim, R., 1996. Melt Enrichment of Shallow Depleted Mantle: a Detailed Petrological, Trace Element and Isotopic Study of Mantle- Derived Xenoliths and Megacrysts from the Cameroon Line. J. Petrol. 37, 15–441.

Lee, D., Halliday, A.N., Davies, G.R., Essene, E.J., Fitton, J.G., Temdjim, R., 1996. Melt Enrichment of Shallow Depleted Mantle: a Detailed Petrological, Trace Element and Isotopic Study of Mantle- Derived Xenoliths and Megacrysts from the Cameroon Line. J. Petrol. 37, 415–441.

Liang, Y.-H., Halliday, A.N., Siebert, C., Fitton, J.G., Burton, K.W., Wang, K.-L., Harvey, J., 2017. Molybdenum isotope fractionation in the mantle. Geochim. Cosmochim. Acta 199, 91–111. https://doi.org/10.1016/J.GCA.2016.11.023

Liu, L., Spasojević, S., Gurnis, M., 2008. Reconstructing Farallon Plate Subduction Beneath North America Back to the Late Cretaceous. Science (80-.). 322. https://doi.org/10.1126/science.1164170

Liu, S., Li, Y., Ju, Y., Liu, J., Liu, J., Shi, Y., 2018. Equilibrium nickel isotope fractionation in nickel sulfide minerals. Geochim. Cosmochim. Acta 222, 1–16. https://doi.org/10.1016/J.GCA.2017.10.018

Lodders, K., 2003. Solar System Abundances and Condensation Temperatures of the Elements. Astrophys. Journal, 591, 1220–1247.

Ma, Z., Thompson, R.N., Lykke, K.R., Pellin, M.J., Davis, A.M., 1995. Time-of-Flight Mass Spectrometer with Improved Resolution Review of. Cit. Rev. Sci. Instruments 66, 1150. https://doi.org/10.1063/1.1145546

Maley, J., Livingstone, D.A., Giresse, P., Thouveny, N., Brenac, P., Kelts, K., Kling, G., Stager, C., Haag, M., Fournier, M., Bandet, Y., Williamson, D., Zogning, A., 1990. Lithostratigraphy, volcanism, paleomagnetism and palynology of Quaternary lacustrine deposits from Barombi Mbo (West Cameroon): preliminary results. J. Volcanol. Geotherm. Res. 42, 319–335.

McCammon, C., 2005. The Paradox of Mantle Redox. Science (80-.). 308. https://doi.org/10.1126/science.1108162

McDonough, W.F., Sun, S. s., 1995. The composition of the Earth. Chem. Geol. 120, 223–253. https://doi.org/10.1016/0009-2541(94)00140-4

Menzies, M.A., Arculus, R.J., G, B.M., Bergman, S.C., Ehrenberg, S.N., Irving, A.J., Roden, M.F., Schulze, D.J., 1987. A record of subduction processes and within-plate volcanism in lithospheric xenoliths of southwestern USA, in: Nixon, P.. (Ed.), Mantle Xenoliths. pp. 59–74.

Meyer, C., 2011. Lunar Sample Compendium.

Meyer, C., 2003. Lunar Regolith - NASA Lunar Petrographic Educational Thin Section Set.

Moorbath, S., Sigurdsson, H., Goodwin, R., 1968. K-Ar ages of the oldest exposed rocks in Iceland. Earth Planet. Sci. Lett. 4, 197–205. https://doi.org/10.1016/0012-821X(68)90035-6

Morand, P., Allègre, C.J., 1983. Nickel isotopic studies in meteorites. Earth Planet. Sci. Lett. 63, 167–176. https://doi.org/10.1016/0012-821X(83)90034-1

Morand, P., Audouze, J., Allègre, C.J., 1980. Search for nickel isotopic anomaly of meteorites, in: 43rd Annual Meeting of the Meteoritical Society.

Moreau, C., Regnoult, J.-M., Déruelle, B., Robineau, B., 1987. A new tectonic model for the Cameroon Line, Central Africa. Tectonophysics 141, 317–334.

https://doi.org/10.1016/0040-1951(87)90206-X

Morgan, W.J., 1983. Hotspot tracks and the early rifting of the Atlantic. Tectonophysics 94, 123–139. https://doi.org/10.1016/0040-1951(83)90013-6

Mostefaoui, S., Lugmair, G.W., Hoppe, P., 2005. 60 Fe: A Heat Source for Planetary Differentiation from a Nearby Supernova Explosion. Astrophys. J. 625, 271–277. https://doi.org/10.1086/429555

Moynier, F., Agranier, A., Hezel, D.C., Bouvier, A., 2010. Sr stable isotope composition of Earth, the Moon, Mars, Vesta and meteorites, Earth and Planetary Science Letters. https://doi.org/10.1016/j.epsl.2010.10.017

Moynier, F., Albarède, F., Herzog, G.F., 2006. Isotopic composition of zinc, copper, and iron in lunar samples. Geochim. Cosmochim. Acta 70, 6103–6117. https://doi.org/10.1016/j.gca.2006.02.030

Moynier, F., Blichert-Toft, J., Telouk, P., Luck, J.-M., Albarède, F., 2007. Comparative stable isotope geochemistry of Ni, Cu, Zn, and Fe in chondrites and iron meteorites. Geochim. Cosmochim. Acta 71, 4365–4379. https://doi.org/10.1016/j.gca.2007.06.049

Moynier, F., Blichert-Toft, J.F., Telouk, P., Albarede, F., 2005. Excesses of 60Ni in chondrites and iron meteorites, in: Lunar and Planetary Science XXXVI.

Neal, C.R., 2001. The Interior of the Moon: The presence of garnet in the primitive deep lunar mantle. J. Geophys. Res. 106, 27865–27885.

Neal, C.R., Taylor, L.A., 1992. Petrogenesis of mare basalts: A record of lunar volcanism*. Geochim. Cosmochim. Acta 56, 2177–2211.

Neal, C.R., Taylor, L.A., 1991. Evidence for metasomatism of the lunar highlands and the origin of whitlockite. Geochim. Cosmochim. Acta 55, 2965–2980.

Newsom, H.E., 1986. Constraints on the Origin of the Moon from the Abundance of Molybdenum and Other Siderophile Elements.

Nicholls, D., 1974. Complexes and First Row Transition Elements. Macmillan, London.

Nier, A.O., 1940. A Mass Spectrometer for Routine Isotope Abundance Measurements. Rev. Sci. Instrum. 11. https://doi.org/10.1063/1.1751688

Niu, Y., Batiza, R., 1997. Trace element evidence from seamounts for recycled oceanic crust in the Eastern Pacific mantle. Earth Planet. Sci. Lett. 148, 471–483. https://doi.org/10.1016/S0012-821X(97)00048-4

Nixon, P.., 1987. Introduction, in: Mantle Xenoliths. pp. 1–3.

Norton, I.O., 2007. Speculations on Cretaceous tectonic history of the northwest Pacific and a tectonic origin for the Hawaii hotspot, in: Plates, Plumes, and Planetary Processes. pp. 451–470.

O'Neill, H.S.C., 1981. The transition between spinel lherzolite and garnet lherzolite, and its use as a Geobarometer. Contrib. to Mineral. Petrol. 77, 185–194. https://doi.org/10.1007/BF00636522

Palme, H., Spettel, B., Bischoff, A., St6ffler, D., 1984. Early Differentiation of the Moon' Evidence from Trace Elements in Plagioclase, in: PROCEEDINGS OF THE FIFTEENTH LUNAR AND PLANETARY SCIENCE CONFERENCE, PART 1 JOURNAL OF GEOPHYSICAL RESEARCH. https://doi.org/10.1029/JB089iS01p000C3

Paniello, R.C., Day, J.M.D., Moynier, F., 2012. Zinc isotopic evidence for the origin of the Moon. Nature 490, 376–379. https://doi.org/10.1038/nature11507

Papanastassiou, D.A., Wasserburg, G.J., 1971. Rb-Sr AGES OF IGNEOUS ROCKS FROM THE APOLLO 14 MISSION AND THE AGE OF THE FRA MAURO FORMATION. Earth Planet. Sci. Lett. 12, 36–48.

Papike, J.J., Fowler, G.W., Adcock, C.T., Shearer, C.K., 1999. Systematics of Ni and Co in olivine from planetary melt systems: Lunar mare basalts. Am. Mineral. 84, 392–399. https://doi.org/10.2138/am-1999-0324

Paslick, C., Halliday, A.N., James, D., Dawson, J.B., 1995. Enrichment of the continental lithosphere by OIB melts: Isotopic evidence from the volcanic province of northern Tanzania. Earth Planet. Sci. Lett. 130, 109–126.

Paslick, C.R., 1995. A Geochemical Study of Volcanism associated with the early stages of Continental Rifting in Northern Tanzanian. University of Michigan.

Paslick, C.R., Halliday, A.N., Lange, R.A., James, D., Dawson, J.B., 1996. Indirect crustal contamination: evidence from isotopic and chemical disequilibria in minerals from alkali basalts and nephelinites from northern Tanzania. Contrib. to Mineral. Petrol. 125, 277–292. https://doi.org/10.1007/s004100050222

Peale, S.J., Cassen, P., 1978. Contribution of tidal dissipation to lunar thermal history. Icarus 36, 245–269. https://doi.org/10.1016/0019-1035(78)90109-4

Perkins, D., Anthony, E.Y., 2011. The evolution of spinel lherzolite xenoliths and the nature of the mantle at Kilbourne Hole, New Mexico. Contrib. to Mineral. Petrol. 162, 1139–1157. https://doi.org/10.1007/s00410-011-0644-1

Pike, J.E.N., Meyer, C.E., Wilshire, H.G., 1980. Petrography and Chemical Composition of a Suite of Ultramafic Xenoliths from Lashaine, Tanzania. J. Geol. 88, 343–352. https://doi.org/10.1086/628512

Pinter, Z., Patko, L., Djoukam, F.T.J., Kovacs, I., Tchouankoue, J.P., Falus, G., Konc, Z., Tommasi, A., Barou, F., Mihaly, J., Nemeth, C., Jeffries, T., 2015. Characterization of the sub-continental lithospheric mantle beneath the Cameroon volcanic line inferred from alkaline basalt hosted peridotite xenoliths from Barombi Mbo and Nyos Lakes. J. African Earth Sci. 111, 170–193. https://doi.org/10.1016/j.jafrearsci.2015.07.006

Porter, S.J., Selby, D., Cameron, V., 2014. Characterising the nickel isotopic composition of organic-rich marine sediments. Chem. Geol. 387, 12–21. https://doi.org/10.1016/j.chemgeo.2014.07.017

Quitte, G., Halliday, A.N., Meyer, B.S., Markowski, A., Latkoczy, C., Gunther, D., 2007. Correlated Iron 60, Nickel 62, and Zirconium 96 in Refractory Inclusions and the Origin of the Solar System. Astrophys. J. 655, 678–684. https://doi.org/10.1086/509771

Quitté, G., Meier, M., Latkoczy, C., Halliday, A.N., Günther, D., Gunther, D., Günther, D., Gunther, D., Günther, D., 2006. Nickel isotopes in iron meteorites–nucleosynthetic anomalies in sulfides with no effects in metals and no trace of 60Fe. Earth Planet. Sci. Lett. 242, 16–25. https://doi.org/10.1016/j.epsl.2005.11.053

Quitté, G., Oberli, F., 2006. Quantitative extraction and high precision isotope measurements of nickel by MC-ICPMS. J. Anal. At. Spectrom. 21, 1249. https://doi.org/10.1039/b607569j

Rai, N., Westrenen, W. Van, 2014. Lunar core formation : New constraints from metal – silicate partitioning of siderophile elements. Earth Planet. Sci. Lett. 388, 343–352. https://doi.org/10.1016/j.epsl.2013.12.001

Ratié, G., Jouvin, D., Garnier, J., Rouxel, O., Miska, S., Guimaraes, E., Cruz Vieira, L., Sivry, Y., Zelano, I., Montarges-Pelletier, E., Thil, F., Quantin, C., 2015. Nickel isotope fractionation during tropical weathering of ultramafic rocks. Chem. Geol. 402, 68–76. https://doi.org/10.1016/j.chemgeo.2015.02.039

Ratié, G., Quantin, C., Jouvin, D., Calmels, D., Ettler, V., Sivry, Y., Vieira, L.C., Ponzevera, E., Garnier, J., Cruz Vieira, L., Ponzevera, E., Garnier, J., 2016. Nickel isotope fractionation during laterite Ni ore smelting and refining : Implications for tracing the sources of Ni in smelter-affected soils. Appl. Geochemistry 64, 136–145. https://doi.org/10.1016/j.apgeochem.2015.09.005

Reedy, R.C., Englert, P., 1986. Workshop on COSMOGENIC NUCLIDES.

Regelous, M., Elliott, T., Coath, C.D., 2008. Nickel isotope heterogeneity in the early Solar System. Earth Planet. Sci. Lett. 272, 330–338. https://doi.org/10.1016/j.epsl.2008.05.001

Reid, A.M., Donaldson, C.H., Brown, R.W., Ridley, W.I., Dawson, J.B., 1975. Mineral chemistry of peridotite xenoliths from the Lashaine volcano, Tanzania. Phys. Chem. Earth 9, 525–543. https://doi.org/10.1016/0079-1946(75)90037-3

Rhodes, J.M., Dawson, J.B., 1975. Major and trace element chemistry of peridotite inclusions from the Lashaine volcano, Tanzania. Phys. Chem. Earth 9, 545–557. https://doi.org/10.1016/0079-1946(75)90038-5

Righter, K., 2002. Does the Moon Have a Metallic Core? Constraints from Giant Impact Modeling and Siderophile Elements. Icarus 158, 1–13. https://doi.org/10.1006/icar.2002.6859

Righter, K., Drake, M.J., Yaxley, G., 1997. Prediction of siderophile element metal-silicate partition coefficients to 20 GPa and 2800°C: the effects of pressure, temperature, oxygen fugacity, and silicate and metallic melt compositions. Phys. Earth Planet. Inter. 100, 115–134. https://doi.org/10.1016/S0031-9201(96)03235-9

Righter, K., Pando, K.M., Danielson, L., Lee, C.-T., 2010. Partitioning of Mo, P and other siderophile elements (Cu, Ga, Sn, Ni, Co, Cr, Mn, V, and W) between metal and silicate melt as a function of temperature and silicate melt composition. Earth Planet. Sci. Lett. 291, 1–9. https://doi.org/10.1016/J.EPSL.2009.12.018

Roden, M.F., Irving, A.J., Murthy, V.R., 1988. Isotopic and trace element composition of the upper mantle beneath a young continental rift: Results from Kilbourne Hole, New Mexico. Geochim. Cosmochim. Acta 52, 461–473. https://doi.org/10.1016/0016-7037(88)90101-9

Rugel, G., Faestermann, T., Knie, K., Korschinek, G., Poutivtsev, M., Schumann, D., Kivel, N., Günther-Leopold, I., Weinreich, R., Wohlmuther, M., 2009. New Measurement of the ^{60}Fe Half-Life. Phys. Rev. Lett. 103, 072502. https://doi.org/10.1103/PhysRevLett.103.072502

Sato, M., Hickling, N.L., McLane, J.E., 1973. Oxygen fugacity values of Apollo 12, 14, and 15 lunar samples and reduced state of lunar magmas, in: Proceedings of the Fourth Lunar Science Conference. pp. 1061–1079.

Satsukawa, T., Michibayashi, K., Anthony, E.Y., Stern, R.J., Gao, S.S., Liu, K.H., 2011. Seismic anisotropy of the uppermost mantle beneath the Rio Grande rift: Evidence from Kilbourne Hole peridotite xenoliths, New Mexico. Earth Planet. Sci. Lett. 311, 172–181. https://doi.org/10.1016/J.EPSL.2011.09.013

Sedaghatpour, F., Teng, F.Z., Liu, Y., Sears, D.W.G., Taylor, L.A., 2013. Magnesium isotopic composition of the Moon. Geochim. Cosmochim. Acta 120, 1–16. https://doi.org/10.1016/j.gca.2013.06.026

Sharp, Z.D., Shearer, C.K., McKeegan, K.D., Barnes, J.D., Wang, Y.Q., 2010. The Chlorine Isotope Composition of the Moon and Implications for an Anhydrous Mantle. Science (80-.). 329. https://doi.org/10.1126/science.1191349

Shearer, C.K., Hess, P.C., Wieczorek, M.A., Pritchard, M.E., Parmentier, E.M., Borg, L.E., Longhi, J., Elkins-Tanton, L.T., Neal, C.R., Antonenko, I., Canup, R.M., Halliday, A.N., Grove, T.L., Hager, B.H., Lee, D.C., Wiechert, U., 2006. Thermal and Magmatic Evolution of the Moon, in: Reviews in Mineralogy & Geochemistry Volume 60: New Views of the Moon. pp. 365–502.

Shimamura, T., Lugmair, G.W., 1983. Ni isotopic compositions in Allende and other meteorites. Earth Planet. Sci. Lett. 63, 177–188. https://doi.org/10.1016/0012-821X(83)90035-3

Shukolyukov, A., Lugmair, G.W., 1993a. 60Fe in eucrites. Earth Planet. Sci. Lett. 119, 159–

166. https://doi.org/10.1016/0012-821X(93)90013-Y

Shukolyukov, A., Lugmair, G.W., 1993b. Live Iron-60 in the Early Solar System. Science (80-.). 259, 1138–1142.

Siebert, C., Nägler, T.F., Kramers, J.D., 2001. Determination of molybdenum isotope fractionation by double-spike multicollector inductively coupled plasma mass spectrometry. Geochemistry, Geophys. Geosystems 2, n/a-n/a. https://doi.org/10.1029/2000GC000124

Silveira, G., Stutzmann, E., Davaille, A., Montagner, J.-P., Mendes-Victor, L., Sebai, A., 2006. Azores hotspot signature in the upper mantle. J. Volcanol. Geotherm. Res. 156, 23–34. https://doi.org/10.1016/J.JVOLGEORES.2006.03.022

Simon, J.I., DePaolo, D.J., 2010. Stable calcium isotopic composition of meteorites and rocky planets, Earth and Planetary Science Letters. https://doi.org/10.1016/j.epsl.2009.11.035

Sobolev, A. V, Hofmann, A.W., Kuzmin, D. V, Yaxley, G.M., Arndt, N.T., Chung, S.-L., Danyushevsky, L. V, Elliott, T., Frey, F.A., Garcia, M.O., Gurenko, A.A., Kamenetsky, V.S., Kerr, A.C., Krivolutskaya, N.A., Matvienkov, V. V, Nikogosian, I.K., Rocholl, A., Sigurdsson, I.A., Sushchevskaya, N.M., Teklay, M., 2007. The Amount of Recycled Crust in Sources of Mantle-Derived Melts. Science (80-.). 316.

Sobolev, A. V, Hofmann, A.W., Sobolev, S. V, Nikogosian, I.K., 2005. An olivine-free mantle source of Hawaiian shield basalts. Nature 434.

Spivak-Birndorf, L.J., Wang, S.-J., Bish, D.L., Wasylenki, L.E., 2018. Nickel isotope fractionation during continental weathering. Chem. Geol. 476, 316–326. https://doi.org/10.1016/J.CHEMGEO.2017.11.028

Steele, A.M., Colson, R.O., Haskin, L.A., 1991. Co and Ni as Incompatible elements in the Lunar Mantle: Implications for fO2 and the Petrogenesis of Apollo 15 Green Glass, in: LPSC XXII.

Steele, R.C.J., Coath, C.D., Regelous, M., Russell, S., Elliott, T., 2012. Neutron-poor nickel isotope anomalies in meteorites. Astrophys. J. 758, 59. https://doi.org/10.1088/0004-637X/758/1/59

Steele, R.C.J., Elliott, T., Coath, C.D., Regelous, M., 2011. Confirmation of mass-independent Ni isotopic variability in iron meteorites. Geochim. Cosmochim. Acta 75, 7906–7925. https://doi.org/10.1016/J.GCA.2011.08.030

Steenstra, E.S., Rai, N., Knibbe, J.S., Lin, Y.H., Van Westrenen, W., 2016. New geochemical models of core formation in the Moon from metal-silicate partitioning of 15 siderophile elements. Earth Planet. Sci. Lett. 441, 1–9. https://doi.org/10.1016/j.epsl.2016.02.028

Strelow, F.W.E., 1990. Distribution coefficients and cation-exchange behaviour of some ammines and aquo complexes of metallic elements in ammonium nitrate solution. Anal. Chim. Acta 233, 129–134. https://doi.org/10.1016/S0003-2670(00)83468-6

Strelow, F.W.E., Weinert, C.H.S.W., Eloff, C., 1972. Distribution coefficients and anion exchange behavior of elements in oxalic acid-hydrochloric acid mixtures. Anal. Chem. 44, 2352–2356. https://doi.org/10.1021/ac60322a001

Sun, C., Graff, M., Liang, Y., 2017. Trace element partitioning between plagioclase and silicate melt: The importance of temperature and plagioclase composition, with implications for terrestrial and lunar magmatism. Geochim. Cosmochim. Acta 206, 273–295. https://doi.org/10.1016/j.gca.2017.03.003

Tachibana, S., Huss, G.R., 2003. The Initial Abundance of 60 Fe in the Solar System. Astrophys. J. 588, L41–L44. https://doi.org/10.1086/375362

Tachibana, S., Huss, G.R., Kita, N.T., Shimoda, G., Morishita, Y., 2006. 60 Fe in Chondrites: Debris from a Nearby Supernova in the Early Solar System? Astrophys. J. 639, L87–L90. https://doi.org/10.1086/503201

Tanimizu, M., Hirata, T., 2006. Determination of natural isotopic variation in nickel using inductively coupled plasma mass spectrometry. J. Anal. At. Spectrom. 21, 1423. https://doi.org/10.1039/b609543g

Taylor, S.R., 1982. A Lunar Perspective. Lunar and Planetary Institute.

Taylor, S.R., 1975. Lunar Science: A Post-Apollo View.

Teng, F.-Z., Dauphas, N., Huang, S., Marty, B., 2013. Iron isotopic systematics of oceanic basalts. Geochim. Cosmochim. Acta 107, 12–26. https://doi.org/10.1016/J.GCA.2012.12.027

Thompson, G., Bryan, W.B., Humphris, S.E., 1989. Axial volcanism on the East Pacific Rise, in: Magmatism in the Ocean Basins. pp. 181–200.

Trappitsch, R., Stephan, T., Savina, M.R., Davis, A.M., Pellin, M.J., Rost, D., Gyngard, F., Gallino, R., Bisterzo, S., Cristallo, S., Dauphas, N., 2018. Simultaneous iron and nickel isotopic analyses of presolar silicon carbide grains. Geochim. Cosmochim. Acta 221, 87–108. https://doi.org/10.1016/J.GCA.2017.05.031

van Kan Parker, M., Sanloup, C., Sator, N., Guillot, B., Tronche, E.J., Perrillat, J.-P., Mezouar, M., Rai, N., van Westrenen, W., 2012. Neutral buoyancy of titanium-rich melts in the deep lunar interior. Nat. Geosci. 5, 186–189. https://doi.org/10.1038/ngeo1402

Vance, D., Little, S.H., Archer, C., Cameron, V., Andersen, M.B., Rijkenberg, M.J.A., Lyons, T.W., 2016. The oceanic budgets of nickel and zinc isotopes: the importance of sulfidic environments as illustrated by the Black Sea. Philos. Trans. A. Math. Phys. Eng. Sci. 374, 20150294. https://doi.org/10.1098/rsta.2015.0294

Vauchez, A., Dineur, F., Rudnick, R., 2005. Microstructure, texture and seismic anisotropy of the lithospheric mantle above a mantle plume: Insights from the Labait volcano xenoliths (Tanzania). Earth Planet. Sci. Lett. 232, 295–314. https://doi.org/10.1016/J.EPSL.2005.01.024

Ventura, G.T., Gall, L., Siebert, C., Prytulak, J., Szatmari, P., Hürlimann, M., Halliday, A.N., 2015. The stable isotope composition of vanadium, nickel, and molybdenum in crude oils. Appl. Geochemistry 59, 104–117. https://doi.org/10.1016/j.apgeochem.2015.04.009

Victor, A.H., 1986. Selective separation of Nickel from other elements by cation-exchange chromatography in dimethylglyoxime/hydrochloric acid/acetone media. Anal. Chim. Acta 183, 155–161.

Wadhwa, M., 2008. Redox Conditions on Small Bodies, the Moon and Mars, in: Reviews in Mineralogy and Geochemistry. GeoScienceWorld, pp. 493–510. https://doi.org/10.2138/rmg.2008.68.17

Walter, L.S., French, B.M., Heinrich, K.F.J., Lowman, P.D., Doan, A.S., Adler, I., 1971. Mineralogical studies of Apollo 12 samples, in: 2nd Lunar Science Conference. M.I.T. Press, pp. 343–358.

Wang, K., Jacobsen, S.B., Sedaghatpour, F., Chen, H., Korotev, R.L., 2015. The earliest Lunar Magma Ocean differentiation recorded in Fe isotopes. Earth Planet. Sci. Lett. 430, 202–208. https://doi.org/10.1016/j.epsl.2015.08.019

Wang, S.-J., Wasylenki, L.E., 2017. Experimental constraints on reconstruction of Archean seawater Ni isotopic composition from banded iron formations. Geochim. Cosmochim. Acta 206, 137–150. https://doi.org/10.1016/J.GCA.2017.02.023

Warren, P.H., 1985. THE MAGMA OCEAN CONCEPT AND LUNAR EVOLUTION. Ann. Rev. Earth planet. Sci 13, 201–241.

Warren, P.H., Wasson, J.T., 1979. The Origin of KREEP. Rev. Geophys. Sp. Phys. 17.

Wasylenki, L.E., Howe, H.D., Spivak-Birndorf, L.J., Bish, D.L., 2015. Ni isotope fractionation during sorption to ferrihydrite: Implications for Ni in banded iron formations. Chem. Geol.

400, 56–64. https://doi.org/10.1016/j.chemgeo.2015.02.007

Weber, R.C., Lin, P., Garnero, E.J., Williams, Q., Lognonné, P., 2011. Seismic Detection of the Lunar Core 331, 309–312.

Wedepohl, K.H., 1974. Nickel, in: Wedepohl, K.H. (Ed.), Handbook of Geochemistry. Springer.

Weis, D., Kieffer, B., Maerschalk, C., Barling, J., de Jong, J., Williams, G.A., Hanano, D., Pretorius, W., Mattielli, N., Scoates, J.S., Goolaerts, A., Friedman, R.M., Mahoney, J.B., 2006. High-precision isotopic characterization of USGS reference materials by TIMS and MC-ICP-MS. Geochemistry, Geophys. Geosystems 7, n/a-n/a. https://doi.org/10.1029/2006GC001283

Weyer, S., Anbar, A.D., Brey, G.P., Münker, C., Mezger, K., Woodland, A.B., 2007. Fe-isotope fractionation during partial melting on Earth and the current view on the Fe-isotope budgets of the planets (reply to the comment of F. Poitrasson and to the comment of B.L. Beard and C.M. Johnson on "Iron isotope fractionation during planetary differentiation" by S. Weyer, A.D. Anbar, G.P. Brey, C. Münker, K. Mezger and A.B. Woodland). Earth Planet. Sci. Lett. 256, 638–646. https://doi.org/10.1016/J.EPSL.2007.01.038

White, W.M., 1985. Sources of oceanic basalts: Radiogenic isotopic evidence. Geology 13, 115. https://doi.org/10.1130/0091-7613(1985)13<115:SOOBRI>2.0.CO;2

White, W.M., McBirney, A.R., Duncan, R.A., 1993. Petrology and geochemistry of the Galápagos Islands: Portrait of a pathological mantle plume. J. Geophys. Res. Solid Earth 98, 19533–19563. https://doi.org/10.1029/93JB02018

White, W.M., Tapia, M.D.M., Schilling, J.-G., 1979. The petrology and geochemistry of the Azores Islands. Contrib. to Mineral. Petrol. 69, 201–213. https://doi.org/10.1007/BF00372322

Wiechert, U., Halliday, A.N., Lee, D.-C., Snyder, G.A., Taylor, L.A., Rumble, D., 2001. Oxygen Isotopes and the Moon-Forming Giant Impact. Science (80-.). 294, 345–348.

Wieczorek, M.A., Jolliff, B.L., Khan, A., Pritchard, M.E., Weiss, B.P., Williams, J.G., Hood, L.L., Righter, K., Neal, C.R., Shearer, C.K., McCallum, I.S., Tompkins, S., Hawke, B.R., Peterson, C., Gillis, J.J., Bussey, B., 2006. The Constitution and Structure of the Lunar Interior, in: Reviews in Mineralogy & Geochemistry Volume 60: New Views of the Moon. pp. 221–343.

Willbold, M., Stracke, A., 2006. Trace element composition of mantle end-members: Implications for recycling of oceanic and upper and lower continental crust. Geochemistry, Geophys. Geosystems 7, 1–30. https://doi.org/10.1029/2005GC001005

Williams, H.M., Bizimis, M., 2014. Iron isotope tracing of mantle heterogeneity within the source regions of oceanic basalts. Earth Planet. Sci. Lett. 404, 396–407. https://doi.org/10.1016/J.EPSL.2014.07.033

Williams, H.M., Mccammon, C.A., Peslier, A.H., Halliday, A.N., Teutsch, N., Levasseur, S., Burg, J.-P., 2004. Iron Isotope Fractionation and the Oxygen Fugacity of the Mantle. Source Sci. New Ser. 304, 1656–1659.

Williams, H.M., Nielsen, S.G., Renac, C., Griffin, W.L., O'Reilly, S.Y., Mccammon, C.A., Pearson, N., Viljoen, F., Alt, J.C., Halliday, A.N., 2009. Fractionation of oxygen and iron isotopes by partial melting processes: Implications for the interpretation of stable isotope signatures in mafic rocks. Earth Planet. Sci. Lett. 283, 156–166. https://doi.org/10.1016/j.epsl.2009.04.011

Williams, H.M., Peslier, A.H., Mccammon, C., Halliday, A.N., 2005. Systematic iron isotope variations in mantle rocks and minerals : The effects of partial melting and oxygen fugacity. Earth Planet. Sci. Lett. 235, 435–452. https://doi.org/10.1016/j.epsl.2005.04.020

Williams, H.M., Prytulak, J., Woodhead, J.D., Kelley, K.A., Brounce, M., Plank, T., 2018.

Interplay of crystal fractionation, sulfide saturation and oxygen fugacity on the iron isotope composition of arc lavas: An example from the Marianas. Geochim. Cosmochim. Acta 226, 224–243. https://doi.org/10.1016/J.GCA.2018.02.008

Wing, B.A., Farquhar, J., 2015. Sulfur isotope homogeneity of lunar mare basalts. https://doi.org/10.1016/j.gca.2015.09.003

Wood, B.J., Bryndzia, L.T., Johnson, K., 1990. Mantle Oxidation State and Its Relationship to Tectonic Environment and Fluid Speciation. Science (80-.). 248.

Wood, B.J., Kiseeva, E.S., Mirolo, F.J., 2014. Accretion and core formation: The effects of sulfur on metal-silicate partition coefficients. Geochim. Cosmochim. Acta 145, 248–267. https://doi.org/10.1016/j.gca.2014.09.002

Yi, W., Halliday, A.N., Alt, J.C., Lee, D.-C., Rehkämper, M., Garcia, M.O. 0, Langmuir, C.H., Su, Y., Rehkämper, M., Garcia, M.O. 0, Langmuir, C.H., Su, Y., 2000. Cadmium, indium, tin, tellurium, and sulfur in oceanic basalts: Implications for chalcophile element fractionation in the Earth. J. Geophys. Res. 105, 18,927-18,948. https://doi.org/10.1029/2000JB900152

Yi, W., Halliday, A.N., Lee, D.-C., Christensen, J.N., 1995a. Indium and tin in basalts, sulfides, and the mantle. Geochim. Cosmochim. Acta 59, 5081–5090.

Yi, W., Halliday, A.N., Lee, D.-C., Christensen, J.N., 1995b. Indium and tin in basalts, sulfides, and the mantle. Geochim. Cosmochim. Acta 59, 5081–5090. https://doi.org/10.1016/0016-7037(95)00342-8

Zhao, Y., Xue, C., Liu, S.-A., Symons, D.T.A., Zhao, X., Yang, Y., Ke, J., 2017. Copper isotope fractionation during sulfide-magma differentiation in the Tulaergen magmatic Ni–Cu deposit, NW China. Lithos 286–287, 206–215. https://doi.org/10.1016/J.LITHOS.2017.06.007

Zindler, A., Hart, S., 1986. CHEMICAL GEODYNAMICS, Ann. Rev. Earth Planet. Sci.

6. Conclusions and outlook

6.1. Conclusions of this thesis

The work presented herein has expanded the limited Ni isotopic dataset for high temperature terrestrial samples, and analysed a number of samples of so far unrepresented lithologies, including pyroxenites, OIBs, and lunar basalts (see Figure 49). With this expanded dataset, further inferences have been made about how Ni isotopes behave in high temperature systems, on Earth and the Moon.

The Ni isotopic composition of the BSE is better known than ever, with three estimates within error (Steele et al. 2011; Gall et al. 2017, this work). The average Ni isotopic composition of unmetasomatised fertile peridotite from this work, $\delta^{60/58}Ni_{SRM986}$=0.20±0.08‰ (n=18), includes no industrially processed reference materials, and more bulk xenoliths of fertile peridotites than previous estimates.

This work investigated the positive correlation observed by Gall and co-workers (2017) between Ni isotopic composition and CPX percentage (in 5 ultramafic xenoliths). Analysis of further xenoliths with modal mineralogy data and analysis of further mineral separates has shown that mineralogy does not control Ni isotope fractionation in the mantle and that the isotopic composition of minerals is in equilibrium within a particular xenolith. The isotopic composition of mineral phases reconstructs to produce the bulk Ni isotopic composition, showing that minor phases and interstitial alteration products do not influence the composition of the mantle. Minerals from hosts described as unmetasomatised have comparable Ni isotopic compositions, and the fractionation between heaviest and lightest phases analysed from various individual xenoliths is limited to <0.12‰. The spinel separates, where analysed, have the heaviest Ni isotopic composition of the mineral phases from that host, with olivine and orthopyroxene identical within error, and clinopyroxene is generally the mineral phase with the lightest Ni isotopic composition.

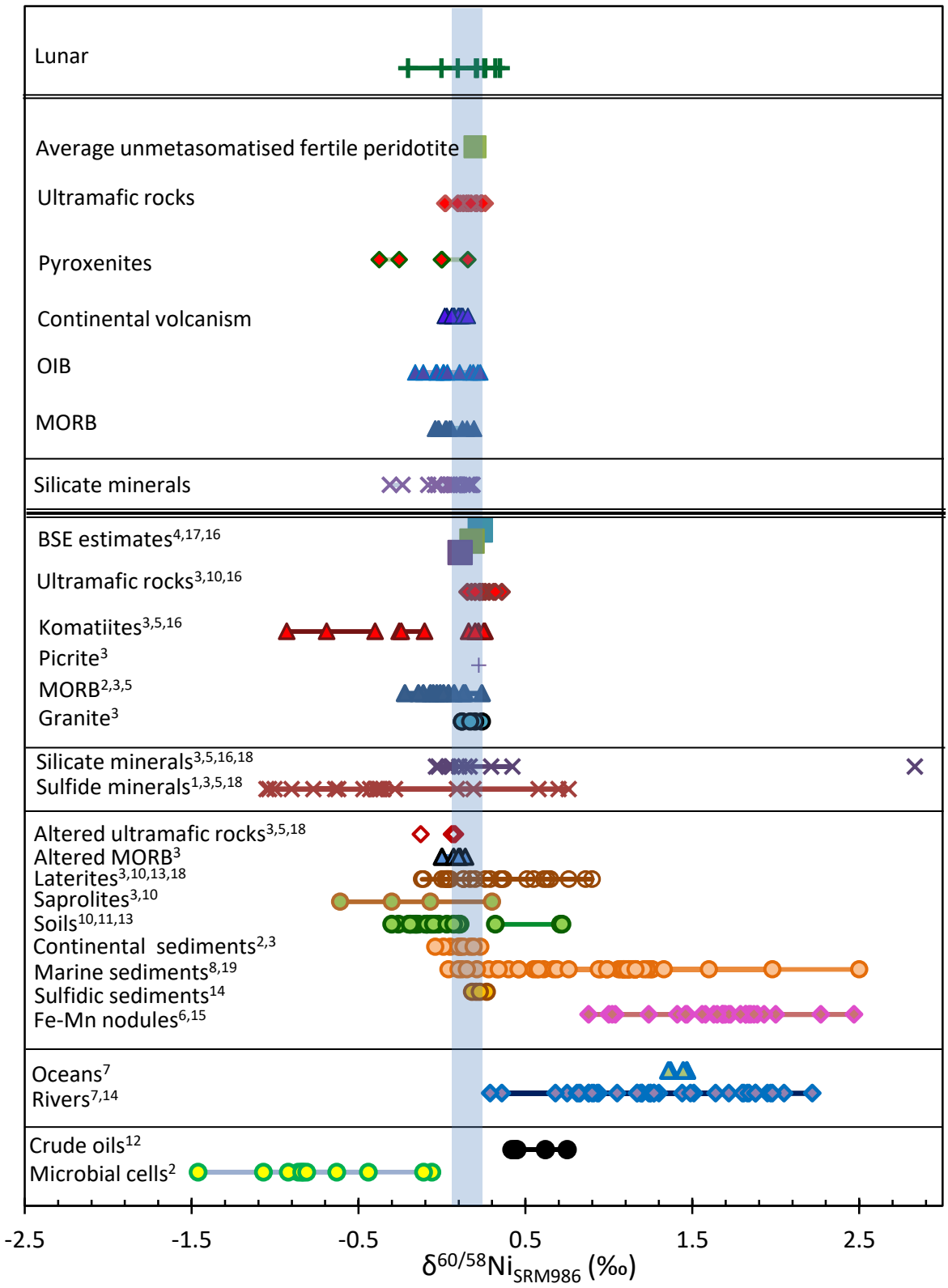

Figure 49

Nickel isotopic compositions analysed in this study compared with published $\delta^{60/58}Ni_{SRM986}$ data for terrestrial samples. BSE estimates for comparison, from (Gall et al., 2017; Steele et al., 2011) and with the estimate of Gueguen and co-workers (2013) recalculated by (Elliott and Steele, 2017) to remove sediments.

[1](Tanimizu and Hirata, 2006); [2](Cameron et al., 2009); [3](Gall, 2011); [4](Steele et al., 2011); [5](Gueguen et al., 2013); [6](Gall et al., 2013); [7](Cameron and Vance, 2014); [8](Porter et al., 2014); [9](Hofmann et al., 2014); [10](Ratié et al., 2015); [11](Estrade et al., 2015); [12](Ventura et al., 2015); [13](Ratié et al., 2016); [14](Vance et al., 2016); [15](Gueguen et al., 2016); [16](Gall et al., 2017); [17](Elliott and Steele, 2017); [18](Spivak-Birndorf et al., 2018); [19](Ciscato et al., 2018)

This study has shown that the terrestrial mantle exhibits Ni isotopic heterogeneity. Heterogeneity within the mantle in such a dominant and highly compatible element was unexpected. Samples of dunite from this work appear to have a light Ni isotopic composition, comparable to the $\delta^{60/58}Ni_{SRM986}$ reported by Spivak-Birndorf and co-workers (2018) for 'altered' dunite. Pyroxenites have been shown to have even lighter Ni isotopic compositions, especially seen in websterites from Cameroon (average $\delta^{60/58}Ni_{SRM986}$=-0.32‰).

Ultramafic xenoliths from Kilbourne Hole show a negative correlation between Ni isotopic composition and Fe content, which indicates that Ni isotopic composition varies with major element chemistry. However, the observed trend with $\delta^{60/58}Ni_{SRM986}$ and Fe shows that the process fractionating Ni isotopes in the Kilbourne xenoliths does not relate to cryptic metasomatism.

The positive correlation between Ni isotopic composition and Nd isotopic composition in the ultramafic xenoliths from Kilbourne Hole supports a common control on both parameters. A less radiogenic Nd isotopic composition is associated with enriched material, and with lighter $\delta^{60/58}Ni_{SRM986}$. Varying proportions of enriched material therefore likely creates a range of Ni isotopic compositions, with a more normal mantle represented by lesser proportions of enriched material. Pyroxenites represent the extreme of enriched material in the mantle, and have the lightest Ni isotopic compositions. In a particular locality, the xenoliths show a continuum of Ni isotopic compositions in relation to the degree of contribution of enriched mantle. Input of enriched material to the mantle is suggested to be related to subduction leading to input of basaltic melt into the mantle wedge.

Light Ni isotopic compositions have been observed in sepentinised and altered oceanic basalts (Gall, 2011; Gueguen et al., 2013), but are insufficiently so to be directly subducted into the mantle and alter the mantle composition sufficient to produce the light Ni isotopic composition in pyroxenites. The lightest $\delta^{60/58}Ni_{SRM986}$ of material that could be subducted is only -0.12‰, whereas the websterites average -0.32‰. Therefore, another process relating to subduction is required. This has been suggested for Mo isotope fractionation, where heavier isotopes are

thought to become enriched in the mantle wedge of subduction zones, during fluid mobilization within the subducting plate in the presence of secondary residual minerals enriched in light Mo (König et al., 2016).

This study has shown that the Ni isotopic composition in mafic samples is invariant with geological setting, with identical average Ni isotopic compositions for OIB and MORB samples. Mafic samples are on average lighter in Ni isotopic composition than the average for unmetasomatised fertile peridotites.

The homogeneous Ni isotopic compositions of Cameroon Line mafic rocks derived by different degrees of partial melting demonstrates that nickel isotopes are not fractionated during partial melting. Incompatible trace element ratios lack correlation with Ni isotopic compositions, also supporting this conclusion. The lack of fractionation between major mantle mineral phases, shown in Chapter 3, also implied that partial melting could not induce a large fractionation in Ni isotopic composition. Lack of correlation with compatible trace element ratios, Ni concentration, and MgO even within a particular volcanic system, suggest that Ni isotopes are also invariant during fractional crystallisation.

The conclusion from Chapter 3 that lighter Ni isotopic compositions were associated with enriched lithologies is further supported by analysis of mafic samples. For example, by the negative trend between chondrite normalised La/Sm (indicator of LREE enrichment) and Ni isotopic composition seen in E-type MORB and N-MORBs from both the Pacific and Atlantic Oceans. The trend forms a continuum, similar to the continuum in Kilbourne Hole xenoliths and Nd isotopic ratio.

With Ni isotopes shown to be invariant to partial melting and magmatic differentiation, the Ni isotopic composition of mafic samples reflect the mantle source region of the volcanic system. Radiogenic isotopic compositions, such as Nd, Sr, and Pb, have been traditionally used to identify potential mantle source endmembers; however, the compositions in radiogenic isotopes are affected by the ratio of parent to daughter and the time since the material carrying that parent-daughter ratio was incorporated into the specific source region. The Ni isotopic

composition could, therefore, separate the influence of time and reveal only the amount of a particular component in the source of a volcanic system.

Therefore, the Ni isotopic composition of a mantle source region is apparently controlled by the amount of recycled pyroxenitic material incorporated into that region. A mass balance calculation suggests that incorporation of 23-29% websterite (-0.32‰) into unmetasomatised fertile peridotite (0.20‰) could produce a source with the Ni isotope signature of the majority of mafic samples (0.05 to 0.08‰). Nickel isotopic composition of terrestrial rocks, therefore, have the potential to isolate the amount of enriched recycled component in the mantle source from both melting processes and time.

The Moon, without plate tectonics and subduction, cannot produce domains of light Ni isotopic composition in its mantle from recycling, as have been sampled on Earth. The average Ni isotopic composition of the lunar basalts is heavier than that of equivalent terrestrial rocks, leading further support that the major process producing lighter $\delta^{60/58}Ni_{SRM986}$ in the terrestrial mantle is not occurring on the Moon.

Therefore, other mechanisms for Ni isotopic fractionation are required. As seen in terrestrial rocks, lunar Ni isotopic compositions have been shown in this work not to vary with traditional indicators of degree of partial melting and magmatic differentiation, although co-genetic origin of the lunar samples is not proven. With melting processes excluded, as well as subduction related processes, this leaves source variations as the most likely cause for variation in Ni isotopic composition, supported by the lightest $\delta^{60/58}Ni_{SRM986}$ being found in the Al-rich basalt, and the single high-Ti sample having one of the heaviest compositions observed.

However, as there are lunar samples with light Ni isotopic compositions, and trends in the geochemical characteristics with Ni isotopic composition, a process has occurred on the Moon to fractionate Ni isotopes in a way that is absent or not observable on Earth, potentially due to being overprinted by subsequent processes over the millions of years of mantle convection and plate tectonics.

We have analysed unspiked and internally normalised Ni isotopic compositions to see if the $\delta^{60/58}Ni_{SRM986}$ variability is an artefact from cosmogenic effects but have found no evidence of this. The unspiked isotopic compositions analysed are normal within uncertainty. In addition, no trend was found between $\delta^{60/58}Ni_{SRM986}$ and exposure age.

There is also no correlation between Ni and Zn isotopic compositions, thought to fractionate by devolatilisation. The few samples analysed for Cl (Sharp, pers. comm) do show a hint of a trend. The lack of a clear trend with Zn and Cl confirms that the relatively refractory Ni is not likely to be fractionated by volatilisation. Only two samples have been analysed for both Mg and Fe stable isotopic composition and Ni isotopic composition, which allows no conjecture for these isotopes. There may be a trend with S isotopic composition, however only 3 samples have been analysed for both systems. There is also a correlation with Ni isotopic composition with S concentration, which may support a joint parent process producing both effects, perhaps linked to sulfides.

Lunar Ni isotopic compositions show a strong negative correlation with plagioclase, and a similar trend is observed in Al_2O_3, and a number of elements incompatible in plagioclase. This suggests that there is an influence on Ni isotopes by a process associated with plagioclase formation. The sample with the lightest Ni isotopic composition has the highest amount of incompatible elements, Al, and plagioclase leading to the suggestion that the greatest Ni fractionation occurs when these factors are all in abundance in the same region of the mantle.

A correlation with Ni isotopic composition and S isotopic composition, and with S content, may suggest that sulphur has a control on Ni isotopic composition on small scales in different lunar source regions, supported by experimental data. This may occur more on the Moon and not on Earth, because the lower oxygen fugacity has forced Ni ions out of the most compatible sites, such as olivine, due to increased competition with Fe^{2+}. The redistribution of Ni between melt, and metal in the proximity of sulfide may fractionate Ni isotopes, and produce the observed variable Ni isotopic compositions, relating to source variations. In mantle sources with

insufficient troilite and metal, this fractionation process may be less, or non-existent, and the resulting basaltic composition would be less significantly affected, or unaltered from bulk.

In summary, these data have shown that the behaviour of Ni isotopes is different in the lunar environment to the equivalent terrestrial environment, resulting in Ni isotopic fractionation by a process that does not occur on the Earth, whereas fractionation on Earth relates to subduction and the presence of different amounts of enriched material.

6.2. Future work

The traditional indicator of mantle sources in mafic rocks is by the radiogenics Sr, Pb, and Nd, The mafic samples analysed in this work with radiogenic isotope data have a relatively restricted range. The range exhibited in the Kilbourne Hole xenoliths, in Nd for example, is ~25 ϵ units, whereas the mafic samples range from 2.3 (from Tanzania) to 10 ϵ units (from the MAR), with no single volcanic system having a range exceeding 4.5 ϵ units. Therefore, in future work, sampling mafic suites from the extremes of the radiogenic mantle array, including those termed EM1 and EM2, could provide further evidence of the extent of the Ni isotopic relationship with enriched mantle source regions. Further extremes may identify if Ni isotopes can identify further endmember compositions in the mantle. In addition, further information of a potential subduction zone fractionation of Ni isotopes could be gained by sampling volcanic material directly from a subduction zone.

Analysis of further lunar materials in order to investigate more of the lunar surface, potentially including volcanic glasses, further high-Ti basalts, and examples of highland anorthosite in order to sample more of the lunar mantle. Analysis of anorthosite could provide context for the apparent relationship between Ni isotopic composition in mare samples and abundance of plagioclase. An expanded dataset could allow a more complete picture of lunar Ni isotopic compositions, and thereby further support or disprove whether lunar Ni isotope fractionation is caused by changing Ni partitioning under reducing lunar mantle conditions. Potentially, an

experimental study of Moon-like compositions under a range of sulphur and oxygen fugacities could be analysed for Ni isotope composition and considered in relation to the lunar basalt data.

7. Appendices

7.1.Specifics of Cleaning

Teflon Cleaning: Six key steps between which the PFA were rinsed 3 times with MQ water in the container or individually. The first step involved wiping with ethanol or isopropanol and immersing in lab detergent and MQ water for a minimum of 24 hours. Then the Teflon beakers were cycled to 50% (by volume) reagent grade HNO_3 acid, which is left on a hotplate at 125°C for a minimum of three days. This cycled to 50% (by volume) reagent grade HCl, and immersed for three days at 125°C. For the fourth step, the PFA is immersed in MQ water for 24 hours at 125°C. Finally, the PFA were refluxed individually with distilled 6M HCl at 125°C before the final rinses with MQ water and drying in an LAF hood. Clean PFA vials are stored individually sealed inside clean plastic bags in a sealed plastic box to remain clean and ready for use. Most vials used are either 7 or 12 ml; however, column storage and cleaning requires much larger vials, as do samples requiring large volumes of rock material. PFA bottles for storage of clean acids are cleaned in the same way, or by refluxing instead of immersion depending on size, and vary in size as necessary.

Columns were cleaned after making over the course of a week. First MQ rinses and use of a cotton bud and MQ, then ethanol and cotton bud. They are then transferred to the clean suite where they are rinsed in MQ again, before they are submerged in PFA in a series of acids and refluxed at 90 °C for two days for each cleaning reagent. All acids used for this cleaning are distilled and in order are 8M HNO_3, 6M HCl, and a final MQ reflux, before storing in 4M HCl. After each reflux, the columns are rinsed in MQ before being submerged in the new reagent. This is a much more thorough procedure than after normal use (which involved immersion in 1M HCl for >1 day on a hotplate at 90°C, and storage in 4M HCl). Two sizes of frits were required for these columns, and it was important they fitted the column exactly, to prevent resin leakage. Frits were punched from porous polyethene and cleaned prior to insertion, without heating, by submersion in 4M HNO_3 for 4 days and then 6M HCl for 4 days, with rinses in MQ water between each step. Frits are then stored in MQ in a PFA beaker until needed.

Batch cleaning of resin: cycling in 2M HCl daily for 6 times.

1. The resin was cleaned on the column by the addition of 4ml 6M HCl, followed by 4ml MQ water, 4ml 6M HCl, 4ml MQ water, 4ml 3M HCl, and 4ml MQ water. Any Ni on the resin was eluting during the addition of HCl, and by cycling between HCl and MQ, the molarities in between will elute many other contaminating ions from the resin. It is possible to pause the cleaning overnight at any point as long as the cleaning process is finished the next day with a minimum of MQ+HCl+MQ before equilibration.
2. Once the cleaned column was filled with resin, the resin was checked for presence of bubbles that adversely affect flow rate. Once again, the addition of MQ water after loading resin was used to check the resin (which expands in water) is at the right level (base of reservoir). Resin was added or removed to adjust to this level if necessary, with careful pipette use. The resin was cleaned on the column by the addition of 1.5ml 6M HCl, followed by 1.5ml MQ water, 1.5ml 6M HCl, 1.5ml MQ water, 1.5ml 3M HCl, and 1.5ml MQ water. Any Ni on the resin will be eluting during the addition of HCl, and by cycling between HCl and MQ the molarities in between will elute many other contaminating ions from the resin.
3. Columns were emptied of resin (to waste, as resin is not reusable after use with ammonia and acetone) with MQ water, and then rinsed with 1M HCl until there were no air bubbles

within the column. The columns were then submerged in 1M HCl and refluxed at 90°C overnight to clean them. Once refluxed the columns can be rinsed with MQ water and stored in 4M HCl until needed

7.2. Acid titration

Date of Titration	Date of Acid tested		HCl	2*SD	n	HNO3	2*SD	n
AVERAGE			**9.96**	**0.200**	**9**	**15.49**	**0.139**	**3**
11-Feb-15	Jane's	New NaOH	**9.77**	0.032	5			
11-Feb-15	04-Dec-15		**9.91**	0.047	7			
31-Mar-15	Feb batch		**9.92**	0.034	7			
31-Mar-15	Dec batch					**15.4**	0.034	8
01-Dec-15	Mid Nov batch		**10.00**	0.089	7			
04-Mar-16	Feb batch					**15.57**	0.029	7
27-Apr-16	20 April batch	New NaOH	**10.11**	0.092	6			
04-Nov-16	02-Nov-16		**9.94**	0.043	6			
20-Feb-17	17-Feb-17		**10.03**	0.020	5			
03-Jun-17	1st June 17		**10.08**	0.045	7	**15.50**	0.040	5
23-Oct-17	Oct-17	New NaOH	**9.942**	0.020	5			
20-Feb-18	20-Feb-18		**9.752**	0.10	5			

7.3. Double spike details

Source: 2003 IUPAC

	Mass	Abundance
Ni58	57.935348	0.680769
Ni60	59.93079	0.26231
Ni61	60.93106	0.011399
Ni62	61.928348	0.036345
Ni64	63.927969	0.009256
Total		1.000079
A_r(Ni) pub	58.6934	
Average atomic weight pub	**58.698091**	in u (g per mol)

Source: Oak Ridge Info Sheet

	61 atomic	62 atomic	**Mixed Spike**
Ni58	0.0013	0.0066	0.004984
Ni60	0.0019	0.0076	0.005862
Ni61	0.9944	0.0006	0.303578
Ni62	0.0005	0.9846	0.684579
Ni64	0.0019	0.0005	0.000927
Total	1	0.9999	0.99993
Total - 64	0.9981	0.9994	0.999004

Source: Louise Gall (Pers Comm)

Weight of each			
mg	31.06	70.82	
ml	103.5	100	1006.735
ppm	300.09662	708.2	**101.1984**
% mix in mixed spike	0.3049	0.6951	
Average atomic weight	**60.931458**	**61.8810218**	**61.59153**
		61/62	0.4386
Conc Ni in Spike		101.198429 ppm	

Table 7-1

	Oak Ridge Assay	
	Spike of isotope 61	Spike of isotope 62
Ni58	0.0013	0.0066
Ni60	0.0019	0.0076
Ni61	0.9944	0.0006
Ni62	0.0005	0.9846
Ni64	0.0019	0.0005
Total	**1**	**0.9999**
Total without isotope 64	0.9981	0.9994

Table 7-2

	Gall (Pers Comm)		
	Isotope 61	**Isotope 62**	**Mixed Spike**
Weight of each added / mg	**31.06**	**70.82**	
Volume of solution made / ml	**103.5**	**100**	1006.735
Conc Ni in each solution / ppm	300.1	708.2	**101.1984**

Fraction of each in the mixed spike	0.3049	0.6951	
	Ratio of 61/62 in the mixed spike		**0.4386**

The calibration results are given below in Table 7-3, and were used in all double spike deconvolution and isotope dilution calculations in this study.

Table 7-3

SRM 986		SPIKE	
Rstd_6058=	0.38544	Rspk_6058=	1.20153
Rstd_6158=	0.016763	Rspk_6158=	56.956
Rstd_6258=	0.053338	Rspk_6258=	141.989

7.4. External Reproducibility

Repeated analyses of standards have been used to calculate a long term external reproducibility, weher each analysis was the product of 30 replicates, during an analytical run.

	SRM	Kambalda	Sudbury	DTS2b	PCC1	BIR1a	BHVO2
Date	**delta**	**delta**	**delta**	**delta**	**delta**	**delta**	**delta**
Published Average		**-1.03**	**0.75**		**0.13**	**0.14**	**0.05**
		0.05	**0.05**		**0.03**	**0.06**	**0.05**
Max	0.072	-0.831	0.828	0.212	0.193	0.206	0.107
Min	-0.045	-0.966	0.726	0.107	0.104	0.099	-0.024
n	**29**	**66**	**60**	**16**	**19**	**22**	**39**
Average	**0.018**	**-0.891**	**0.771**	**0.157**	**0.145**	**0.147**	**0.028**
2SD	**0.058**	**0.064**	**0.049**	**0.063**	**0.063**	**0.062**	**0.065**
	0.035	-0.877	0.775	0.165	0.187	0.190	0.011
	0.040	-0.892	0.824	0.163	0.158	0.206	0.064
	0.003	-0.850	0.807	0.107	0.193	0.164	-0.024
	-0.010	-0.867	0.795	0.212	0.172	0.173	0.066
	0.011	-0.866	0.763	0.185	0.155	0.152	0.097
	0.072	-0.863	0.828	0.164	0.182	0.170	0.066
	0.060	-0.871	0.790	0.114	0.124	0.183	-0.018
	0.042	-0.880	0.821	0.199	0.133	0.160	0.030
	0.048	-0.923	0.796	0.147	0.119	0.140	0.001

0.072	-0.929	0.747	0.205	0.192	0.157	0.017
0.025	-0.923	0.821	0.181	0.192	0.125	-0.006
0.011	-0.921	0.766	0.140	0.172	0.123	0.023
0.033	-0.890	0.809	0.156	0.104	0.186	0.031
0.016	-0.866	0.799	0.157	0.104	0.106	0.068
-0.009	-0.885	0.746	0.183	0.118	0.168	0.107
-0.015	-0.899	0.791	0.123	0.145	0.108	0.071
0.026	-0.926	0.788		0.136	0.126	0.066
0.005	-0.907	0.765		0.112	0.137	0.043
0.006	-0.875	0.784		0.141	0.161	0.015
0.009	-0.898	0.809			0.099	-0.007
-0.010	-0.908	0.751			0.104	0.004
0.033	-0.958	0.785			0.180	0.027
0.056	-0.910	0.760				0.006
-0.007	-0.868	0.790				0.030
0.022	-0.864	0.783				0.009
-0.018	-0.908	0.756				0.001
-0.016	-0.943	0.819				0.024
-0.045	-0.831	0.827				0.007
-0.011	-0.901	0.800				-0.004
	-0.859	0.761				-0.015
	-0.837	0.797				0.013
	-0.927	0.803				0.015
	-0.842	0.783				-0.008
	-0.937	0.795				0.022
	-0.908	0.792				0.056
	-0.898	0.785				0.022
	-0.939	0.749				0.024
	-0.908	0.743				0.083
	-0.875	0.778				0.016
	-0.883	0.787				
	-0.966	0.810				
	-0.944	0.781				
	-0.924	0.771				
	-0.917	0.790				
	-0.889	0.801				
	-0.910	0.792				
	-0.904	0.810				
	-0.925	0.767				
	-0.911	0.775				
	-0.950	0.746				
	-0.941	0.783				
	-0.951	0.752				
	-0.925	0.735				
	-0.959	0.764				
	-0.911	0.764				
	-0.933	0.770				
	-0.934	0.793				

-0.863	0.795
-0.900	0.726
-0.889	0.818
-0.951	
-0.908	
-0.947	
-0.921	
-0.925	
-0.919	

7.5. Room temperature related drift

During some runs of samples on the mass spectrometer used in this work, the resulting data were found to be inexplicably irreproducible during the run. The delta values appeared to drift enormously so that the same vial of sample analysed three times could give three completely un-relatable values. On some occasions, it was clear the room temperature was varying by significantly more than the given specifications for a Nu plasma MC-ICP-MS, so this possible effect on the data was investigated further with the aim of producing evidence of the temperatures adverse influence on measuring high precision delta values in Ni.

During an overnight run where both room temperature and centre field number were logged and later transcribed to correspond with the measured delta. This run used the check peak centre and offset to measure programming, so the resulting delta values of the secondary standards are correct and stable (**Figure 50**) despite a raw delta value of SRM 986 of +0.524±0.048. Previous runs aimed towards getting raw delta of the SRM to 0.2 to be sure of interference free measuring, which is no longer necessary using this programming. It is clear from Figure 50 that there is a strong anti-correlation between the centre of the peak's field number and the room temperature. For measuring Ni the interference free shoulder is <400 field numbers wide on average, and therefore without being able to track the peak drift the measurement mass would quickly and irretrievably fall of the peak completely or begin measuring on interference plus Ni58. More extreme temperature drift than occurred during this test has been witnessed (up to 6 °C from night to day) and it is unknown at this time if the peak centre programming can completely remove all effects of such extreme drift from showing up in the resulting deltas.

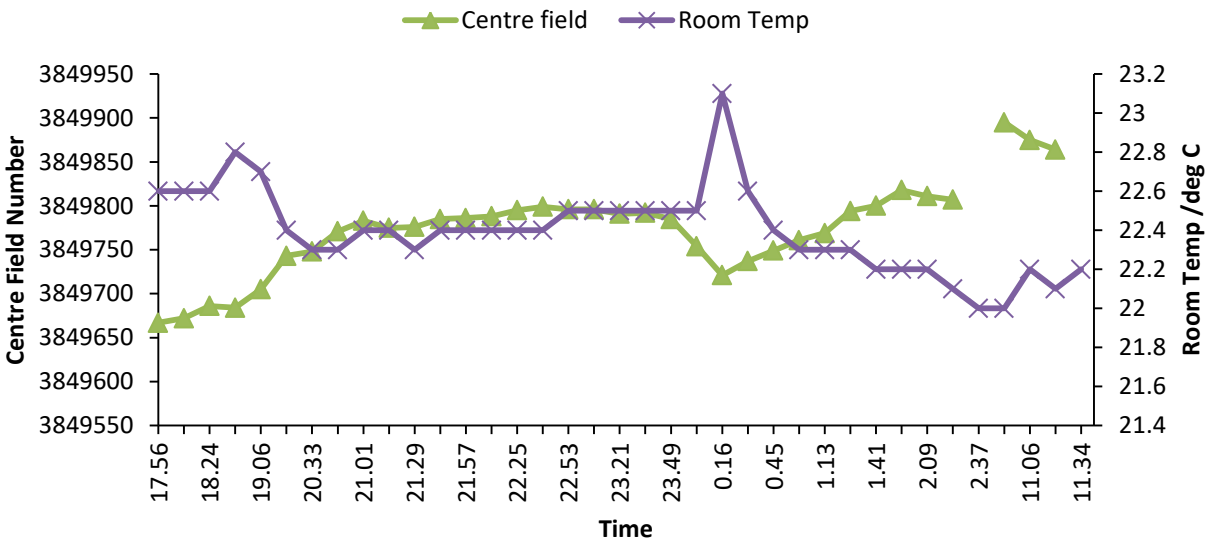

Figure 50

Plot of the room temperature (measured by Ebro EBI300 logger) throughout an overnight run on the mass spectrometer used in this work (real time on the x axis) and of centre field number (logged by the mass spectrometer used in this work) for the same times. The two lines clearly anti-correlate, showing that a temperature fluctuation of less than 1 °C can cause a drift in the centre of the peak of >150 field numbers. This is sufficient to cause a measurement to drift away from the interference free shoulder on the 58 mass peak onto interference or off the peak entirely. This highlights the necessity of checking the peak centre before each measurement and measuring a set offset form this onto the interference free shoulder.

7.6. Mass balance model for Ni isotopic composition in mafic rocks

				Average mantle		0.2
Sample	**Rock Type**	**Loc**	**$\delta^{60/58}$Ni**	**fraction websterite %**	**fraction pyroxenite %**	**fraction KH pyroxenite %**
				-0.32	-0.1	0.05
C134	Mafic Nephelinite	Etinde	0.117	15.962	27.667	55.333
C151	Mafic Nephelinite	Etinde	0.063	26.290	45.569	91.138
C22	Nephelinite	Etinde	0.075	24.033	41.658	83.316
C20	Nephelinite	Etinde	0.069	25.121	43.542	87.084
C152	Hauyne Nephelinite	Etinde	0.105	18.239	31.614	63.227
C150	Olivine	Etinde	0.069	25.232	43.735	87.470

	melanephelinite					
C51	Alkali Basalt	Manengouba	0.063	26.386	45.736	91.471
C65	Hy-normative basalt	Manengouba	0.060	26.923	46.666	93.332
C72	Alkali Basalt	Manengouba	0.073	24.470	42.414	84.828
C146	Alkali Basalt	Mandara Mts	0.017	35.176	60.972	121.9
C192	Basanite	Mt Cameroon	0.066	25.808	44.734	89.469
C30	Basanite	Mt Cameroon	0.113	16.672	28.898	57.796
C112	Basanite	Bambouto	0.098	19.650	34.060	68.120
P18	Olivine Nephelinite	Príncipe, Island in Cameroon Line	0.030	32.784	56.826	113.7
FP44	Alkali Basalt	Bioko, Island in Cameroon Line	0.101	19.100	33.106	66.212
H93-3	Foidite	Kwaraha, N Tanzania	0.156	8.499	14.731	29.462
BD105	Ol-Melilite nephelinite	Oldoinyo, Loolmurwak, Tanzania	0.127	14.100	24.441	48.882
ST38	Basalt	N, Iceland	0.189	2.115	3.667	7.333
GS18	Tholeiite	N, Iceland	0.217	-3.269	-5.667	-11.333
CX11		E, Iceland	0.231	-5.906	-10.238	-20.475
CX19		E, Iceland	0.106	18.068	31.319	62.637
SNB19		W, Iceland	0.012	36.151	62.661	125.3
SNB40	Tholeiite	W, Iceland	0.033	32.180	55.779	111.56
AZF3	Transitional basalt	Flores, Azores	-0.035	45.193	78.335	156.67
AZP6	Alkali Basalt	Pico, Azores	-0.160	69.146	119.853	239.71
AZFY2	Alkali Basalt	Fayal, Azores	-0.111	59.830	103.705	207.41
PL02 25-1	Alkali Basalt	Galapogos	-0.030	44.177	76.573	153.15
PL02 30-1	Tholeiite	Galapogos	0.008	36.957	64.058	128.12
D4-6G	Alkali Basalt	Loihi	0.170	5.805	10.061	20.123
R82-1	N type Basalt	EPR	0.192	1.538	2.667	5.333
R93-7	E type Basalt	EPR	0.045	29.825	51.697	103.39
R94-2	N type Basalt	EPR	0.193	1.318	2.285	4.569
A127 D5-5	N type Basalt	Famous Ridge	0.151	9.377	16.254	32.508
A127 D8-2	N type Basalt	Famous Ridge	0.056	27.677	47.974	95.948
A127 D10-2A	MORB	Famous Ridge	0.123	14.715	25.506	51.013
A127 D15-1	E type Basalt	Famous Ridge	0.028	33.004	57.208	114.42
A127 D17-3	E type Basalt	Famous Ridge	-0.041	46.410	80.443	160.89
A127 D21-3	E type Basalt	Famous Ridge	-0.017	41.656	72.204	144.41
A127 D22-5	E type Basalt	Famous Ridge	0.021	34.505	59.808	119.62

A127 D26-5	E type Basalt	Famous Ridge	-0.023	42.823	74.227	148.46
A127 D27-5	E type Basalt	Famous Ridge	-0.038	45.804	79.394	158.79

				Max mantle		0.26
Sample	**Rock Type**	**Loc**	**$\delta^{60/58}$Ni**	**fraction websterite %**	**fraction pyroxenite %**	**fraction KH pyroxenite %**
				-0.32	-0.1	0.05
C134	Mafic Nephelinite	Etinde	0.117	24.655	39.722	68.095
C151	Mafic Nephelinite	Etinde	0.063	33.915	54.641	93.670
C22	Nephelinite	Etinde	0.075	31.892	51.382	88.083
C20	Nephelinite	Etinde	0.069	32.867	52.952	90.775
C152	Hauyne Nephelinite	Etinde	0.105	26.697	43.011	73.734
C150	Olivine melanephelinite	Etinde	0.069	32.966	53.113	91.050
C51	Alkali Basalt	Manengouba	0.063	34.001	54.780	93.908
C65	Hy-normative basalt	Manengouba	0.060	34.482	55.555	95.237
C72	Alkali Basalt	Manengouba	0.073	32.283	52.012	89.163
C146	Alkali Basalt	Mandara Mts, Cameroon	0.017	41.882	67.477	115.675
C192	Basanite	Mt Cameroon	0.066	33.483	53.945	92.478
C30	Basanite	Mt Cameroon	0.113	25.292	40.748	69.854
C112	Basanite	Bambouto, Cameroon	0.098	27.962	45.050	77.228
P18	Olivine Nephelinite	Príncipe, Island in Cameroon Line	0.030	39.737	64.021	109.751
FP44	Alkali Basalt	Bioko, (Island in Cameroon Line)	0.101	27.469	44.255	75.866
H93-3	Foidite	Kwaraha, N Tanzania	0.156	17.964	28.943	49.616
BD105	Ol-Melilite nephelinite	Oldoinyo, Loolmurwak, Tanzania	0.127	22.987	37.034	63.487
ST38	Basalt	N, Iceland	0.189	12.241	19.722	33.810
GS18	Tholeiite	N, Iceland	0.217	7.414	11.944	20.476
CX11		E, Iceland	0.231	5.049	8.135	13.946
CX19		E, Iceland	0.106	26.544	42.765	73.312
SNB19		Iceland	0.012	42.756	68.884	118.087
SNB40	Tholeiite	Iceland	0.033	39.196	63.149	108.256
AZF3	Transitional basalt	Flores, Azores	-0.035	50.863	81.946	140.479

AZP6	Alkali Basalt	Pico, Azores	-0.160	72.338	116.544	199.790
AZFY2	Alkali Basalt	Fayal, Azores	-0.111	63.985	103.088	176.722
PL02 25-1	Alkali Basalt	Galapogos	-0.030	49.952	80.478	137.962
PL02 30-1	Tholeiite	Galapogos	0.008	43.478	70.049	120.083
D4-6G	Alkali Basalt	Loihi	0.170	15.549	25.051	42.945
R82-1	N type Basalt	EPR	0.192	11.724	18.889	32.381
R93-7	E type Basalt	EPR	0.045	37.085	59.748	102.424
R94-2	N type Basalt	EPR	0.193	11.526	18.570	31.835
A127 D5-5	N type Basalt	Famous Ridge	0.151	18.752	30.212	51.792
A127 D8-2	N type Basalt	Famous Ridge	0.056	35.159	56.645	97.106
A127 D10-2A	MORB	Famous Ridge	0.123	23.538	37.922	65.009
A127 D15-1	E type Basalt	Famous Ridge	0.028	39.935	64.340	110.297
A127 D17-3	E type Basalt	Famous Ridge	-0.041	51.953	83.703	143.490
A127 D21-3	E type Basalt	Famous Ridge	-0.017	47.692	76.836	131.720
A127 D22-5	E type Basalt	Famous Ridge	0.021	41.280	66.507	114.012
A127 D26-5	E type Basalt	Famous Ridge	-0.023	48.738	78.523	134.611
A127 D27-5	E type Basalt	Famous Ridge	-0.038	51.411	82.828	141.992

7.7. Lunar Ni isotopic composition averages

Sample	Cut	[Ni]	d60Ni	2SD	n
10017	**405**	5.521	**0.288**	0.001	2
12002	**598**	102	**0.095**	0.048	4
12018	**277**	63.39	**0.320**	0.011	2
12054	**13**	18.27	**0.343**	0.037	6
12054	**146**	9.607	**-0.003**	0.069	2

12054	**150**	5.827	**0.187**	0.000	2
12063	**343**	29.05	**0.210**	0.029	4
15016	**240**	58.34	**0.248**	0.034	5
15535	**165**	62.03	**0.267**	0.046	5
15556	**258**	44.16	**0.198**	0.028	5
14053	**305**	11.2	**-0.203**	0.017	4

7.8. Lunar Ni isotopic compositions and mineralogy

The only mineral with a trend with Ni isotopic composition

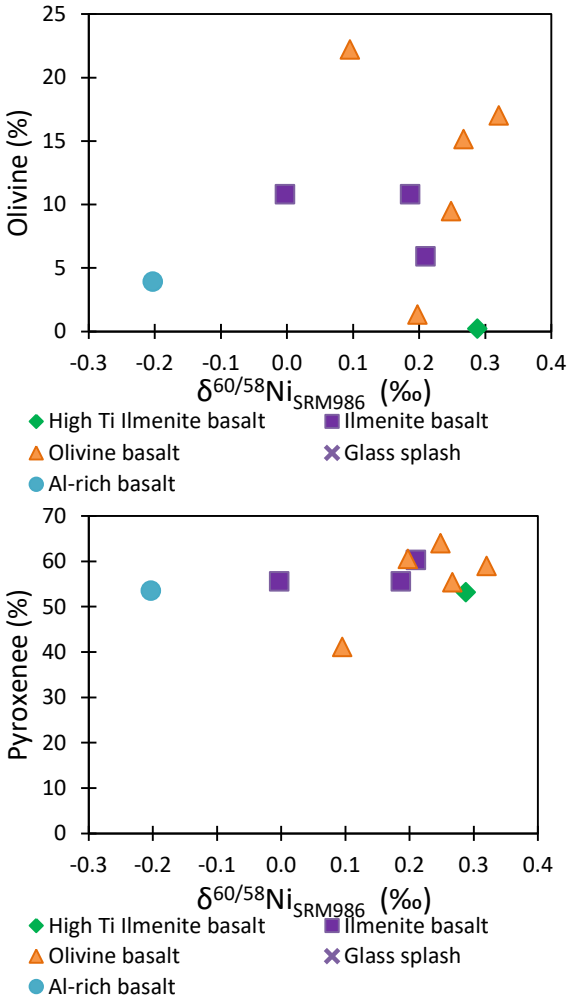

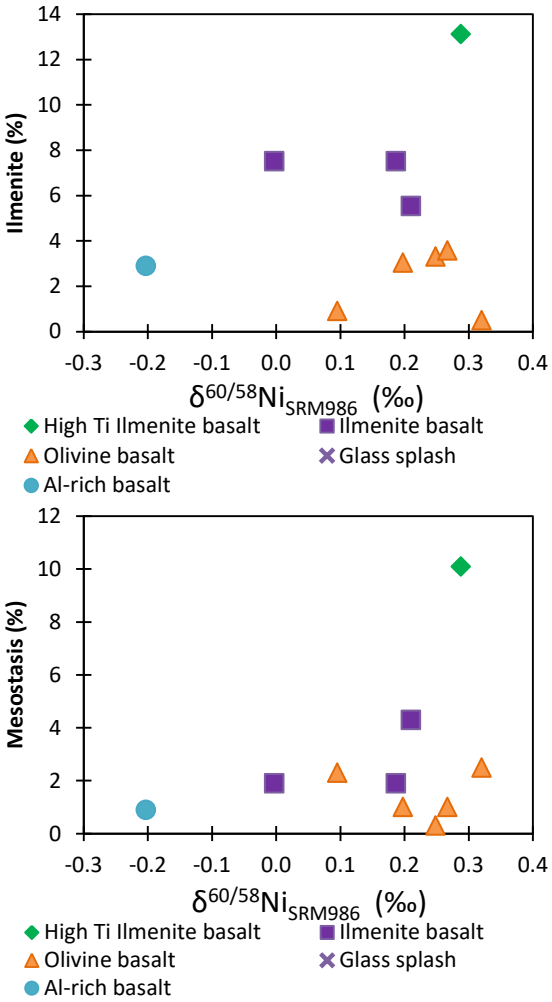
Ilmenite (%)
14
12
10
8
6
4
2
0
-0.3
-0.2
-0.1
0.0
0.1
0.2
0.3
0.4
δ60/58NiSRM986 (‰)
High Ti Ilmenite basalt
Ilmenite basalt
Olivine basalt
Glass splash
Al-rich basalt
Mesostasis (%)
12
10
8
6
4
2
0
-0.3
-0.2
-0.1
0.0
0.1
0.2
0.3
0.4
δ60/58NiSRM986 (‰)
High Ti Ilmenite basalt
Ilmenite basalt
Olivine basalt
Glass splash
Al-rich basalt

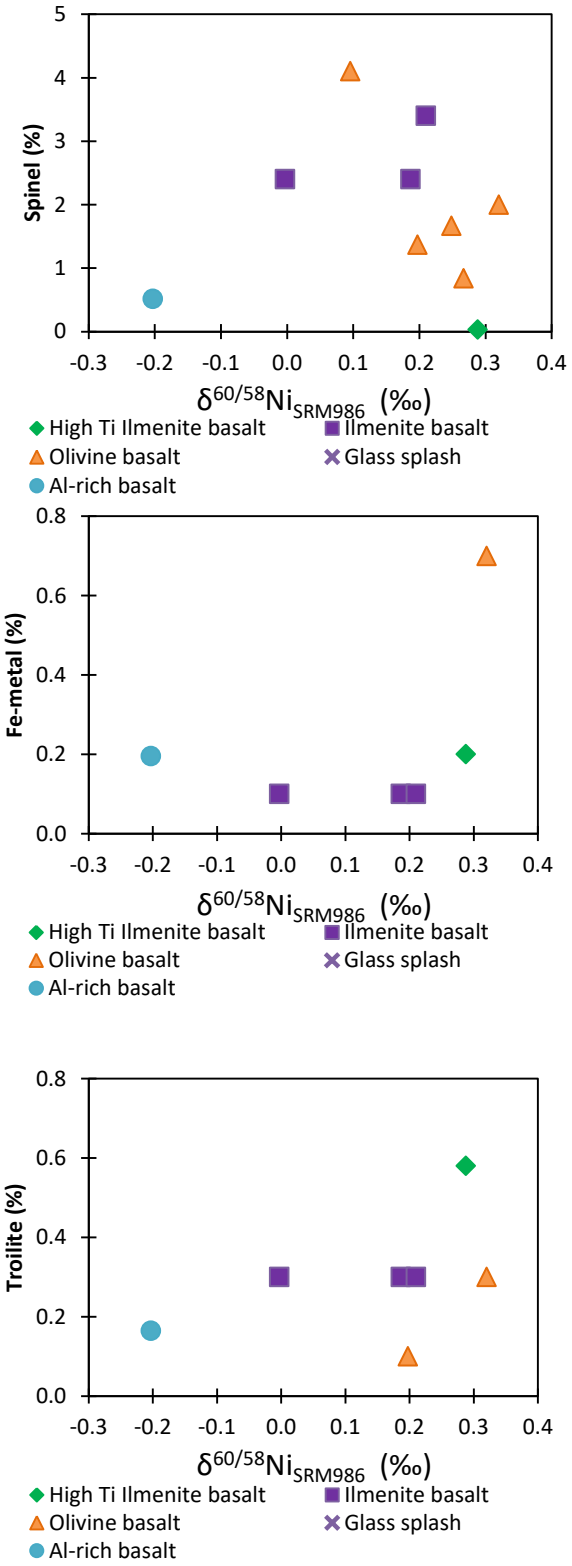

Figure 51

Nickel isotopic composition of the lunar samples plotted against the mineralogy in modal percent (Meyer, 2011). Limited data for spinel reflects the fewer data points for this plot. 12054 was analysed as an interior and exterior samples, plus the glass splash (mineralogy unknown) but mineralogy is assumed invariant between interior and exterior. No linear trend is seen with olivine, ilmenite, pyroxene, spinel, mesostasis, troilite or Fe-metal. Spinel, excluding the Al rich sample, may have a weak negative trend (r^2=0.308). In contrast, nickel isotopic compositions in terrestrial rocks show no trends with mineralogy. External reproducibility in Ni isotopic composition is 0.06‰.

7.9. Lunar $\delta^{60/58}Ni_{SRM986}$ as averages of both Zn matric cuts and fresh powders

Table 7-4

Table of mass dependent Ni isotopic compositions from lunar samples measured relative to SRM986. Lithological designations taken from (Meyer, 2011). Sample numbers include sample (5 digits) and cut (3 digits). Nickel concentrations from isotope dilution, and n is the number of separate analyses of the sample. Samples analysed more than three times were duplicated with the matrix Zn cut. External reproducibility on Ni isotopic composition measurements = 0.06‰.

Sample	Rock Type		Ni (ppm)	$\delta^{60/58}$Ni (‰)	2sd	n
High-Ti Basalt						
10017 405	High K ilmenite basalt	Interior	5.52	**0.288**	0.001	2
Low-Ti Basalt						
12002 598	Olivine basalt		101.80	**0.095**	0.048	4
12018 277	Olivine basalt		63.39	**0.320**	0.011	2
12054 13	Glass splash from an ilmenite basalt	Glass	18.27	**0.343**	0.037	6
12054 146	Glass-coated ilmenite basalt	Interior	9.61	**-0.003**	0.069	2
12054 150	Glass-coated ilmenite basalt	Exterior	5.83	**0.187**	0.000	2
12063 343	Ilmenite basalt		29.05	**0.210**	0.030	4
14053 305	Al-rich basalt		11.16	**-0.203**	0.017	4
15016 240	Vesicular olivine-normative basalt		58.34	**0.248**	0.035	5
15535 165	Olivine normative basalt		62.03	**0.267**	0.046	5
15556 258	Vesicular olivine normative basalt		44.16	**0.198**	0.028	5

7.10. Lunar major element data analysed by quadrupole mass spectrometer

Sample	Cut		TiO2		Al2O3		FeO		MgO		MnO		K2O	
			wt%	±	wt%	±	wt%	±	wt%	±	wt%	±	wt%	±
10017	405	int	11.3	0.22	8.3	0.27	19.9	0.29	7.9	0.16	0.2	0.01	0.3	0.002
12054	13	glass	NA		NA		NA		NA		NA		NA	
12054	146	int	5.28	0.28	10.6	0.12	20.8	0.37	6.74	0.20	0.28	0.01	0.08	0.001
12054	150	ext	4.06	0.12	11.2	0.29	20.4	0.43	6.80	0.13	0.28	0.01	0.07	0.001
12063	343		4.91	0.13	8.10	0.30	21.4	0.45	9.82	0.27	0.27	0.01	0.06	0.001
12002	598		NA		NA		NA		NA		NA		NA	
12018	277		2.10	0.11	7.35	0.45	20.6	0.31	15.1	0.38	0.27	0.00	0.05	0.001
15016	240		2.09	0.08	8.51	0.40	22.3	0.33	11.3	0.31	0.28	0.01	0.04	0.001

15535	165	2.06	0.12	7.95	0.37	23.0	0.41	11.1	0.33	0.29	0.01	0.04	0.001
15556	258	2.35	0.12	8.58	0.36	21.4	0.64	8.58	0.28	0.28	0.01	0.04	0.001
14053	305	2.71	0.18	13.16	0.50	17.2	0.32	8.75	0.25	0.26	0.02	0.10	0.001
Detection Limit		0.003	wt%	0.005	wt%	0.01	wt%	0.005	wt%	0.0004	wt%	0.048	wt%

7.11. Lunar trace element data analysed by quadrupole mass spectrometer

Sample	**Cut**		Sc		V		Cr		Co		Ni		Cu		Sr	
			ppm	±	ppm	±	ppm	±	ppm	±	ppm	±	ppm	±	ppm	±
10017	405	int	90.5	6.4	70.4	2.5	26383	0.0	26.7	0.8	5.5	0.1	4.7	0.5	182	7.5
12054	13	glass	NA		NA		NA		NA		NA		NA		NA	
12054	146	int	77.2	4.1	112	6.3	26065	0.0	24.4	0.9	4.99	0.6	5.71	0.4	162	6.4
12054	150	ext	75.5	2.2	143	3.7	24412	0.0	33.9	0.6	9.57	0.4	7.82	0.2	176	6.3
12063	343		62.5	3.1	115	3.9	36936	0.0	32.3	1.2	23.6	0.9	4.16	0.4	136	4.9
12002	598		NA		NA		NA		NA		NA		NA		NA	
12018	277		46.3	3.9	182	5.1	43714	0.0	57.6	1.0	75.5	2.8	20.3	1.2	79.9	3.1
15016	240		43.0	2.4	234	4.1	57713	0.0	51.9	1.2	65.1	1.9	6.31	0.5	82.8	4.0
15535	165		44.3	1.8	217	1.1	45788	0.0	55.8	1.3	67.9	1.7	7.63	0.6	89.4	3.7
15556	258		47.5	3.3	211	6.3	43699	0.1	45.5	1.5	47.6	1.4	7.44	0.7	101	3.8
14053	305		61.5	5.9	108	4.7	27695	0.0	25.2	1.0	10.6	0.8	19.17	0.7	105	3.9
Detection Limit			0.16	ppm	0.06	ppm	0.09	ppm	0.04	ppm	0.10	ppm	0.05	ppm	0.07	Ppm

Sample	**Cut**		Y		Zr		Nb		Ba		La		Ce	
			ppm	±	ppm	±	ppm	±	ppm	±	ppm	±	ppm	±
10017	405	int	175	2.7	504	8.6	23.3	0.4	294	6.7	27.8	0.7	80.3	2.8
12054	13	glass	NA		NA		NA		NA		NA		NA	
12054	146	int	44	1.1	113	4.5	6.78	0.2	50.9	2.2	5.44	0.3	16.3	0.3
12054	150	ext	55	1.4	127	2.3	4.18	0.2	74.0	1.9	7.20	0.1	20.8	0.6
12063	343		36	0.4	91.6	2.2	0.46	0.1	39.2	2.4	4.09	0.3	12.5	0.5
12002	598		NA		NA		NA		NA		NA		NA	
12018	277		30	1.5	89.4	2.6	1.22	1.4	52.0	1.5	5.28	0.3	13.9	0.4
15016	240		24	1.1	90.3	3.0	5.61	0.3	46.6	0.6	5.08	0.2	14.0	0.6
15535	165		24	1.5	87.4	1.0	0.70	0.4	48.5	2.3	5.04	0.2	13.9	0.4
15556	258		24	1.1	89.0	3.3	0.89	0.4	49.7	2.2	5.00	0.1	13.8	0.2
14053	305		53	1.8	208	6.1	2.94	0.8	151	2.2	12.9	0.3	34.7	0.6
Detection Limit			0.04	ppm	3.37	ppm	0.07	ppm	0.02	ppm	0.01	ppm	0.01	ppm

Sample	**Cut**		Pr		Nd		Sm		Eu		Gd		Tb	
			ppm	±	ppm	±	ppm	±	ppm	±	ppm	±	ppm	±
10017	405	int	11.9	0.5	59.6	1.3	20.8	0.4	2.3	0.0	28.2	0.7	5.2	0.2

12054	13	glass	NA		NA		NA		NA		NA		NA	
12054	146	int	2.56	0.2	13.58	1.1	5.03	0.9	1.22	0.1	7.25	0.7	1.29	0.0
12054	150	ext	3.36	0.2	17.05	1.3	6.18	0.2	1.64	0.1	9.22	0.5	1.67	0.1
12063	343		2.01	0.1	10.52	1.7	4.07	0.3	0.99	0.1	5.87	0.1	1.08	0.1
12002	598		NA		NA		NA		NA		NA		NA	
12018	277		2.06	0.1	10.33	0.5	3.59	0.6	0.84	0.0	4.97	0.5	0.89	0.0
15016	240		2.03	0.2	10.00	1.0	3.20	0.5	0.87	0.0	4.38	0.6	0.76	0.0
15535	165		2.08	0.2	10.86	1.0	3.13	0.5	0.91	0.1	4.44	0.3	0.77	0.0
15556	258		2.10	0.2	9.88	0.9	3.54	0.5	0.98	0.0	4.58	0.4	0.77	0.1
14053	305		4.86	0.2	20.40	1.8	6.19	0.7	1.31	0.0	7.91	0.4	1.55	0.1
Detection Limit			0.01	ppm	0.08	ppm	0.03	ppm	0.004	ppm	0.01	ppm	0.001	ppm

Sample	**Cut**		Dy		Ho		Er		Tm		Yb		Lu	
			ppm	±	ppm	±	ppm	±	ppm	±	ppm	±	ppm	±
10017	405	int	34.2	1.7	7.4	0.3	21.3	0.3	3.0	0.1	18.5	0.8	2.6	0.1
12054	13	glass	NA		NA		NA		NA		NA		NA	
12054	146	int	8.81	0.3	1.79	0.1	5.24	0.2	0.75	0.0	4.69	0.3	0.65	0.1
12054	150	ext	11.58	0.3	2.32	0.1	6.87	0.4	1.00	0.0	5.99	0.4	0.86	0.0
12063	343		7.16	0.3	1.46	0.1	4.48	0.4	0.62	0.0	3.90	0.6	0.53	0.1
12002	598		NA		NA		NA		NA		NA		NA	
12018	277		6.06	0.3	1.19	0.0	3.62	0.1	0.54	0.0	2.88	0.2	0.44	0.0
15016	240		5.10	0.3	0.97	0.1	2.83	0.1	0.37	0.0	2.26	0.1	0.31	0.0
15535	165		5.21	0.2	0.97	0.1	2.83	0.2	0.42	0.0	2.32	0.1	0.29	0.0
15556	258		5.01	0.4	0.96	0.1	2.90	0.3	0.38	0.0	2.14	0.2	0.33	0.0
14053	305		10.23	1.0	2.12	0.1	6.55	0.4	0.98	0.0	6.38	0.4	0.85	0.1
Detection Limit			0.004	ppm	0.006	ppm	0.005	ppm	0.004	ppm	0.005	ppm	0.003	ppm

Sample	**Cut**		Hf		Pb		Th		U		Li	
			ppm	±	ppm	±	ppm	±	ppm	±	ppm	±
10017	405	int	16.1	0.6	1.2	0.1	3.5	0.1	0.8	0.0	19.1	2.1
12054	13	glass	NA		NA		NA		NA		NA	
12054	146	int	3.86	0.1	0.19	0.1	0.90	0.1	0.13	0.0	7.15	1.5
12054	150	ext	4.47	0.3	0.29	0.1	1.10	0.1	0.18	0.0	11.10	1.4
12063	343		3.08	0.1	0.15	0.0	0.63	0.1	0.10	0.0	5.87	1.7
12002	598		NA		NA		NA		NA		NA	
12018	277		2.60	0.2	0.39	0.1	1.00	0.1	0.15	0.1	7.05	1.4
15016	240		2.67	0.1	0.15	0.0	0.79	0.0	0.07	0.0	6.84	0.9
15535	165		2.40	0.3	0.17	0.0	0.74	0.0	0.06	0.0	6.29	0.6
15556	258		2.65	0.1	0.15	0.0	0.75	0.1	0.09	0.0	6.77	1.1
14053	305		5.23	0.3	1.11	0.1	2.20	0.1	0.46	0.0	11.87	0.8
Detection Limit			0.050	ppm	0.026	ppm	0.404	ppm	0.035	ppm	0.090	ppm